



The
University
Of
Sheffield.

Impact of alternative fuels on atomisation, noise, vibration and combustion instabilities of gas turbines

By Charith J. Wijesinghe

Supervisors;

Dr. B. Khandelwal

Prof. W. Nimmo

A thesis submitted in partial fulfilment of the requirements for the degree of

Doctor of Philosophy

Faculty of Engineering

Department of Mechanical Engineering

University of Sheffield

May 2021

Abstract

With increasing requirements for alternative fuels, a significant proportion of researchers around the world concentrate on emissions and fuel systems compatibility of novel alternative fuels. Whilst the impact of alternative fuels on combustion instability, noise, vibrations and the mechanisms behind it are relatively unexplored. In this study an investigation has been conducted to determine the impact of fuel properties on atomisation characteristics with a wide variety of novel alternative fuels and several low aromatic surrogate fuels. One investigation has been a study observing the noise and vibrations emanating from a gas turbine combustor running on alternative fuels. which has found how fuel properties have impacted the noise, vibrations and pressure oscillations of the combustor. It was found that fuels with lower density, viscosity and cetane number produce lower vibrations from a gas turbine and that increased H/C ratio has a beneficial impact on noise and vibrations. In addition, this investigation observed the noise and vibrations characteristics of a full in-service gas turbine in the form of a Honeywell APU running on 20 alternative fuels of varying properties. A key finding of this investigation is that fuel properties play a crucial role in the noise and vibrations of gas-turbines and therefore has an impact upon the wear life of engine hot-section components, which would be amplified at elevated operating pressure ratios. This finding is unique to this study.

Moreover, this investigation has determined that atomisation plays a key role in the noise, vibrations and instability a fuel generates in a gas turbine combustor and a full gas turbine. The impact of atomised fuel droplet size on engine vibration was studied, which showed that as fuel droplet size increases so does the vibrations produced by the engine. The final knowledge contribution of this work has been the study of several aromatic species and their properties with respect to their atomisation, noise and vibrations

characteristics. To this end several aromatic compounds were tested for their droplet sizes as well as noise and vibrations to determine the best aromatic for blending with kerosene. The results showed that Ethylbenzene and Cumene produced the lowest droplet sizes and vibrations.

Acknowledgements

I wish to express my sincere appreciation to my supervisors Dr Bhupendra Khandelwal and Professor Bill Nimmo for their patience, guidance, and support throughout my time at the University of Sheffield.

I would also convey my utmost gratitude to my parents Dr. N. D. Wijesinghe and Professor P. S. Wijesinghe for their unwavering support throughout my life and more specifically proofreading my sometimes erratic writings.

Moreover, I would like to thank the technical and research staff at the LCCC, Mr. I. Ahmed, Mr. D. Dunstan and Mr. T. Haycock without them this endeavour would not have been possible.

Finally, I would like to thank the *two* magpies who decided to nest on a tree outside my window; to them I attribute any measure of luck I have experienced during the writing of my thesis.

This is my thesis. There are many like it, but this one is mine.

Contents

Abstract	i
Acknowledgements	iii
List of figures	xiii
List of tables	xiv
Nomenclature	xv
List of publications	xvii
1 Introduction	1
1.1 Thesis structure	2
1.2 Research question	4
2 Literature Review	5
2.1 Alternative fuels	5
2.1.1 Motivations	6
2.1.2 Composition and feedstocks	8
2.1.2.1 Sugars and starch crops	10
2.1.2.2 Lignocellulosic biomass	11
2.1.2.3 Triglycerides and other plant derived oils	12
2.1.3 Production pathways	13
2.1.3.1 Fischer-Tropsch process	13
2.1.3.2 Hydroprocessing	14

2.1.3.3	Alcohol to jet	15
2.1.4	Aromatics and emissions	16
2.1.4.1	Particulate emissions	17
2.1.4.2	Seal compatibility	22
2.2	Combustion instability	25
2.2.1	Combustion fundamentals	25
2.2.1.1	Flame stabilisation	28
2.2.2	Combustion instability of gas turbines and their combustors	30
2.2.2.1	Acoustic oscillations	32
2.2.2.2	Effect of fuel type on instabilities	33
2.2.3	Atomisation	37
2.2.3.1	Sheet and droplet formation (classical atomisation)	38
2.2.3.2	Prompt atomisation	41
2.2.3.3	Effect of atomisation characteristics on combustion instability	42
2.2.3.4	Effect of alternative fuels on spray characteristics	47
2.2.4	Controlling combustion instability	53
2.3	Signal processing	53
2.3.1	Fundamentals of signal analysis	54
2.3.1.1	Sampling theorem	56
2.3.2	Root mean square value.	56
2.3.3	Acoustic octaves	57
2.3.4	Fourier Analysis	57
2.3.5	Knowledge gaps	58
2.3.6	Aims and objectives	59
3	Fuels, their properties and experimental methods	60
3.1	Aromatic compounds and their blends	60
3.2	Reference and other drop-in alternative fuels	64
3.3	Properties of conventional Jet fuel.	66
3.3.1	Density	66

3.3.2	Flash point	67
3.3.3	Viscosity	68
3.4	Experimental methodology of atomisation rig	68
3.4.1	Atomization	72
3.4.2	Laser particle analyser	72
3.4.2.1	Data acquisition and processing	76
3.4.3	Mean diameters	77
3.5	Experimental setup of atmospheric pressure combustor	78
3.5.1	Tay combustor	81
3.5.2	Sensors and data processing	82
3.6	Gas turbine experimental methods	88
3.6.1	The gas turbine engine	88
3.6.2	APU operating procedure and conditions	90
3.6.3	Sensors and data processing	92
4	Spray characteristics of low aromatic and alternative fuels	95
4.1	Introduction	95
4.2	Results and discussion	96
4.2.1	Droplet size distributions	96
4.2.2	Comparison against fuel properties	105
4.3	Conclusions	111
5	Noise, vibrations and instability characteristics of an atmospheric pressure combustor running on low aromatic surrogate fuels	113
5.1	Introduction	113
5.2	Results	114
5.2.1	RMS Analysis	117
5.2.2	Octave band analysis	120
5.2.3	Peak height analysis	131
5.3	Conclusions	135

6	APU testing	137
6.1	Introduction	137
6.2	Results	138
6.2.1	RMS Analysis	142
6.2.2	Octave analysis	148
6.3	Conclusions	152
7	Overall conclusions of alternative fuels and combustion instability and future work	154
7.1	Overall conclusions	154
7.2	Future work	157
	Bibliography	159
	Appendices	180

List of Figures

2.1	Choke-points of current oil transit routes and route volume [21].	7
2.2	The energy ‘Trilemma’ [22].	8
2.3	Pathways for the production of alternative fuels from fossil and bio-based feedstocks [23].	8
2.4	Production schematic for sugar cane derived jet fuel [30].	11
2.5	Production of bio diesel by country [33].	12
2.6	FT process schematic adapted from [40].	14
2.7	Production process for HRJ [43].	15
2.8	Production process for Alcohol to jet (ATJ) [46].	16
2.9	Molecular configuration of Toluene.	17
2.10	General mechanism of soot formation during combustion [47].	18
2.11	Aromatic content of a fuel vs emission indices of the non-volatile particulate matter emitted upon the burning of the fuel in a gas turbine. Coloured lines indicate engine power setting as a percentage [55].	20
2.12	Organic mass emitted by CTL, GTL and Jet-A1 against measurement locations and power settings [57].	21
2.13	Particulates measured for fuels at size of 75 nm. fuel 1 is Jet-A1 [59]. . .	22
2.14	Seal contraction process[1].	23
2.15	. Swelling effect of nitrile O-rings in mixture of 25% aromatic and SPK [66].	24
2.16	Relaxation behaviour of nitrile O-rings in the triangle [42].	25
2.17	Gas turbine cycle schematic [67].	26

2.18	Types of combustors, where the shaded areas depict the combustion zones of each type [68].	27
2.19	A can-annular combustion chamber [69].	28
2.20	Bluff body flame stabilised combustor schematic, adapted from [70].	29
2.21	Swirl stabilised combustion chamber schematic, adapted from [70].	30
2.22	Combustion instability feedback loop [1].	31
2.23	Causes of combustion instability [77].	31
2.24	Vibration amplitude and frequency with 4 fuels [85].	34
2.25	Vibration amplitude and frequency with 3 fuels [86].	35
2.26	The average pressure (a), RMS pressure oscillations (b) and instability frequencies (c) with respect to inlet air-temperature for the fuels tested by Chen et al. [87].	36
2.27	FFT vibration data for the fuels tested by Othman et al. [88].	37
2.28	Peak vibrations in dB at the first 4 harmonics for the fuels tested against their carbon to hydrogen ratio [88].	38
2.29	Classical representation of a simple jet disintegration [68].	39
2.30	Classical representation of a sheet breakup [91].	40
2.31	Spray break up for jets across various flow regimes [96].	42
2.32	Spray characteristic of the two combustor conditions investigated by García et al. [97]. The series have been shifted by 30dB for illustrative purposes.	43
2.33	SMD characteristics of the swirl cup injector investigated by Liu et al. [98]. Left figure indicates ‘ignition condition’ and the right ‘LBO condition’.	44
2.34	Critical blow-off limits for a natural gas and air mixture exiting into a n environment consisting of the gases shown in the figure with respect to flow speed and the equivalence ratio [101].	45
2.35	Spray characteristics variation between normal ignition conditions and LBO [98].	46
2.36	Spray characteristics variation between normal ignition conditions and LBO [73].	46

2.37 Droplet size with respect to radial distance as investigated by Vouros et al. [102].	48
2.38 SMD comparison with Weber number for several lengths away from in- jector ‘z’ [103].	49
2.39 SMD for 2 alternative and one conventional fuel [105].	50
2.40 Spray cone measurement locations of Kannaiyan and Sadr [106].	51
2.41 SMD at various locations of the spray field for the 3 fuels. Top and bottom indicate 0.3MPa and 0.9MPa injection pressures respectively [106].	51
2.42 F-T vs RP3 fuel SMD with increasing injection pressures [107].	52
2.43 Active instability controller for a premixed combustor using microphones and loudspeaker [108].	54
2.44 An illustration of the 3 main types of signals; periodic, transient and random.	55
3.1 Spray testing rig.	69
3.2 Spray rig bottom vents and liquid drainage.	70
3.3 Nitrogen pressurised fuel tank.	70
3.4 Injector assembly and fuel filters.	71
3.5 Air-blast atomiser and schematic from the Rolls-Royce Tay engine.	72
3.6 Malvern 2600c Particle sizer [129].	73
3.7 Particle scattering mechanism[129].	74
3.8 Alignment display [129].	75
3.9 Examples of photographs collected of the raw data.	76
3.10 Comparison of SMD vs DMD [134].	78
3.11 Atmospheric pressure combustor schematic.	79
3.12 Combustor control panel.	80
3.13 Tay combustion chamber.	82
3.14 Dynamic pressure sensor schematic [136].	83
3.15 From left to right: pressure sensor base, sensor probe, signal interrogator. The images were acquired after the flooding of the LCCC hence the rust on the probe.	83
3.16 Combustor and sensors (microphones are not visible in this image).	84

3.17	Accelerometers and microphones used [137, 138].	84
3.18	DAQ user interface.	85
3.19	Raw time series data.	86
3.20	Spectrogram of C11 for Accelerometers (X1, Y1 and Z1) both microphones (M1, M2) and pressure oscillations (P).	87
3.21	APU schematic diagrams.	89
3.22	Gas turbine and key components.	90
3.23	picture of APU showing its key components.	91
3.24	APU test bed schematic and sensor locations.	92
3.25	Spectrogram of 3 accelerometers X1, Y1, Z1 and 2 microphones M1, M2 for fuel RF14.	94
4.1	Jet-A1 droplet size distribution and cumulative frequency charts	97
4.2	Injection pressure comparison of fuel RF2.	99
4.3	SMD plots for fuel groups A and B against the blend density.	100
4.4	SMD of aromatics normalised to Jet A1 (RF1).	102
4.5	SMD of aromatics normalised to JP 8 (RF2).	103
4.6	SMD plots for reference fuels against their density.	104
4.7	Reference fuel SMD against surface tension at $60psi$	106
4.8	Reference fuel SMD against viscosity at $60psi$	106
4.9	Reference fuel SMD against derived cetane number (DCN) at $60psi$. Red marker indicates RF8.	107
4.10	Injection pressure comparison of fuel RF1(A2) and RF4(C1).	108
4.11	Injection pressure comparison for two reference fuels from Buschhagen et al. [105].	109
4.12	Theoretical vs experimental comparison for SMD.	110
5.1	Single sided FFT of all 8 sensors (accelerometers (X1, Y1 ,Z1 ,X2 and Y2), microphones (M1 and M2) and pressure sensor (P)) for A2. Red, green and blue lines indicate conditions 1,2 and 3 respectively.	115

5.2	RMS data for A and B groups at Condition 1 (Blue) Condition 2(Orange) and Condition 3 (Grey).	118
5.3	RMS accelerometer data compared to fuel blend density for all 3 conditions.	119
5.4	Octave band analysis for B group and Jet A1 for M2 at condition 1. Reference pressure $1Pa$	122
5.5	Octave band analysis for B group and Jet A1 for M2 at condition 2. Reference pressure $1Pa$	123
5.6	Octave band analysis for B group for M2 at condition 3. Reference pressure $1Pa$	124
5.7	Octave band analysis for B group and Jet A1 for M2 at condition 1. Reference pressure $20\mu Pa$ which corresponds with human hearing range. . .	125
5.8	Octave band analysis for B group and Jet A1 for M2 at condition 2. Reference pressure $20\mu Pa$ which corresponds with human hearing range. . .	126
5.9	Octave band analysis for B group for M2 at condition 3. Reference pressure $20\mu Pa$ which corresponds with human hearing range.	127
5.10	Octave band analysis conducted by Simons et al for Jet A and 2 alternative fuels [86].	130
5.11	Peak height analysis for A and B groups for X1 at condition 2.	131
5.12	Peak height analysis for A and B groups for Y1 at condition 2.	132
5.13	Peak height analysis for A and B groups for P at condition 3.	133
5.14	Peak height analysis for A and B groups for X1 at condition 2 with respect to H/C ratio.	134
6.1	Single sided FFT of all 5 sensors (accelerometers (X1, Y1 ,Z1), microphones (M1 and M2) for RF14. Red, green and blue lines indicate conditions 1,2 and 3 respectively. Tooltips indicate peak amplitudes and their corresponding frequency.	139
6.2	Single sided FFT of X1 for the three engine conditions with RF14 (reference Jet A1).	141
6.3	RMS data for each fuel at Condition 1 (Blue) Condition 2(Orange) and Condition 3 (Grey).	143

6.4	RMS Analysis of 3 Jet A1 repeats conducted with respect to engine condition	144
6.5	RMS acceleration of fuels tested in APU against the viscosity. Note not all fuels' viscosity data were available.	145
6.6	RMS acceleration of fuels tested in APU against the fuel density.	146
6.7	RMS acceleration of fuels tested in APU against the hydrogen to carbon ratio. Note not all fuels' H/C ratio data were available.	146
6.8	RMS acceleration of fuels tested in APU against the cetane number. Only fuels with cetane number available are depicted (RF3, RF7, RF8, RF10, RF11, RF12, RF13).	147
6.9	Octave band analysis M1 at condition 1. Reference pressure $20\mu Pa$ which corresponds with human hearing range.	149
6.10	Octave band analysis M1 at condition 2. Reference pressure $20\mu Pa$ which corresponds with human hearing range.	150
6.11	Octave band analysis M1 at condition 3. Reference pressure $20\mu Pa$ which corresponds with human hearing range.	151
7.1	RMS acceleration for X1 condition 3 against the SMD at $60psi$ for fuels RF7, RF8, RF10, RF11, RF12 and RF13 for the APU.	155
7.2	Peak height of T2 X1 against the SMD at $60psi$ for fuels both A and B group fuels tested on atmospheric combustor.	156
7.3	Data acquisition VI for acceleration, noise and pressure.	181

List of Tables

2.1	PM mass and number reductions for alternative fuels with respect to Jet-A1 [54].	19
3.1	List of low Aromatic blends	60
3.2	Properties of Banner NP1014 used	63
3.3	List of reference and prospective drop-in alternative fuels	64
3.4	Uncertainty of controllable quantities.	80
3.5	Description of combustor conditions.	81
3.6	Description of APU gas turbine conditions.	91

Nomenclature

D_{32} Sauter Mean Diameter

kt Kilo-ton

AFR Air-fuel Ratio

ANSI American National Standards Institute

APU Auxiliary Power Unit

ASTM American Society for Testing and Materials

ATJ Alcohol To Jet

CI Compression ignition (Usually describes a diesel engine.)

cPM condensible Particulate Matter

CTL Coal To Liquid

DEF STAN Defense Standard

DFT Discrete Fourier Transform

EGT Exhaust Gas Temperature

EPA Environmental protection agency

FAR Fuel-air Ratio

FFT Fast Fourier Transform

FT Fischer-Tropsch

GTL	Gas To Liquid
HEFA	Hydro-processed Esters and Fatty Acids
IPK	Isoemerised Paraffinic Kerosene
LBO	Lean Blow Off
LTO	Landing and Take off cycle
nvPM	non-volatile Particulate Matter
OPR	Overall Pressure Ratio
PM	Particulate Matter
PTFE	Polytetrafluoroethylene
RMS	Root Mean Square
RPM	Revolutions Per Minute
SAF	Sustainable jet fuel
SPK	Synthetic Paraffinic Kerosene
SPL	Sound Pressure Level
TRL	Technology Readiness Level
UCO	Used Cooking Oil
vPM	Volatile particulate matter

List of publications

Authored during the course of this PhD programme.

Book chapters

- B. Khandelwal, C. Wijesinghe, S. Sriraman. Effect of Alternative Fuels on Emissions and Engine Compatibility in; *Energy for Propulsion : A Sustainable Technologies Approach* [1]. **It should be noted that sections 2.1.4.1 and 2.1.4.2 have been adapted from this book chapter.**

Conference papers

- C. Wijesinghe, B. Khandelwal. Impact of alternative fuel on gas turbine noise, vibration and instability. *AIAA Scitech 2019 Forum* [2]. *Awarded best paper from AIAA terrestrial energy systems committee for 2019.*
- C. Wijesinghe, Y. Ling, B. Khandelwal. Experimental Investigation and Assessment of Combustion Instability and Engine Vibrations; as an Impact of Using Novel Alternative Fuels with Low Aromatics in a Gas Turbine Engine *GPPS Beijing, 2019 Proceedings* [3].
- Patrick King, Andre Filipe Carneiro dos Santos, Amir Al-Sheboul, Charith Wijesinghe, Bhupendra Khandelwal. The Feasibility of Hydrogen Assisted Combustors and Fuel Reformation Technologies. *AIAA Propulsion and Energy 2019 Forum* [4].

Journal papers

- B. Khandelwal, J. Cronly, I. Ahmed, C. Wijesinghe, C. Lewis . The effect of alternative fuels on gaseous and particulate matter (PM) emission performance in an

auxiliary power unit (APU). *The Aeronautical Journal* 2019 Volume 123 Issue 1263
Pages 617-634[5].

Under review/ In preparation

- C. Wijesinghe, B. Khandelwal. Impact of aromatic species selection and alternative fuels micro and bulk properties on atomization. *The Aeronautical Journal- under review, currently completing corrections.*
- C. J. Wijesinghe, B. Khandelwal, W. Nimmo. Noise, vibrations and instability characteristics of an atmospheric pressure gas turbine combustor running on low aromatic surrogate fuels. *In-preparation.*
- C. J. Wijesinghe, B. Khandelwal, Combustion instability, Gaseous Emissions and Lean blow out (LBO) in Bhupendra Khandelwal Editor, Aviation fuels First Edition, Academic Press Elsevier, ISBN: 9780128183144. Due to be published 1st April 2021.

Chapter 1

Introduction

With the rapid onset of climate change looming in the intermediate future and the drive to curb emissions, it is natural for alternative fuels to be considered for aviation gas turbines as aviation accounts for 2% of all anthropogenic greenhouse gas emissions [6]. However, with the introduction of alternative fuels comes with it many challenges one such challenge is the unknown nature of how existing combustion infrastructure will react to the alternative fuel. This investigation focuses upon the effect of alternative fuels on combustion noise, vibration and instabilities.

Noise in general is considered a nuisance at best and can lead to social tensions and can hinder the quality of life of those persons directly impacted by high noise situations on a daily basis such as those who live near a busy road such as motorways or A roads in metropolitan city centres [7]. Another such issue is the constant noise pollution emitted by busy airports such as London's Heathrow [8].

Noise and vibrations are generally considered to be distinct when considering the domain of dynamics. However, both are interconnected in that they both describe the convection of molecular motional energy in different domains usually noise in fluids (most notably air) and vibrations in solid media (i.e. the dull vibrations in the cabin of an aircraft caused by the gas turbines) [9].

Noise from aviation and aircraft can be classified into three categories; systems derived noise (i.e. air-conditioning, pressurisation derived noise), Aerodynamic noise (from the interaction of the aircraft fuselage on the free-stream airflow) and finally the largest

contributor the engine derived noise. Engine noise in itself is dichotomous, in that it is comprised of the mechanical noise from the compressors and fan as well as the jet noise produced by the high-velocity jet of air leaving the rear of the engine.

Noise generated in the core of aerospace gas turbines can be separated into two categories namely direct and indirect combustion. Direct combustion noise is formed when the burning gas mixtures of a combustion chamber expand unsteadily causing pressure and temperature fluctuations which form the ideal conditions for noise generations. Indirect combustion noise on the other hand is a result of entropy waves generated by the temperature fluctuations caused by the unstable combustion propagating towards the turbine blades and generating noise there [10].

This investigation focuses upon the vibration and noise generated by the combustion system of the gas turbine and how it is impacted by the variation in fuel. It also sheds light on how the variation in combustion noise and vibrations caused by combustion instability impacts the noise and vibrations characteristics of the wider gas turbine. This is possible as the gas turbine is a complex dynamic system that is rigidly linked in its entirety save for the rotational components which have some degree of freedom but are still linked to the wider engine by means of bearings and other mechanical fittings.

With the increasing attention that anthropogenic emissions have garnered in recent times and the drive towards cleaner carbon neutral fuel intensifying, it is prudent to investigate the possible alternatives for conventional fossil derived jet fuel. Whilst liquid alternative fuels have been researched for the past 20 years, especially with an emphasis on their emissions characteristics, their operability has yet to be explored thoroughly in terms of the noise and vibrations variation caused by fuels. Hence this investigation focuses on a small segment of that operability namely the noise, vibrations and instability characteristics of alternative fuels running on conventional gas turbines and combustors.

1.1 Thesis structure

The structure of this thesis is as follows, chapter 1 is a introduction providing a general overview of thesis. Chapter 2 contains the background literature regarding the state of

art as it pertains to the noise, vibrations and combustion instability of gas turbines. It has been subdivided into 3 sections; alternative fuels and their pathways including the legislation surrounding the adoption of sustainable aviation fuel (SAF) as drop in alternatives to conventional jet fuel, secondly combustion and instability which explores the current knowledge around combustion instability, combustion fundamentals and atomisation which impacts combustion instability greatly, finally the literature informs the reader about the signal processing techniques used in the analysis of the noise and vibration data acquired in this investigation.

Chapter 3 describes the fuels chosen and the experimental apparatus used in this investigation. It is divided into four sections. The first of which is the fuel section where all the aromatics and drop-in fuels are listed with their fuel properties as well as the reasoning behind their selection. The other 3 sections describe the 3 experimental campaigns undertaken as a part of this investigation. Namely, atomisation testing using a particle sizer, combustor testing using a can-type combustor and finally a full test campaign using an APU.

Chapters 4, 5 and 6 describe the results obtained from the experiments conducted as part of this investigation. The structure of this thesis has been designed to showcase the overarching theme of how fuel variation impacts the combustion characteristics of an engine. Firstly starting with the impacts of fuel type on atomisation as shown in chapter 4, how the atomised fuel impacts the noise and vibrations characteristics of a combustor in chapter 5 and finally how combustion and atomisation of various fuels impact an entire gas turbine in terms of noise, vibrations and combustion instability.

Finally, chapter 7 serves to act as a section aiming to draw correlations from the 3 experimental campaigns and to showcase the links between atomisation, combustion and their impacts on rotational machinery and the wider gas turbine. In addition to this chapter 7 also includes a section on future work that could be carried out to further enhance the findings of this investigation.

1.2 Research question

This project will evaluate the impact of conventional and synthetic (alternative) fuel composition on engine vibration, noise and combustion instability by using a range of combustion systems including a Rolls-Royce Tay combustor and a commercially available Honeywell APU (Auxiliary power unit). Furthermore, it will investigate the impact of the alternative fuels on spray characteristics as spray and mixing of fuel is a known factor affecting combustion instability. The contribution to knowledge from this PhD is new knowledge about how different novel alternative fuels impact combustion instability, noise and vibrations as well as any implications on engine life and maintenance of engines. The contribution to knowledge also includes detailed understanding on instability phenomenon, when alternative fuels are burned in conventional combustion systems. One of the future impacts of the work could be designer fuels, optimised for current combustion systems and better combustion systems in future. Both combustion systems and the fuels they use require new strategies to cope with increasing environmental considerations.

Chapter 2

Literature Review

This chapter contains review of the current state of art relating to the current research and has been divided into the following topics;

- Liquid alternative fuels. With a view to exploring variations in composition and production methods with respect to conventional fuels.
- Combustion instability in gas turbines and combustors. With a view to determining how a variation in fuel composition could impact the instability characteristics of a given engine.
- Signal processing as pertains to the acquisition and visualising of noise, vibrations and pressure data.

2.1 Alternative fuels

Alternative fuels are defined as fuel that are capable of being used instead of conventional fossil fuels. This review is focussed upon liquid alternative fuels which can be used to replace liquid aviation fuels (i.e. Jet A1, Jet A, JP8 and TS1). That said it should be noted that according to the International energy agency; of the 3.8 million kt(kilo-tons) of crude oil produced in 2017 only 300,000kt was refined into ‘jet kerosene’, with 1 million kt and 1.3 million kt refined into ‘motor gasoline’ (i.e. Petrol) and Diesel respectively [11]. This compares to only 8600 and 9500 kt of renewable fuel of all sources being produced in 2017 and 2018 respectively [12]. This means that compared to fossil fuels alternative fuels make

up only 0.25% of total crude oil production. However, since the year 2008 alternative fuel production has undergone a 94% increase indicating the increasing demand for alternative fuels as well as showcasing the increasing maturity of the production technologies [12].

2.1.1 Motivations

The motivations for using alternative fuels are complex multifactorial, this section aims to elaborate on them. The most obvious motivation for further developing alternative fuels and proliferating their use stems from the climate crisis the world is currently facing. Alarming rises in emissions due to anthropogenic activity causing the atmospheric CO_2 concentrations to exceed $400\mu mol\ mol^{-1}$ and set to increase at a rate of $2\mu mol\ mol^{-1}$ per year [13]. These emissions impact the mean temperature of the planet by means of radiative forcing mainly. This is defined as the remainder of solar energy in the atmosphere after taking into account the energy that has been reflected back into space. This trapped energy is essential to life on earth, however anthropogenic activity has increased the greenhouse gasses present in the atmosphere to an extent that it is causing increases to the global mean temperatures and other climatic events (i.e. Drought's, warmer winter's, coastal flooding etc.) [14].

The second reason behind the argument for alternative fuels stem from the localized emissions from the combustion of fossil fuels which emit particulate matter (PM) and NO_x and CO (carbon monoxide) which are known to be carcinogenic when inhaled and can lead to respiratory illnesses in those who are subjected to long term exposure in poor air quality environments such as in megacities around the world [15–17]. Therefore it stands to reason that using alternative fuels with proven lower emissions specially in terms of PM can be of profound utility [5, 18]. Other impacts of atmospheric air pollution take the form of acid rains, smog and ozone layer depletion.

Finally, and most importantly are the economic and security of supply arguments for the implementation of jet fuels of non-conventional origin. It is well known that when the price of crude oil is high (i.e. from 2008-2014 when the price of Brent crude was consistently above \$100 a barrel) it has been observed that research into alternative fuels has received increased funding due to the perceived increase in profitability for the sup-

pliers of alternative fuels [19, 20]. Furthermore, the other economic argument for the use of alternative fuel involved security of supply. That is to say that countries which do not possess reserves of crude oil (or cannot produce enough on their own to be self-sufficient) must secure their oil supplies from abroad, leading to an obligation with that country and a possibility of fuel shortages if geopolitical issues arise among supplier and customer countries. Figure 2.1 depicts the current routes of oil movements across the planet by maritime means. As can be seen the major routes of transit involve the straits of Hormuz, Suez Canal and the straits of Malacca. All three of these choke-points are known hot-spots piracy and/or terrorism which have threatened the supply of crude to customer nations at various points in time; the most recent being the attacks on crude oil tankers in the straits of Hormuz in 2019 (at the time of writing). This type of uncertainty and instability in the supply of crude oil has given political reason and will to explore alternative fuels especially in countries such as the U.S. and the U.K.

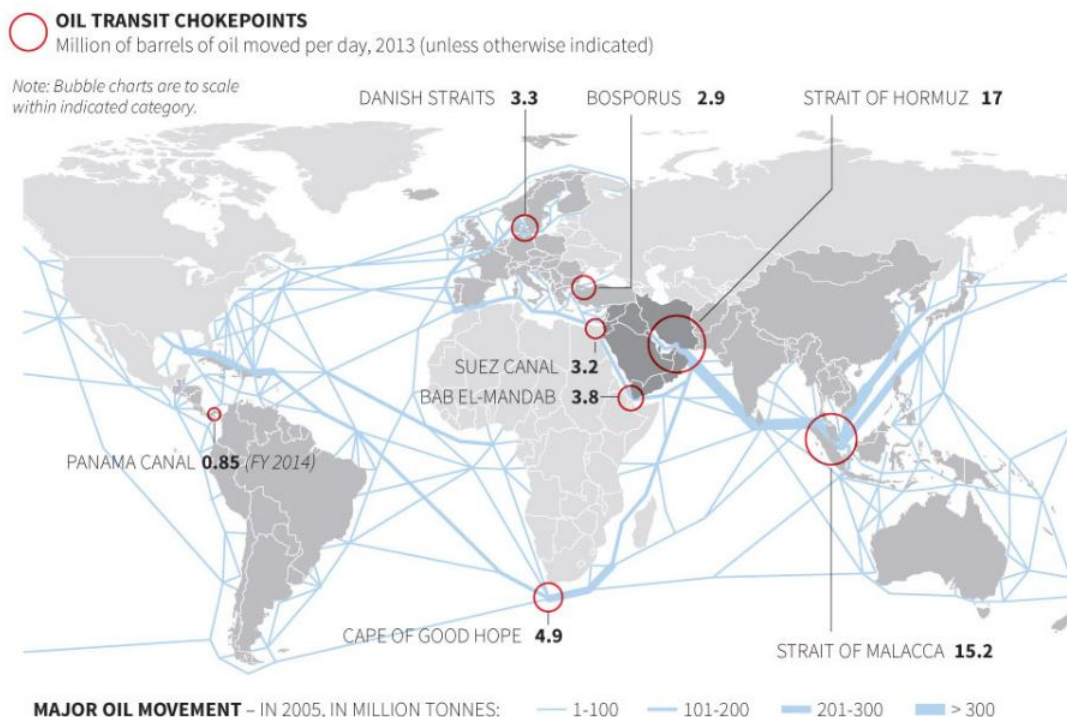


Figure 2.1: Choke-points of current oil transit routes and route volume [21].

Combined, the motivations for the use of alternative fuels are known as the ‘energy trilemma’, which are 3 issues that must be balanced in order to achieve a sustainable energy policy for a given state.

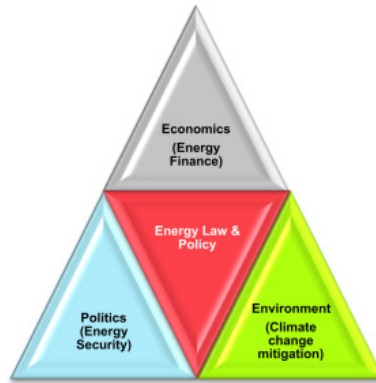


Figure 2.2: The energy 'Trilemma' [22].

2.1.2 Composition and feedstocks

Feedstocks for liquid alternative fuels of gas turbines are dichotomous; divided into bio-based and fossil-based feedstock. Bio-based feedstock is considered to be a renewable fuel source. That said fossil-based alternatives are the more mature technology having been used in some form or another for the better part 70 years.

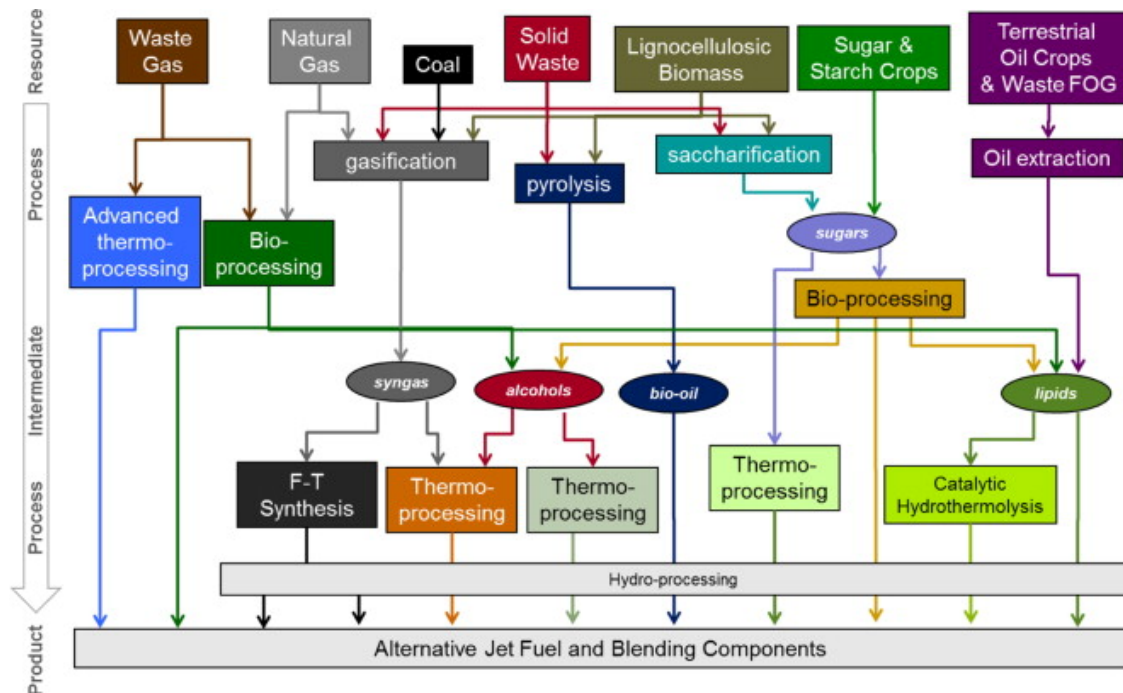


Figure 2.3: Pathways for the production of alternative fuels from fossil and bio-based feedstocks [23].

Figure 2.3 depicts the most commonly used pathways to derive alternative jet fuels from both types of feedstocks. Biological feedstocks can be from almost any plant based

source however when considering the economic feasibility and the energy density of the plant based source the number of viable candidates are reduced to those mentioned in Fig. 2.3. The key objective of these various pathways is to develop a jet fuel surrogate. To understand the requirements of alternative fuels it is important to first understand the composition of conventional jet fuel as it currently stands. There exists two main standards which set the composition jet fuel namely; the U.K.'s DEF STAN 91 and the U.S.' ASTM D1655 [24, 25]. These standards go on to describe the required composition in terms of % aromatic hydrocarbons present in the fuel, distillation curve, density, boiling point, flash point, viscosity, energy density (net heat of combustion) etc. however this document assumes the feedstock used for the production of the aviation fuel is fossil based and requires further approvals before alternative fuels are able to be certified for use in jet engines even if they meet the aforementioned standards. There exists a specific standard from ASTM's Committee on 'Petroleum products, Liquid fuels and lubricants' named D7566 "Standard Specification for Aviation Turbine Fuel Containing Synthesized Hydrocarbons" [26]. This standard provides a method by which synthetic fuels can be certified for commercial use in aircraft as blends with jet A1.

That said the above standards are 'fit for purpose' in nature, having been developed from empirical and anecdotal evidence. Therefore, they do not describe the individual chemical components present in the fossil derived jet fuel. According to Bernabei et al. the average fossil derived jet fuel contains 20% aromatics (arenes), 20% naphthenes (cycloalkanes), 20% paraffins (straight chain alkanes) and 40% iso-paraffins (branched alkanes) [27]. The method used by them involved gas chromatography and ion detection for mass.

In general, it seems that it's possible to produce a liquid fuel that matches the above composition and agrees with the aforementioned standards relatively easily from a chemistry perspective from a number of sources, after-all all biological matter are carbon and hydrogen based. The core issue lies in the efficiency of converting the alternative feedstock into the final useable product in-terms of cost with respect to fossil based fuel, energy efficiency (there is little point in producing a very clean burning fuel if the production pathways of the fuel require vast amounts of energy which offset any gains made by burning

it clean) and finally the life cycle emissions of manufacture through to final use must be better than fossil based fuel. Here bio-based feedstocks have a certain advantage as overall they tend to be carbon neutral due to the plants grown to produce the fuel absorb carbon from the atmosphere. What follows is a brief overview of the commonly used feedstock to derive alternative fuels both bio and fossil based.

When considering biofuel feedstocks there are 4 generations of biofuels with the latest being 4th generation biofuels. 1st are derived from edible feedstock such as sugar-cane, wheat, barley and potato. This poses the obvious dilemma of food vs fuel, whereby fuel producing crops compete with food crops which is detrimental to the efforts regarding the elimination of hunger amongst humans. 2nd generation biofuels were developed with the aim of combating drawbacks of the 1st. These are comprised of non-edible feedstock such as wood-chip, forest residue etc. Principle advantage of these being they do not compete with human food crops and also in general require no purposeful cultivation as they are usually by-products of the forestry and other biomass producing industries. The disadvantage of 2nd generation biofuels stem from the high capital costs involved in the pre-treatment processes required to obtain the fermentable sugars which can be utilised for biofuels. 3rd generation biofuels are derived from micro-algae. This has the distinct advantage of not requiring arable land coupled with a fast growth rate. The drawbacks of the 3rd generation biofuels stem again from high capital costs of the production process. Finally, 4th generation biofuels are derived from genetically modified micro algae which can be grown in waste water and also capture large amounts of CO₂ [28].

2.1.2.1 Sugars and starch crops

Sugars made from agricultural starch crops are the premier method for manufacturing biofuels currently, specifically the sugar cane crop which is extremely efficient photosynthetically and contains almost 20% of its mass in sucrose [6]. Increasing amounts of this resource is being diverted from conventional sugar to biofuel production specially ethanol. Other sugar producing crops include whey, sorghum and sugar beets. The precursor required for the production of fuels stems from the sugar hydrolysate or from molasses, which are a by-product from sugar produced for human consumption [29]. Whilst sugar

cane is an effective feedstock for aviation fuel the land use requirement for the large scale production of it is problematic due to the specific climate required as well the achievable crop density for a given land area. One such sugar cane derived aviation fuel is Farnesane, the method of production for which is depicted in Fig. 2.4.

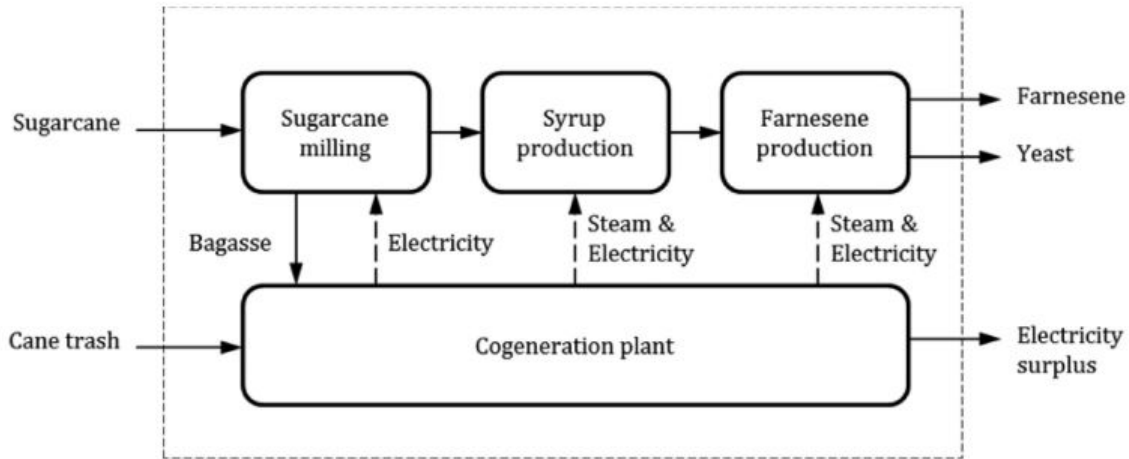


Figure 2.4: Production schematic for sugar cane derived jet fuel [30].

2.1.2.2 Lignocellulosic biomass

Due to the drawbacks of sugar cane which is a first generation biofuel there is much interest in lignocellulosic feedstocks, these are mainly derived from plants which do not compete with the world food supply chain. Examples of lignocellulosic feedstock include food waste, agricultural residues (chaff, silage etc.), wood residue (woodchips, sawdust etc.) and other crops grown especially as energy crops. Several studies have conducted on the feasibility of converting wood derived biomass into drop-in alternative fuels using a method known as alcohol to jet (ATJ) [31, 32]. Ganguly et al. claims that using woody biomass derived jet fuel totally instead of fossil jet fuel a 78% saving in global warming potential can be achieved. the practicality of such claims must be considered in the light of the complex production pathways required as well as the competition existing for the use of said feedstock [32]. Due to these reasons lignocellulosic biomass is of limited utility in the production of jet fuel, due to the increased complexity and therefore lack of economic viability in producing a liquid fuel. This type of feedstock is far more common in power generation where for example food waste on a large scale can be used as fuel via anaerobic

digestion.

2.1.2.3 Triglycerides and other plant derived oils

For several decades it has been common practice to formulate biodiesel using plant-based (vegetable) oils as well as used cooking oil (UCO). Whilst it is possible to run almost straight vegetable oils in diesel engines with only minor modifications; this is not ideal for aviation gas turbines due to the heterogeneous nature of the oils in question leading to unpredictable combustion characteristics which are not of great concern in a land based engine. Biodiesel however is produced by transesterification, where the fats are reacted with an alcohol (most commonly methanol although ethanol is also a possibility) to produce a methyl-ester. This is the most common method of production for bio diesel and is known as FAME (Faty-Acid-Methly-Ester). The most common feedstock used in the manufacture of biodiesel are soybean, rapeseed (canola), coconut and oil palms depending on the geographic region of growth. Oil based biofuels along with sugar derived fuels are considered to be first generation fuels. Their utility has been called into question on the grounds of sustainability, competition with food production and finally the environmental benefits of using them [33]. Figure 2.5 depicts the major producers of biodiesel's as of 2008.

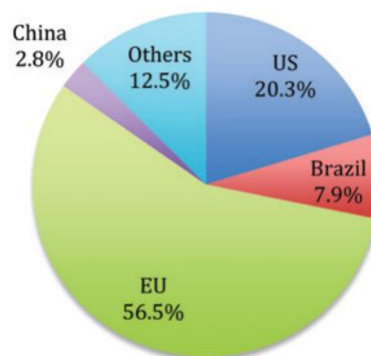


Figure 2.5: Production of bio diesel by country [33].

The efficiency of using bio-diesel in aviation engines has been called into question by Wardle [34]. This is presumable due to the innate nature of FAME having fuel borne oxygen which is undesirable in aviation fuels as it reduced the energy density of the fuel.

2.1.3 Production pathways

The chemical process by which a given fuel, be it fossil or bio based has been formulated has an imperative impact upon the resulting fuels chemical characteristics. Moreover, the production pathway used also impacts the economic viability of the fuel as well the environmental impact of the overall fuel life-cycle. Several of these pathways have been approved under the ASTM D7566 standard for the derivation of synthetic jet fuels. Others are in the process of gaining this approval.

2.1.3.1 Fischer-Tropsch process

First invented by Franz Fischer and Hans Tropsch in 1925, the Fischer-Tropsch (FT) process is the premier method by which gaseous mixtures of carbon monoxide and hydrogen (Syngas) are converted into liquid Hydrocarbons at a temperature range of 150 – 300°C in the presence of metal catalysts (Iron, Cobalt and Ruthenium) [35, 36]. The process is mainly used to derive liquid hydrocarbons from Solid feedstocks via gasification (i.e. Coal to liquid (CTL)). That said there are many methods by which to derive Syngas including from biomass which can then via the FT process be converted to liquid fuels [37]. According to Kandaramath et al. fuels produced via the FT process are non-toxic, and exhibit lower NO_x emissions, increased cetane number and low PM emission fuels [36]. Drawbacks of the FT process include the cost of implementation and the fact that it is relatively energy intensive [38]. Moreover, FT fuels tend to be free from aromatics and sulphur as well as the minor trace contaminants present in conventional fuels [39]. It has also been observed by Kreutz et al. that irrespective of feedstock used in the FT process the ultimate fuel characteristics will be determined by the operational conditions of the FT process [40].

The economics of the FT process is quite uncompetitive with respect to fossil fuels as the cost of producing syngas and the FT process itself is energy intensive. Furthermore, the fuels produced by the FT process tend to be straight chain paraffins causing the fuel to be significantly homogenous compared to fossil fuels. This process has the advantage of producing fuels that are the cleanest burning while still combusting liquid hydrocarbons. However, it has some undesirable effects in the form of low lubricity and poor seal com-

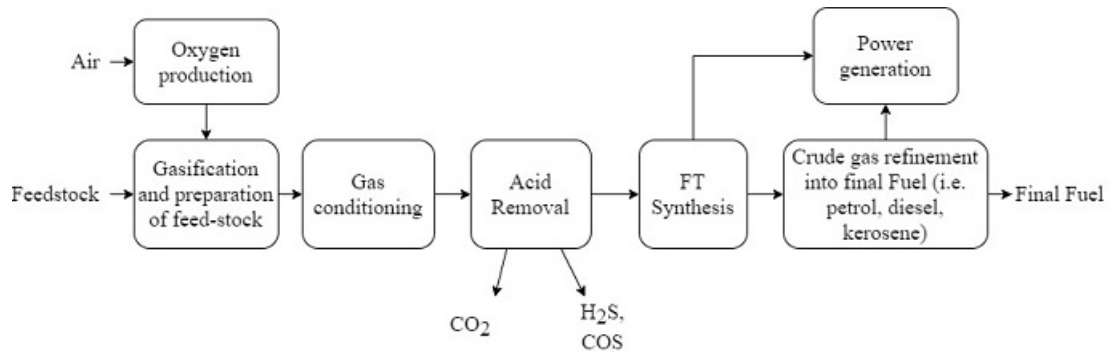


Figure 2.6: FT process schematic adapted from [40].

patibility, which results in increased wear and leaks respectively [1, 41, 42]. As of now the method of certification for biojet fuel involves gaining approval through ASTM D7566. Several fuels using the FT process have been approved for use in commercial flights as a percentage blend with conventional jet fuel. Examples include Sasol corporations FT synthetic fuel approved up to 50% blend this fuel is FT derived from coal and natural gas and Syntroleum's FT synthetic jet from natural gas [38].

2.1.3.2 Hydroprocessing

Hydroprocessing is the umbrella term used by the petroleum industry to describe three separate processes; hydrogenation, hydro-cracking and hydro-treating. Hydrogenation refers to the process of adding hydrogen atoms to unsaturated molecules to increase the combustion efficiency and H/C ratio. Hydro-cracking is the process where long chain hydrocarbons from heavy oils are 'cracked' into shorter molecules fit for use as liquid fuels at standard temperatures and pressures and finally hydro-treating refers to the process of using hydrogen atoms to replace other undesirable compounds in hydrocarbons, specifically oxygen.

Due to this utility hydro-processing is used for almost all feedstocks as a final or penultimate step in the journey to produce a usable fuel [23]. Fuels generated from these processes are known as hydroprocessed renewable jet (HRJ) and tend to contain almost no aromatics, trace impurities (i.e. sulphur, metals) and oxygen. Therefore, the thermal stability of these fuels tend to be very good. However, the lack of aromatics tend to deliver fuels with low lubricity and seal compatibility which need to be overcome by means of

either blending or additives. In terms of renewable fuels, the main feed-stocks used for Hydroprocessing are triglycerides and other bio based fats and oils. The detailed process for which has been described by Wang and Tao [43]. This process is relatively mature with test flights having been conducted using HEFA fuels [44].

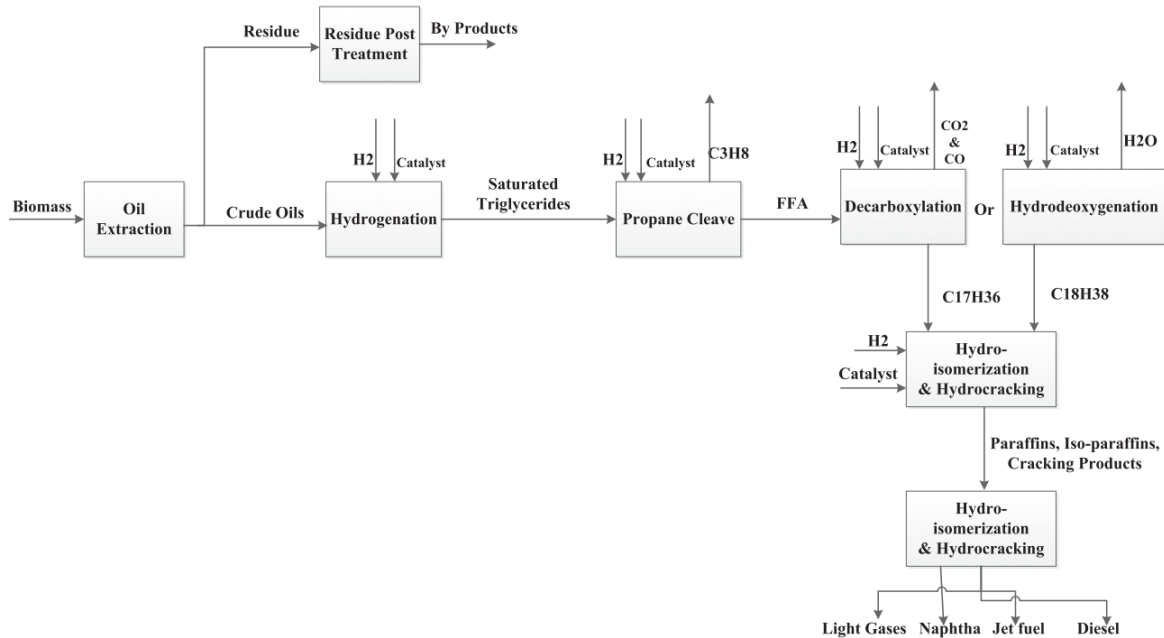


Figure 2.7: Production process for HRJ [43].

2.1.3.3 Alcohol to jet

Alcohol to jet or ATJ for short is a relatively new process that aims to convert alcohols into jet fuels through a process of oligomerisation. A distinct advantage of ATJ derives from the fact that they do not require unproven, unscalable technologies to manufacture. The total process chain involves the dehydration of alcohol (most production pathways are not pure, they include at-least some percentage of water), oligomerisation (the building of longer chain hydrocarbons) distillation (heating the resulting hydrocarbons to derive distillate fractions suited for various purposes) and finally hydrogenation as mentioned in the previous section [45]. ATJ has also been approved for blending into jet fuels through annex 5 of ASTM D7566. Figure 2.8 depicts the generalised process of deriving hydrocarbons from alcohols. Whilst it is possible to run alcohols neat in gas turbines, this is not ideal as pure alcohols have low energy density around 29 MJ/l (calorific value of 34 MJ/kg) for

butanol whereas Jet A1 has close to 35MJ/l (calorific value of 43MJ/kg). This would cause a significant increase in the required fuel per flight. Furthermore pure alcohols have poor lubricity characteristics and also are highly volatile with very low flash points which would affect the safety and operability of aircraft.

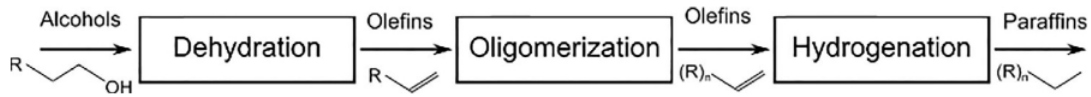


Figure 2.8: Production process for Alcohol to jet (ATJ) [46].

Several organisations are actively involved in the production of ATJ fuel with approval from ASTM D7566 such as ‘LanzaTech’ whose process involves recycling industrial off-gasses and syngas from biomass, ‘Gevo Inc.’ who specialise in butanol based ATJ’s. Several of these alternative fuels have been successfully blended with conventional fuels in commercial flights.

2.1.4 Aromatics and emissions

When it comes to fuels and emissions with respect to aviation, there exists a vast quantity of research conducted into the effect of alternative fuels on gas turbines. This section aims to provide a brief overview of how alternative fuels impact emissions, and what role aromatics play in the emissions process and also why they are of interest in this study.

Aromatics are by definition considered to be hydrocarbon molecules which consist of a ring of 6 carbon atoms with a ring of delocalized electrons and a minimum of 6 hydrogen atoms attached (in the case of Benzene). Aromatics gain their name from the fact that they have an aroma and were named as such before the advent of molecular chemistry. They form one of the 2 main types of hydrocarbons in organic chemistry. The other being aliphatic hydrocarbons which do not contain the double bonded 6 carbon ring, although they can still be cyclic with single bonds. Figure 2.9 depicts the simplest aromatic apart from Benzene which is Toluene. As can be seen there is a ring of 6 carbon atoms double bonded to each other with a single methyl group attached to the number 1 carbon atom instead of the lone hydrogen atom.

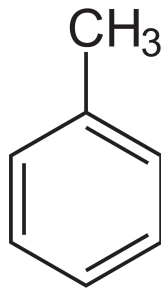


Figure 2.9: Molecular configuration of Toluene.

Aromatics have formed a proportion of naturally extracted hydrocarbon-based fuels from the dawn of fossil based fuel production.

2.1.4.1 Particulate emissions

Particulate emissions, when considered in the airborne context, traditionally can be split into two subsections, PM_{2.5} used for particles $2.5\mu m$ or less in diameter and PM₁₀ for particles of diameter $10\mu m$ or less. Particle emissions, widely known as particulate matter (PM), refers to solids or liquids present in the exhaust gases following combustion. These particles can include carbonaceous particles, abraded metals, inorganic acids, as well as PM present in the ambient air generated from more mundane natural sources like soil and dust particles. Hence the shapes and sizes of the discrete particulates as well as their chemical composition can be irregular. To develop an accurate descriptor for particulate matter therefore would require clarification of their chemical composition, morphology and the abundance of each particle as a function of particle size. Therefore, some common descriptors of particulate matters include nvPM and vPM, non-volatile and volatile particulate matter. NvPM are solid particles at the exit plane of the engine exhaust whereas vPM is liable to change state (forms precursors) when it encounters the ambient conditions outside the engine, as the exhaust is at extremely elevated temperatures some gaseous emissions may condense into liquid and coat the solid particles when cooled down in the exhaust downstream of the turbine. The rate these gaseous emissions condense is somewhat dependent upon their vapour pressure and other ambient conditions such as temperature and humidity, a classic example of this phenomena are contrails from jet aircraft, which appear sometimes but not others. This is due to water vapour being condensed due to the

prevailing ambient conditions, as well as the exhaust temperature at the time.

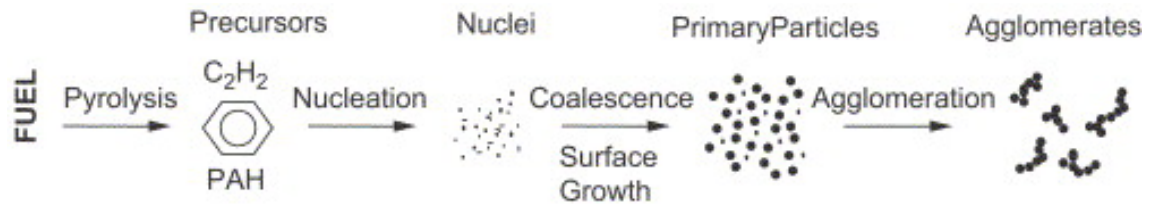


Figure 2.10: General mechanism of soot formation during combustion [47].

Volatile particulate matter (vPM) are formed by the nucleation of gaseous pre-cursors mainly consisting of sulphuric acid and other such organic compounds formed in the cooler exhaust gas downstream of the combustor [48, 49]. Furthermore, it has been observed that these gaseous precursors condense to around the nvPM as illustrated in Fig. 2.10 . The volatile PM definition also fits the condensable PM (CPM) terminology mostly used by the Environmental Protection Agency (EPA).

The main reason particulate emissions have garnered attention is due to the fact that they are an air pollutant, which among other things is mainly responsible for the smog that permeate industrial and heavy-traffic oriented cities such as Beijing and Delhi. Furthermore, particulates pose a significant health risk to humans, it is well-established in literature that individuals exposed to particulate matter on a regular basis are subject to increased risk of mortality and loss of life expectancy due to respiratory and cardio-pulmonary illnesses, such as lung-cancer and cardiac arrest[50–53].

Therefore, it is imperative that particulate emissions be reduced and to this end alternative fuels of diverse types have been scrutinized for their particulate emission levels. In one of the studies conducted by Lobo et al. comparison of PM emissions from a commercial gas turbine (CFM-56) while using alternative fuel was performed [54]. Different types of biomass and FT based fuels were used which were then compared with Jet A-1 as a standard. Several blends of FAME (Fatty-Acid-Methyl-Esters) and Jet A-1 and 100% Fischer-Tropsch fuels were tested. The turbine was operated for full LTO (Landing and take-off) cycles for each blend of fuel. The results of this these test show that PM emissions is reduced significantly when FAME and FT fuels are used, as shown in table 2.1.

Table 2.1 presents the PM emissions reductions as a percentage when compared to

Table 2.1: PM mass and number reductions for alternative fuels with respect to Jet-A1 [54].

Alternative Fuel	PM number reduction	PM Mass reduction
20% FAME 80%JET-A1	22%±7%	20%±8%
40% FAME 60%JET-A1	35%±6%	52%±5%
50% FT 50%JET-A1	34%±7%	39%±7%
100% FT	52%±4%	62%±4%

standard Jet A-1, with 100% F-T fuel providing the greatest reduction in particulates matter, however all the alternative fuels tested had lower PM emissions number and size than Jet A-1, this can be attributed to the fact the fuels in this study has been chosen for their low aromatic content and high H/C ratios. Though it is to be noted that some the fuels tested by Lobo et al. may not be suitable to be used as jet fuel. There are a substantial number of studies in literature which shows that the increase in aromatic content of a given fuel has a tendency to increase PM emissions in gas turbine exhausts. This effect has also been observed by Brem et al. where an in-production high-bypass turbofan and injected fuel mixed with solvents to increase the aromatic content of the fuel, the results of which have been summarised in Fig.2.11 [55].

From Fig. 2.12 it can be observed that as the aromatic content of the fuel increases the emission indices for nvPM also increases showing a clear causal relation-ship. Brem et al. goes on to support the view that soot formation is the result of aromatic content in the fuel as opposed to incomplete combustion, as modern day turbines are highly efficient achieving 99.9% combustion efficiency [55]. Moreover a study conducted by DeWitt et al. corroborates the fact that aromatic content of a fuel is proportional to PM emissions [56]. The study measured the number of particles emitted and their size for JP-8 and F-T derived fuels and found that F-T derived fuels emitted particles that were a full order of magnitude smaller than those emitted whilst running JP-8.

Williams et al. has described the effects alternative fuels have on vPM by measuring the organic matter concentrations in the exhaust duct of a Rolls-Royce Artouste Auxil-

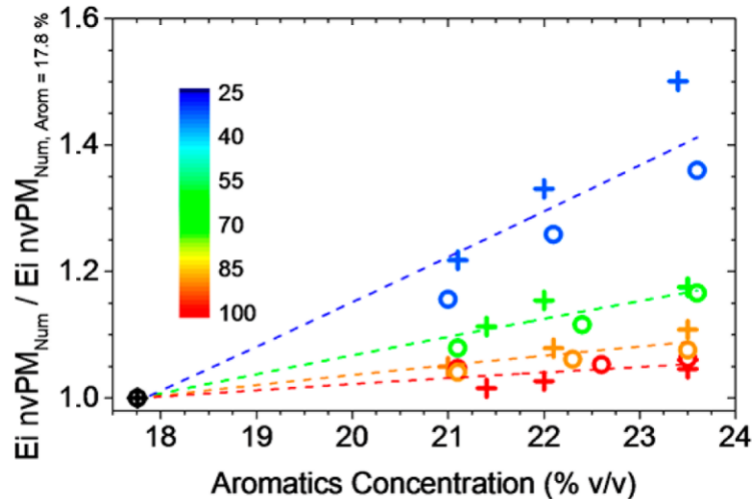


Figure 2.11: Aromatic content of a fuel vs emission indices of the non-volatile particulate matter emitted upon the burning of the fuel in a gas turbine. Coloured lines indicate engine power setting as a percentage [55].

ary Power Unit (APU) during tests conducted in 2009 [57]. During the course of this investigation several coal-to-liquid (CTL), gas-to-liquid (GTL), diesel and biodiesel fuels were compared with the reference Jet A1. It was observed that the organic mass emitted by Jet A1 was higher than that of the CTL and GTL blends used at the various power levels tested, this lends credence to the view that alternative fuels emit less vPM. Furthermore, the paper goes on to suggest that the vPM content in a given exhaust is sensitive to its measurement location as vPM is gaseous at first and condenses onto the nvPM particles down-stream in the exhaust due to temperature drops. The resulting organic mass emissions results from the study are shown in Fig. 2.12.

In another study conducted by Liati et al. the size distributions of nvPM produced by a CFM-56 gas turbine with respect to engine power using electron microscopy was studied [58]. It was found that at 100% engine static thrust the nvPM particles are larger and more numerous compared with 65% engine power. With lower engine settings, the amount of nvPM drops dramatically and also the mean size of the particles also drops, however these smaller particles are more oxidative and reactive with respect to larger particles. Reduction in PM emissions therefore can be achieved in several ways such as, combustor designs that limit the fuel rich areas in the combustion domain and reducing

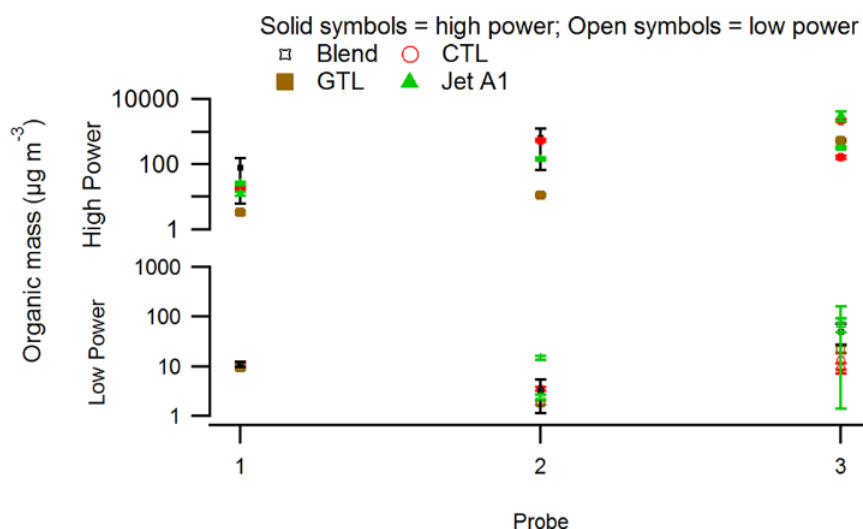


Figure 2.12: Organic mass emitted by CTL, GTL and Jet-A1 against measurement locations and power settings [57].

residence times of the fuel in very high temperature zones within the combustor [58].

A separate study under the Continuous Lower Energy, Emissions and Noise (CLEEN) program at the University of Sheffield's Low Carbon Combustion Centre, gaseous and PM emissions from gas turbines were measured for several alternative fuels and then compared to reference Jet-A1 where fuels 1-4 were blends of Jet-A1 and SPK (Synthetic Paraffinic Kerosene) and fuels A through D were potential alternative jet fuels. The turbine in used for the tests was a Honey-well GTCP85 APU [59]. Figure 2.13 shows the number of particles produced of size 75nm particulates for all the fuels tested in the study. Again, it can be observed that the fuels with lower aromatic content show reduced PM density. Similar trends were attained for 27 nm particulates, validating the pivotal role of aromatics in particulate emissions.

Dewitt et al. studied various aromatic solvents, which are consistent with the molecular weight distribution shown by jet fuel used by military users (JP-8) [56]. These were then added to F-T fuels as blends and individual components. The study observed an increased output of soot precursors which in turn indicated higher PM concentrations which was attributed to the increased aromatic content.

In conclusion it has been highlighted by Dewitt et al. that aromatic content of a fuel has a very strong impact upon the amount, and size distribution of particulate matter emitted

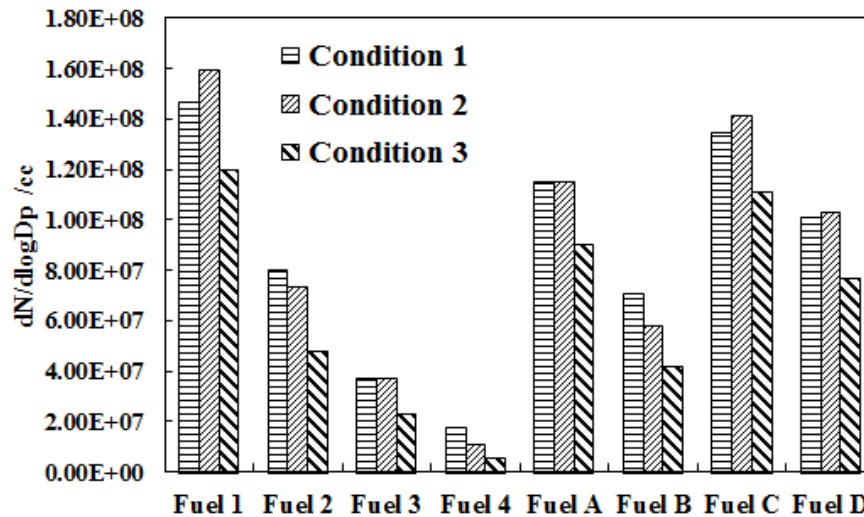


Figure 2.13: Particulates measured for fuels at size of 75 nm. fuel 1 is Jet-A1 [59].

from gas turbines [56]. Furthermore, as the composition of alternative fuels such as those from the F-T process can be altered to reduce their aromatic content, they produce less particulate emissions. This being said It has been agreed by Brem et al. that Hydrogen content is a better metric than aromatic content as a marker for PM emissions prediction [55].

2.1.4.2 Seal compatibility

The main reason behind aromatic compounds being need in the composition of alternative fuels has been to enhance the seal swell and lubricity of the fuel therefore it is imperative to shed some light upon the manner by which aromatics aid a fuels seal capacity.

Although in the previous sections it was determined that alternative fuels, on the whole, are beneficial to the aviation industry, as well the environment, there remains the issue of whether these alternatives are compatible with existing fuel systems and infrastructure. Even though alternative fuels (as a blend with Jet A1) have been approved for use in gas turbines, there exists a possibility of fuel leaks due to the varying composition of the alternative fuels. This happens because the seals in the engine and wider fuel system are not compatible with the new fuels. One of the main reasons for the seals not to work is due the absence or reduction of aromatics in the new fuels. Seal-swell reduction has been attributed to the lack of aromatic content in alternative fuels [18, 55, 56, 60]. Seal

shrinkage can cause seal failures and damage in the fuel system and eventually leakages. In essence seal-swell is defined as the increase in volume experienced by a seal when in contact with a liquid and vice-versa. This swelling normally means that the inner-diameter as well as the volume of the seal increases due to the absorption of fuel components such as aromatic content. Generally, naphthalene is considered a good hydrogen donor as opposed to alkanes or alkyl benzenes. DeWitt et al. found that fuel component separation and assistance to seal-swell as in equation 2.1 [56].

$$\text{Alkanes} < \text{Alkyl} - \text{Benzenes} < \text{Naphthalene's} \quad (2.1)$$

As observed by Thomas et al. the swelling of seal elastomers as a reaction against the fuel, moreover it has been determined by Qamar et al. that seal swelling is caused by the seal absorbing hydrocarbons from the fuel [61, 62]. In the aviation field acceptable seal swell ranges from approximately 18% to 30% whereas in the automotive industry seal swell is at roughly 12%, this can be attributed to the fact that ground vehicles do not experience the same variation in ambient conditions as aircraft and hence require less seal-swell performance [63]. When considered in greater detail it was observed by Graham et al. that several reaction takes place where intermolecular bonds of the fuel and polymer seal break and form new bonds with each other [64]. Overall these reactions are in equilibrium and are energy balanced. On the contrary seal shrinking ensues in the event that particular molecules of the seals seep into the fuel causing the seal to reduce in volume, the lack of plasticizer in the seals can be a cause for seal shrinkage. This process is shown in the Fig. 2.14 and Baltrus et al. observed that the shrinking process involves the release of fuel components absorbed by the seals [65].

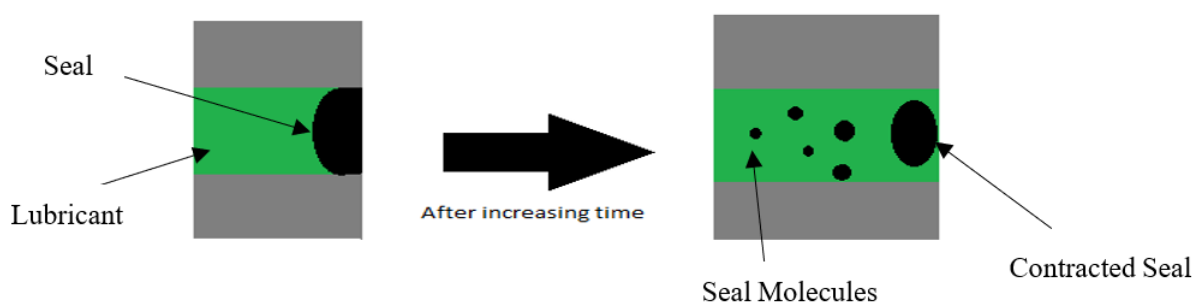


Figure 2.14: Seal contraction process[1].

Figure 2.15 shows the effect on seal swell different aromatics has on nitrile seal using a stress relaxation technique. It can be clearly observed from the figure that tetralin induces a significantly higher seal swell with respect to propyl benzene or P-xylene [66].

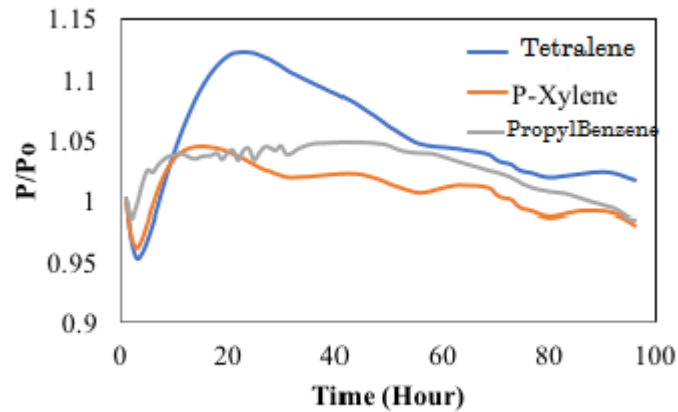


Figure 2.15: . Swelling effect of nitrile O-rings in mixture of 25% aromatic and SPK [66].

A study carried out by Liu and Wilson where a stress relaxation technique was utilised to observe the effects of several solvents including n-decane, iso-paraffins and cycloparaffins on seals composed of several materials [42]. It was observed during this study that O-rings manufactured from fluorosilicone and fluorocarbons performed well in the presence of all the fuel blends tested. Furthermore, it has been found that nitrile O-rings are susceptible to substances other than aromatics and that n-decane causes seals to lose performance.

Figure 2.16 shows the amount of seal swell achieved while using different compositions of Decalin, Decane and Shellsol T. It can be clearly observed from the figure that there are compounds which lead to seal swell, while others may not take any part in swelling or lead of shrinkages. It is also found from the study that not just aromatics are responsible for swelling of seals. Similar patterns have also been observed by DeWitt et al. and Graham et al. [42, 56, 64]. It was also found that several types of aromatics lead to different amount of seal swell. According to available literature, it can be inferred that further optimisation and research is required in the alternative fuel industry so that appropriate seal swell can be achieved without compromising other fuel suitability parameters.

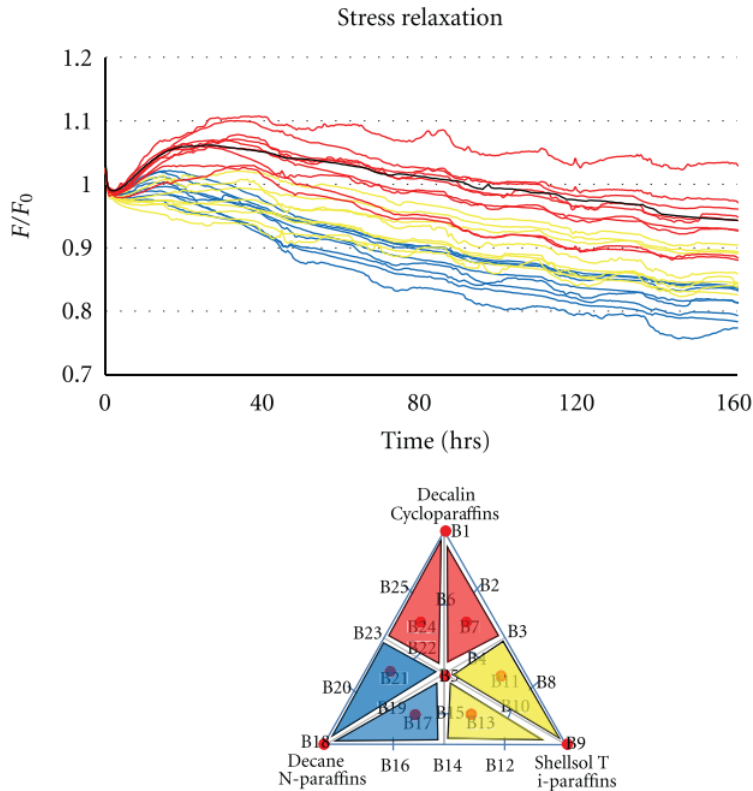


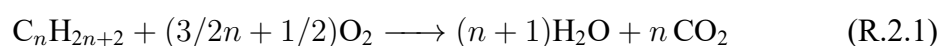
Figure 2.16: Relaxation behaviour of nitrile O-rings in the triangle [42].

2.2 Combustion instability

This section will aim to explore the literature surrounding combustion instability and will aim to provide background information as to why combustion instability is important, why it exists and how it manifests in gas turbine engines.

2.2.1 Combustion fundamentals

Combustion is defined as the reduction and oxidation (Redox) reaction in which heat is released in a controlled exothermic fashion. The reactants involved are named the fuel and the oxidizer. this investigation is concerned with the burning of mainly hydrocarbon fuels (fuels that consist of molecules containing mainly if not only hydrogen and carbon atoms in their molecular structure). Combustion reactions for linear alkane type hydrocarbons generally are of following formula;



The above equation is the ideal scenario for a combustion reaction in that it assumes that the reactants are present in the right quantities and are reacting uniformly, in other words it is a stoichiometric equation. However in practice combustion is a highly unstable process where multiple variables contribute to the outcome such as, equivalence ratio, mixing, fuel composition etc.

The above equation applies to combustion in many settings where liquid fossil fuels are used (i.e. land based, marine, automotive etc.). However this investigation focusses upon aviation gas turbines. All aviation air breathing gas turbines follow the Brayton thermodynamic cycle. They also consist of several basic components including a compressor, combustion chamber and a turbine (the combustion chamber and turbine are together identified as the 'hot section').

Image redacted due
to Copyright.

Figure 2.17: Gas turbine cycle schematic [67].

Figure 2.17 depicts the open cycle schematic for a gas turbine. Where intake air is subjected to isentropic (constant entropy) compression at 1-2 in the compressor. From 2-3 the system undergoes heat addition from the combustion process in a relatively constant pressure. Finally from section 3-4 the gas undergoes isentropic expansion where work is extracted from the turbine completing the mechanism of a conventional gas turbine engine.

This investigation focuses upon the combustion section of the process. Combustion in a gas turbine takes place in a combustion chamber. There exists several types of conven-

Image redacted due to Copyright.

Figure 2.18: Types of combustors, where the shaded areas depict the combustion zones of each type [68].

tional gas turbine combustors namely; 'can' type, annular and can-annular (a compromise solution between the two aforementioned types of combustor) [68].

Figure 2.18 illustrates the various types of combustors present in modern gas turbines. As can be seen the can combustors comprise of several tubular liners arranged in a circular pattern encased by the outer casing of the combustors. This type of combustor is the most basic and economically viable of combustors. However these tend to be excessively heavy, bulky and do not lend themselves easily to packaging a modern engine. Some of aviation worlds pioneering gas turbines such as the Power Jet W.2 (Designed by Frank Whittle), Jumo 004 (World's first production gas turbine) used this type of combustor with varying numbers of cans from around 6 up to 16 cans per engine [68].

The more modern engines tend to use annular combustion chambers, which are in effect a single flame chamber that surrounds the engine in an annular manner and is contained using an outer and inner casing. This type of combustion chamber tends to be more efficient in terms of packaging the engine as whole. The increased volume of combustion allowed when using an annular configuration means the chamber can overall be significantly (around 25%) shorter than a can-annular combustor allowing greater weight and cost savings [69]. However when considering the research and development of this type of combustor it becomes impractical. This is due to the fact that to replicate this type of combustion would require an entire gas turbine to be used as a research rig, which is cost prohibitive in terms of building and commissioning as well as the fuel cost to run the

Image redacted due
to Copyright.

Figure 2.19: A can-annular combustion chamber [69].

rig. Modern gas turbines such as Rolls Royce Trent series and General Electric's GE-90 engines use annular combustors.

The final hybrid type of combustors are the turbo-annular or can-annular type combustors. Where several combustion cans are placed concentrically around the main engine shaft and then interconnected with each other using cross-fire tubes. Figure 2.19 depicts a typical can-annular combustion chamber. This type of combustion chamber has the advantage of sharing a common air casing amongst all the cans and therefore have a common outer liner saving weight and volume.

2.2.1.1 Flame stabilisation

Before considering the instability of flames in a combustor it is worth considering how a flame is stabilised in a gas turbine in the first instance. The magnitude of this task in a gas turbine can be analogous to attempting to light a candle outdoors in the midst of a hurricane. In a gas turbine for instance the air flow velocities are much greater than the flame velocity; hence without a method of stabilisation sustaining flame in those conditions would be near impossible. It is commonly known that the airflow speed and the flame speed are key in flame stabilisation. Higher airflows with respect to the flame speed would mean the flame is flushed down the combustor and would blowout. The key to sustaining a flame in a gas turbine involves some type of recirculation process. Where by some of the combustion products circulates inside the combustor and perpetually ignites the new combustion products coming from upstream. The most basic of these recirculation methods involves what is known as 'bluff body flame stabilisation'. Where a so called bluff body impedes the fuel air mixture and caused a recirculation zone downstream of it,

Image redacted due to Copyright.

Figure 2.20: Bluff body flame stabilised combustor schematic, adapted from [70].

allowing the flame to be ‘anchored’ to this body. Figure 2.20 depicts a classical model of bluff body flame stabilisation. Where the bluff body in this case is the fuel injection system which causes a low velocity turbulent zone behind it stabilising the flame whilst aiding mixing as well; where the flame stabilises behind it.

Another more relevant method employed in gas turbines for flame stabilisation involves what is known as swirl stabilisation of flames. Where swirlers are used to impart a rotational component to the airflow which creates a recirculation zone where the flame can be stabilised. The swirl can be induced using a swirling vane or even a directional injection of air. Figure 2.21 shows a schematic of a combustor with swirl stabilised flame. It should be noted that in both cases only around a fifth of the total inlet air passes through the swirlers or bluff body into the primary zone, which ensures a rich air-flow mixture locally that sustains the flame. Approximately a third of the inlet air passes into the secondary zone through the dilution holes (which may or may not be angled to impart further swirl depending on individual combustor design). Leaner conditions in the secondary zone serves to complete the combustion process by combusting the remainder of the combustion products from the primary zone. This secondary air also aids in the cooling of the combustion liner. The remainder of the inlet air then mixes with the combustion products in the tertiary zone adding mass flow and cooling the gases so that the down stream turbine does not need to encounter the extreme combustion temperatures.

It must be noted that even a small deviation in either the air flow or fuel flow properties would have a significant impact upon the combustion quality and therefore emissions,

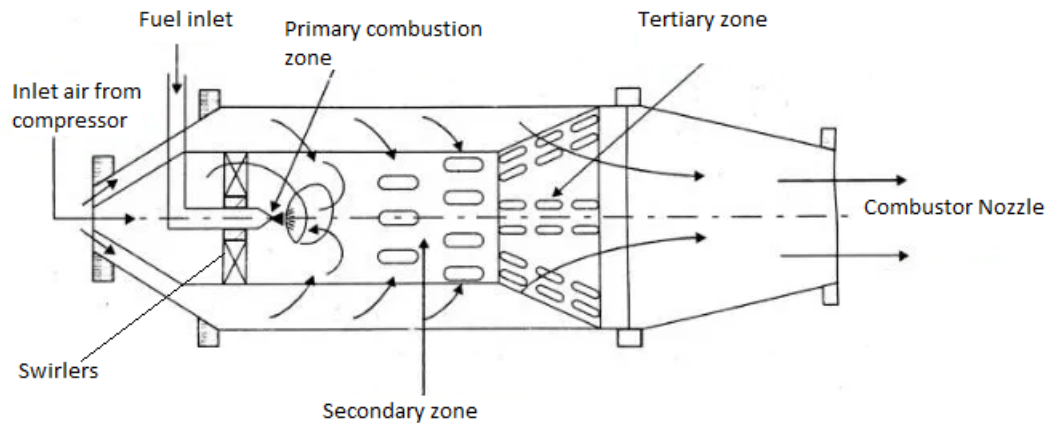


Figure 2.21: Swirl stabilised combustion chamber schematic, adapted from [70].

performance (instability and liner wear) [2, 3, 5, 71–73]. This therefore leads to a gap in the knowledge regarding how various fuels with differing properties impact the combustion process in a combustor or turbine that has been designed solely for use with conventional aviation fuels.

2.2.2 Combustion instability of gas turbines and their combustors

Combustion instability has been defined as the large-amplitude perturbations of the acoustics and pressure fields of a reacting flow (such as a flame) which can impact the flow in a physical manner if allowed to progress untended [74, 75]. This type of instabilities have been encountered in almost all types of combustors from rocket engines to land based industrial gas turbines. Instabilities of this nature are caused by a feedback loop between the combustion process and the acoustic characteristics of the combustion chamber in question. This type of behaviour can be avoided by designing the combustion chamber to cooperate well with the fuel being utilised. However with the push towards more and more lean combustion and alternative fuels it is not practical to redesign engines to match the myriad of alternative fuels currently being developed.

Figure 2.22 depicts the feedback loop of instability, where the flame of combustion creates the thermal oscillations which in turn develop acoustic oscillations which in turn interact with the flow characteristics of the reacting flow and finally this impacts the flame itself. If this behaviour is present in a given combustor it poses several undesirable effects.

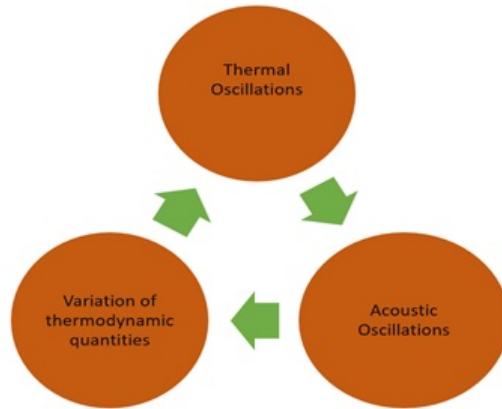


Figure 2.22: Combustion instability feedback loop [1].

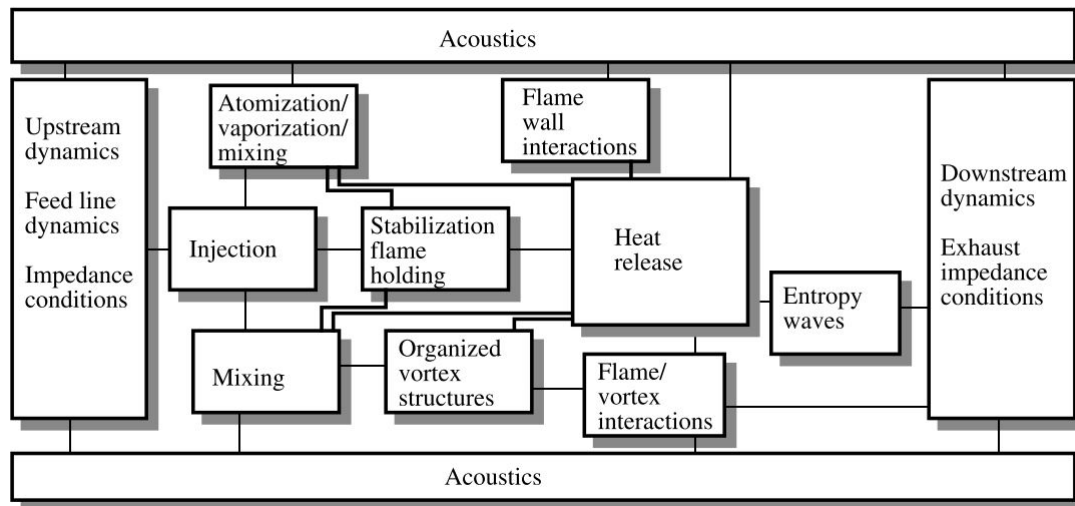


Figure 2.23: Causes of combustion instability [77].

Namely these could progress onto becoming large amplitude oscillations of pressure and velocity, this in turn could manifest itself as thrust oscillations. Moreover these fluctuations could induce severe vibration of the combustor which would cause increased wear and fatigue of engine components [71, 76, 77]. Finally combustion instability is known to cause flame blow-off's and even compressor surges in gas turbines.

Lord Rayleigh first introduced a criterion (Rayleigh's criterion) that described the conditions in which unsteady heat release adds energy to the acoustic field [78]. It describes the interaction of heat release oscillations and the acoustic mode of the combustor. The instability condition takes place when driving forces of oscillation are greater than the damping of oscillations [75]. The above definition is numerically given by equation 2.2.

Where p' and q' represent pressure and heat release fluctuations, T is the temporal term, V is a volumetric term, S is a area component, u' is a velocity term, and lastly n is length term from the surface of the chamber.

$$R = \int_0^T \int_v p' q' dV dt > \int_0^T \int_s p' u' .n dS dt \quad (2.2)$$

In the main it is well established that combustion instabilities occur at frequencies near or around the natural modes of the combustor [75]. This type of instabilities can be of bulk instabilities (also known as Kelvin-Helmholtz instabilities), axial or tangential to the combustor [79]. However it is also possible for instabilities to occur that are not related to the modes of the combustor itself. An example of this is the excitation of the downstream nozzle when an entropy wave from the combustor or even a vortex from the flame is propagated impinges on the nozzle and then is reflected back towards the combustor [80, 81]. this type of instability is considered to occur at lower frequencies than the natural modes of the combustor itself and are more prevalent near the lean blow off limit.

2.2.2.1 Acoustic oscillations

Whilst there is no general terminology agreed upon to define the various noises emitted from a combustion chamber of a gas turbine Lefebvre et al. proposed several names; 'rumble' and 'growl' for low frequency noises (50-180 Hz) and 'howl'/'humming' for the acoustics above these frequencies [68]. Rumble and growl are known to occur from ignition up until idle speed and maybe detrimental towards proper engine running as it has a tendency to increase start-up time for the engine and also impacts compressor stall margins [68]. As combustor inlet air temperature increases the intensity of growl is decreased but increased combustion pressure has the inverse effect. Howl, whilst intimately linked to rumble occurs at increased engine RPM and has a frequency range of approximately 200-500Hz. Like rumble elevated inlet air temperature mitigates howl which is prominent around ambient air temperatures (288K). Lefebvre further goes onto explain that howl is affected by the fuel type in use and is mitigated by more volatile fuels [68].

2.2.2.2 Effect of fuel type on instabilities

The fuel type's effect on combustion instability is closely linked to how it impacts the reaction time of combustion. Where the characteristic time is calculated as per equation 2.3 [68]. Which denotes the time taken from the injection of the fuel into the chamber until the maximum heat release.

$$t_{combustion} = t_{mixing} + t_{evaporation} + t_{reaction} \quad (2.3)$$

When the characteristic combustion time approaches equilibrium with a characteristic acoustic time for the combustor (representing the acoustic modes of the combustor) combustion instabilities occur. Therefore, it stands to reason that a given fuel type has the propensity to change the difference between combustion time and the acoustic times of the combustor [68]. Research carried out to date regarding the effect of fuel type on combustion instability mainly focuses upon gaseous fuels for gas turbines. Janus et al. conducted a study where a miniature (8cm) combustor was fed with varying proportions of propane, hydrogen and natural gas and measured the instability characteristics using optical and piezoelectric pressure transducer methods [82]. Other typical measurements of ambient conditions and temperature were also made. Their results indicate that inlet air temperature and equivalence ratio (defined as the ratio of the ratio of fuel/air and the stoichiometric fuel to air ratio) have a visible impact on the pressure oscillations observed in the tests with respect to the fuel composition used. The key point that was raised was that pressure oscillations increased with increased ambient humidity and with increasing equivalence ratio. The authors conclude that the transport time is heavily linked to the stability characteristics of the combustion taking place [82].

A separate study conducted by Vandsburger et al. explored the theme of spray vaporization effect upon the heat release pattern and instability characteristics of a dump combustor [83]. It was observed that liquid spray and gaseous combustion have remarkably different instability characteristics. Moreover it corroborates the idea that as overall equivalence ratio increases the pressure oscillations increase. Further work was carried out regarding liquid fuels by Mehta et al. where a gas turbine combustor was examined for heat release fluctuations and pressure oscillations to determine how the volatility of

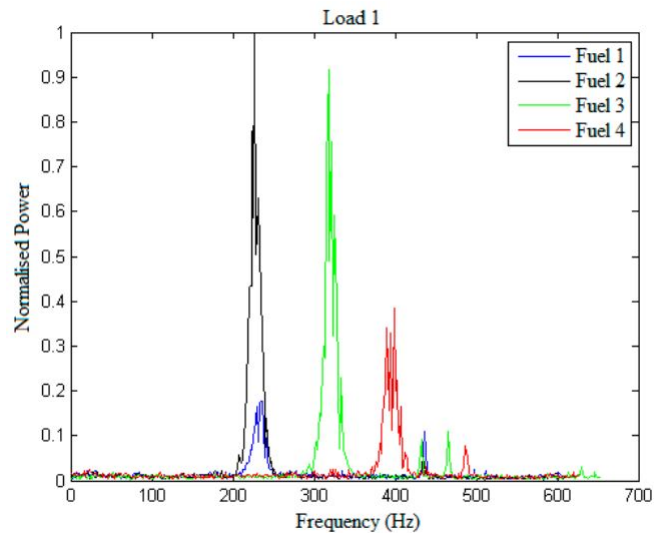


Figure 2.24: Vibration amplitude and frequency with 4 fuels [85].

different fuel are showcased in terms of instability [84]. The main finding of this research was that for liquid fuels spray vaporisation and droplet size had a significant effect upon the pressure oscillation produced by the combustion. Fuels used in this research were JP 4, JP 5, a blend and diesel [84]. A key finding of this research involved states that the equivalence ratio effect on pressure oscillations is much the same as for the previous studies mentioned afore. However, Mehta has observed that the pressure oscillations drop after a peak equivalence ratio.

The extent to which vibration and noise manifest is partially dependent on the different properties of the fuel. Khandelwal et al. investigated the role of different fuel composition and its impact on combustion vibrations [85]. Testing was done on a Honeywell GTCP85 APU using four different fuels in Fig. 2.24. Fuel 1 and Fuel 2 were Jet A-1 sourced from two different sources, whereas fuel 3 and 4 are FT process produced fuel from different sources. It was observed that the FT process fuel which had lowest density from the fuels tested in this study produced higher frequency spectra of vibrations. Though highest amplitude of the vibration was produced by Jet A-1 from fuel 1. It is to be noted that Jet A-1 sourced from two different sources have similar frequency but significantly different amplitudes indicating power of the vibrations. Furthermore, the relationship between fuel density and vibration is more explicitly considered in the work done by Khandelwal et al., where a higher density, coconut oil blend, biodiesel was compared with conventional

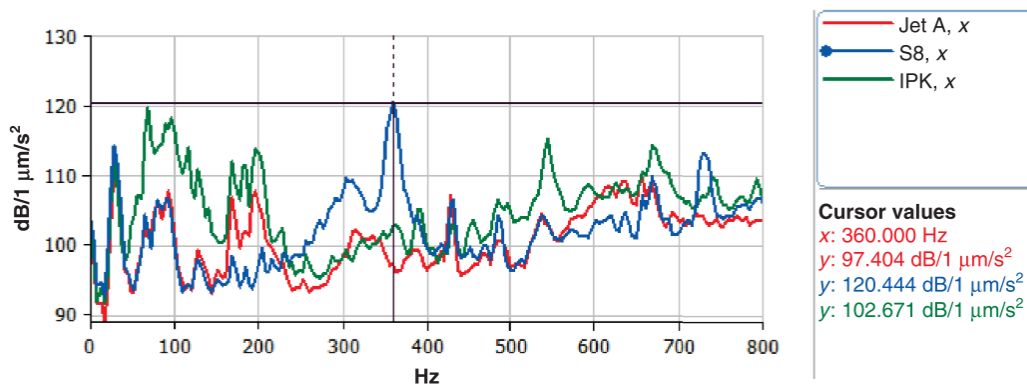


Figure 2.25: Vibration amplitude and frequency with 3 fuels [86].

diesel [85]. In this study, the higher density fuel blend displayed a significant reduction in vibrational acceleration. an illustration of this is depicted in Fig. 2.24.

A Study conducted by Simons and Soloiu regarded the impact of noise and vibrations of alternative fuels on a miniature gas turbine [86]. The fuels used were Jet A and 2 alternative fuels S-8 and IPK. The authors concluded that the noise produced due to combustion was low with respect to the turbo-machinery noise generated by the turbine, concluding that the viscosity of fuels play an impact in the atomisation of fuel and therefore the combustion instability. Furthermore, they added that their alternative fuels have displayed lower sound pressure levels with respect to standard jet fuel.

Figure 2.25 depicts a vibration frequency domain plot for the fuels tested by Simons and Soloiu. It is clearly visible that all the fuels in question show a similar frequency content, with minor variations in amplitude amongst the fuels. An interesting fact in this plot is that the vibration amplitude for Jet A is consistently lower than that for the alternative fuels, especially in the 360Hz range where S-8 shows a peak but Jet A and the IPK do not. This type of result bears further investigation.

Chen et al. investigated the impact of inlet air temperature and fuel modulation on combustion instability using a model gas turbine combustor. The fuels tested were basic hydrocarbons of an aliphatic nature such as n-decane and iso-octane, a cyclo-alkane methyl-cyclohexane (MCH) and finally RP-3 which is a Chinese analogue of Jet A1. The main variation of this investigation was the ability to modify the inlet air temperature from 383K-483K. The authors concluded that Increasing the inlet- air temperature has an

adverse impact on combustion instability with respect to RP-3 and n-decane and that the other 2 fuels were unstable throughout the investigation irrespective of the air temperature.

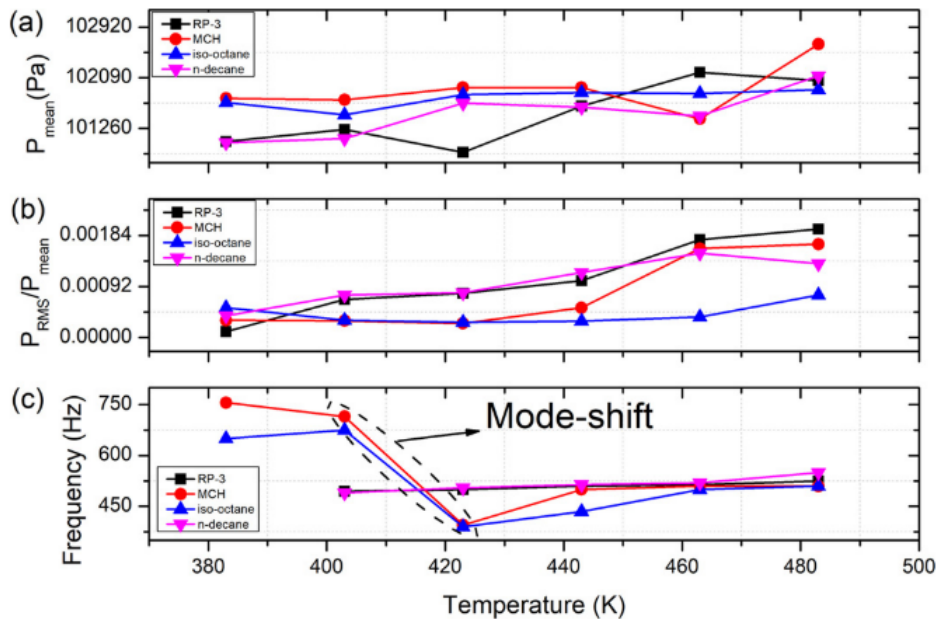


Figure 2.26: The average pressure (a), RMS pressure oscillations (b) and instability frequencies (c) with respect to inlet air-temperature for the fuels tested by Chen et al. [87].

Figure 2.26 shows the mean pressure oscillations, RMS pressure characteristics as well as the instability frequencies of the fuels tested by Chen et al. with respect to their varied inlet air temperature [87]. As is clearly visible all fuels depict a rise in combustion pressure oscillations as the temperature increases. Moreover, it is clear that the instability frequencies are mainly concentrated around the 700Hz range.

Another study has been conducted by Othman et al. investigating the effect on vibrations by fuels in gas turbines [88]. Whilst not strictly regarding alternative fuels in the sustainable sense, it does observe the impact fuel variation has on vibrations of a gas turbine. The fuels tested in this investigation were Kerosene, Gas oil, Methanol and a 50%-50% blend of Kerosene and Methanol.

The gas turbine used by Othman et al. comprised of a single stage radial compressor driven also by a radial turbine. Power was generated using a power turbine after the compressor turbine. The power turbine is attached to a dynamometer. The maximum power output was 8kW. Figure 2.27 depicts the vibration FFT for all fuels tested by Othman et al.,

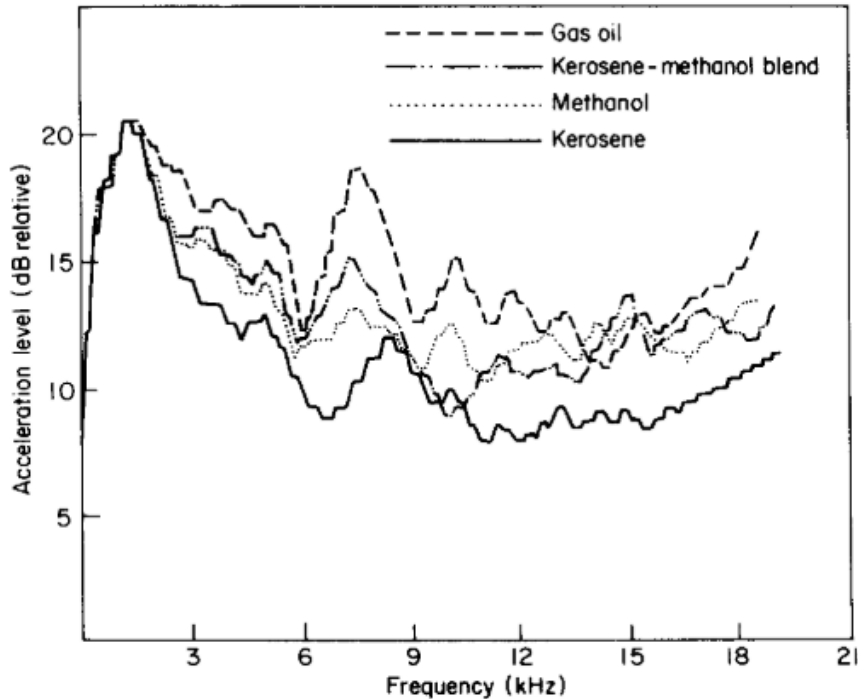


Figure 2.27: FFT vibration data for the fuels tested by Othman et al. [88].

overall it is clear that Kerosene has the lowest vibrations and gas oil the highest. Othman et al. concludes that the combustor produces the main source of vibrations. They have also noted that as carbon to Hydrogen ratio increases vibrations also increase as shown in Fig. 2.28.

2.2.3 Atomisation

Spray characteristics of fuel atomisation is considered to be paramount in determining the performance characteristics of a gas turbine. In essence this is due to the injector's role in the mixing of the air and fuel in given combustion chamber; the more thoroughly mixed the fuel and air the better the combustion will be in terms of instability efficiency and even emissions. Therefore, it stands to reason that if a fuel can adversely affect the atomisation of a given fuel injector the vast majority of which are optimised for use with Jet-A, Jet-A1; it would affect the combustion instability characteristics of the engine. Fuel injection for gas turbines is a vast topic in itself but it would be prudent to discuss the salient points in this review as the first stage of this investigation aims to establish the spray characteristics of several alternative fuels with respect to Jet A1.

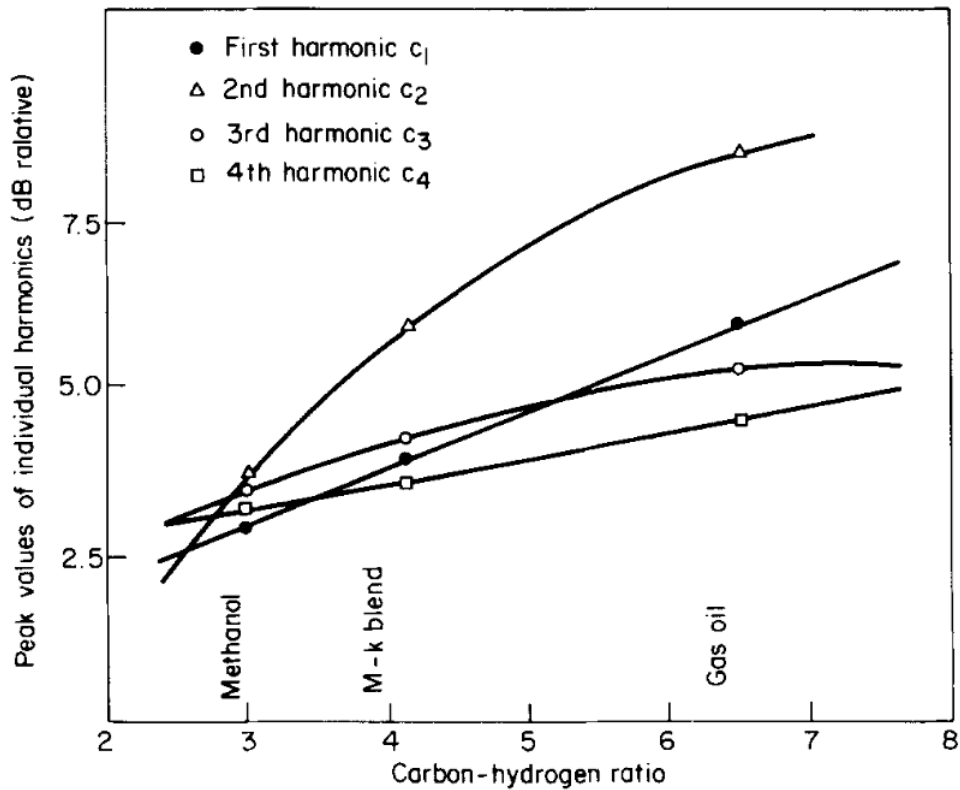


Figure 2.28: Peak vibrations in dB at the first 4 harmonics for the fuels tested against their carbon to hydrogen ratio [88].

2.2.3.1 Sheet and droplet formation (classical atomisation)

Atomisation is a term used to describe in essence transformation of liquid fuel into small droplet or a spray prior to being burned in a gas turbine combustor or any other liquid fuel burner. Contrary to what the name suggests these liquids are not literally broken into individual atoms but more of a fine mist. A more elegant definition has been provided by Mansour and Chigier “atomisation is process in which the surface to mass ratio of a liquid is increased” [89]. Of a given liquid two properties stand out in affecting droplet size, shape and ease of formation; these are namely the surface tension and the viscosity of the liquid. Surface tension is commonly defined as the inclination of like liquid molecules to stick together forming a shape with the smallest possible surface area assuming no outside forces act upon it. This is the reason that most injectors produce droplets which are spherical in nature (the shape with the least surface area). The process of atomisation is generally considered to be formed of 3 sub-processes known a nozzle ejection, primary

Image redacted due
to Copyright.

Figure 2.29: Classical representation of a simple jet disintegration [68].

atomisation and secondary atomisation. Primary atomisation is the first process where the fuel is divided up into ‘shreds’ and ‘ligaments’. Secondary atomisation is where the larger ‘strands’ and ‘ligaments’ are broken further into smaller near spherical droplets [68]. Figure 2.29 depicts the process by which a laminar flowing jet ejected from a nozzle into a stationary gaseous environment behaves. This mechanism was first described by Lord Rayleigh, who goes on to determine that small perturbations in the fluid cause its disintegration into drops when the perturbation with the fastest growth reaches a critical wavelength [90]. This is still relevant in the modern day because modern fuel injection systems tend to increase the perturbations imparted on the fluid stream to expedite the formation of smaller and smaller droplets using swirlers or other such geometry which aid in mixing and lead to stable combustion.

Whilst the break-up of jets serves to easily portray the mechanism of atomisation, most modern injectors do not rely on simple pressure atomisation through a nozzle, mainly because a single orifice jet has to be sized to the maximum fuel flow rate for a given application. Which poses a problem where the injector cannot atomise well under lower fuel flow rates where the orifice is not operating at maximum pressure and would lead to larger drop sizes and poor combustion. This is where twin fluid atomisers have come to dominate the field of jet fuel injection. In essence a twin fluid atomiser has an orifice or orifices sized to deliver the required maximum fuel flow rate and in addition have extra orifices where high pressure air is used to impinge upon the fuel jet to shatter it and increase the rapidity of the atomisation process. This type of atomiser therefore does not produce jets but conical sheets of fuel, due to the fact the orifices are not axial to the flow of air but are usually tangential to the flow coming out of helical or angular slots in the injector

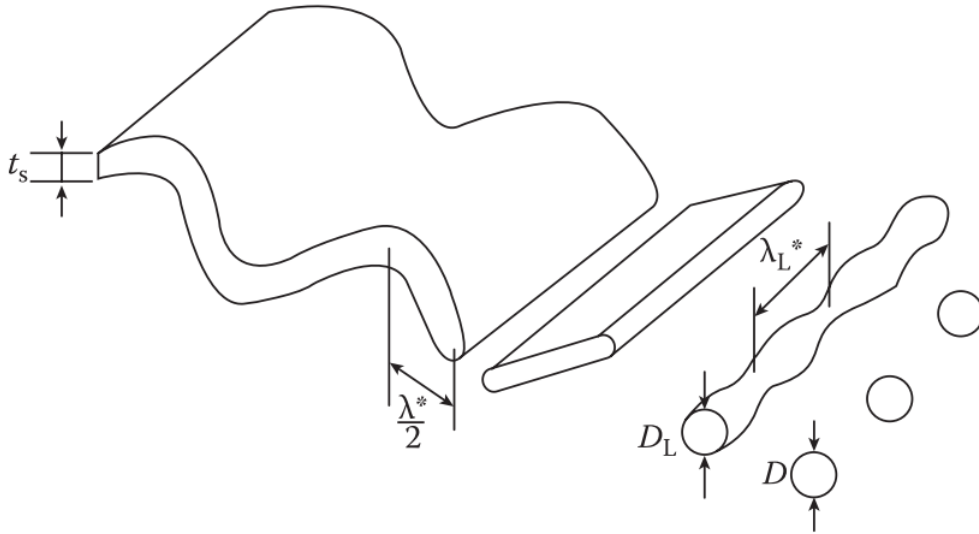


Figure 2.30: Classical representation of a sheet breakup [91].

for better mixing and increased interaction between the atomisation air and the fuel.

The breakup of fuel sheets was described thoroughly by Fraser et al. [91]. Figure 2.30 depicts the mechanism of sheet breakup which is relatively similar to the breakup of jets. The key metric in determining the behaviour of the breakup of the sheet is the relative velocity between the sheet and the medium into which it has been injected (usually air). As this relative velocity increases the breakup of the sheet gets closer to the nozzle or injection orifice, and the drop diameters and ligament sizes decrease.

Whilst the above methods describe the atomisation of fuels there are also several methods used to theoretically derive the SMD of a given fuel. most notably by Lefebvre [68]. The main purpose of these equations is to define the characteristic SMD's of a given atomiser. And therefore, various equations exist for the different types of atomisers. The equation for a simple pressure atomiser has been described by Elktob et.al in equation 2.4 [92].

$$D_{32} = 6156v^{0.385}\sigma^{0.737}\rho_f^{0.737}\rho_a^{0.06}\Delta P^{-0.54} \quad (2.4)$$

Where D_{32} is the SMD in μm . v and σ are the viscosity and surface tension of the fuel respectively. ρ_f and ρ_a represent the density of the fuel and air respectively and finally ΔP is the differential pressure drop across the nozzle. There are relatively few equations for simple pressure atomisers due to the dense sprays they create which make experimental SMD measurement problematic due to obscuration. That said another equation for plain

orifice atomisers have been described by Hiroyasu et al. and is shown by equation 2.5 [93]. In this equation Q is the fuel volume flow rate and A is a constant varying with the nozzle geometry.

$$D_{32} = A\Delta P^{-0.135} \rho_a^{0.121} Q^{0.131} \quad (2.5)$$

Both of these equations are only applicable to fuel injected into standing air as is the case when testing the performance of an injector. This is caused by the fact that the drop sizes of a injection is dependent upon the relative velocity of the fuel and the air unto which it is injected, therefore if the fuel is injected into a flowing field the equations would need modification to reflect that.

However, as this investigation focuses upon an airblast atomiser it is more relevant to discuss the estimation of SMD for twin-fluid atomisers. The seminal equation for SMD of twin-fluid atomisers has been conducted by Nukiyama and Tanasawa and has been improved upon by Lefebvre [68, 94]. The base equation for SMD by Nukiyama and Tanasawa is shown by equation 2.6. Where μ is the viscosity of the liquid fuel and Q is the volume flow rate. the subscripts L and A denote liquid and air respectively. The air terms in this equation refer to the atomisation air and not atmospheric air. A noticeable omission in this equation is the fact that a characteristic dimension for the nozzle geometry is omitted. This has been done due to the fact that in experimental studies it has been shown that nozzle geometry does not impact the droplet diameters [94]. Furthermore, it should be noted that in equation 2.6 there are terms for the density, surface tension and viscosity of the fuel which indicate that these properties have an impact on the drop size produced by the injector. Therefore these properties will be used in this investigation to compare the alternative fuels and their injection characteristics.

$$D_{32} = 0.585(\sigma/\rho_L U_R^2)^{0.5} + 53(\mu_L^2)^{0.225}(Q_L/Q_A)^{1.5} \quad (2.6)$$

2.2.3.2 Prompt atomisation

The aforementioned process of droplet formation is known as the classical mechanism of jet and sheet breakup in atomisation. The other method is known as prompt atomisation

where the fuel jet or sheet breaks up in an extremely short time duration after exiting the nozzle. Instances this occur are for instance when a fuel jet is impinged upon by a high-velocity air jet at a suitable angle or when a high velocity fuel jet is released into a stagnant or low velocity air pocket [95]. Therefore, prompt atomisation can be defined as injection where the fuel jet or sheet immediately disintegrates upon release from the nozzle. This leads to the observation that the breakup of the fuel jet or sheet is instantaneous. However, it should be noted that no full explanation of the prompt atomisation mechanism has been described as of yet and is a subject which is under investigation.

The the methods of jet break up with respect to the flow regimes has been described in Fig. 2.31. Where ‘Oh’ is Ohnesorge number and Re is the flow Reynolds number.

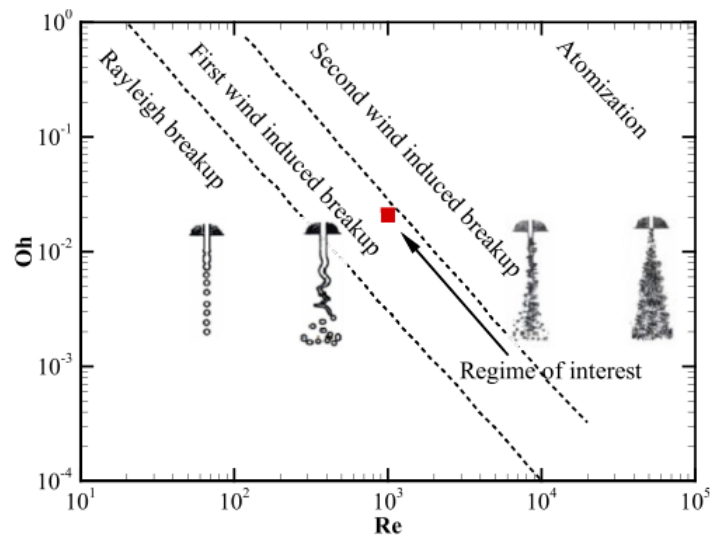


Figure 2.31: Spray break up for jets across various flow regimes [96].

2.2.3.3 Effect of atomisation characteristics on combustion instability

In literature there exists some studies which have investigated the impact various fuels have upon spray characteristics and by extension the effect spray characteristics have upon combustion instability. some of which have been critiqued below.

A study conducted by García et al. where a small scale gas turbine combustor with heated inlet air and atmospheric pressure running on Jet-A1 was subjugated to CH* chemiluminescence and Mie scattering to determine how equivalence ratio and other performance characteristics impacted the instability [97]. Results for this study indicate differ-

ent spray characteristics in when the combustor was known to be undergoing self-excited oscillations. Figure 2.32 depicts the spray characteristics of the combustor in the two engine conditions that were investigated by García et al. Condition A is the leaner condition and condition B is a richer condition; although the global equivalence ratio has been kept constant at 0.75. As can be seen from the figure the Leaner condition has 2 pronounced peaks around 440 and 646 Hz and the richer condition has overall more peaks but they not as powerful.

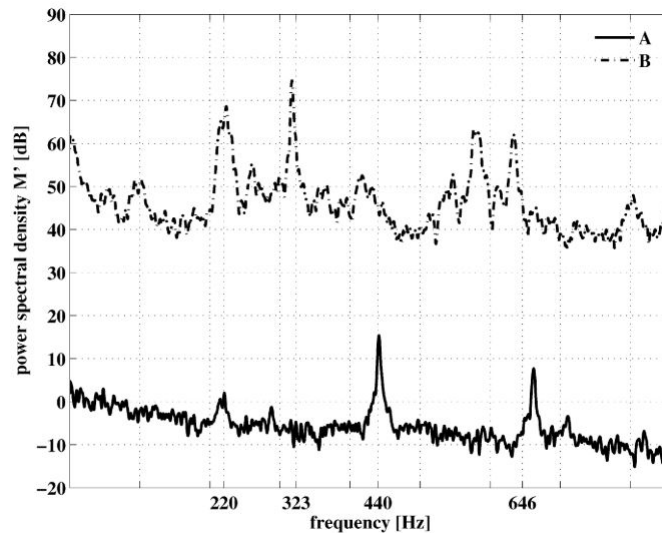


Figure 2.32: Spray characteristic of the two combustor conditions investigated by García et al. [97]. The series have been shifted by $30dB$ for illustrative purposes.

The method used by García et al was termed Mie scattering imaging where a 476-514 mm laser is centred along combustors injection plane. The light scattered by the injection spray is then monitored by a CMOS fast camera. This data then is presented as a function of the whole spray fluctuation along the laser beam from which the PSD has been depicted in Fig. 2.32. The major conclusion of their investigation was that their combustor shows instabilities at 2 separate AMF's (air mass flow rate) and that at these conditions the spray behaviour was affected. It was observed that at high AMF's the spray is compact and the higher air velocity induces increased mixing and evaporation. And finally, it was concluded that the observed combustion instabilities are linked to oscillations of the spray and its evaporation. This investigation leads credence to the fact that the spray characteristics directly impact the combustion instabilities of a given combustor. This in

effect validates this investigation into the effect on fuel type on spray characteristics as this will in turn impact the combustion instabilities caused by those fuels.

Another study has been conducted by Liu et al. investigating the effect of atomisation characteristics on combustion stability in a ‘swirl-cup’ combustor [98]. Several combustor conditions were investigated with varying FAR (fuel-air ratio), distance from injector etc. Figure 2.33 depicts some of the results. The authors have compared the SMD with increasing reference velocity which shows a negative trend, showing decreased droplet sizes with respect to increasing velocity. This is in keeping with the literature where faster velocities correspond to smaller drop sizes. h in this case refers to the gap between the nozzle shroud of the authors atomiser.

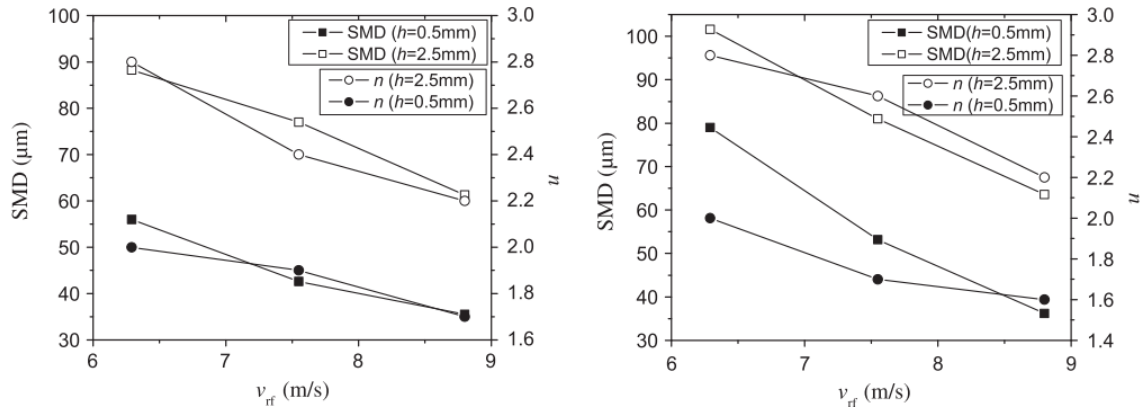


Figure 2.33: SMD characteristics of the swirl cup injector investigated by Liu et al. [98]. Left figure indicates ‘ignition condition’ and the right ‘LBO condition’.

Figure 2.33 also depicts the ‘droplet diameter distribution index’ n which in effect acts as an analogue to the standard deviation of the droplet diameters to the extent that the higher n is the more uniform the droplet size distribution. With this in mind it appears that as the reference velocity increases the n value decreases leading to decreased uniformity of distribution. It also appears that the ignition condition (left) and the LBO condition (right) have little impact on the SMD. A key conclusion of this investigation seems to be that the smaller the droplets get, the less uniformly distributed they are.

A key facet of instability is defined by the phenomenon known as Lean Blow-off (LBO), which is defined as a static instability [99, 100]. This type of instability becomes increasingly important with the current drive towards leaner and cleaner burning engines

where the ideal situation is dictated by the lowest viable equivalence ratio (Φ). Thereby operating as close to the blow off limit as possible. Figure 2.34 depicts the blow-off limits of gaseous and air fuel mixture operating in various atmospheric conditions. As can be seen from the figure the margins for stable flames without blow-off, flashback or quenching is a narrow triangular section where if the flow speed drops excessively the flame will flash back and if the equivalence ratio drops and the air speed stays constant the flame will blow off.

Image redacted due
to Copyright.

Figure 2.34: Critical blow-off limits for a natural gas and air mixture exiting into a n environment consisting of the gases shown in the figure with respect to flow speed and the equivalence ratio [101].

These phenomena are greatly impacted by the spray characteristics of a given injector and combustor combination. This is due to the fact that as equivalence ratio drops (in effect reducing fuel flow rate through the injector) the spray pattern will be altered. The impact of the spray characteristics at or near LBO condition have been depicted well by Liu et al. [98].

As is visible from Fig. 2.35 as the equivalence ratio drop to LBO condition the spray pattern is visibly poorer with respect to the ignition condition where the droplets much more uniformly distributed and are symmetrical with the spray vertical axis. Yoon et al. conducted a study observing the combustion instability characteristics of a combustor under variable fuel air mixture ratios [73]. As can be seen from Fig. 2.36 the inlet fuel air mixture has a great impact on the mean pressure fluctuations which indicates unstable flame conditions. The high equivalency instability have been determined to be caused by the classical dynamics instability mechanism of the coupling of the heat release rate and the pressure oscillations, leading to the classical combustion instability feedback loop

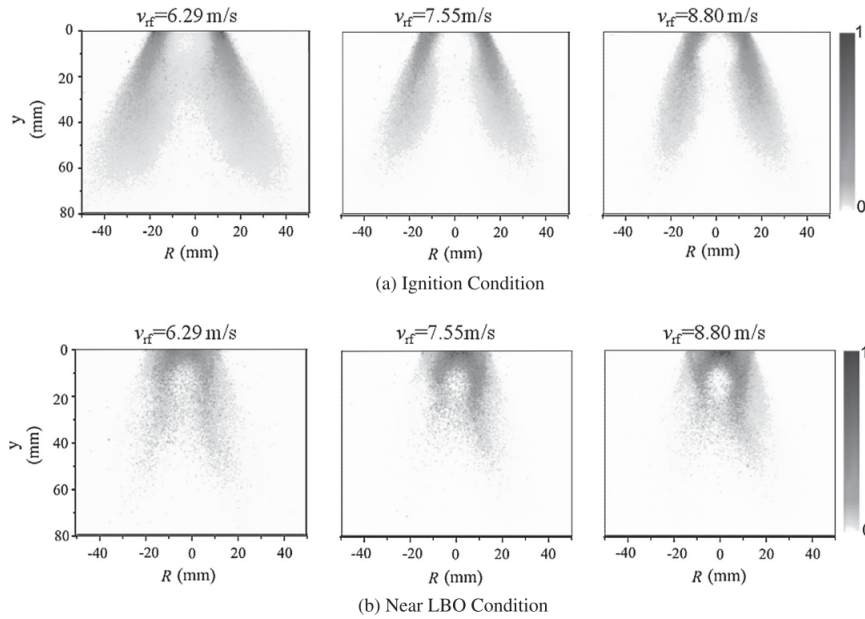


Figure 2.35: Spray characteristics variation between normal ignition conditions and LBO [98].

described by Rayleigh's criterion [73, 78]. The low frequency instabilities are apparently more mysterious in origin according to Yoon et al. however, the authors have observed that this phenomenon may be caused by fluid turbulence mechanisms such as vortex shedding [73].

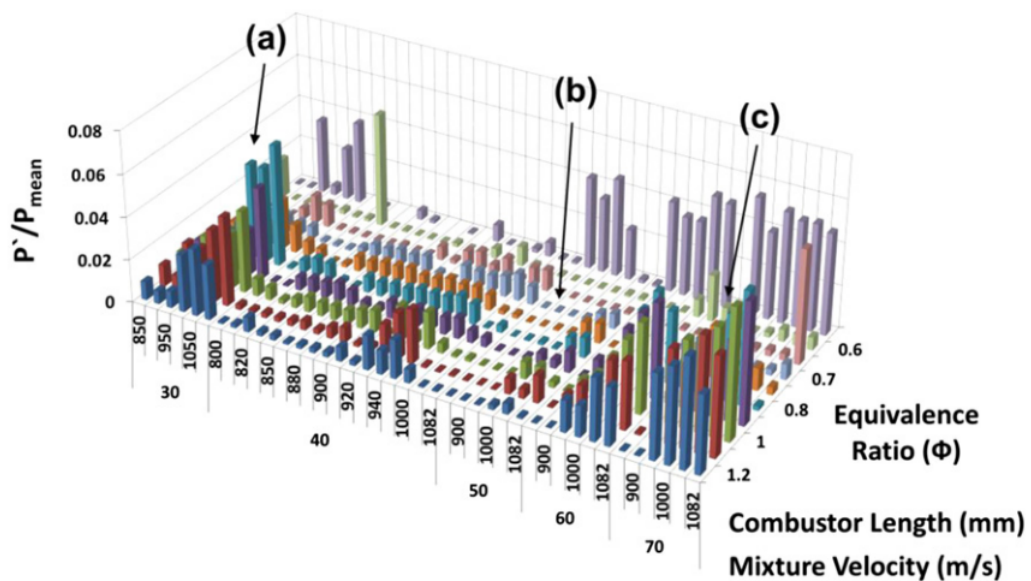


Figure 2.36: Spray characteristics variation between normal ignition conditions and LBO [73].

2.2.3.4 Effect of alternative fuels on spray characteristics

A separate study conducted by Vouros et al. has investigated the spray characteristics of several alternative fuel surrogates with respect to conventional jet-A1. The measurement techniques used included PDA (phase Doppler anemometry) which enable the acquisition of volumetric data regarding the sample particle as well as velocity. The tests have been run with the spray nozzle at various distances away from the detector to determine how the spray develops with distance from the nozzle. Moreover several injection pressures have been utilised to determine the effect pressure has upon the spray characteristics [102]. Figure 2.37 depicts the results obtained in this investigation where the vertical axis represents SMD (Sauter mean diameter) and the horizontal axis depicts radial distance from the centre of the spray. z/d depicts the axial distance from the injector normalised to the nozzle diameter.

The Fuels used in this investigation involve several basic blends involving pure paraffins (P), a blend of paraffins (80%) and aromatics (20%) named P-Ar, a blend of paraffins (60%) and naphthenes (40%) and finally a combination blends involving all three at 50% paraffins, 30% naphthenes and 20% aromatics. The study does not specify which aromatics, paraffins or naphthenes were in the blends; instead providing the total percentage by volume. Yet this is still of use as we can see which particular type of compounds impact the SMD. In figure 2.37 it can be seen that the pure paraffin blend consistently shows a reduced SMD at all axial distances and shows a rapid decrease in particle size with increasing radial distance. Reference jet-A1 performs the poorest with respect to all the fuels tested. They go onto conclude that SMD is a good indicator of the impact fuel properties have upon the spray characteristics of a given fuel.

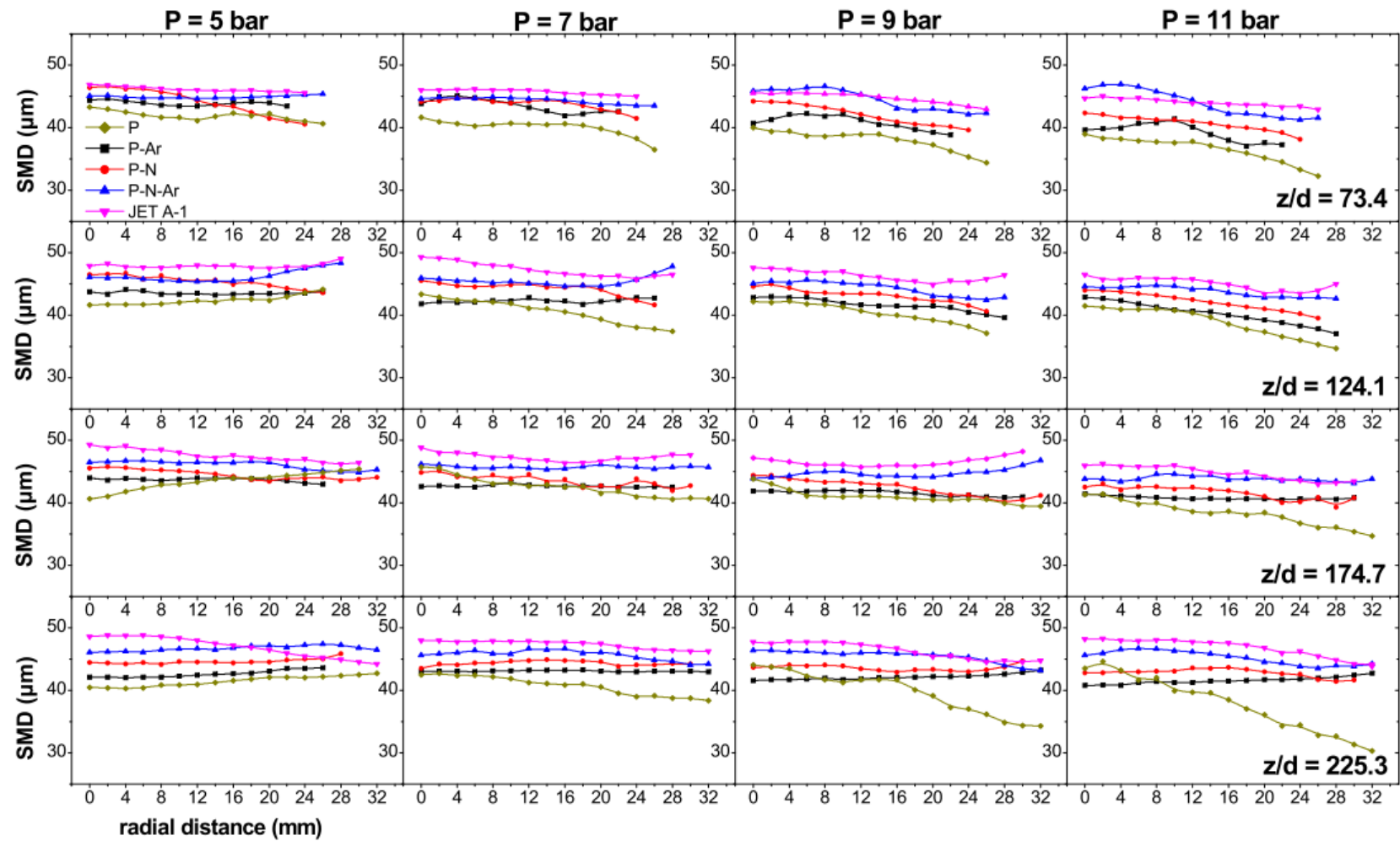


Figure 2.37: Droplet size with respect to radial distance as investigated by Vouros et al. [102].

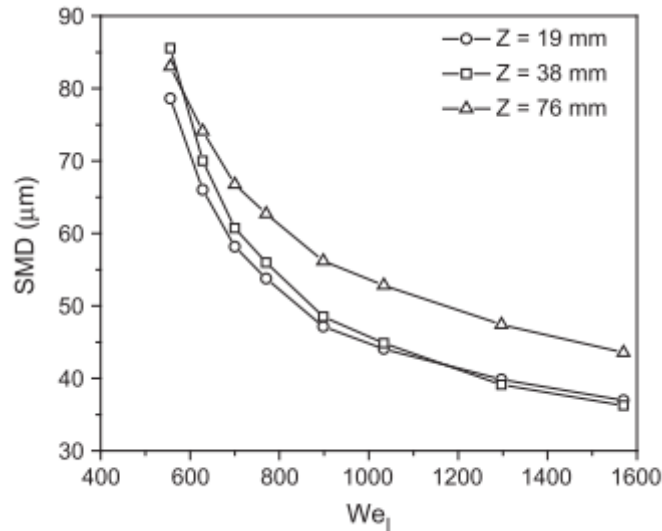


Figure 2.38: SMD comparison with Weber number for several lengths away from injector ‘ z ’ [103].

Another study has been conducted by Sivakumar et al. investigating the impact a camelina derived bio fuel on atomisation in a simple swirl atomiser [103]. The authors used Weber number in their analysis, which is a good method of analysing multiphase flows. The equation for which has been depicted in equation 2.7. Where ρ is the density of the fluid, v is the fluid velocity, l a characteristic length (in this case corresponding to drop size) and σ is the surface tension of the fluid.

$$We = \frac{\rho v^2 l}{\sigma} \quad (2.7)$$

A key point of the Weber number is that it depicts the effect surface tension has upon the drop sizes and proves that as surface tension of the sprayed liquid decreases the drop sizes also decrease. This phenomenon was first credited to R. Tolman [104]. Figure 2.38 depicts a comparison of the bio fuel injected from a swirl atomiser for SMD vs Weber number, it is clearly visible that the SMD drops in a decaying fashion with the increase of the Weber number. Furthermore, Sivakumar et al. have concluded that at high fuel flow rates the SMD decreases closer to the atomiser but starts to increase due to evaporation of the fuel and coalescence of the droplets [103].

Moreover, a study was conducted by Buschhagen et al. where it was observed that the spray characteristics of several sustainable jet fuels using a twin fluid atomiser (air-blast

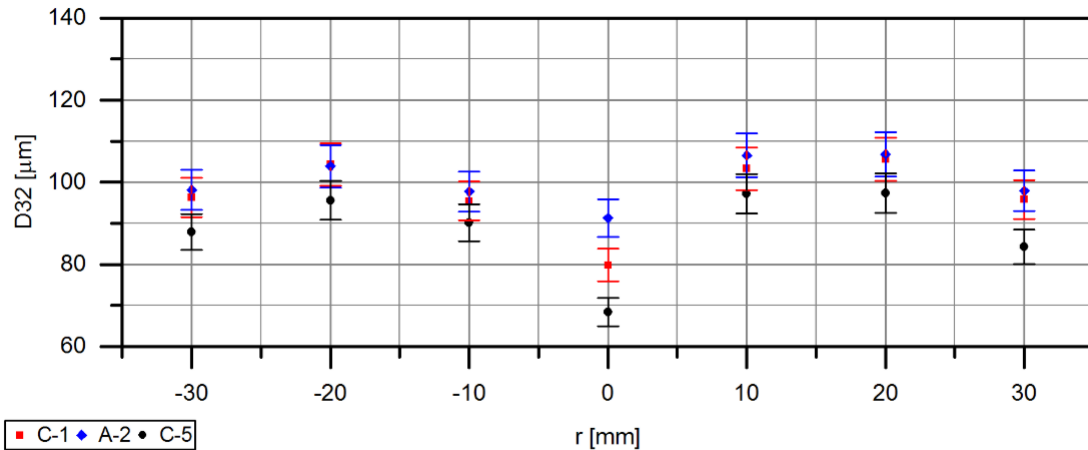


Figure 2.39: SMD for 2 alternative and one conventional fuel [105].

type). The key findings of this investigation were that as injection temperature decreases the spray quality decreases by 17% in terms of Sauter mean diameter (SMD, D_{32}).

Figure 2.39 depicts the SMD for 3 fuels C1, A2 and C5 at varying radii from the centre of the spray cone. Where A2 is reference Jet A1 as can be seen from the figure all three fuels show only minute differences in their SMD. It is also visible that the SMD does not appear to change with distance from the centre of the vertical spray plane indicating a uniform atomisation. The figure depicts SMD 1 inch (25.4mm) downstream of the injector which is indicative of the very high droplet size and also explain the uniform distribution where the droplets have not yet had the time to undergo secondary atomisation and it also explains why the fuel properties seem to have little impact upon the atomisation.

Kannaiyan and Sadr investigated the spray characteristics of a GTL fuel known as CSPK (commercial SPK), Jet A1 and a blend of the fuel and a product named “Shellsol” [106]. The investigation was conducted using PDA (pulse doppler anemometry) using 2 dimensions and hence 2 lasers which precludes the need for calibration. It was observed the particle sizes at several locations of the spray cone as shown in Fig. 2.40. The injector used was a pressure swirl type atomiser.

Figure 2.41 depicts the results obtained by Kannaiyan and Sadr, where the SMD has been plotted for the 3 fuels against radial distance of the spray cone. As expected the mean drop size increases as the distance from the nozzle axis increases due to poorer mixing occurring at the edges of the spray field as the injector used is only pressure swirl

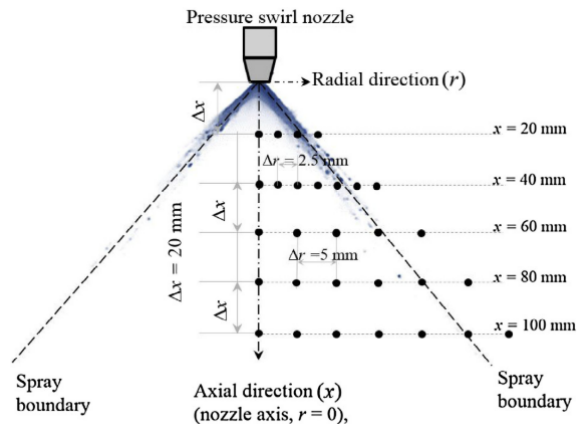


Figure 2.40: Spray cone measurement locations of Kannaiyan and Sadr [106].

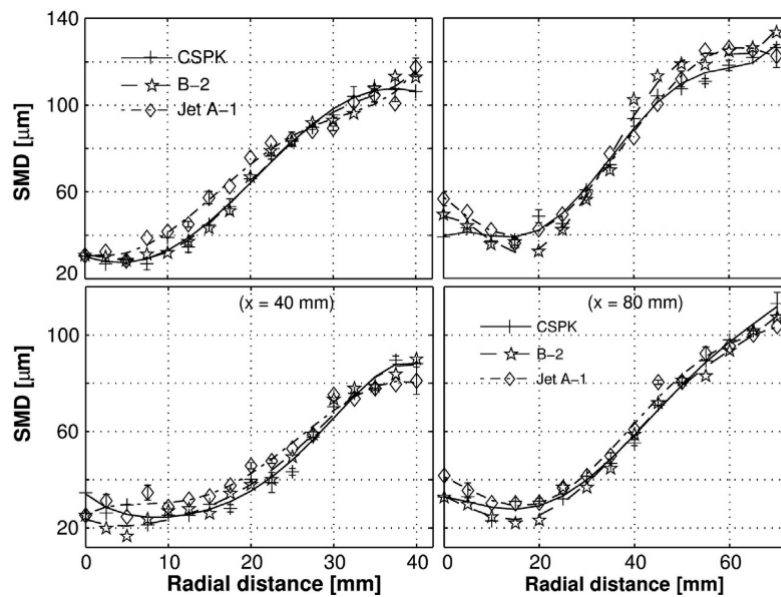


Figure 2.41: SMD at various locations of the spray field for the 3 fuels. Top and bottom indicate 0.3MPa and 0.9MPa injection pressures respectively [106].

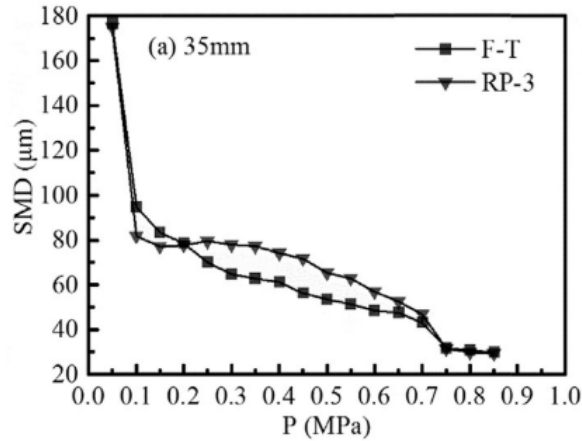


Figure 2.42: F-T vs RP3 fuel SMD with increasing injection pressures [107].

and not air assisted. However, there appears to be no statistically significant difference in the SMD between the fuels; which can be attributed to the fact that all three fuels have a very narrow range in their bulk properties that impact atomisation (i.e. density, surface tension and viscosity). The only variation in the fuels observed in this study with respect to the spray quality is in the mean axial velocity of the droplets with respect to the radial location.

Another study conducted by Zhao et al. Compare a FT derived fuel to RP3 (Chinese equivalent of Jet A1) using a pressure swirl atomiser and a Malvern particle sizer [107]. The particle sizes were measured at several axial lengths away from the nozzle as well as several injection pressures. The results are depicted in Fig. 2.42.

As can be seen from the figure the SMD's at pressures below 0.1MPa show extremely high drop sizes for both fuels indicating poor mixing and breakup as is to be expected at low injection pressures. The SMD drops and stabilises between 0.2MPa and 0.7MPa where the FT fuel performed better than the RP3 fuel indicating around a 10% decrease in particle size. Above 0.7MPa there is a sharp drop in the SMD which could indicate a change in the atomisation mechanism from classical to prompt indicating that the droplets are instantaneously vaporised. The variation in the SMD between the alternative and conventional fuel maybe attributed to the chemical composition of the fuel.

2.2.4 Controlling combustion instability

The classical methodology for the control and damping of combustion instabilities has been termed ‘passive control of combustion instability’. These are processes and modifications that are independent of time and are fixed in nature. Examples of passive control involve hardware modification in the form of changing the combustor geometry which will serve to modify the acoustic modes of the combustor which will serve to induce a difference between the natural frequency of the combustor and the frequency combustion and heat release which allows tends to damp the acoustic waves from combustion. Another example of passive instability control varying the flame stabiliser geometry which causes the turbulent vortex shedding frequencies to be changed moving them further away from the combustors natural modes as well as changing the flame propagation speed [74].

Active control systems involve the use of mechanical actuators and valves introduced to control the equivalence ratios of the combustor to either generate acoustic waves and fuel flow rate fluctuations to induce instability in a research setting or to damp the very same in an operational situation [74]. Furthermore, acoustic drivers can be used to damp acoustically coupled instability by means of a closed loop control system which can collect the combustion input parameters and produce a suitably phase shifted acoustic wave which will damp the instability waves generated by the combustion process. Such a system for a premixed combustor has been studied by Lang et al. and is depicted in Fig 2.43 [108].

2.3 Signal processing

This section aims to give a brief overview of the signal processing techniques used in the representation of digitally acquired signals specifically noise, vibrations and dynamic pressures. Signal processing is a vast subject area covering basic data acquisition to complex control systems. Firstly, it is imperative to define what is considered a signal for the purposes of this investigation and in the wider field of signal analysis. A signal is considered to be a physical quantity that has a variation over the course of time, which in this case refers to noise (sound pressure waves propagating toward the emplaced microphones from the engine), vibrations (the forces caused by either rotating machinery of the gas

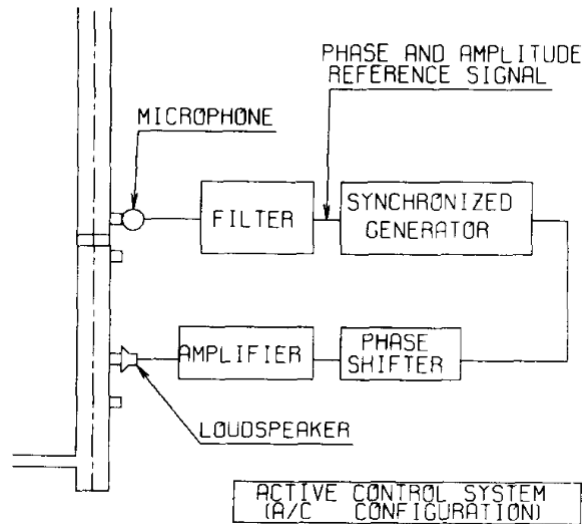


Figure 2.43: Active instability controller for a premixed combustor using microphones and loudspeaker [108].

turbine or the heat release derived pressure fluctuations in a combustion chamber being translated through the solid metal surfaces of the engines to the fixed accelerometers) and the pressure oscillations (directly measured from the combustion liner) themselves.

2.3.1 Fundamentals of signal analysis

The first step of signal analysis is to classify the signal into one of 3 categories. The first of which is a periodic signal, which is a signal that repeats itself after a particular period (T_p) of time. The second type of signal is a random signal (i.e. stochastic process), which does not repeat itself and the values of a the signal at a given point in time is not immediately relatable to the other points. The final type of signal is a transient signal, which means they are not constant over time and can either decay or expand with respect to time [109]. From the above definitions it is natural to state that vibrations and noise generated by the combustion process is would fall into the random signal category. Therefore the rest of this section will focus upon how random signals are treated and analysed, with a view to developing a framework to compare the noise and vibrations data acquired in this investigation. Random signals in the mean are generated when the forces being measured (e.g. Thermoacoustic pressure oscillations) are caused by a multitude of sources such as turbulent flow impinging on a solid surface.

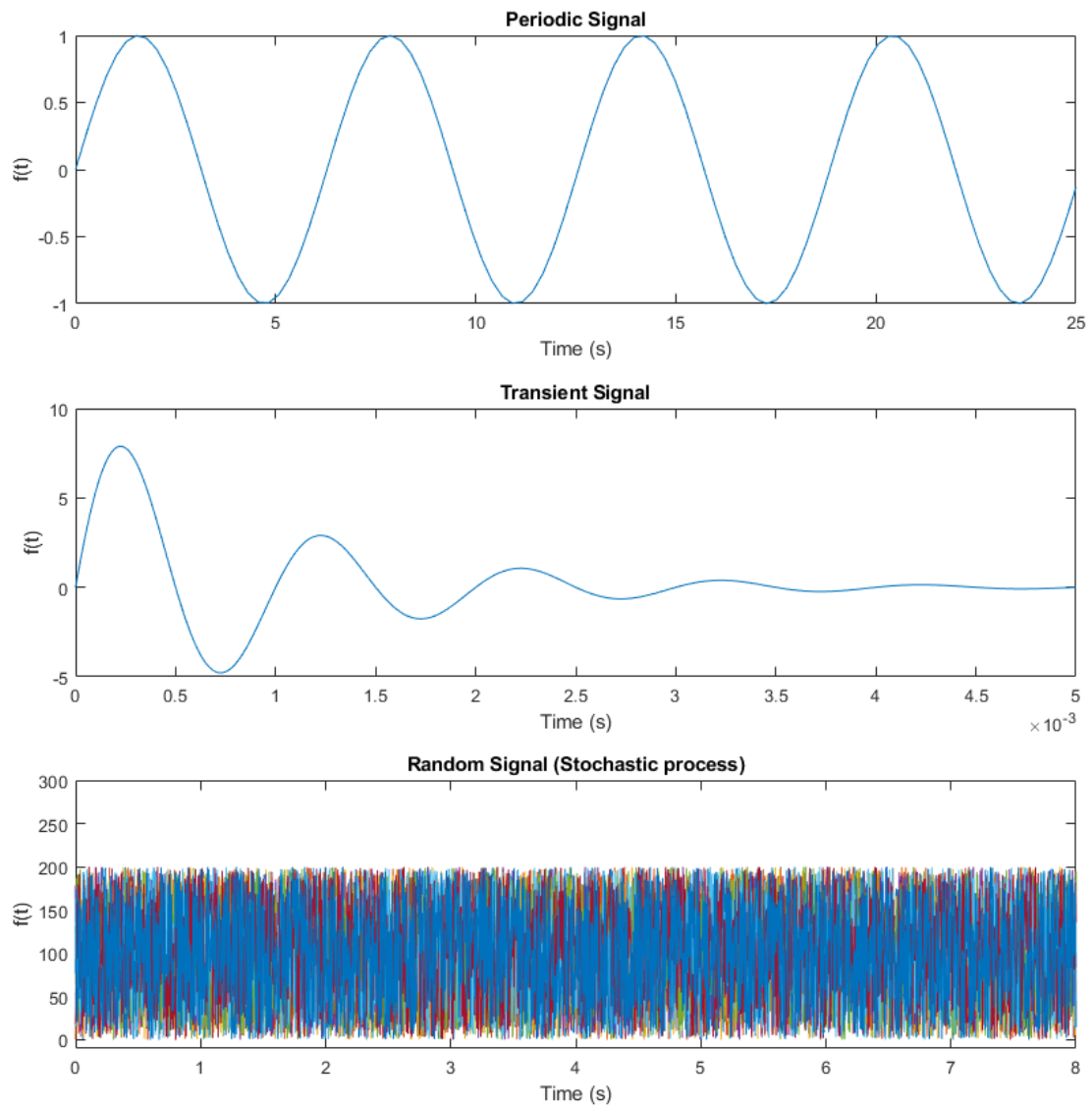


Figure 2.44: An illustration of the 3 main types of signals; periodic, transient and random.

Figure 2.44 shows an example of periodic signals, transient signals and a random signal.

2.3.1.1 Sampling theorem

The above classifications depict signal in analogue format in that they are continuous. However, when considering data acquisition and analysis using digital sensors which cannot comprehend analogue signals discretization must be considered. In essence this means acquiring the continuous data by sampling only discrete instances of it. The seminal work on sampling continuous signals in a discrete fashion was conducted by Nyquist [110] who described mathematically the number of samples required to capture a continuous sample discretely. The common definition given for the Nyquist frequency is ‘one half of the sampling frequency’. Which means that if one requires to observe the frequency criteria of a discretized analogue signal it must be below the Nyquist frequency and in effect the discretization must have been conducted at twice the Nyquist frequency.

2.3.2 Root mean square value.

RMS or Root Mean Square value is a method of comparing the magnitude of dynamic signals it is derived by calculating the squared mean amplitude of a signal. The formula for the RMS of a given signal $x(t)$ is shown in equation 2.8 [109].

$$X_{RMS} = \sqrt{\frac{1}{\tau} \int_0^{\tau} x^2(t) dt} \quad (2.8)$$

In equation 2.8 τ signifies the time constant of the signal. Hence it can be said that the RMS value describes the strength of a given signal. So in terms of vibrations how forceful the vibrations are. That being said, RMS is a mean value of an entire signal along its frequency spectrum and therefore has a tendency to not reflect the highest peaks of a signal as it averages the spectrum. Also it should be noted that the RMS value is heavily impacted by the noise in a signal.

2.3.3 Acoustic octaves

An octave band is defined in such a way that the upper bound of the band is double the lower bound of the band. This type of filtered frequency analysis is very commonly used in acoustics to determine the frequency content of the signals [86, 109].

$$SPL = 10 \log_{10}(P^2/P_{ref}^2) \quad (2.9)$$

Equation 2.9 denotes the mathematical formula used to calculate Sound Pressure Level (SPL) in decibels. Where P is the measure sound pressure in Pascals and P_{ref} is the reference pressure with which to convert to decibels. The reference pressure for use with respect to human hearing as per ANSI S1.11-2014 is $20\mu\text{Pa}$ [111]. Decibels are useful in acoustic analysis to convert raw sound pressure to a logarithmic scale that matches the nature in which the human ear perceives sound. The human ear does not perceive sound linearly, it does so in an exponential manner between the frequencies of 20Hz-20kHz (there is some variation in the frequency band of human hearing dependant on the age of the human in question). Therefore in practical terms it is not useful to interpret sounds in terms of pressure linearly.

2.3.4 Fourier Analysis

The fundamentals of frequency analysis is comprised of the Fourier transform which enables the conversion of a continuous signal into the frequency domain. This is crucial when considering random and transient signals as the time domain signal is relatively meaningless for random and transient signals in the main. The Fourier transform can be calculated using equation 2.10. Where the time domain function $x(t)$ is multiplied by an analysing complex variable composed of sinusoids $e^{-j2\pi ft}$. In which f is the frequency and t is the time. Immediately it is clear that this equation would not be practical in its application as it is derived for continuous functions with a known equation. The data acquired in practice have an unknown equation and has been acquired digitally.

$$F[x(t)] = X(f) = \int_{-\infty}^{\infty} x(t)e^{-j2\pi ft} dt \quad (2.10)$$

The solution to this issue is known as the discrete Fourier transform (DFT). The DFT

allows the calculation of the Fourier transform using a set of equally spaced samples. This is the reasoning behind sampling the data at a fixed sampling frequency. The DFT can be calculated using equation 2.11. Where the k^{th} frequency of X is equal to the sum of $x_n e^{\frac{-2j\pi kn}{N}}$ for N samples.

$$X_k = \sum_{n=0}^{N-1} x_n e^{\frac{-2j\pi kn}{N}} \quad (2.11)$$

The DFT can relatively easily be solved with real solutions using Euler's formula (equation 2.12) to remove the complex aspects. However considering that in practice millions of data points are gathered in normal investigations which according the DFT requires the calculation of millions of summation points per frequency k . The raw DFT is very computationally intensive in practice.

$$e^{jx} = \cos(x) + j\sin(x) \quad (2.12)$$

The solution to this issue is known as the Fast Fourier Transform (FFT). Whilst there exists many different algorithms for the FFT in essence their basic principles involve the simplification of the DFT by factorising the DFT matrix into products mainly comprised of zeros. This process reduces the amount of calculation required per DFT by an order of magnitude. The resulting FFT's are in general more accurate than the preceding DFT's due to the lower quantity of rounding off errors encountered computationally [112].

2.3.5 Knowledge gaps

Whilst there are many studies conducted upon the affect fuel injection plays upon combustion instability as well as how various fuel properties impact spray characteristics, very few studies have observed the impact of alternative fuels on spray characteristics. The main studies on this subject area are described in the literature review [102, 103, 105]. However these studies do not investigate the impact of aromatic species and their properties on spray characteristics. At best these studies focus upon the total aromatic content not the composition of aromatics. The reason for investigating the spray characteristics of aromatic compounds stems from the fact that they produce an inordinate amount of particulate emissions with respect to aliphatic hydrocarbons as described in the literature

review. Furthermore, whilst there exists a large amount of literature regarding the impact of atomisation on combustion instability (mainly concerning flow rate fluctuations [113–118]), there is a gap in the literature regarding the impact alternative fuels spray characteristics have on combustion instabilities.

Another knowledge gap identified in this investigation is the almost total lack of literature regarding the noise and vibrations emitted by commercial gas turbine combustion devices during the combustion process when running on alternative fuels. This is especially important when considering alternative fuels which are due to play a key role in the short to medium term with respect to the global drive for cleaner combustion. Therefore, it is imperative to glean some knowledge regarding how noise and vibrations are impacted by fuel composition and in gas turbines and gas turbine combustors. That being said some the literature that was found regarding the impact of fuel composition on noise and vibrations of gas turbines are either using a non-representative engine (i.e. a miniature gas turbine [86]), or are concerned with the adaptation of other fossil fuels for use in gas turbines such as diesel [88].

2.3.6 Aims and objectives

Considering the literature and the knowledge gaps that have been found, the aims and objectives of this investigations are defined as follows.

- Investigate the impact of alternative fuel properties on spray atomisation.
- Investigate the impact of alternative fuels and blends on the noise, vibrations and pressure oscillations of an atmospheric pressure combustor.
- Investigate the impact of alternative fuels and fuel properties on the noise and vibrations of a full gas turbine APU to observe if correlations from combustor holds.
- Derive conclusions as to what aromatic compounds can be added to alternative fuel blends to improve lubricity and seal swell whilst keeping noise vibrations and instability levels manageable.

Chapter 3

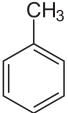
Fuels, their properties and experimental methods

This chapter describes fuels used in this investigation and their properties. These particular aromatics have been chosen after consulting the literature surrounding the average composition of hydrocarbon jet fuel; which points to alkyl-benzenes and poly-aromatic hydrocarbons being in the majority of hydrocarbon compounds found in jet fuel [27, 119].

3.1 Aromatic compounds and their blends

As has been discussed in section 2 of this investigation, 16 varying aromatic species that appear in jet fuel have been chosen to form fuel blends to determine which aromatics can be added to fuels to maintain lubricity and seal compatibility, table 3.1 depicts the candidates.

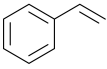
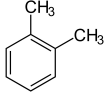
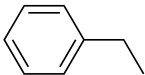
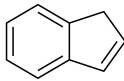
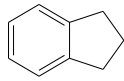
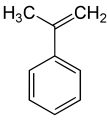
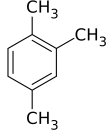
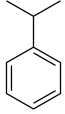
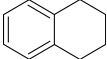
Table 3.1: List of low Aromatic blends

Fuel Code	Aromatic	Density (kg m^{-3})	H/C Ratio	Illustration of compound
1	Toluene	865	1.143	

Continued on next page

3.1. AROMATIC COMPOUNDS AND THEIR BLENDS

Table 3.1 – *Continued from previous page*

Fuel Code	Aromatic	Density (kg m ⁻³)	H/C Ratio	Illustration of compound
2	Styrene	906	1	
3	O-Xylene	879	1.25	
4	Ethylbenzene	867	1.25	
5	Indene	996	0.889	
6	Indan	965	1.111	
7	α -Methylstyrene	909	1.111	
8	Pseudocumene	876	1.333	
9	Cumene	864	1.333	
10	Tetralin	973	1.2	

Continued on next page

Table 3.1 – Continued from previous page

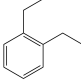
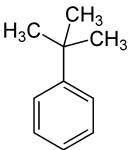
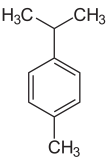
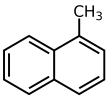
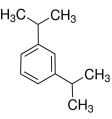
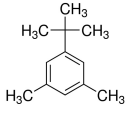
Fuel Code	Aromatic	Density (kg m ⁻³)	H/C Ratio	Illustration of compound
11	Diethylbenzene	870	1.4	
12	Tert-butylbenzene	867	1.4	
13	p-Cymene	860	1.4	
14	Methylnaphthalene	1001	0.909	
15	3-Isopropylcumene	856	1.5	
16	Tert-Butyl-m-Xylene	867	1.5	

Table 3.1 depicts the aromatic compounds used in this investigation. These for the most part consist of poly-cyclic and mono-cyclic aromatic compounds. The density noted has been obtained from the manufacturer (bottle label) and is accurate at 15°C. The hydrogen to carbon ratio (H/C ratio) has been calculated. Due to cost the impracticalities of testing these compounds neat it was decided to blend these aromatics with a baseline straight

Table 3.2: Properties of Banner NP1014 used

Properties	Value
Density at 15°C	751kg/m ³
Aromatic content (mass fraction)	0.15% wt
Flash point	67°C
Viscosity at 20°C	1.8cSt

chain solvent which contained 99% C9,C10,C11,C12 and C14 by volume. The balance impurities are stated by the manufacturer to be hydrocarbons larger than C14 amounting to a maximum of 1%. The solvent was commercial in nature manufactured by Banner chemicals U.K. under the moniker Banner NP1014.

The aromatics were blended in two ratios namely 8% and 18% aromatic with the balance being solvent. These particular ratios were arrived at after considering the average total aromatic content present in jet fuel according to literature being approximately 18% and the minimum aromatic content present in the mainstream jet fuel (i.e. Jet-A, Jet-A1 and JP-8) around 8% [120–123]. The two blend ratios were given a code for ease of reference in this study with 8% being ‘A’ and 18% being ‘B’. So for example the blend of Tetralin at 8% would be fuel ‘A10’ and the 18% blend would be fuel ‘B10’. This method of notation will be carried on through out the investigation and will be referred to frequently. Table 3.2 describes the physical properties of the Banner NP1014 solvent used in this investigation.

The blending was achieved by volume in 10 litre batches of each aromatic blend. As the density of the aromatics and solvents were provided by the manufacturers (tested using ASTM D4052) the blending was completed by mixing the masses of solvent and aromatic required to achieve the required blend ratios of 18% and 8%. The reason for blending masses to achieve a volume blend instead of measuring cylinders is the large batch size of 10 litres for which scales accurate to $\pm 0.1g$ were used.

3.2 Reference and other drop-in alternative fuels

The main reference fuel used in this study was Jet A1. Which has been given the reference code RF1. RF2 is also largely analogous to Jet-A1 with some minor additives included for corrosion resistance properties and improve anti-icing characteristics. Table 3.3 portrays the reference fuels used in this investigation where the density has been tested at 15°C and the viscosity at 40°C. The viscosity for RF8 and RF9 have been extrapolated using their viscosity at 20°C and -20°C using the viscosity curve for reference jet fuel.

Table 3.3: List of reference and prospective drop-in alternative fuels

Fuel Code	Description	Density (kg m⁻³)	Flash Point (°C)	Viscosity (cSt)	Cetane number
RF1	Jet A1	803.2	48	1.31	48.3
RF2	Jet kerosene with anti-corrosion additives	779.9	42	1.14	48.8
RF3	High flashpoint jet kerosene	826.8	60	1.57	39.2
RF4	ATJ produced by Gevo inc	759.7	49.5	1.53	17.1
RF5	Highly viscous fuel blend (64% JP5 balance farnesane)	807.7	66	1.78	47
RF6	Low cetane fuel blend (60% Sasol IPK balance ATJ)	759.2	46	1.25	28
RF7	Narrow boiling point blend (73% C10 balance trimethyl benzene)	768.9	44	1.9	39.6

Continued on next page

3.2. REFERENCE AND OTHER DROP-IN ALTERNATIVE FUELS

Table 3.3 – *Continued from previous page*

Fuel Code	Description	Density (kg m ⁻³)	Flash Point °C	Viscosity <i>cSt</i>	Cetane number
RF8	blend of fuel high in cyclo-paraffins	818.1	64	1.65 ¹	42.85
RF9	High Aromatic blend	823.0	56	1.35 ¹	43.1
RF10	High cetane number blend achieved using only HEFA and SPK's	759.0	48	1.6	63.3
RF11	cetane verified blend	777.0	50	4.33 ²	31
RF12	cetane verified blend	786.0	38	4.6 ²	44
RF13	cetane verified blend	786.0	56	5 ²	54
RF14	Conventional Jet A1	791.7	42	3.369 ²	-
RF15	Jet A1 blend with intermediate aromatics	844.6	-	-	-
RF16	Jet A1 blend with low aromatics	836.8	-	-	-
RF17	Jet A1 blend with High aromatics	862.5	>75	-	-
RF18	Conventional Jet A1 of other provenance	785.3	36	3.421 ²	-
RF19	Alcohol-to-jet SPK	758.8	46	-	-
RF21	Blend of 49% RF24, 34% RF23 and 17% HEFA	796.1	42	3.961 ²	-
RF22	Blend of 70% RF23 and 30% HEFA	777.2	40.5	3.276 ²	-

Continued on next page

¹ indicates fuel for which the viscosity has been extrapolated using the viscosity curve for Jet A1

² indicates fuel for which the viscosity has been obtained at -20°C.

Table 3.3 – *Continued from previous page*

Fuel Code	Description	Density (kg m⁻³)	Flash Point °C	Viscosity <i>cSt</i>	Cetane number
RF23	Pure Jet A1	790.1	43	3.154 ²	-
RF24	Pure Jet A1	814.4	43.5	4.591 ²	-
RF25	Blend of 51% RF24 and 49% HEFA	784.0	43	4.364 ²	-
RF26	Blend of Jet A1 and Camelina derived HEFA 47.7%	779.6	40	5.107 ²	–

3.3 Properties of conventional Jet fuel.

As has been discussed in the literature review the standard specification for commercial jet fuel is set by the aviation governing bodies of various countries, with the main contenders being ASTM D1655 [25] from the USA (specifying Jet A), Def Stan 91-091 [24] from the UK (specifying Jet A1). Other grades of jet fuels exist in the form of TS1 from Russia (higher volatility and lower freeze point compared to Jet A1; this is to suite the cold start requirements of the Russian far east) and No 1 and No 3 Jet fuel from China (No 1 is similar to TS1 and No 3 is similar to Jet A1) [124]. That said it is important to clarify the specific properties the aforementioned standards specify, as these are used this investigation to draw conclusions from and compare the surrogate blends to each other.

3.3.1 Density

The most commonly compared property in this investigation will be density, which is in essence the mass of a given substance per unit of its volume. The density of a jet fuel must be measured by either IP 160 [125], IP365 [126] or D4052 [127] tests before

being declared fit for use. The standard measurement of density involves the use of a glass hydrometer or an oscillating U-tube density meter. The specifications for jet fuel allow a range of densities between $775\text{kg}/\text{m}^{-3}$ and $840\text{kg}/\text{m}^{-3}$ at 15°C . The density of a Jet fuel is specially important when considering volume occupied by aircraft fuel tanks (i.e. less dense fuels will tend to occupy more volume within the aircraft for the same range and more dense fuels will impact the total maximum take off weight of the aircraft leading to reduced payload and range, assuming the energy density of the fuel is constant). Furthermore density of a fuel tends to be an indicator of fuel composition in that denser fuels would be composed of heavier hydrocarbons and vice versa. This in turn would impact the combustion quality of the fuels as it is well known that heavier hydrocarbon fractions are more difficult to burn and produce more soot. However, if the fuel is too light it would be composed of more volatile compounds which would impact the flash and freeze points of the fuel leading to increased danger in handling the fuel.

3.3.2 Flash point

Flash point is defined as the lowest temperature at which a volatile substance will ignite into a flame when exposed to an ignition source. The standards specify a minimum required flash point at 38°C [24, 25]. The flash point should not be confused with the autoignition temperature (the temperature at which a fuel will ignite spontaneously, which is important when considering diesel compression ignition engines) or the fire point (the temperature at which a substance will continue to burn after the ignition source has been removed, this is important for consumer goods safety characteristics etc.). The flash point of a fuel is closely related to its vapour pressure, which is defined as the pressure exerted on a closed system containing the fuel in its condensed states (either solid or liquid). In essence this a measure of how likely the fuel is to evaporate under standard conditions, fuels which have a high vapour pressure are known to be volatile. The vapour pressure relates to flash point in that a high vapour pressure creates a small cloud of vapours above the liquid surface which is easily combustible therefore lowering the flash point. This is important in fuel because as a non-homogenous liquid a given fuels flash point correlates highly towards its most volatile component. Hence the flash point of a fuel can be easily

manipulated to suit by adding high vapour pressure compounds to the fuel (i.e. to reduce the flashpoint for winter operations). Flash point is tested using a closed cup tester, which heats a small volume of the fuel to a constant temperature and then dipping a small flame into the cup to monitor whether ignitions occurs. These methods are specified in ASTM 3828 and ASTM 3278.

3.3.3 Viscosity

Viscosity of a liquid is closely related to the resistance it shows towards deformation when subjected to forces. In essence it is a measure of the frictional forces between the fluids shear layers. For liquids the most practically visible aspect of viscosity is the fluids ability to flow and its visual thickness. Therefore viscosity is usually measured by the distance it flows at a given angle in a defined period of time. The viscosity of a liquid is strongly impacted by the temperature. High temperatures result in lower viscosities and vice versa. Measurement of viscosity is conducted with the aid of a viscometer where either a solid object moves through the sample liquid or the liquid itself is made to flow through a narrow tube between two bulbs as in Ostwald viscometers. The standard for the measurement of fuel viscosities is defined in ASTM D445 [128]. Viscosity is an important factor when considering fuels in gas turbines because it impacts the atomisation process of the fuel at the injection stage. This can lead to poor and non-uniform atomisation which in turn leads to unstable combustion and increased emissions due to the non-uniform nature of the fuel air mix.

3.4 Experimental methodology of atomisation rig

This section aims to define the experimental equipment used and the procedures followed to conduct the spray experiment. The basic requirement was to test the spray characteristics of the fuel, to this end a droplet size analysis was conducted by spraying the fuel using an injector from a Rolls Royce Tay combustor. The cubicle itself is continuously purged with nitrogen from a cylinder bank to maintain a low oxygen environment to reduced unrequited combustion from occurring inside. The nitrogen ingress rate into the chamber

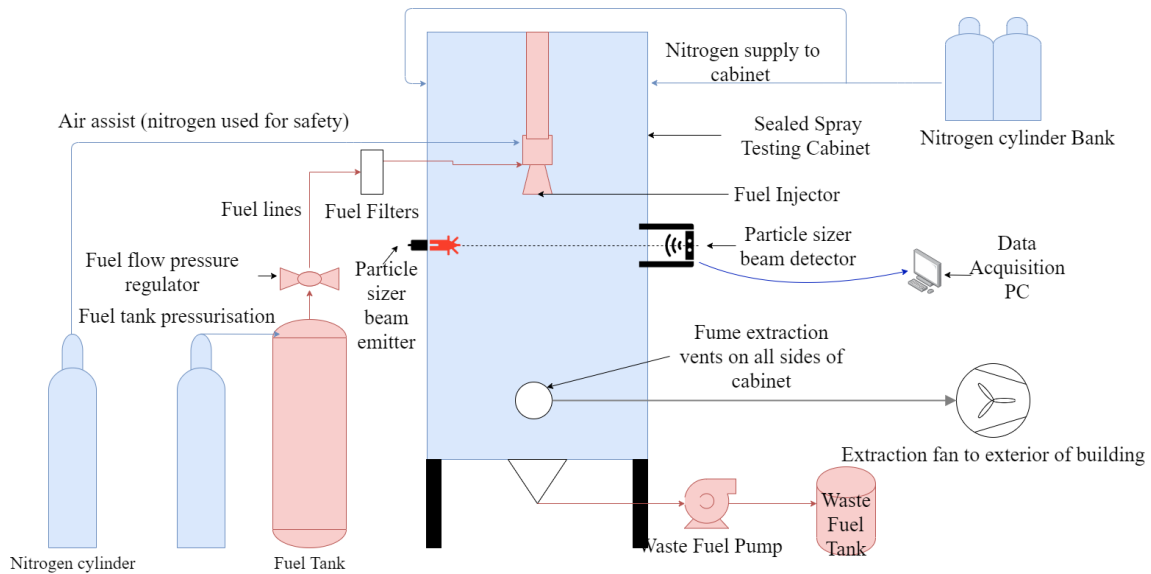


Figure 3.1: Spray testing rig.

is around $20l/m$ so as not to disturb the spray with undesirable air turbulence inside the cubicle. The chamber is continuously evacuated from a low level to remove the heavier fuel vapours also to mitigate the risk of spontaneous combustion. This process also allows time between tests to be reduced as the previous test's vapours are dissipated rather quickly. Figure 3.1 depicts the entirety of the spray rig. The chamber itself was mainly constructed from perspex with aluminium supports with the injection assembly suspended from the roof of the chamber. The Particle sizer has been mounted in the same plane as the injector assembly but $07cm$ below the atomiser, which enables the sizer to capture a good cross section of the spray so as to be able to successfully compare the different fuels as well the literature [102]. Approximately $0.5m$ below the analyser level are the fume extraction vents which vent the fuel vapours to the exterior of the building.

Figure 3.2 portrays the lower portion of the spray cubicle where the vapour extraction system and the liquid drain are located. The liquid drain is connected to a waste fuel pump and then onto a small waste fuel-drum also slightly visible in Fig. 3.2.

The fuel system involved a pressurised fuel tank (also pressurised using nitrogen for safety reasons) which was connected using PTFE tubes and Swagelok compression fittings to the injector assembly. Figure 3.3 depicts the fuel tank in which fuel pressure gauge is visible.

During the experiment the tank was filled with a given fuel using plastic hand pumps.

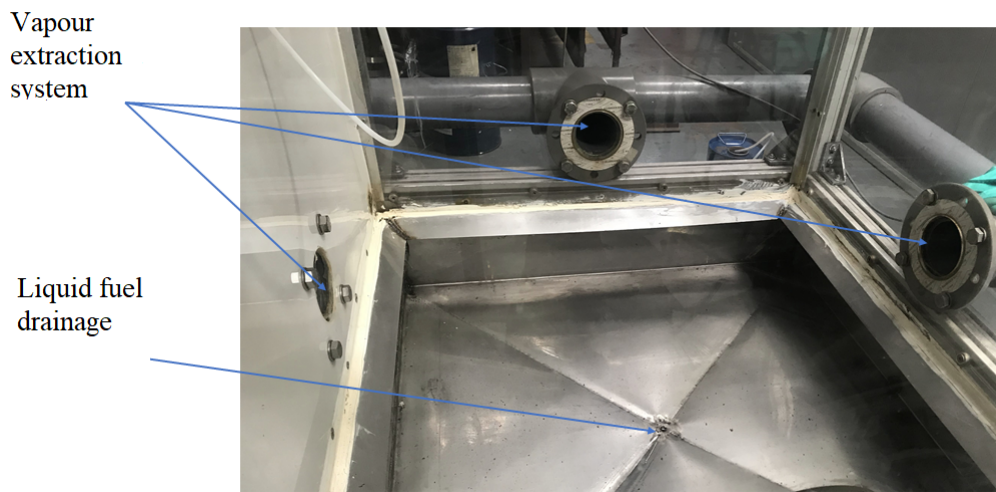


Figure 3.2: Spray rig bottom vents and liquid drainage.

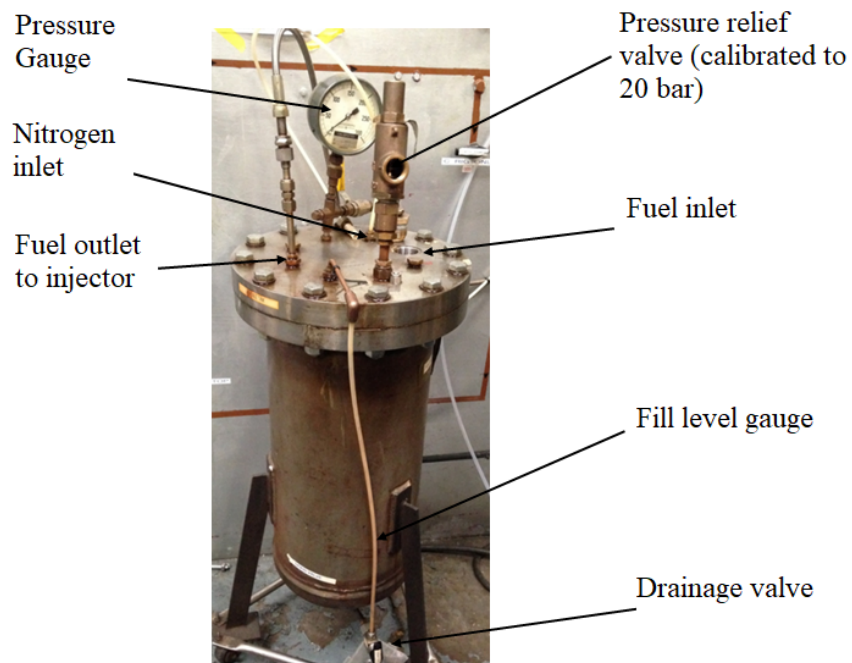


Figure 3.3: Nitrogen pressurised fuel tank.

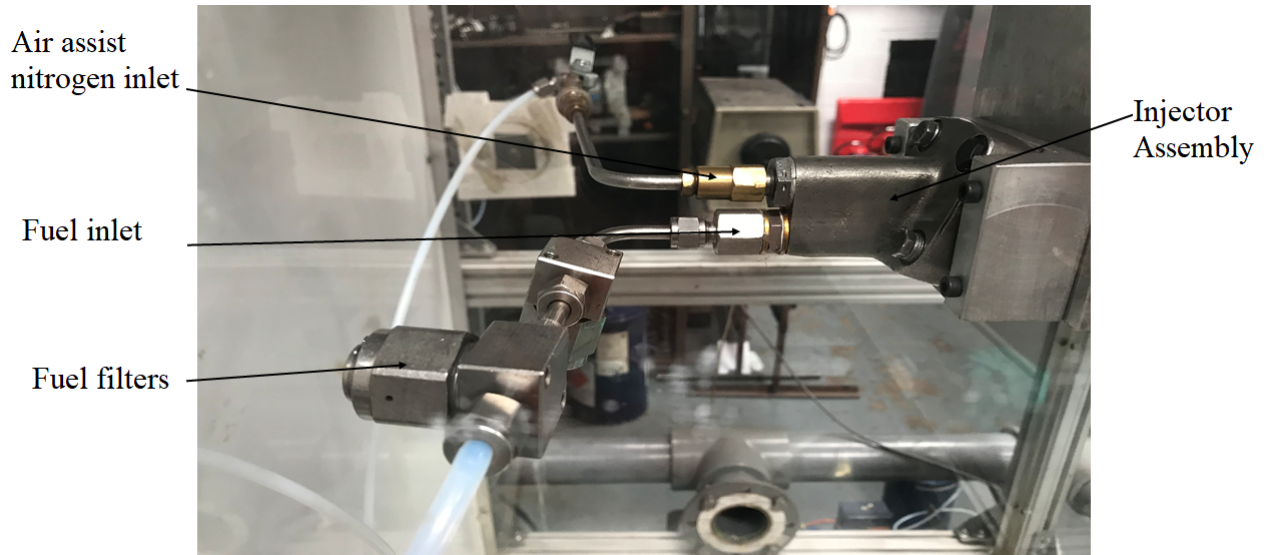


Figure 3.4: Injector assembly and fuel filters.

The tank was filled with approximately 3 litres of fuel per test. This was more than enough to complete the 9 test-points per fuel conducted in the investigation. At the end of each test the fuel tank was drained using the valve located in the bottom of the tank. This was done while the tank was pressurised to expedite the draining process and the injector was also opened so that any remaining fuel in the lines would either drop back into the tank or be injected into the chamber and evacuated that way. Once drained the tank was flushed using isopropyl alcohol to effectively ‘clean’ the tank in preparation for the next fuel. Isopropyl alcohol was chosen for this procedure due to its quick-drying nature. The next fuel was then pumped into the tank and pressurised and the injector opened without taking a reading so as to make sure droplets of the previous fuel in the line will be flushed out and only the current fuel remains in the line and injector. Figure 3.4 depicts the injector assembly with the fuel and air assist inlets, the figure also portrays the fuel filters used in the testing. These were included in the testing to avoid clogging the injectors with any foreign objects or particle present in the fuel. Whilst this was an unlikely event in a research fuel where the tank was cleaned regularly it was decided to include the filters to maintain homogeneity with the methods used when the injector was in service as well the research rig used in chapters 5 and 6. The filters were $60\mu\text{m}$ in pore size, and were of the Swagelok TF series T-type filter in the 0.5in size.

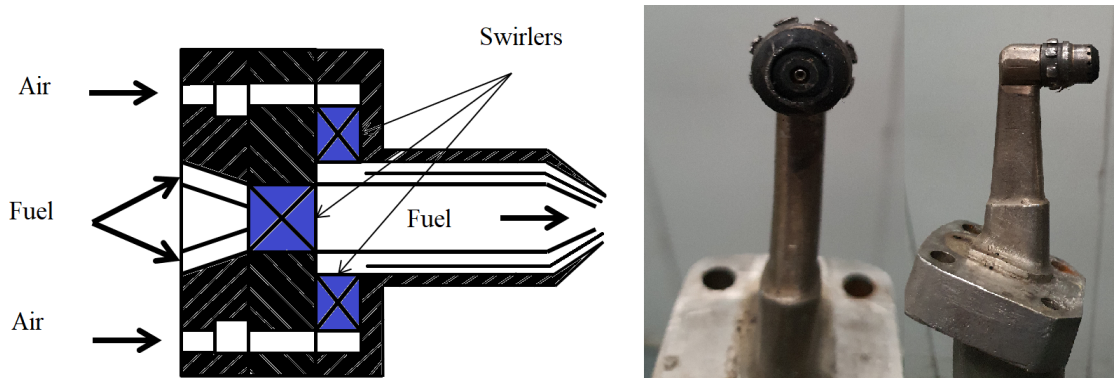


Figure 3.5: Air-blast atomiser and schematic from the Rolls-Royce Tay engine.

3.4.1 Atomization

Atomization was achieved using a twin-fluid atomiser from a Rolls-Royce Tay engine. This atomiser along with a combustion test rig was donated to the LCCC by Rolls-Royce. Advantages of using a twin-fluid atomiser as opposed to a pressure-atomiser (which as the name suggests uses the pressure of the fuel to force it through a small discharge orifice to achieve atomization) lies in the fact that for a given combustor design the fuel discharge orifice is sized to the maximum fuel flow rate. Which means that anything below maximum fuel flow rate would incur poor atomization from a pressure atomiser due to the lower differential fuel pressure. Twin-fluid atomisers mitigate this issue by supplementing the fuel atomization with high speed air which will aid the atomization at a wide range of fuel flow conditions. The twin fluid atomisers themselves are dichotomous in that some are classified as ‘air-assist’ and others as ‘air-blast’ atomisers. Whilst both are largely similar technologies the differentiating factor is the amount of air assist involved and its velocity. Air-blast atomization is used in this investigation as it is most representative of in-service aircraft engines due to their lower fuel pump pressure requirements. In this investigation the atomization air pressure was regulated and maintained constant at 1bar .

3.4.2 Laser particle analyser

The particle sizer used in this study was a Malvern 2600c particle sizer. This particular device is classified as a ‘non-imaging optical analyser’ due to it operating without the need to form and image of the scanned particles on the detector module. Figure 3.6 depicts a

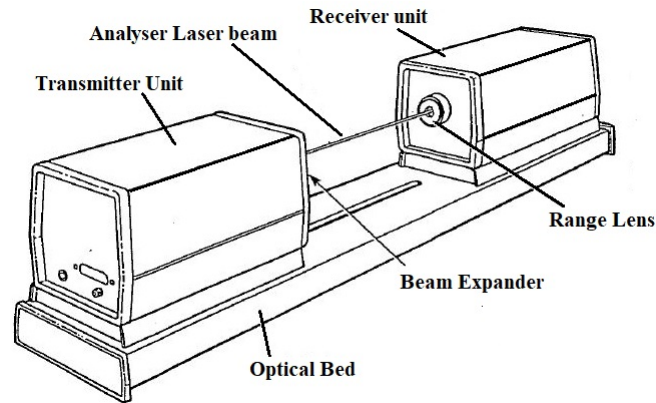


Figure 3.6: Malvern 2600c Particle sizer [129].

schematic of the device.

The particle sizer operates using the fundamentals of 'conventional Fourier optics' where a helium-neon (He-Ne) laser develops a beam of diameter 18mm . The laser beam is monochromatic (red in colour as this is dependent on the wavelength of the laser) and collimated i.e. the beam is composed of only parallel rays of photons. This beam is then projected to the receiving unit; the gap between the emitter and the receiver minus a minimum detection distance forms the usable detection area of the device. The perfectly parallel (collimated) beam is interrupted by particles (i.e. the substance used as a sample in the sizer) and is scattered, this scattering is measured by the detector and analysed to determine the size of the particles.

Both the diffracted and unaffected elements converge onto the detector lens which determines the diffraction pattern of the light using 31 different sections which corresponds to angles of scattering. The unaffected light then is discarded from the optical system. Sample's volume concentration is determined from measuring the power of the light passing out of the system. The interaction of the particles and laser beam as received by the detector is depicted in Fig. 3.7. The detector reading in a given instant is not representative of the sample as the result would only be computed using a small portion of the sample within the laser beams cross-section at that point. To combat this phenomenon, the detector is swept multiple times per test enabling a time averaged result to be computed which intern produces an accurate description of the fluid tested. The typical time required to form time averaged reading is 5 seconds. The analyser then uses Fraunhofer

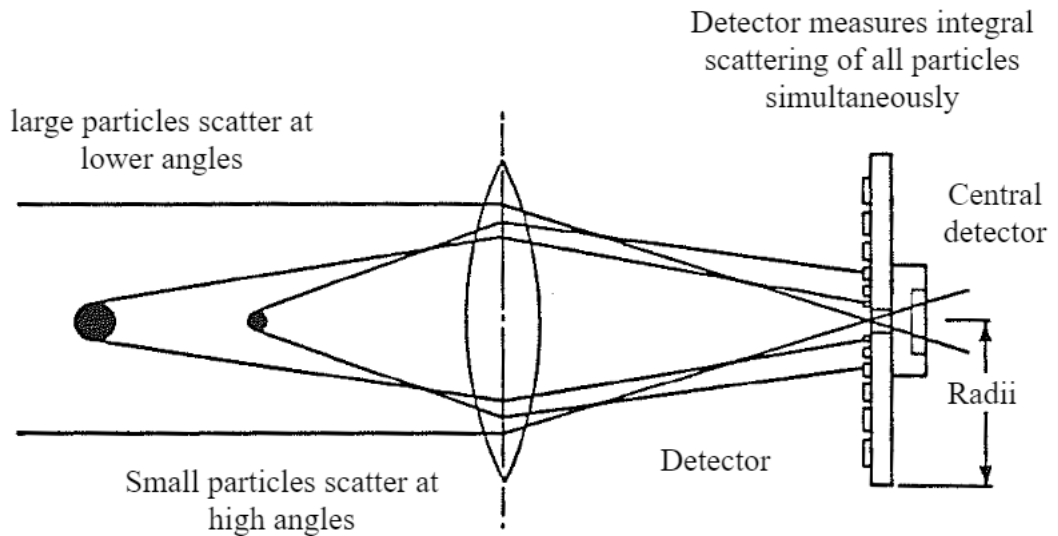


Figure 3.7: Particle scattering mechanism[129].

diffraction methods to determine the number of particles counted in each of the detection zones. Moreover, the analyser also has built-in correction algorithms to combat the effects for obscuration which takes effect when the obscuration of a given sample exceeds 0.5 (with 1 being fully obscured and 0 being unobscured). These corrections only and methods are mode specific to the analyser and are only effective in the 'lds' mode which corresponds to liquid drop sprays; which is the case in this investigation.

The Malvern 2600 particle sizer is well suited for this application as it involves the measurement of continuous spray flows and has been used to characterise spray atomisers in the literature [130, 131]. In terms of practicalities required particle sizer was calibrated (aligned) before commencing the experiment. This proved to be a long and laborious process which involved making minute adjustments to the mountings of the receiver and emitter units so that the laser beam is in the same plane as the detector. The alignment of the sizer was checked before each test point was carried out, as it was found that the sizer was prone to misaligning itself were someone to walk too close-by it. The alignment was graded as 'good' or 'bad' by the sizer as per Fig. 3.8. The range lens used in this investigation was the 800mm lens, capable of detecting particles between 15.5 and 1503 microns. This range covers the expected droplet size ranges as found in the literature

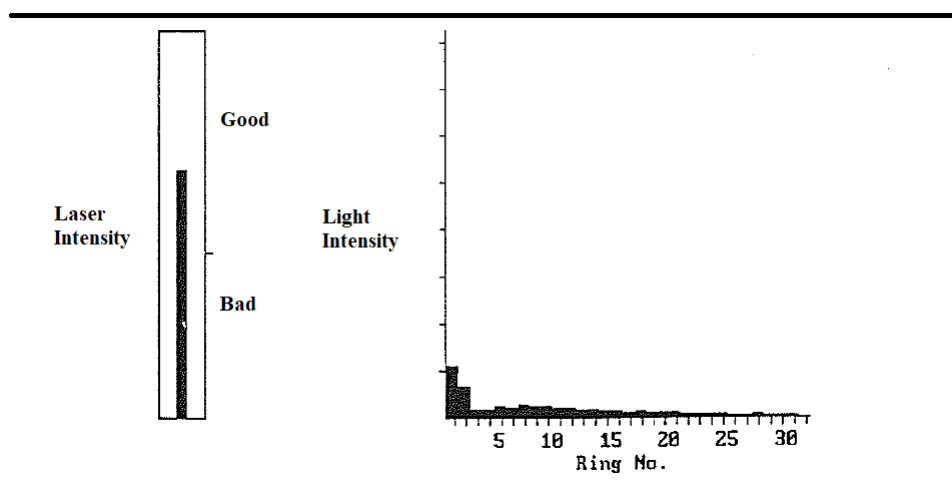


Figure 3.8: Alignment display [129].

[98, 102, 103]. This lens has a lens cut off distance of 1050mm. Which means that if the sample is beyond this distance the result will be subject to vignetting, this was not an issue in this investigation as the distance between the laser beam emitter and the detector in this investigation was 1m. This lens was used in conjunction with the 18mm beam expander.

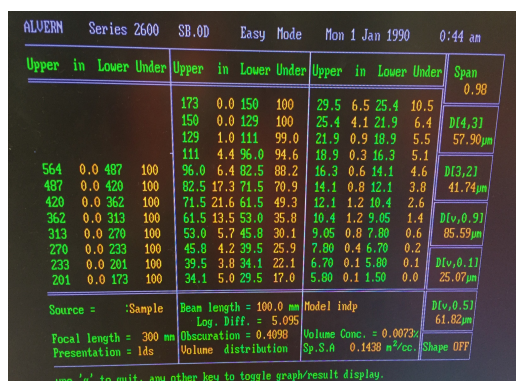
Furthermore, it was necessary to account for the background light and other scattered particles inside the cubicle to obtain an accurate reading. The particle sizer accounts for this using the 'set-zero' function where a background reading is taken and is used to subtract from the sample reading to ameliorate the effects of the background light conditions or even residual particles from a previous spray. This process was carried out for every fuel tested. In addition, during the preparatory tests it was noted that after each spray there was a tendency for the cubicle to become misted with fuel vapour which made the cubicle almost opaque. This phenomenon tended to skew the particle sizer data as the laser beam was highly scattered by the mist. To rectify this issue the extraction system was modified so that it would also extract from the top of the cubicle as well as the bottom corners. Whilst this ameliorated the issue to a great extent the SOP was amended to increase the time between tests so that the fuel mist would dissipate further with the aid of increased extraction.

The procedures and equipment used in this investigation were subjected to the rigours of university health and safety policy including but not limited to risk assessments, CoSHH (conduct of substances hazardous to health) assessments, SOP's (standard operating pro-

cedures) and laser safety declarations as well as laser equipment training.

3.4.2.1 Data acquisition and processing

Given the vintage of the particle sizer the data acquisition proved quite challenging in that the Malvern connects to a pc using a PCI (Peripheral Component Interconnect) card which in turn is connected via a broad cable to the sizer assembly. This in itself is not a major issue as conventional PCI is still in use. The major issue encountered was from the fact that the Malvern software was only compatible with a MS-DOS operating system. A system that was obsolete in the early 90's. Further more, the data transfer possible using this system required 3 1/2 floppy disks. Whilst it was possible to get the software running on the oldest computer still functioning in the LCCC the transfer of the soft data copies proved unfeasible (partly due to the cumbersome nature of diskette drives and the proprietary nature of data formats produced by the sizer). Therefore, the decision was taken to take photographic evidence of the results from the acquisition computer and manually record the data into more modern systems. Figure 3.9 depicts the type of results obtained via photographic methods and then manually entered into a PC for analysis. Figure 3.9a depicts the numerical results of the particle counting done by the sizer as well other parameters of mean volumes and diameters that have been calculated. Figure 3.9b depicts the particle distribution and cumulative % undersize curve of a given spray.



(a) Example of raw data



(b) Example of raw particle size distribution

Figure 3.9: Examples of photographs collected of the raw data.

3.4.3 Mean diameters

The most common metric of comparing droplet sizes of a given liquid is considered to be using the mean diameters of the droplets which are for technical reasons assumed to be perfectly spherical. This assumption is relatively valid for low density and viscosity liquids which fuels are considered to be. There are several different diameters which are used to describe liquid droplets; the most commonly used is known as the ‘Sauter mean diameter’ (SMD) which is sometimes referred to as $D[3,2]$. Whilst these are called ‘mean diameter’s they are not diameters in the conventional sense; in that the SMD is actually better described as a mean of the surface area to the volume ratio of the droplets [132]. The equation for the SMD has been eloquently described by Pacek et al. and depicted in equation 3.1 [133]. Where d^2 is the second moment of probability density and d^3 is the third. The utility of the SMD stems from it being more representative of the finer droplets present in a given sample which is the case in this investigation.

$$d_{32} = \frac{\int_{d_{max}}^{d_{min}} d^3 p(d) \delta d}{\int_{d_{max}}^{d_{min}} d^2 p(d) \delta d} \quad (3.1)$$

Another mean diameter used in sample statistics is the ‘volume moment mean’ (known as DeBrouckere mean diameter) or the $D[4,3]$ which is more representative of the bulk of the droplets present in a given sample and therefore is affected by outsize droplets more than the SMD. An illustration of where the SMD and DMD fall on a generic droplet distribution is shown in Fig. 3.10. The Malvern droplet sizer used in the investigation calculates both the aforementioned metrics and as we are more interested in the finer droplets for this study the SMD was the main metric used. Error bars have been derived from the standard deviation of the data range. It should also be noted that SMD is especially useful for combustion purposes as it serves a good indication of the evaporation rate of the droplet which in turn give insight into the rate and consistency of combustion.

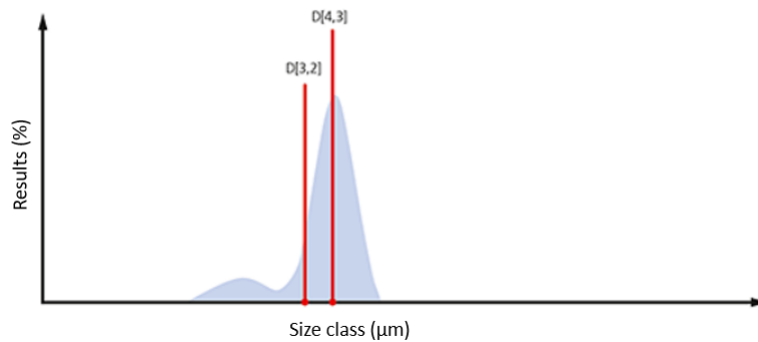


Figure 3.10: Comparison of SMD vs DMD [134].

3.5 Experimental setup of atmospheric pressure combustor

This section aims to elaborate on the experimental apparatus used and the procedures that were adhered to in the conduct of this experiment conducted using a Tay combustor. The primary purpose of this investigation was to test the pressure oscillations, noise and vibrations emitted by the 16 aromatic species listed in table 3.1 in an actual gas turbine combustor from a Rolls Royce Tay engine. The individual fuels were stored for the tests in the same nitrogen pressurized fuel tank from the previous section and illustrated in Fig. 3.3. A similar cleaning and refuelling procedure was used (i.e. fuel transfer from hand pumps and cleaning the tank using Isopropyl alcohol. Then filling the tank with new fuel and running the combustor for several minutes to ensure only the new fuel remained in the lines). The atmospheric pressure combustor and the associated sensors are depicted in Fig. 3.11.

As can be seen from Fig.3.11 the combustor is supplied with air from a large industrial grade fan which and the line is throttled with a butterfly valve and associated air flow meter (venturi type). Both the fan and the valve are controlled by the NI SCXI control unit according to readings provided by the air flow sensor. This allows the control of the inlet air mass flow rate to a total uncertainty of $\pm 2\%$. The SCXI control unit also controls the fuel system (both the fuel injection and the air assist). The nitrogen pressurized fuel tank is connected to a control panel that includes a Coriolis flow meter which controls

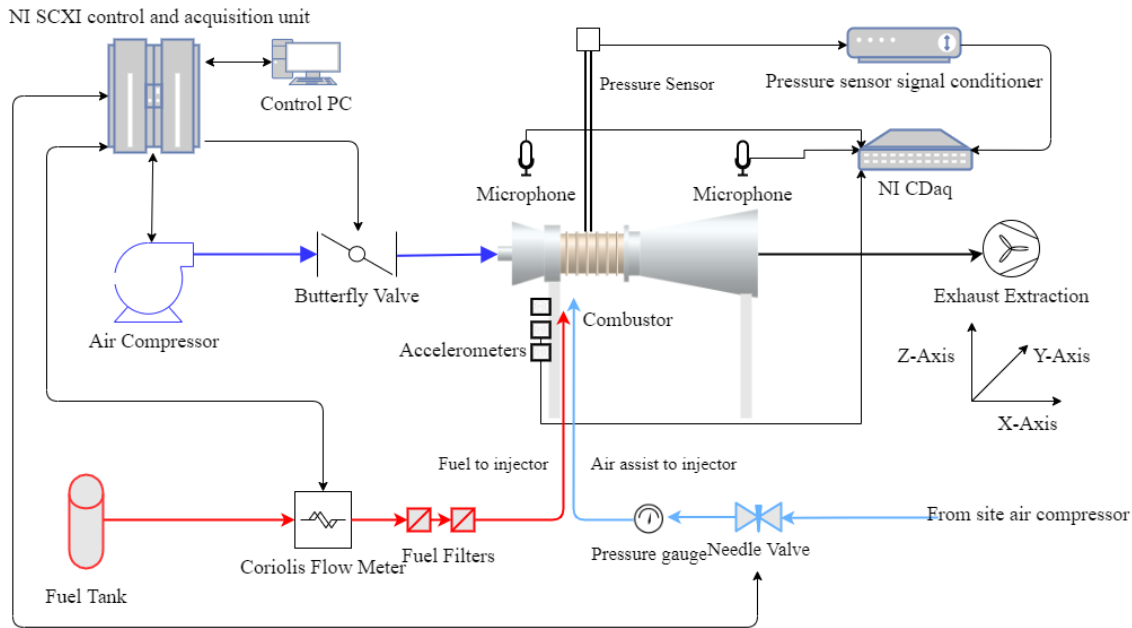


Figure 3.11: Atmospheric pressure combustor schematic.

the fuel flow. Prior to the injector 2 fuel filters are fitted of a cartridge type. The Air assist is supplied with dry compressed air from the LCCC's site compressor. This compressed air is control by pressure gauges and a needle valve. The air assist is maintained at 1bar throughout the test campaign. The barometric pressure varied between 1003HPa and 1007HPa and the inlet air temperature varied between 16 and 18 Celsius. Fuel exiting the tank is then controlled by twin series (coarse and fine) air actuated needle valves and an air actuated fuel shut off solenoid. Finally, the SCXI unit also controls the extraction system which vents the exhaust air to the building exterior. It should also be noted that the inlet air was not preheated and was supplied at standard room temperature. Furthermore, the inlet air pipe contains flow straighteners and other geometry that stabilises the flow and reduces the impact caused by the flow meters and the butterfly valve. This process is key as depending on the valve position a considerable amount of turbulence could be introduced which would introduce an unknown variable to and test. The inlet air is delivered through a $6''$ pipe and the inlet section is designed with accordance to BS:5167. It should also be noted that the SCXI system is run on a 5Hz control frequency.

Figure 3.12 depicts the SCXI control unit with physical power switches and an emergency stop switch. The fuel, air, ignition is controlled by the LabVIEW VI specifically developed for this research rig. The program also allows the monitoring of several temper-

3.5. EXPERIMENTAL SETUP OF ATMOSPHERIC PRESSURE COMBUSTOR

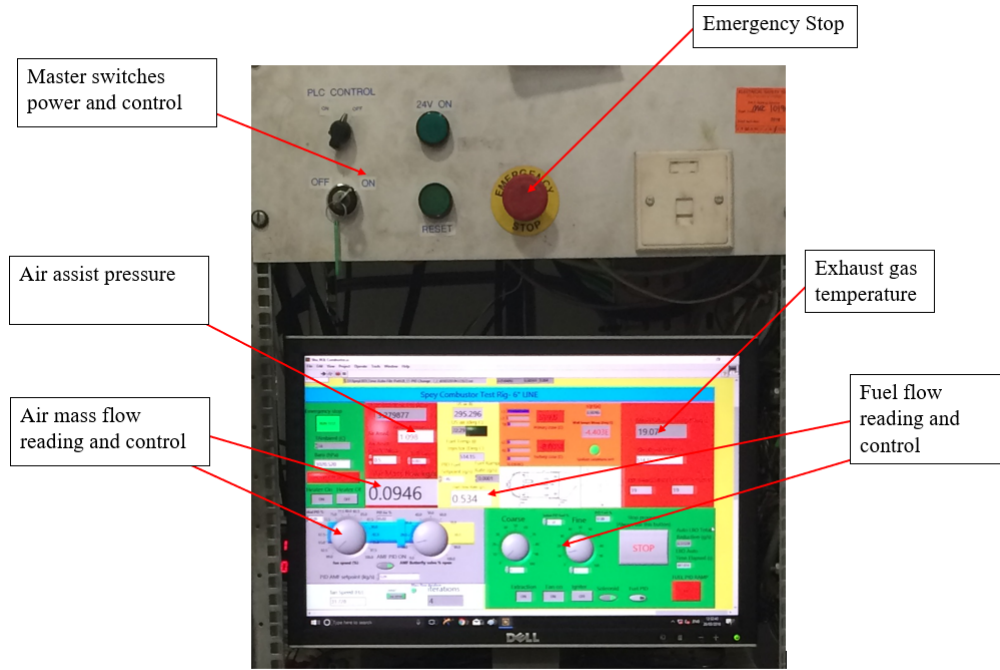


Figure 3.12: Combustor control panel.

atures along the rig the most important being inlet air and exhaust gas temperature (EGT). Table 3.4 shows the measurement capacities and associated uncertainties of the combustor control system. As has been mentioned above the SCXI control system is inherently low speed by virtue of its 5kHz sampling rate. This is the reason as to why the pressure sensor, accelerometers and microphones data has been acquired by a separate DAQ sampling at 20kHz.

In this investigation the combustor was run at 3 separate conditions for each fuel blend.

Table 3.4: Uncertainty of controllable quantities.

Variable	Measurement capacity	Uncertainty
EGT ($^{\circ}\text{C}$)	0-500	$\pm 2K$
Air flow rate (g/s)	0-320	$\pm 2\%$
Fuel flow rate (g/s)	0-5	$\pm 3\%$

Table 3.5: Description of combustor conditions.

Condition	Fuel flow rate (g/s)	Air mass flow rate (g/s)	Calculated AFR
1	0.5	130	260
2	1.7	200	117.64
3	0.5	60	120

The first condition was a middle ground condition with a moderate fuel and air flow considered a control condition reflecting normal operating conditions of the combustor. The second condition was a rich high air and fuel flow condition where emissions were expected to be high, but the combustion was not expected to be unstable. The final condition was an extremely lean condition close to the LBO point of the combustor and fuels where instability was anticipated. The details of the engine conditions are elaborated in table 3.5.

It should be noted however, that the air flow rate does not include the mass flow from the air assist supplied to the injector of the combustor. Therefore, the calculated AFR would carry some systematic inaccuracy which is not of concern in this investigation as the primary purpose was to compare the instability noise and vibrations characteristics of the fuel blends. This air assist was kept constant at 1 bar for all conditions throughout the investigation. To ensure the air assist functions without blockages the fuel injector was checked at the beginning of each test day for soot deposits. This was found not to be a significant issue due to the lean conditions used in this investigation.

3.5.1 Tay combustor

Figure 3.16 shows the combustor proper and the associated thermocouples and other sensors attached to monitor the combustion process. The combustor itself is encapsulated inside an iron pressure vessel which acts as the outer casing of an engine. Figure 3.13 depicts the combustion liner proper where the first stage is the swirler which agitates the inlet air and allows for improved mixing. It should be noted that the liner is part of a

multi-can Tay engine (where in operational situations there would be 6 cans arranged in a circular pattern around the engine core and shafts. The cans would be in a turbo-annular arrangement). The fuel injector is located on the ventral side of the rig and protrudes directly into the combustion chamber via a perforation in the liner. This arrangement creates the necessary bluff body for the flame to stabilise inside the chamber.



Figure 3.13: Tay combustion chamber.

3.5.2 Sensors and data processing

A principle variable measured in this particular investigation was the pressure oscillations inside the combustor using a dynamic optical pressure sensor manufactured by Oxsensis Ltd. The sensor was designed to be capable of tolerating the elevated temperatures inside the combustion chamber. A schematic of the sensor layout is presented in Fig. 3.14 where the sensor probe is connected via fibre optic cable to the interrogator unit which converts and conditions the signal so that it may be acquired by standard data acquisition systems (DAQ) which in this case was a NI cDAQ 9178. The interrogator communicates with the DAQ via a standard coaxial BNC (Bayonet Neill–Concelman) connector. This sensor is calibrated according to a voltage to pressure curve provided by the manufacturer. The sensor has a maximum soak temperature of 600°C hence it has only been inserted into the gap between the outer casing of the combustor and the liner. The technical mechanisms of the optical method has been described in detail by the manufacturer in a case study [135].

Figure 3.15 depicts the actual images of the pressure sensor and interrogator. The probe itself includes a thermocouple to measure the temperature of the probe.

3.5. EXPERIMENTAL SETUP OF ATMOSPHERIC PRESSURE COMBUSTOR

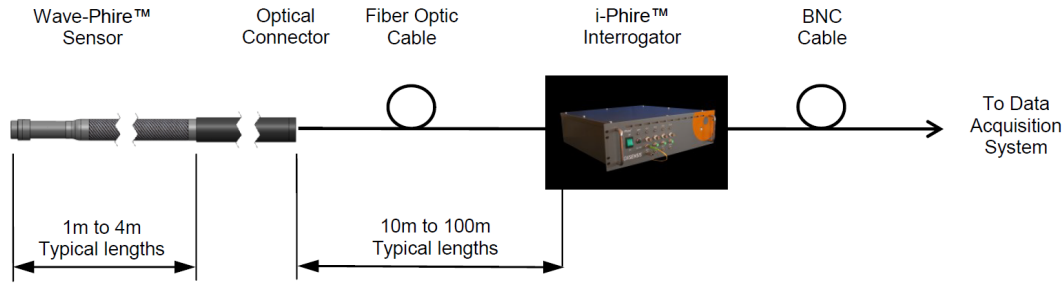


Figure 3.14: Dynamic pressure sensor schematic [136].



Figure 3.15: From left to right: pressure sensor base, sensor probe, signal interrogator. The images were acquired after the flooding of the LCCC hence the rust on the probe.

The Accelerometers used in this investigation were Dytran Instruments model 3225F1 miniature accelerometers. These are manufactured using titanium shells with a sensing element of quartz, and are designed to be adhesively fixed to the target surfaces. They have an advertised sensitivity of $10\text{mV/g} \pm 3\%$ and were received calibrated from the manufacturer. The maximum measurable force for a $\pm 5\text{V}$ input is 4905m/s^2 and the frequency response was 1.6-10000Hz with a resonant frequency of well over 60kHz. This particular accelerometer was chosen for its ability to withstand elevated temperatures of up to 125°C . The accelerometers and microphones were connected to NI9234, NI 9213, and NI 9203 modules on the cDAQ which were in IEPE mode due to the sensors being

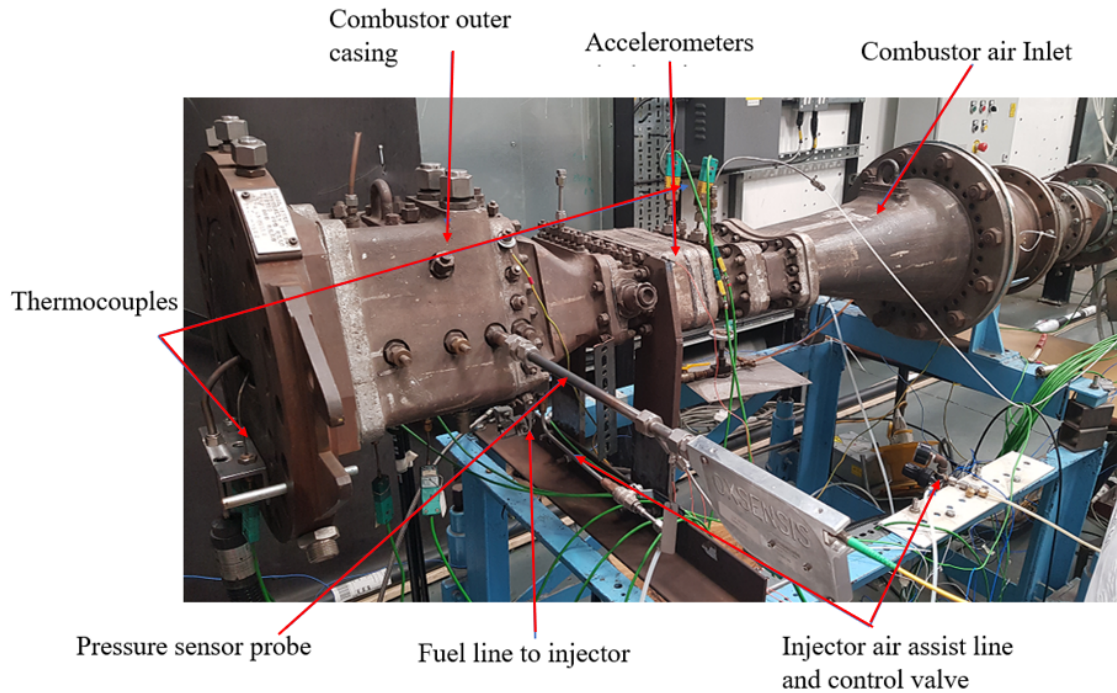


Figure 3.16: Combustor and sensors (microphones are not visible in this image).

IEPE compliant and supplied with $\pm 5V$. In this investigation 5 accelerometers were used, they were termed X1, Y1, Z1, X2 and Y2. As can be inferred from the naming scheme 3 accelerometers were affixed to the frame of combustor in the 3 planes X, Y and Z. The remaining 2 accelerometers were used as backups for the X and Y plane to verify the data and also to see how the vibrations changed based on the location of the accelerometers on the same plane.



Figure 3.17: Accelerometers and microphones used [137, 138].

The microphones used in this investigation were PCB Piezotronics HT378B02 condenser microphones. The sensitivity was 50mV/Pa with the microphone diameter being 0.5 inches. The maximum frequency response of the microphones were 20kHz. 2 microphones were placed 1m apart and affixed to the floor using stands, to correspond with the inlet of the combustor and the exhaust plane of the combustor respectively. The microphones were located 0.2m away from the combustor.

3.5. EXPERIMENTAL SETUP OF ATMOSPHERIC PRESSURE COMBUSTOR

The data acquisition from the cDAQ was conducted using a laptop running a LabView VI specifically developed for this purpose. Where the sampling rate and other variables could be adjusted. The output data was collated in .lvm file format which could easily be exported to Matlab for further processing. As mentioned above the sampling rate was 25kHz and the output file contained readings from the 8 sensors and a time stamp. Each test point was recorded for approximately 2 minutes which gives around 2.4 million readings per test point at the above sampling rate.

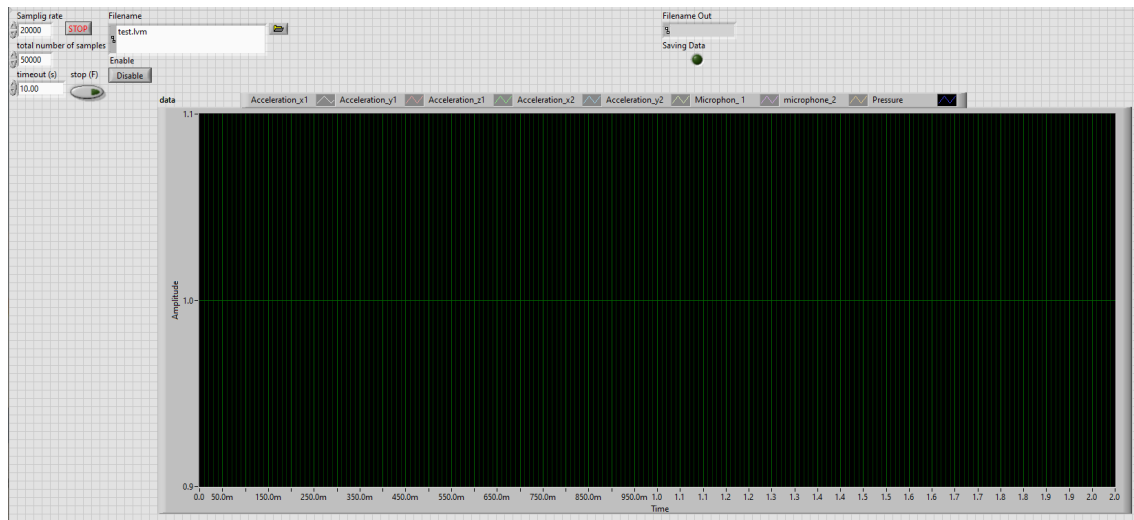


Figure 3.18: DAQ user interface.

Figure 3.18 depicts the user interface for the VI where the data collection could be initiated and the file saved for processing. The Block diagram for the VI has been attached in Appendix 2. Once the data has been acquired it was then imported into Matlab for final processing. The first step was to clean the data. That is to say the data was scanned for NaN variables and if present these deleted. Due to the high sampling rate used there was a possibility of data being lost during the saving process. This would affect the actual sampling rate of the data. This uncertainty is caused by the DAQ PC write speed being lower than the incoming data rate into RAM. Therefore this error in collection only appears once every 50000 samples which is the interval at which the data is written to the disk. This was rectified in Matlab by deleting the affected rows of data and resampling the whole dataset.

The sampling rate is a key criterion which was determined by means of an iterative process. The higher the sampling rate the better the resolution of the data. However and

increased sampling rate leads to increased file sizes and increased computational requirements specially in this investigation as there were a total of 75 test points. That being said a very low sampling rate would lead to poor quality data resolution. Moreover in digital signal processing the usable frequency content is known as the Nyquist frequency, which is half the sampling rate. Therefore, using a sampling rate of 25kHz would only yield a usable frequency range of 12.5kHz. This range was deemed sufficient as in the pilot studies conducted for this investigation no frequency content above 10kHz was visible.

The bulk of the processing of data involved converting the raw data acquired in the time series to the frequency domain. This is standard practice as per ISO 1638 and due to the fact that the time series data has little detail of note. Figure 3.19 depicts the raw time domain data for condition 2 for Jet A1, as can be seen little practical details can be made out from this type of format. To convert the data to frequency domain a process of the Fast Fourier Transform (FFT) was conducted, which is a form of the Discrete Fourier transform (DFT) for digital (i.e. stepwise) data. The mathematics behind the DFT and FFT have been described in the literature review section.

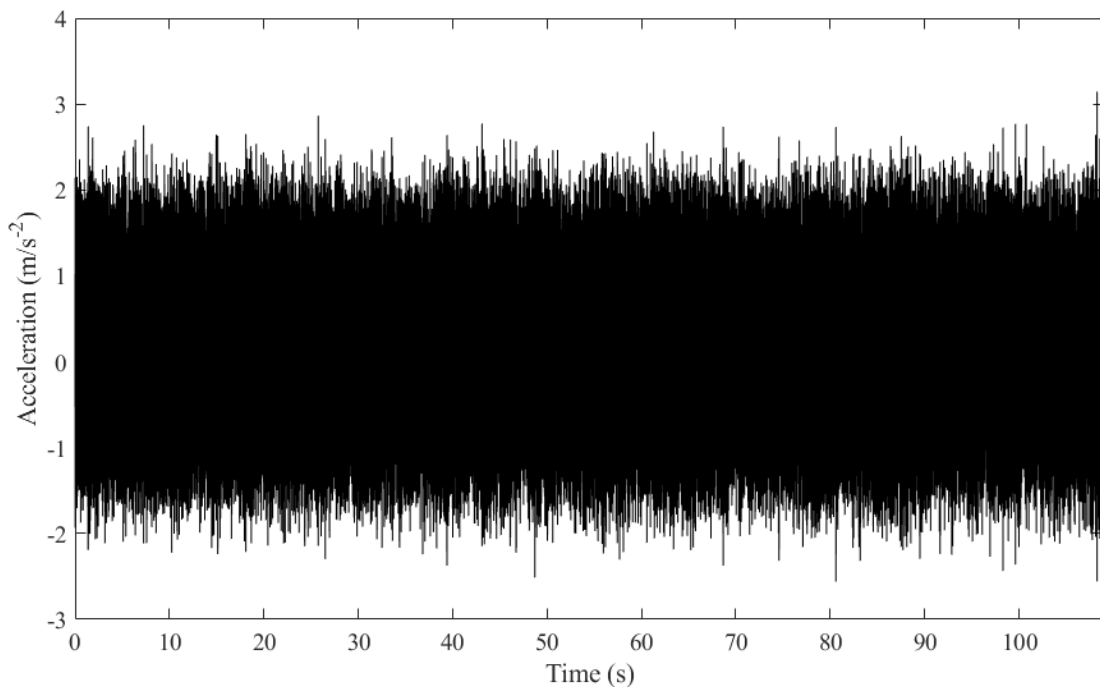


Figure 3.19: Raw time series data.

Given the large quantity of data acquired per test and the large file sizes of the data, a method was sought to observe whether the whole 2 minutes of data would be required

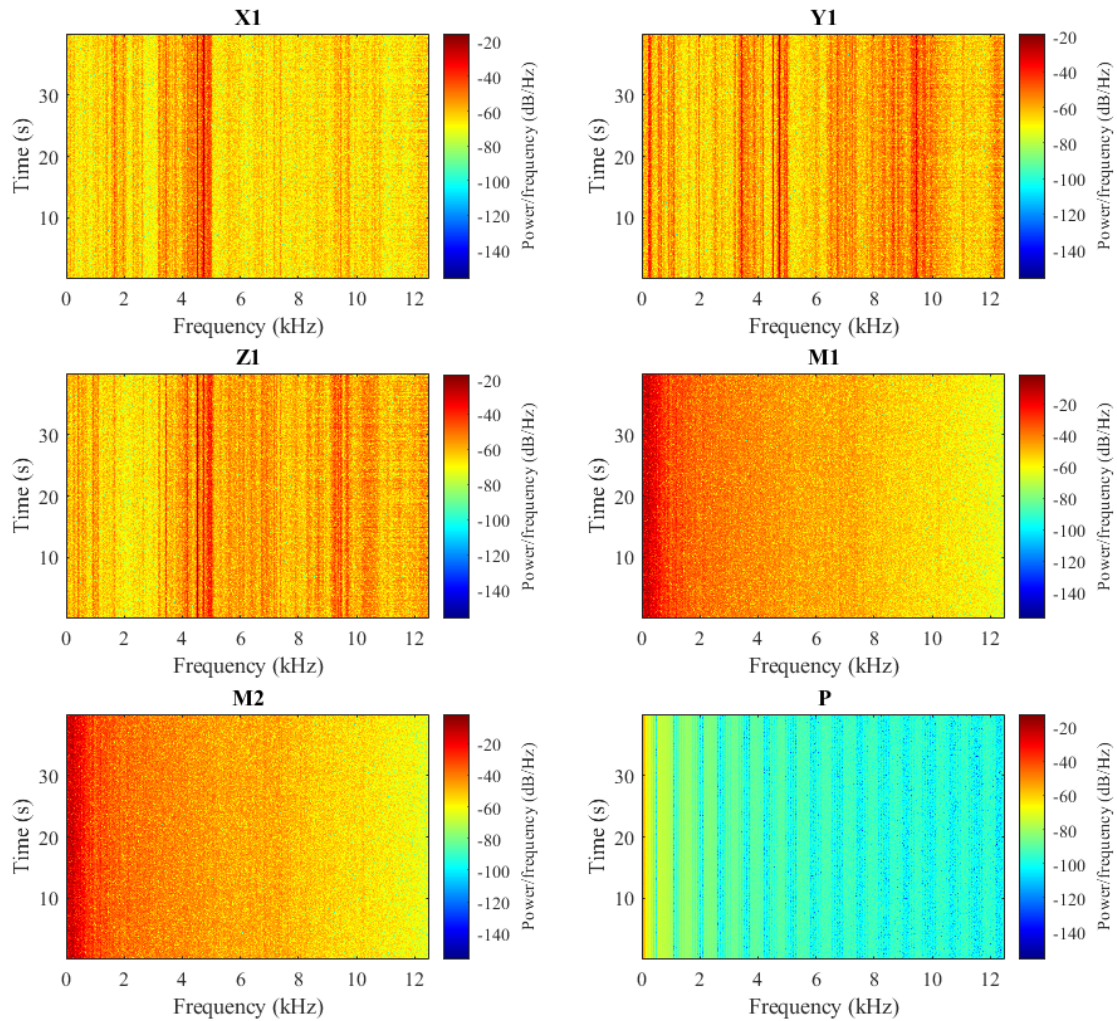


Figure 3.20: Spectrogram of C11 for Accelerometers (X1,Y1 and Z1) both microphones (M1, M2) and pressure oscillations (P).

for analysis. Figure 3.20 depicts the spectrogram for C11 and all its sensors. The spectrogram shows how the frequency content of a signal would vary with time. The colour map indicates the power of the signal with the darker colours being increased power. The key fact of this analysis is that in the case of this combustor the signal frequency content does not vary with time. This indicates that the signals are random by stationary signals. From a combustion perspective this makes sense as the combustor operating conditions were kept constant during the test phase, with the only variable per test point being the fuel. Therefore, we can safely reduce time period analysed per signal without affecting the data. After analysing the spectrograms for each test point, a standard sample window of 10000 samples was arrived at between the 500000th sample and the 510000th sample.

This sampling window was kept constant throughout the analysis and results presented in Chapter 5.

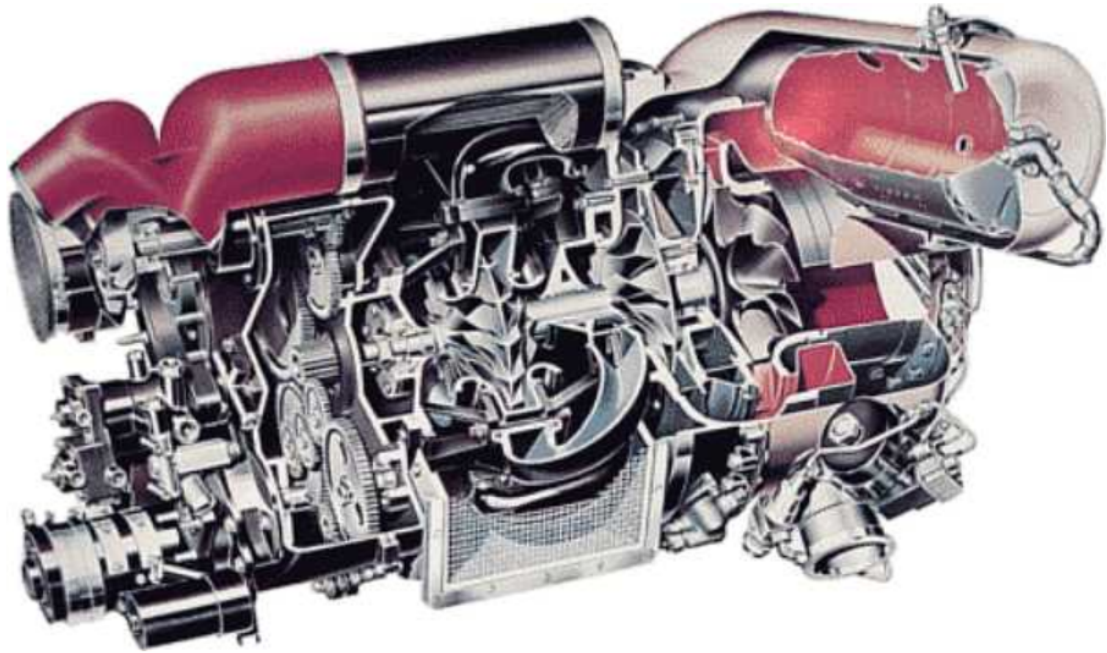
3.6 Gas turbine experimental methods

This section aims to describe the experimental apparatus used to measure the noise and vibrations emanating from a full gas turbine APU (Auxiliary Power Unit). The primary purpose of this investigation was to determine the variation in noise and vibrations caused by the fuel used and to link the vibrations and noise to the fuel properties. To this end the fuels listed in table 3.3 were tested on the APU at 3 conditions where the noise and vibrations data were observed.

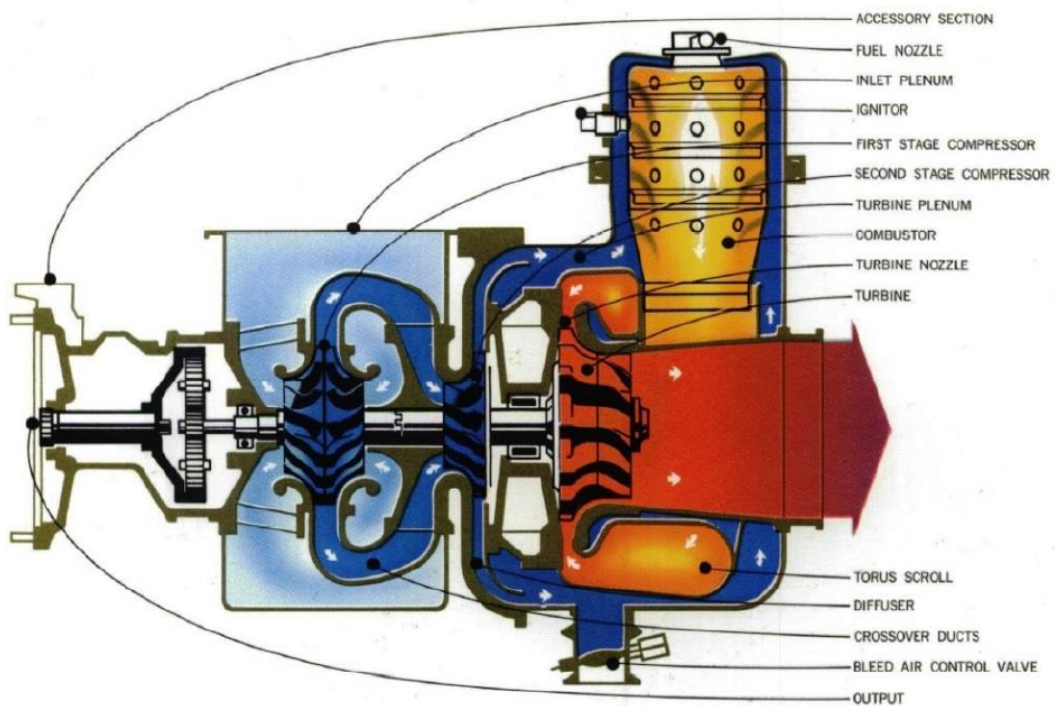
3.6.1 The gas turbine engine

The gas turbine used in this investigation is a Honeywell (formerly Garrett) GTCP85CK type auxiliary power unit commonly found on aircraft such as C-130 Hercules, Boeing 727 and 737(original series and next generation) etc. The model designation stands for 'gas turbine compressor and power'. The APU is also fitted with a 32kW power generator which in practice would be used to provide electrical power to the aircraft whilst on the ground or in the event of a main engine failure whilst airborne. The APU's other main function is to provide compressed air to start the main engines. This function is achieved via a bleed valve from the second stage compressor. The APU uses a 2 stage compression system comprised of 2 centrifugal compressors as shown in Fig.3.21. The compressors provide a overall compression ratio of 5:1. The hot section of the APU is made up of a single can type combustor as described in 2 and a single radial turbine. The bleed air is rated at $58\text{kg}/\text{min}$ at an EGT of 220°C with no shaft power. The shaft power is rated to 150kW and the maximum EGT of the engine is 620°C .

The APU is used as a research engine at the University of Sheffield's Low Carbon Combustion Centre (LCCC) and is mounted in a sound isolated room atop a purpose built frame. pressure transducers and thermocouples have been added to the rig to monitor various temperatures and pressures. The advantage of this particular setup is with respect to



(a) Cutaway image of a GTCP85 type APU unit [139].



(b) Schematic image of a GTCP85 type APU unit [139].

Figure 3.21: APU schematic diagrams.

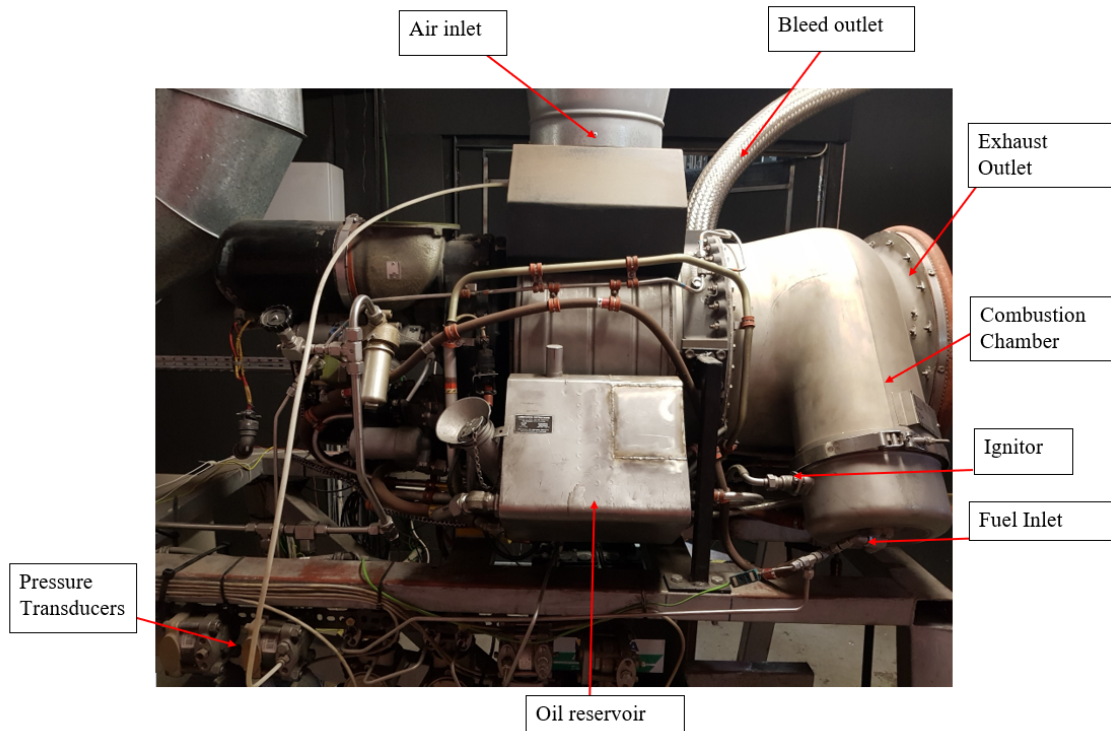


Figure 3.22: Gas turbine and key components.

a lab-scale combustor is that it provides a full scale gas turbine with its turbo-machinery attached, which allows the accurate simulation of combustion phenomena. The advantage of running this rig as opposed to a full- scale propulsion gas turbine is in the cost of operation in terms of maintenance and especially fuel ad the ease of switching fuels.

3.6.2 APU operating procedure and conditions

Table 3.6 portrays the 3 gas turbine test conditions. The APU was operated under 3 conditions named No Load (NL), Environmental Control system Start (ECS) and Main Engine Start (MES) from least to greatest power output and fuel flow rates. The engine condition has been varied by changing the position of the engine bleed valve allowing less or more air to escape into the bleed system.

The APU itself if operated using in house developed lab-view VI's which enable the safe start-up and monitoring of key engine temperatures and other parameters. The VI also controls the bleed air valve position which regulates the engine power output. The fuel for the APU was sourced in the form of 200 litre barrels and a permanent fuel tank which

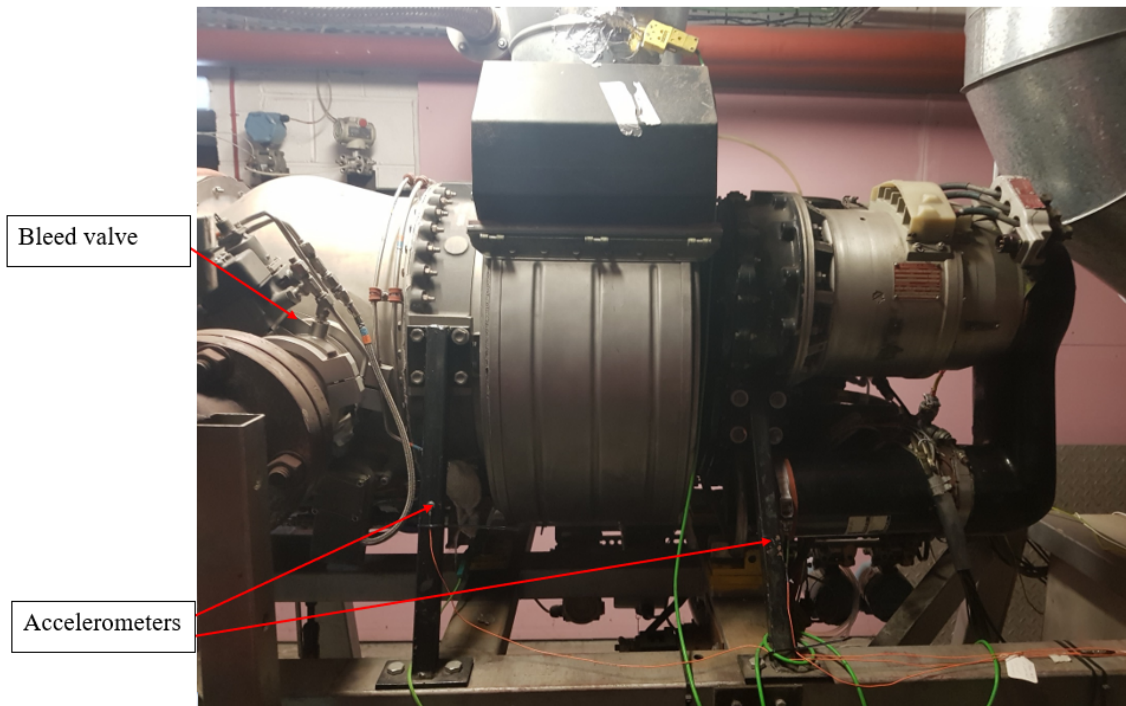


Figure 3.23: picture of APU showing its key components.

Table 3.6: Description of APU gas turbine conditions.

Engine property	Condition 1 (NL)	Condition 2 (ECS)	Condition 3 (MES)
Fuel flow rate (g/s)	18±0.2	25±0.3	32±1.0
Main shaft speed (RPM)	41900±150	40800±300	40100±750
Air/Fuel Ratio AFR	135±3.9	84.4±0.8	62.2±1.0
EGT (°C)	320±6	430±5	570±8

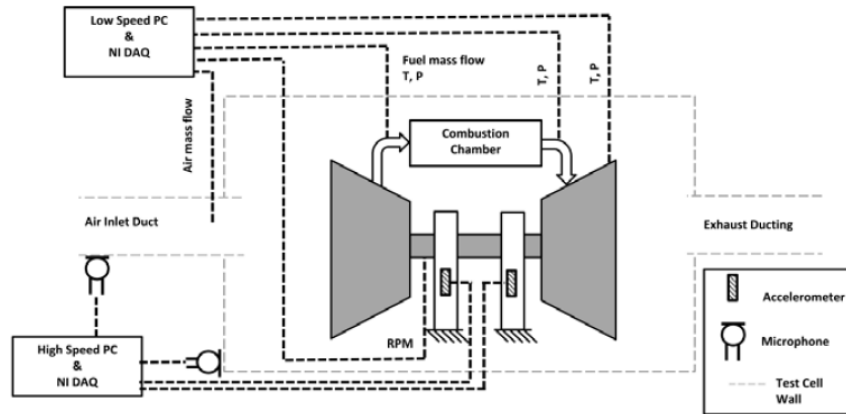


Figure 3.24: APU test bed schematic and sensor locations.

contained conventional Jet A1. The engine would be brought up to operating conditions using the Jet A1 and then the alternative fuel in the barrel would be connected to the fuel lines using a 3-way valve. This enables hot-swapping of fuels and also allows the engine to remain running whilst the next fuel is made ready. For a given fuel the procedure was to bring the engine up to condition 3 and wait for stability, record the data and then reduce to condition 2 and so forth. The length of each test point was approximately 10 minutes of stable running. This increased length of time was required as several experiments were being run simultaneously, including particulate and gaseous emissions over and above then noise and vibrations measured in this investigation. A repeat of each test point was conducted to ensure increased accuracy.

3.6.3 Sensors and data processing

The sensors used in this particular experiment are largely similar to those described in section 3.5.2. 3 accelerometers and 2 microphones were used to measure the noise and vibrations emanating from the APU at a given test point. The data acquisition and processing work flow was identical to that which has been described in section 3.5.2 with the exception that the pressure probe was omitted due to the impracticability of drilling a hole through the combustion liner of a perfectly functional gas turbine. A notable variation of the acquisition process for the APU was the sampling rate, which was increased to 51.2kHz. This step was taken after several pilot tests to determine where the key frequency content of the APU were located in the spectrum. A sampling rate of 51.2kHz

allows a Nyquist frequency of 25.6kHz. This allows the clear visualisation of the highest frequency components of the APU signal which were located around 20kHz. The reason for the increased frequency content in the APU compared to the combustor is the myriad of rotational and moving components of the APU which produces high frequency vibrations.

The microphones were at first mounted inside the sound isolated room where the APU was located (straddling the combustor of the APU), however this proved to be a futile effort as the noise generated by the APU saturated the microphones. The microphones have a maximum dynamic range of 135dB at a reference pressure of $20\mu\text{Pa}$. Indicating that the APU produces a greater noise than the capability of the microphones. It was therefore decided to locate the microphones directly outside the APU room where they could still record the noise emanated from the APU albeit damped by the rooms sound dampening walls. Even through the damping of the walls the microphones were able to pick up noises around the 80dB range.

The accelerometers were mounted on the support arms of the APU as depicted in Fig.3.23 The X and Y accelerometers were affixed to on the right support arm in the figure and the Z accelerometer was affixed to the left support arm of Fig.3.23. The reason for not fitting the accelerometers directly to the combustion chamber or the main APU body itself stems from the temperature tolerance of the accelerometers and the difficulty of finding a flat surface onto which a solid contact can be made with the accelerometers.

Moreover, it should also be noted that like the combustor testing the signals emanating from the APU were classified as random stationary signals as the signal did not change during the recording interval. This is attributed to the engine being at stable condition when the recordings were obtained. Transient signals obtained at start-up and shutdown are outside the scope of this investigation. The spectrogram for RF14 is depicted in Fig. 3.25. As is clearly visible from the figure the signal does not change with respect to time, as indicated by the vertical stripes on the sub figures. The stripes themselves indicated increased power frequencies in the spectrum, the greatest of which is located around 21kHz which is well below the Nyquist frequency of 25.6kHz.

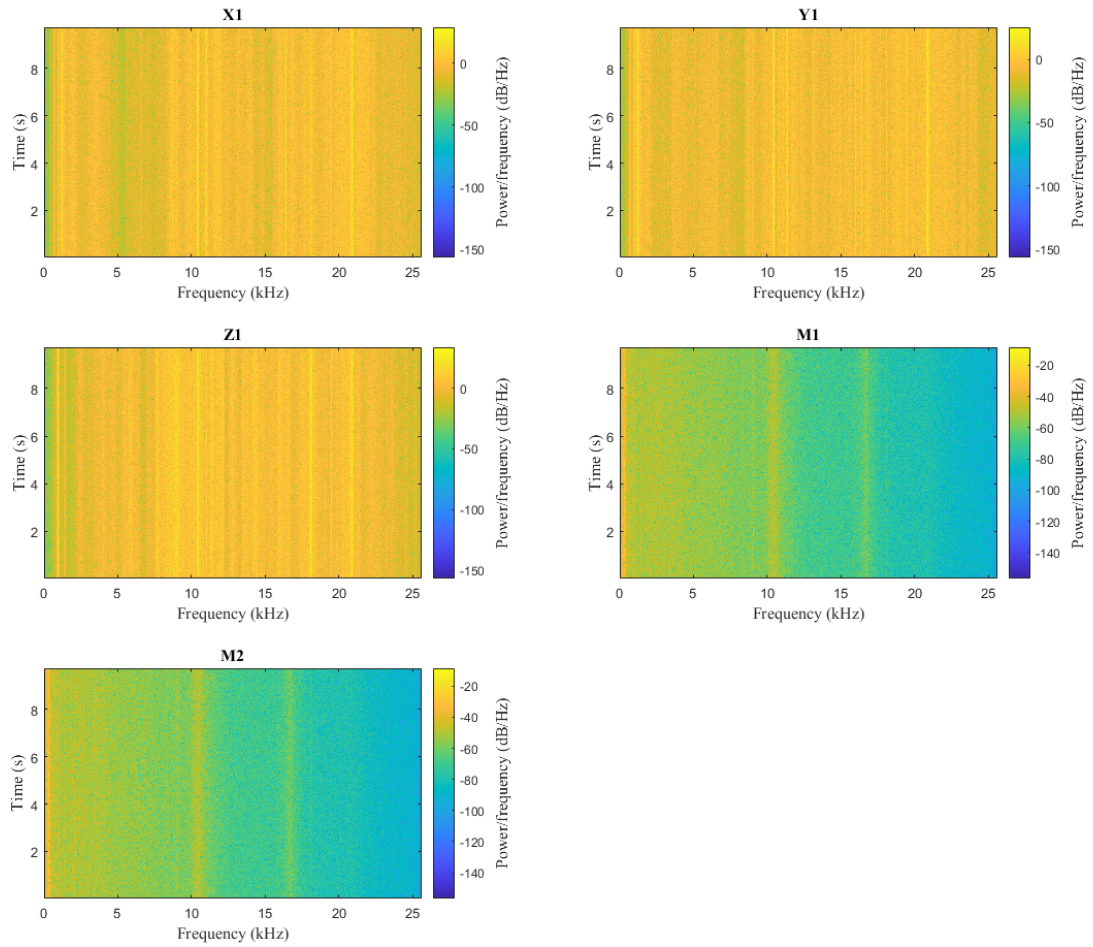


Figure 3.25: Spectrogram of 3 accelerometers X1, Y1, Z1 and 2 microphones M1, M2 for fuel RF14.

Chapter 4

Spray characteristics of low aromatic and alternative fuels

4.1 Introduction

The importance of fuel injection methods and fuel atomization characteristics of those methods has been well described in the literature [97, 98, 102, 103, 105, 140–144]. Also, there are large number of studies in literature detailing impact of bulk conventional fuel properties on atomization and spray characteristics. Though there is a lack of knowledge around how different alternative fuels, especially with selected species of aromatics would impact the atomization and spray characteristics. Hence in this investigation it was considered prudent to compare how the chosen fuels behaved when injected through a gas turbine fuel injector, therefore this chapter details the atomisation testing conducted upon aromatic jet fuel surrogates and some fully synthetic ready to use jet fuel detailed in the fuel details chapter 3. Another contribution to knowledge which this chapter would deliver is how different aromatic structures, bonds and other micro properties of aromatics species impacts spray and atomization. One of the major outcome of this particular study is to investigate how these alternative and aromatic fuels perform in the fuel injection phase of combustion. To achieve this objective testing was conducted at using a spray chamber test rig and laser particle sizer. It was found that the droplet sizes in the form of SMD correlate well against the fuel properties of density, viscosity and surface tension. New knowledge

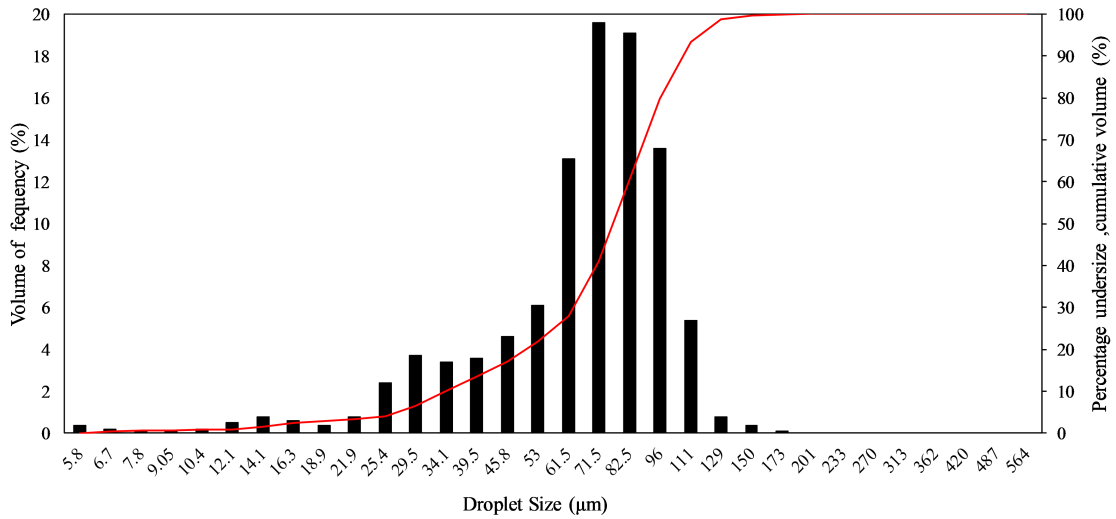
was found in the spray characteristics of several aromatic species with the best performers being Ethylbenzene, Cumene and Tert-Butylbenzene. Which indicates that the size of aliphatic groups attached to the benzene ring in the aromatic molecule has an impact on the drop-size and therefore the combustion characteristics. The worst performers were the poly-aromatic naphthalene compounds.

4.2 Results and discussion

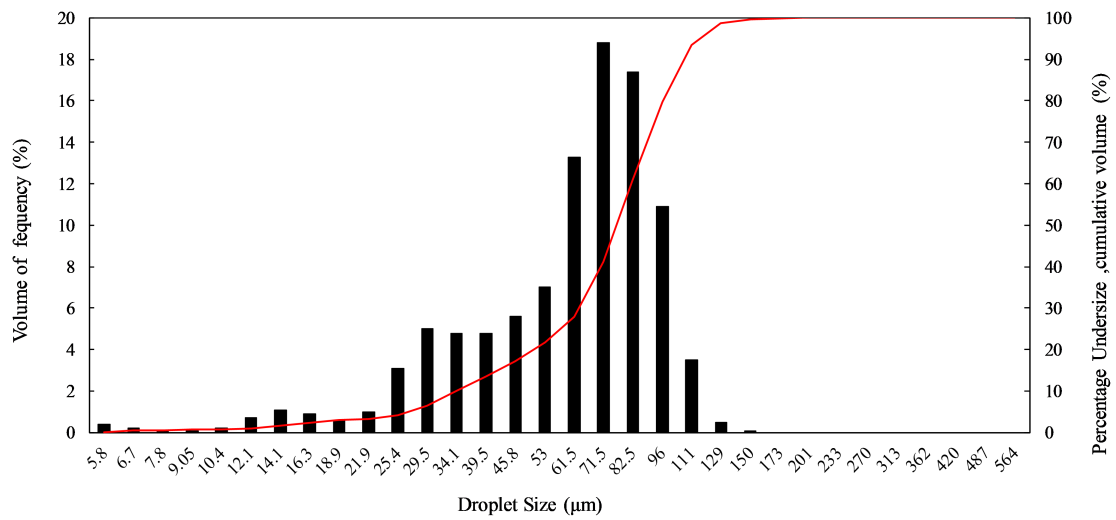
This section depicts the results and the discussions surrounding the results obtained during the droplet size analysis. The fuels used in this investigation are the 16 Aromatics depicted in table 3.1 blended with banner NP1014 in two ratios 8% known as the A group (fuels A1-A16) and 18% known as the B group (fuels B1-B16). Also tested in this investigation are the reference fuels described in table 3.3. These fuels were then tested as using the apparatus described previously in the experimental setup section. The fuels were tested at 3 specific fuel injection pressures 50psi (3.45bar), 60psi (4.13bar) and 70psi (4.83bar). The air assist pressure was kept constant at 1bar . The experiment was conducted under room temperature conditions of 20°C over the period of several weeks. Three repeats were conducted for each test point and the average taken for the variables collected.

4.2.1 Droplet size distributions

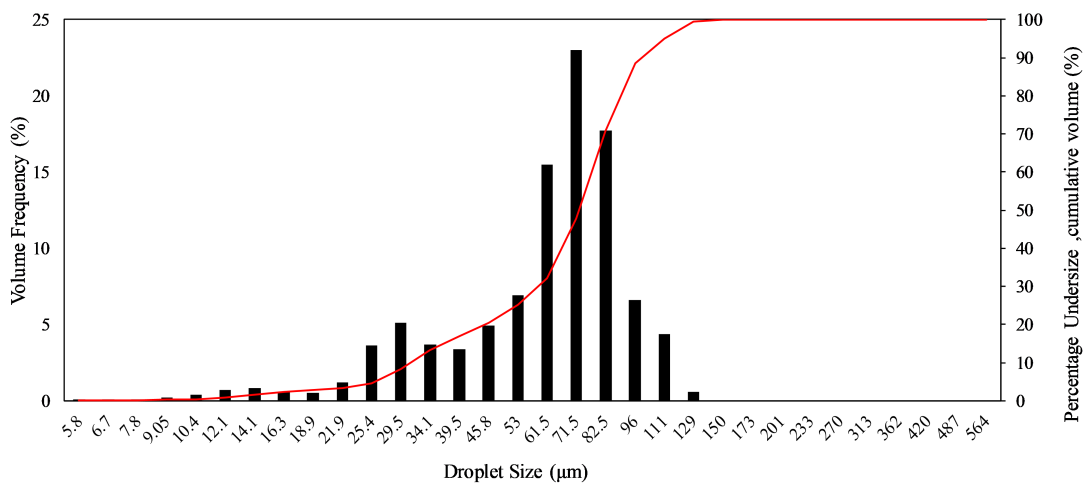
The first set of data of note stems from the droplet size distributions themselves. Figure 4.1 depicts the droplet size distributions for reference Jet A1 at injections pressures 50psi (Fig. 4.1a), 60psi (Fig. 4.1b) and 70psi (Fig. 4.1c). The horizontal axis portrays the droplet size in bins (due to space considerations and clarity only one bound of the bin is depicted). For instance, the peak at $61.5\mu\text{m}$ of Fig. 4.1a corresponds to the % volume of droplets that fall in-between $61.5\mu\text{m}$ and $71.5\mu\text{m}$. The minimum droplet size detected by the Malvern was $1.5\mu\text{m}$. The left vertical axis depicts the % total volume of droplets detected per bin (i.e. for Fig. 4.1a around 19% of all droplets detected fell into the $71.5\mu\text{m}$ - $82.5\mu\text{m}$ category). The right vertical axis corresponds to the cumulative frequency (the crimson line), which for Fig. 4.1a shows that around 90% of droplets fall below $111\mu\text{m}$.



(a) Jet A1 Frequency undersize plot for 50psi injection pressure.



(b) Jet A1 Frequency undersize plot for 60psi injection pressure.



(c) Jet A1 Frequency undersize plot for 70psi injection pressure.

Figure 4.1: Jet-A1 droplet size distribution and cumulative frequency charts

An interesting feature of Fig. 4.1 is the slight bi-modality of all three sub-figures. It is clearly visible that the main volume of counts is in the 71.5-82.5 micron bin for all three pressures, however there is a smaller peak centred around the 29.5-34.1 micron bin. This phenomenon comes into better focus at the highest injection pressure of 70psi where the second peak is more consolidated and visible. This slight bi-modality can be explained by the twin fluid nature of the injector where the fuel at the edge of the fuel sheet is encountering the greatest impingement from the atomization air and is undergoing a more rapid atomization process resulting in smaller droplet sizes and a second peak in the figure. It should also be noted that all the fuels tested show a similar droplet distribution pattern with the exception of a few outliers where the misting of the cubicle skewed the results to impossible drop sizes in excess of 400 microns.

Furthermore, it can also be seen that as the injection pressure increases in 4.1 the distributions become sharper and consolidated. That is to say the peaks become narrower and more defined, for instance with respect to Fig. 4.1a, Fig. 4.1c shows narrower more defined peaks. This is in keeping with the literature where increased injection pressures show sharper and more uniform atomization [145, 146].

Figure 4.2 depicts the size distributions at the 3 injection pressures overlaid on each other for the fuel RF2 which is a JP-8 fuel considered the nominal fuel used in this investigation. This holds to the trend that as the injection pressure increases the droplet distribution becomes more consolidated and the peaks narrower indicating a more uniform atomization; in keeping with the literature. Again, a minor peak is visible at a lower mean diameter which can be attributed to the twin fluid nature of the atomiser. One interesting aspects of Fig. 4.2 is that the 70psi peak is much stronger than that of the other two injection pressures indicating that a step change in the atomization mechanism is taking place. It might be postulated that as the pressure approaches 70psi the atomization is advancing to becoming what is known as ‘prompt’ atomization [95]. Where the fuel velocity is appreciably higher and is being shot into what is effectively a stagnant flow field and the fuel has limited opportunity to form into the ligaments and strands and waves structures mentioned in the literature review. Instead the fuel is immediately disrupted into fragments without the process of primary and secondary atomization occurring (classical

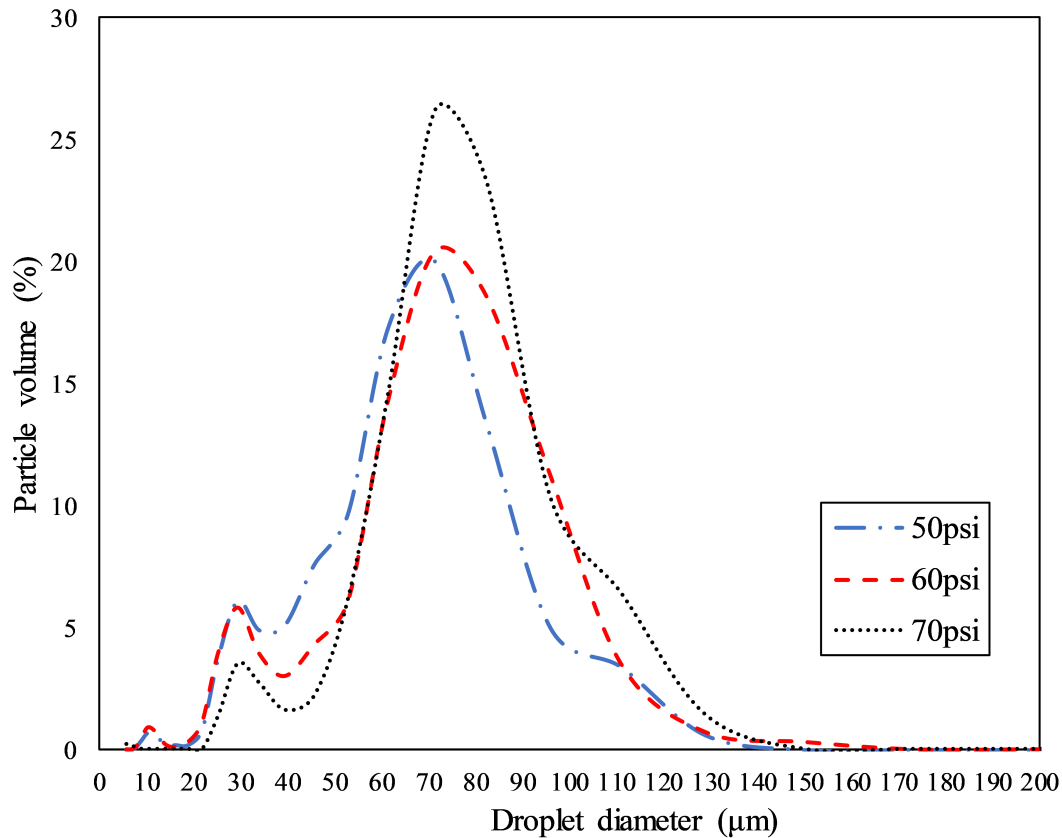
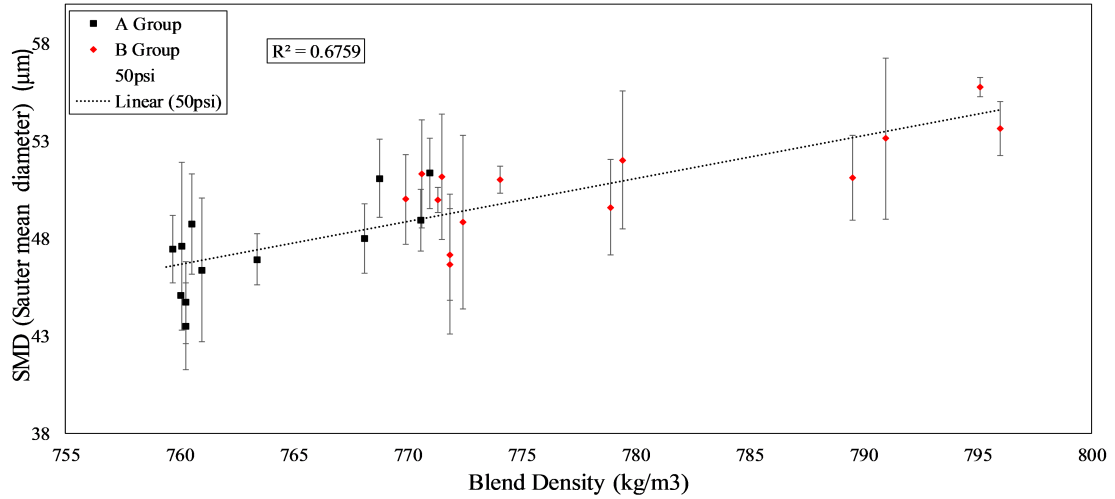


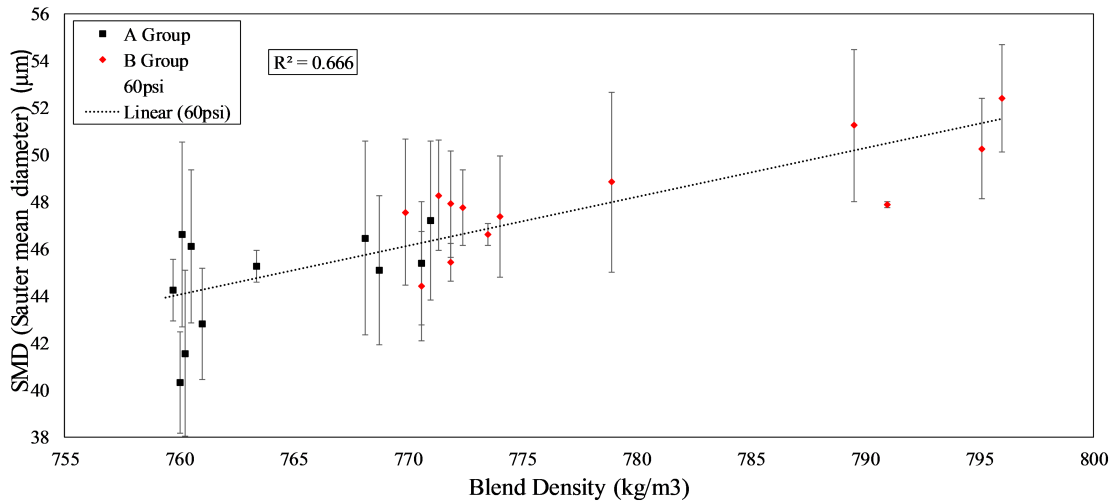
Figure 4.2: Injection pressure comparison of fuel RF2.

atomization). However, Lefebvre et al. goes on to state that prompt atomization if occurring would cause drop diameters to be independent of liquid characteristics such as viscosity. This was found not to be the case later on as the viscosity plots show a small correlations [68]. It should also be noted that the method of atomization is highly dependent upon the operating conditions of the atomiser, and it is also possible that inside a combustor this atomiser would not behave the same way as it would inside the spray cubicle which has almost stationary airflow save for the presumably slight suction created by the extraction system in place. Whilst this may not be an absolutely accurate depiction of spray behaviour inside a combustor it would be plausible to consider this setup meaningful in comparing the behaviour of several fuels.

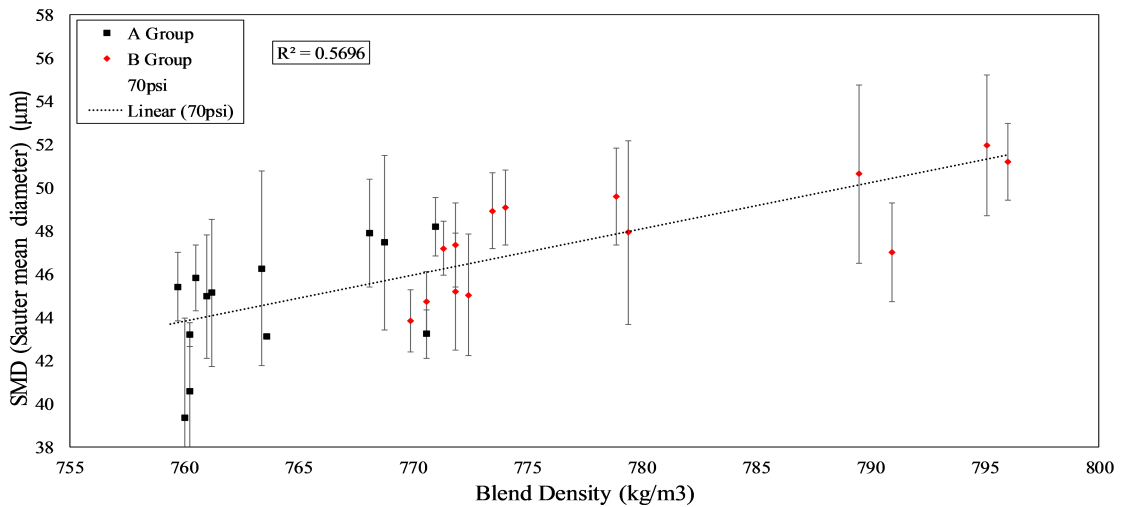
Figure 4.3 depicts the SMD against the blend density for the aromatic blends both A group and B group for the 3 injection pressures. Firstly, of note is that as expected the A group have a lower SMD on the whole with respect to B group. This is due to the A group being blended with only 8% by volume of aromatics as opposed to B group which had



(a) 50psi injection pressure.



(b) 60psi injection pressure.



(c) 70psi injection pressure.

Figure 4.3: SMD plots for fuel groups A and B against the blend density.

18%. This holds true for all injection pressures. Secondly, all three plots show a positive correlation with respect to blend density with an R^2 value of at least 0.5. This is in keeping with the literature where the increased density would impede the atomization process. However, it should be noted that ASTM D1655 allows for a total fuel density range of $775\text{-}840\text{kgm}^{-3}$ [25]. The majority of the A group have densities around 760kgm^{-3} and the B group coalesces around 770kgm^{-3} . The worst performers were Indene (A5 and B5) and Methyl naphthalene (A14 and B14) respectively. Both of these aromatics are polycyclic meaning they have more than one carbon ring with at least several double bonds between them as well as the highest density compound densities of all the aromatics tested. Therefore, it is to be expected that they would spray poorly. The effect of density on droplet formation is well known in the literature where as the liquid density increases the droplet sizes increase as the greater mass of the liquid in a given volume has a greater resistance to the injection forces. Hence for a given atomisation pressure a denser liquid will have larger droplet sizes [145, 147]. The best performers were the least dense compounds Tert-butylbenzene, Ethylbenzene and Cumene all of which corresponds to a blend density of 760kgm^{-3} the lowest tested in the A group. The B group showed similar results. A compound significant in its absence from the best performers list is Toluene the simplest possible aromatic (therefore the least dense) with the exception of pure benzene. Toluene performed just above the best aromatic compounds at the trend line. This would indicate it to be within the 1 standard deviation confidence interval. Furthermore, it is clearly visible the correlations are a little dispersed, this can be attributed to the droplet sizer used in this investigation; a multiple laser setup would provide a cleaner trend as more data points per spray would be obtained from a different angle increasing the measurement accuracy. Another observation is that with the increase in injection pressure the R^2 value drops indicating poorer correlations, this may be attributed to the fact that we are approaching the prompt atomization thresholds and some of the droplets are instantaneously atomised.

Figure 4.4 depicts the A Groups SMD normalised to Jet A1 (RF1) as can be seen the blends with the simpler aromatics perform better than the Jet and the poly cyclic aromatics perform poorly. It should be noted that RF1 is a relatively dense Jet A1 (803.2kgm^{-3})

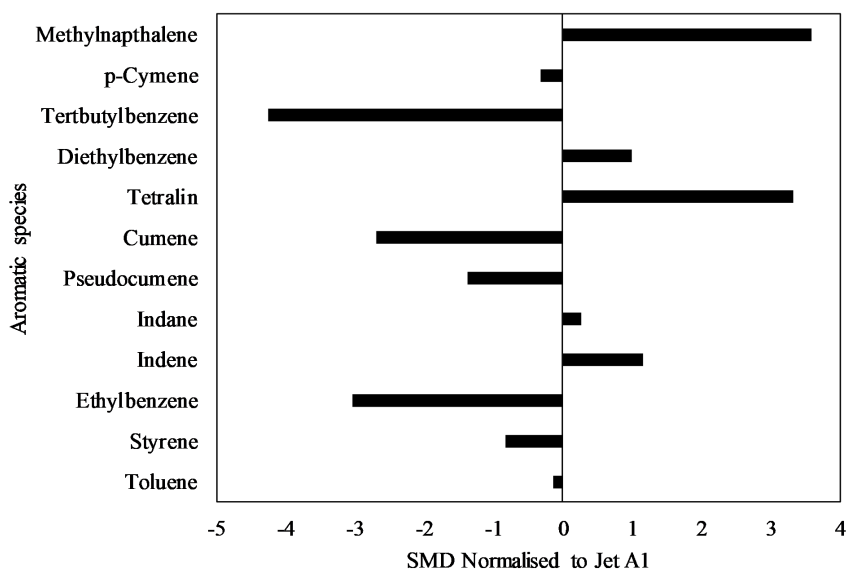


Figure 4.4: SMD of aromatics normalised to Jet A1 (RF1).

with an aromatic content of 19% by mass although the exact composition of the aromatic content remains unknown. With this information it would be natural that most of the blends would outperform the nominal Jet A1. A more useful comparison is made in Fig. 4.5 with JP 8 the best possible jet fuel available to this investigation with an aromatic content of only 13%. Here we can see that most of the aromatic blends perform poorly with respect to RF2 which is much less dense at only 779.9 kg m^{-3} which is just within the regulations. Here the only compounds that manage to outperform RF2 are Ethylbenzene, Cumene and Tert-butylbenzene. An interesting fact that the SMD against density curves show is that chemically the aromatics that are closest to pure benzene (i.e. with a benzene ring a few methyl groups) tend to be denser than compounds with a larger aliphatic group attached indicating that the benzene ring is disproportionately contributing to the density of the compound. This is reflected by the fact that the best performers were mono-aromatic compounds with large aliphatic-groups attached. This effect is further emphasized by the poly-aromatic compounds which overall performed the worst in this investigation (Methylnaphthalene, Indene, Indan and Tetralin). Even amongst the poly compounds, the worst performer was Methylnaphthalene which is the only true poly aromatic compound tested (with 2 full benzene rings in the molecule) the others only having an Ali-cyclic group attached to the benzene ring.

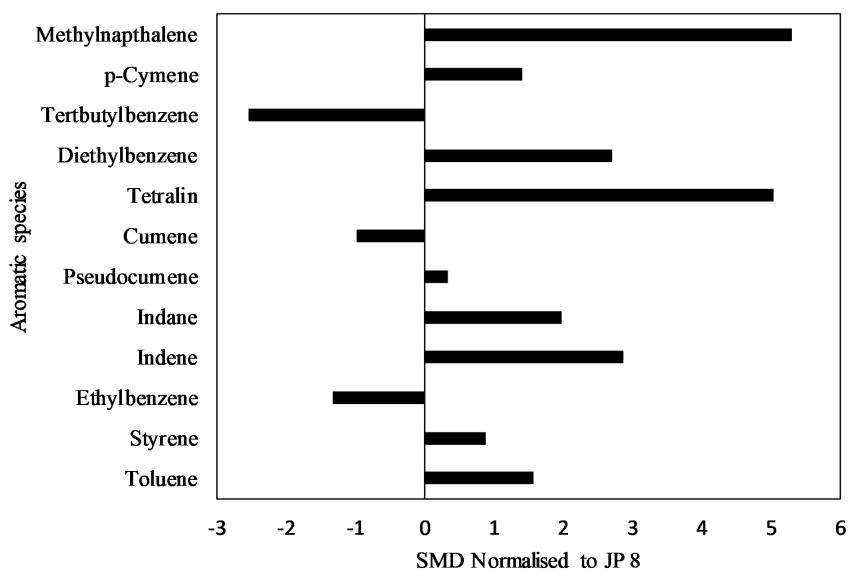
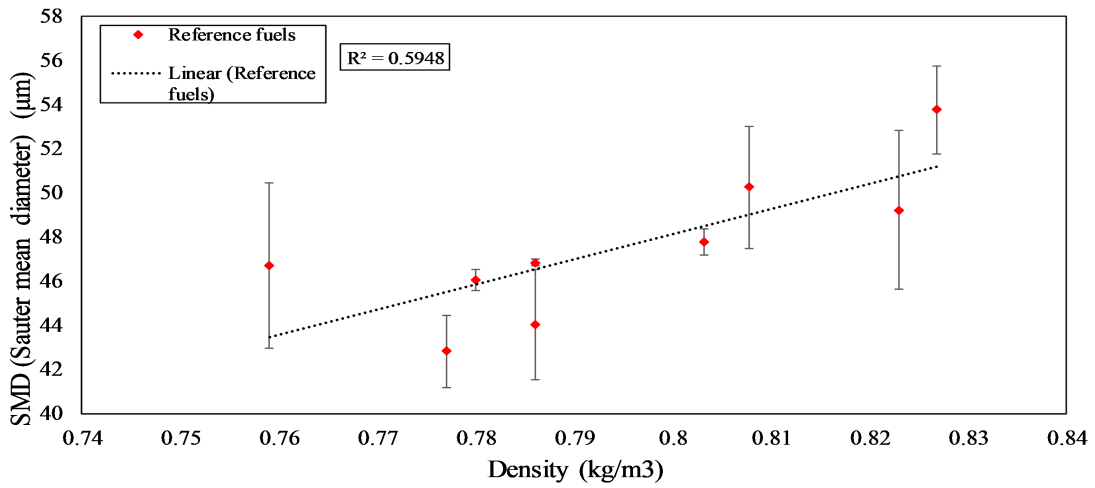


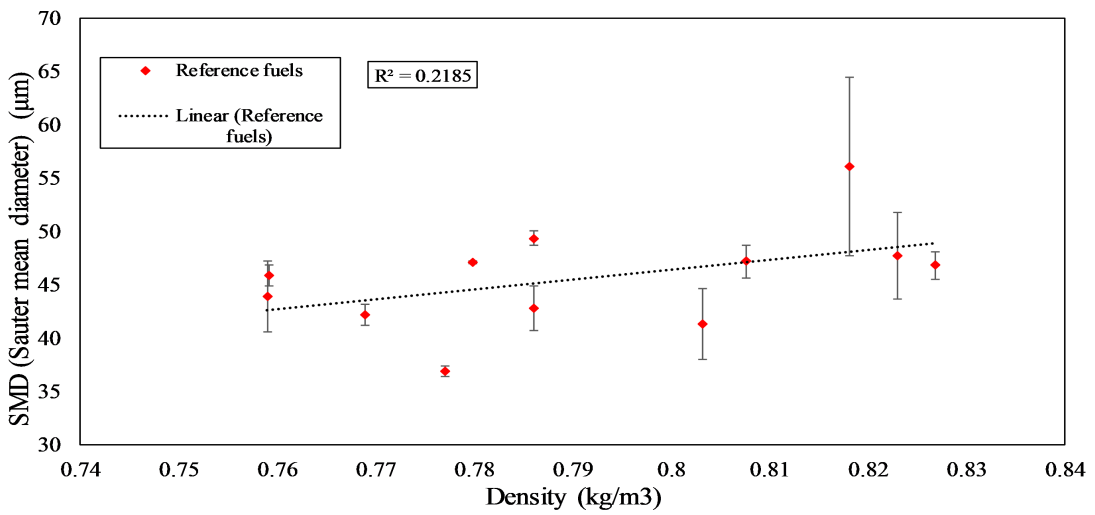
Figure 4.5: SMD of aromatics normalised to JP 8 (RF2).

Figure 4.6 depicts the SMD against density for the reference fuels against their density for the three injection pressures. At 50 *psi* the correlation is relatively sound with an R^2 value greater than 0.5 however it degrades to around 0.2 with increasing injection pressure. It is plausible that as the injection pressure increases the atomization mechanism changes from classical to prompt atomization. Furthermore, it should be noted that at 70 *psi* there exists an outlier coming in at 43 μm which corresponds to RF1 which is due to suspected experimental error with regards to the time in-between tests which mists up the cubicle. Moreover, reference fuels RF5, RF7, RF8 and RF9 are not depicted in the 50 *psi* plot as they were not conducted due to lack of fuel (50 *psi* was the last series of tests conducted) and the inability to replace these fuels which were left over from other experimental campaigns at the LCCC. The best performing fuel amongst the reference fuels in terms of SMD was the RF4 fuel which was a 100% ATJ fuel with less than 1% aromatic content. The worst performing fuel was as expected fuel RF3 which is the worst case JP5 fuel with a very high flash point and an aromatic content exceeding 20%.

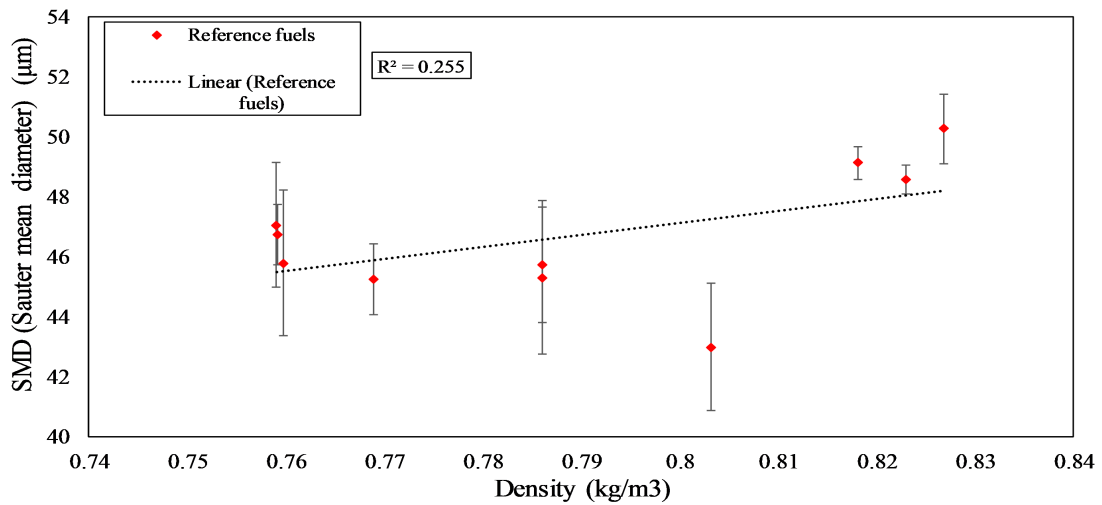
Furthermore, it should be noted that compared to the aromatic blends the reference fuels show poor correlations on the whole, it is theorized that this is due to three possible reasons; firstly that the density ranges of the fuels are closer together with respect to the aromatic blends which causes even minor deviations in the SMD to have a greater impact



(a) 50psi injection pressure.



(b) 60psi injection pressure.



(c) 70psi injection pressure.

Figure 4.6: SMD plots for reference fuels against their density.

on the R^2 value. The second and more likely reason for this is due to the fact that the reference fuels compositions are more complex and other components than aromatics may be impacting the spray characteristics. Finally, it is also known that density is not the only variable of a liquid that would affect the spray characteristics and with a multitude of chemical compounds it is possible that for example; a compound with relatively low density but high viscosity and surface tension would degrade the spray characteristics of a given reference fuel. The following section will focus on deeper explanations of the impact of fuel properties on droplet formation.

4.2.2 Comparison against fuel properties

This section aims to explore how various other available fuel properties have an impact on the spray characteristics of the fuels. This section only pertains to the reference fuels as the standard tests required to obtain the data are cost prohibitive and therefore have not been applied to the aromatic blends. Figure 4.7 depicts the SMD for the reference fuels against their surface tensions measured in dynes ($gcm\ s^{-2}$). As can be seen there is a slight correlation with an R^2 value of greater than 0.2. This is in keeping with the literature as surface tension is one of the key variables in determining spray characteristics and droplet formation as explained in the Section 2. The reason for the lower correlation coefficients can be explained by the fact that the entire range of viscosities are less than 5 dynes. As per table 3.3 it should be noted that the surface tension data for fuels RF11, RF12 and RF13 were unavailable and therefore are not represented in Fig. 4.7.

Figure 4.8 depicts the viscosity in centistokes ($mm^2\ s^{-1}$) against the SMD of the reference fuels. A slight positive correlation with increasing viscosity was observed. Again, the viscosity range in question is very small for these fuels at only 1.4 centistokes even less than the range for surface tension. The correlation is again in keeping with the literature as the ease with which a liquid is able to flow is crucial to how it would be have under atomization conditions.

Figure 4.9 portrays the derived cetane number of the reference fuels against their SMD. This show effectively no correlation implying that cetane number of a fuel is independent of its spray characteristics. This is to be expected as the spray characteristics of a given fuel

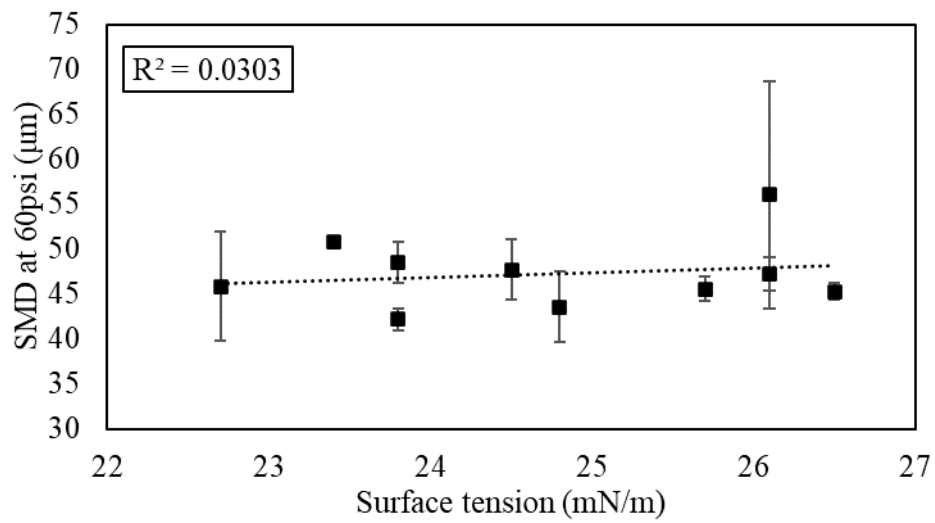


Figure 4.7: Reference fuel SMD against surface tension at 60psi.

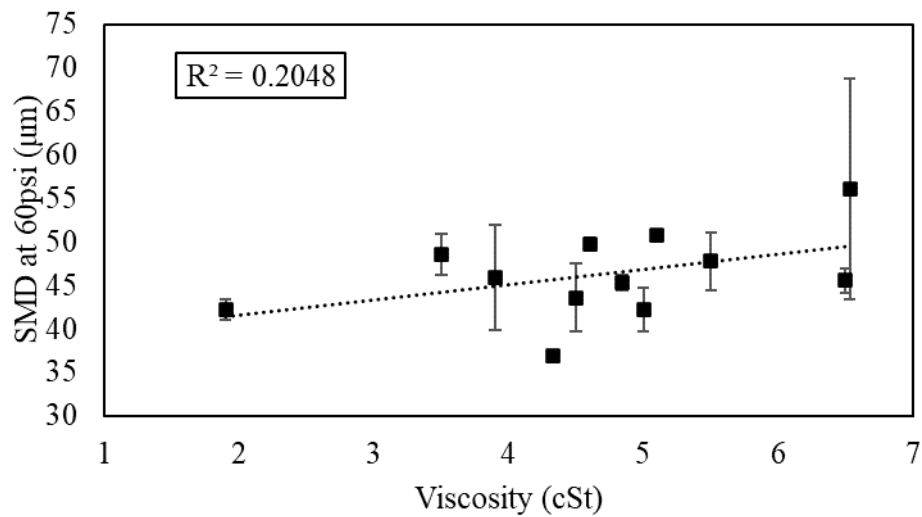


Figure 4.8: Reference fuel SMD against viscosity at 60psi.

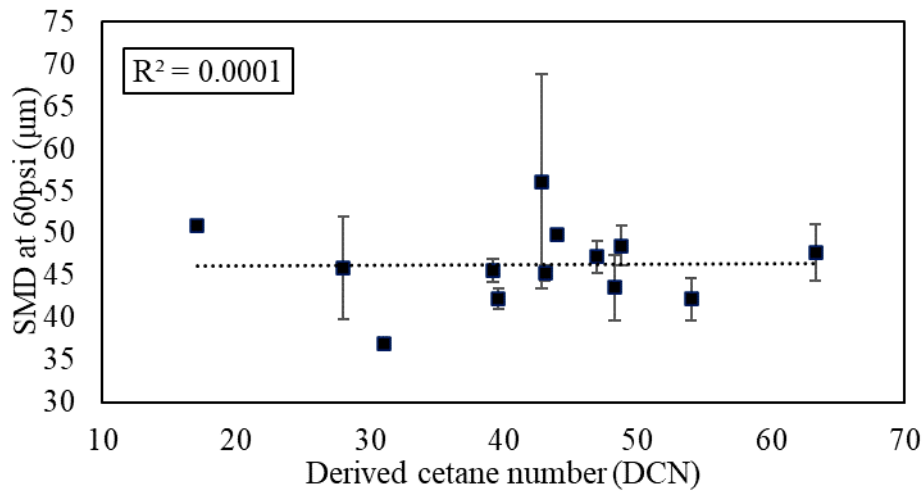


Figure 4.9: Reference fuel SMD against derived cetane number (DCN) at 60psi. Red marker indicates RF8.

is heavily dependent on its bulk fluid properties but cetane number is more dependent upon the bond and activation energies of the individual compounds in a fuel. Which means that cetane number is impacted disproportionately by certain compounds such as di-tert-butyl peroxide which increases a fuels cetane number and compounds such as of pentamethyl heptane which reduces the cetane number. Jet fuels in general have high cetane numbers which is useful in producing good combustion characteristics. Whilst the cetane numbers of the aromatic blend have not been tested, the solvent used to achieve the blends must have an extremely high cetane number as it contains at least 22% by volume pure cetane which has a cetane number of 100.

Two sources from the literature have been selected to validate this study against. Firstly, the study conducted by Vouros et al. which has been described in Chapter 2 and specifically Fig. 2.37 [102]. Where they have measured the SMD of several fuel blends considering the total aromatic paraffin content at different radii of the spray and varying distances from the from the discharge nozzle. They also verify the trends we have seen with respect to density, viscosity and surface tension. Furthermore, the absolute values for SMD for all their fuels are within the $40\mu m - 50\mu m$ range as are the ones measured in this study lending credence to the accuracy of our measurements.

Secondly, some of the same reference fuels were tested by Buschhagen et al. and the

results published the injection pressures used were similar so was the atomiser [105]. Although the measure position is quite different and so was the spray angle generated by their injector. However, they have produced an SMD graphs with respect to injection pressure as shown on Fig. 4.11. The curve for this investigations data is depicted in Fig. 4.10. As can be seen the figure the trends are similar, however the absolute SMD values are much higher for the reference curve, this is explained by the fact that their measurements were taken much closer to the discharging orifice with respect to this investigation. Which means the Droplets analysed by Buschhagen et al. are probably still in the primary atomization zone as opposed to this investigation. However, it should be noted that these 2 sources provide a good validation for this study; whose aim has been to identify which aromatic compounds affect the spray characteristics the least.

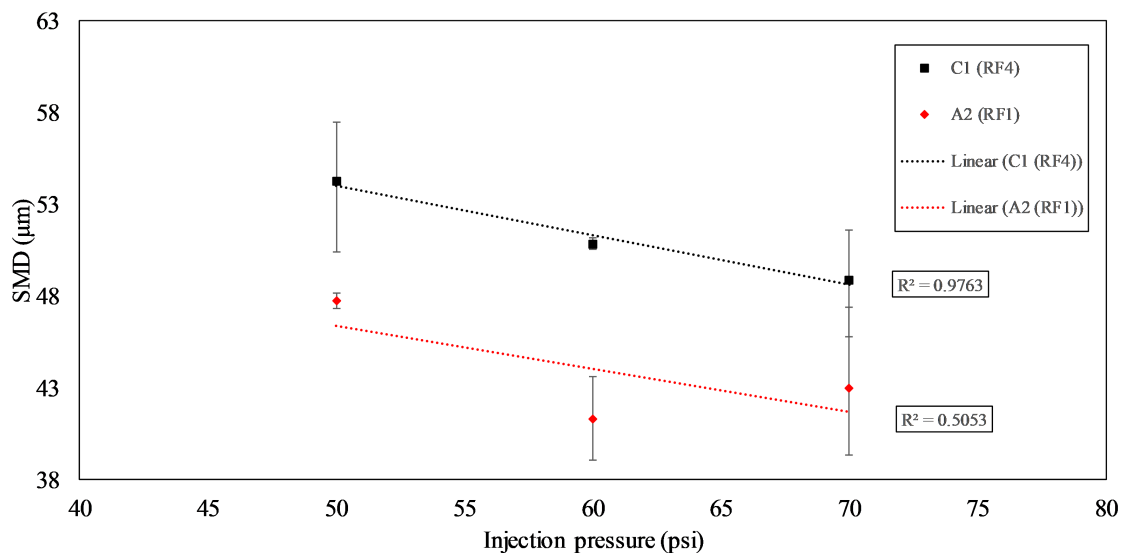


Figure 4.10: Injection pressure comparison of fuel RF1(A2) and RF4(C1).

Figure 4.12 depicts the experimental results against those calculated using a modified version of Nukiyama Tanasawa equation for experimental characterisation of SMD for twin-fluid atomisers depicted in equation 2.6 [94]. Furthermore it should be noted that this equations primary purpose is to derive the characteristics of a given injector not to observe the impact of a various fuels on a single injector which is why the ALR and other constant features (in this investigation) are more prominent in the equation as opposed to the fluid properties of the fuel. The original equation has been modified by using the Air-Liquid ratio instead of the individual volume flow rates as that data was not available.

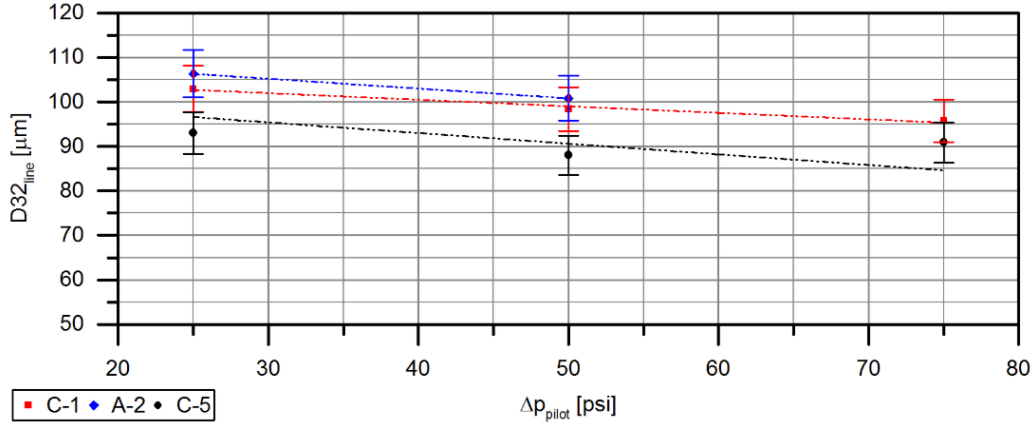
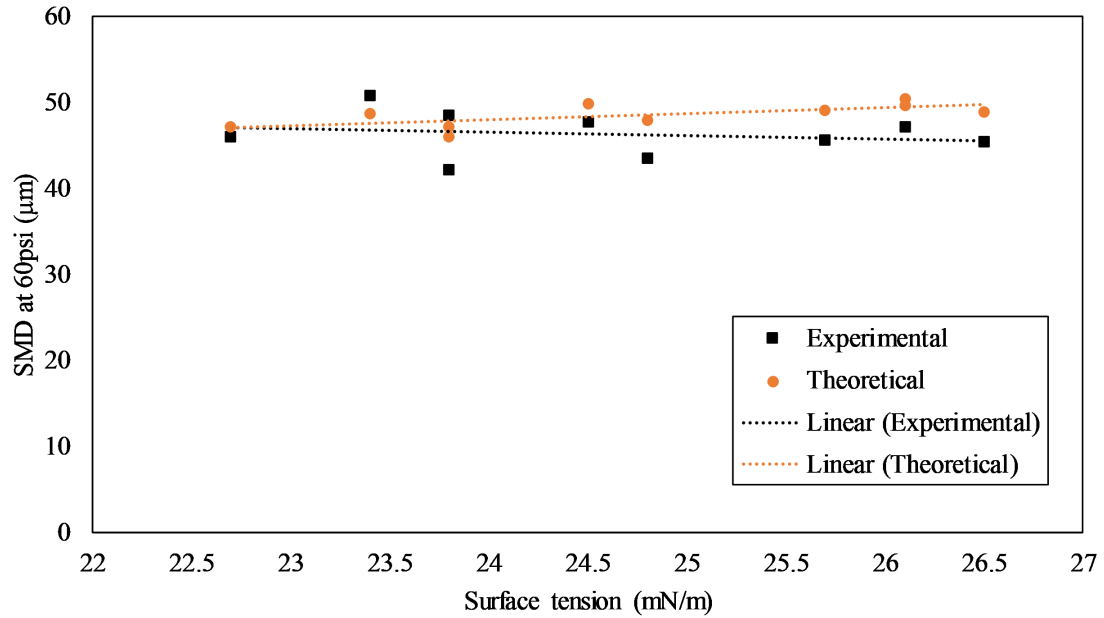


Figure 4.11: Injection pressure comparison for two reference fuels from Buschhagen et al. [105].

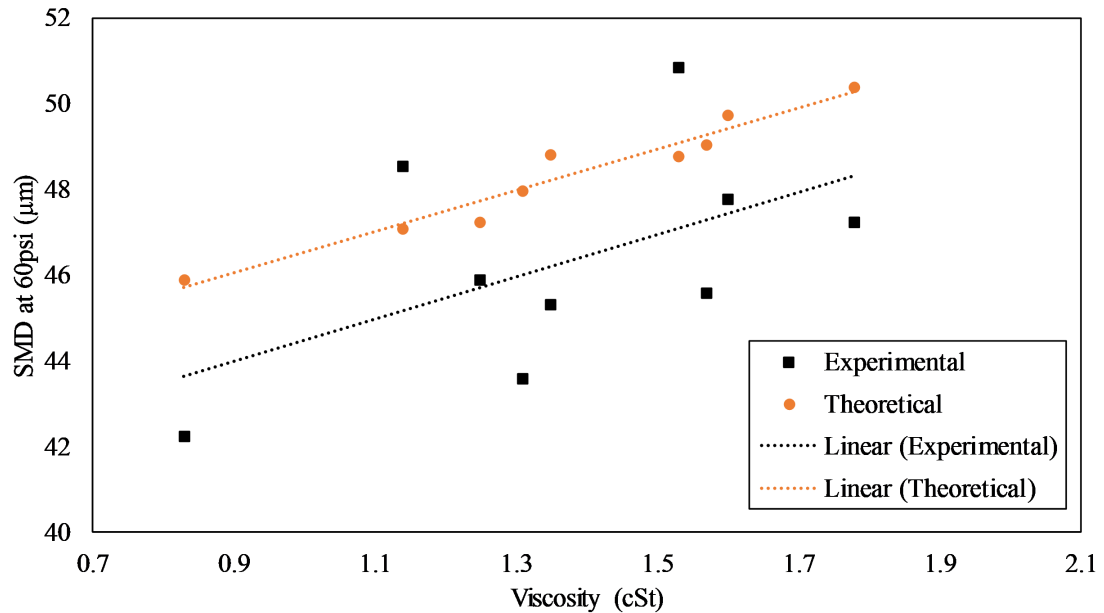
Moreover, as the differential velocity between the liquid and the stationary air has been back calculated from SMD value for Jet A1 as the differential velocity could not be measured in this investigation. The modified equation is depicted in 4.1 . As can be seen from the figures the viscosity and surface tensions of the fuels correlate well with the theoretical values. Moreover, it can be seen that for both surface tension and for viscosity the results for theoretical and experimental tends to get closer together with increasing SMD and base variable indicating that the experimental accuracy increases with increasing SMD, this is as it should be as the larger the droplet sizes the better they can be detected by the detectors in the Malvern. It is of obvious note that the trends are slight in both the experimental and theoretical values. This can be attributed to the fact that in the grand scheme of things all the fuels tested were very similar in fuel properties less than 17% variation in the range for surface tension and 40% variation in range for the viscosity. This is as it should be as there would little be utility in testing fuels with large property variations which would obviously be poor quality fuels.

$$D_{32} = 0.585(\sigma/\rho_L U_R^2)^{0.5} + 53(\mu_L^2)^{0.225}(ALR)^{1.5} \quad (4.1)$$

Finally, it should be noted that this investigation has tested several surrogates of aromatic blends and found that density, surface tension and viscosity play a key role in their spray characteristics in keeping with the literature [97, 102, 105]. Furthermore, it was



(a) Theoretical vs experimental SMD against surface tension.



(b) Theoretical vs experimental SMD against viscosity.

Figure 4.12: Theoretical vs experimental comparison for SMD.

found that the benzene ring in particular contributes to molecular density disproportionately and this is reflected in the experimental results by the fact that the best performing aromatics were those with a large aliphatic group attached to the benzene ring. In keeping with this hypothesis, it is possible to conclude that the worst performers were the molecules with 2 benzene rings (i.e. poly-aromatic hydrocarbons) again this has been reflected in the experimental results. It would be prudent in future to test aromatic compounds with even greater aliphatic groups attached as this would presumably result in better spraying characteristics, however it remains to be seen whether this type of compound can still effectively contribute to the lubricity and seal swell capability expected of jet fuels.

4.3 Conclusions

With respect to new knowledge the best and worst performing aromatics have been identified with a view to determining what aromatic can be added to jet fuel whilst impacting the spray characteristics the least and yet maintaining the crucial role they play on lubricity and seal capability. The best performing aromatics were the Ethylbenzene, Tert-Butylbenzene and Cumene. Which it should be noted are aromatics with a branched aliphatic compound attached which stands to affect the compounds density which would explain the better spray characteristics. Another way to describe this phenomenon is to say the compounds with the least aromaticity. Furthermore, as it is widely accepted that larger drop sizes correlate to poorer combustion it can be expected that the best performing aromatics in terms of spray characteristics would also be higher performing in the noise and vibrations portions of this investigation. Another conclusion that can be made is that the benzene ring contributes disproportionately to the density of the aromatic molecule, indicating that an aromatic with a large aliphatic group attached would be able to spray better than a pure aromatic or poly-aromatic compound. This is reflected by the fact that all three top performing compounds Ethylbenzene, Tert-Butylbenzene and Ethylbenzene have aliphatic compounds attached to the benzene ring.

The results for SMD observed in this investigation compare well against those that have been found in the literature with similar trends being observed in all cases which

lends credence to the findings of this experiment into the spray quality of specific aromatic compounds. The observed trends would be far greater were the pure aromatics were tested however this was found not be practical and cost prohibitive. Moreover, this would not have been representative of operating conditions as aviation fuels do not only comprise of aromatics, but aromatics do contribute to the lion's share of the particulate emissions produced during combustion of liquid fuels.

Another contribution to knowledge which this chapter would deliver is how different aromatic structures, bonds and other micro properties of aromatics species impacts spray and atomization. One of the major outcomes of this particular study is to investigate how these alternative and aromatic fuels perform in the fuel injection phase of combustion.

Whilst this investigation has several knowledge contributions, some weaknesses also exist. Firstly, the measurement of the droplets at one distance from the nozzle deprives the generation of a global SMD for droplet size, secondly the lack of a flow meter and the flow rates being governed by pressure alone may induce errors in flow rate due to pressure loss in the fuel system due to blockages in the fuel filters, lines and injector. The justification for not having a flow meter was cost as a sensitive Coriolis-type flow meter was deemed to be prohibitively expensive.

Finally, in conclusion it can be said that the contribution to new knowledge in this chapter stems from the direct comparison of 16 aromatic species in 2 different blend ratios in terms of their sprayed drop size. This has implications in how well these individual aromatic species behave in terms of combustion quality, therefore a direct impact on the emissions generated. This has lead to some clarity as to which aromatics can be added in an alternative fuel with the least impact on atomisation.

Chapter 5

Noise, vibrations and instability characteristics of an atmospheric pressure combustor running on low aromatic surrogate fuels

5.1 Introduction

The importance of pressure oscillations, acoustic and vibrations characteristics and their impact on the combustion instability process have been described in the literature [71, 75–77, 86, 148–151]. In this investigation 16 separate low aromatic surrogate fuels were tested for their combustion instability characteristics. The results showed that the vibration both correlate well with the increase in density. This provided some clarity into the effect aromatics species have upon combustion instability.

This investigation was cut short without the ability to test the reference fuels due to the flooding and destruction of the LCCC in the autumn of 2019. Even though the flooding cut short this particular experimental campaign, it did not impact the overarching scientific goals of this investigation which was to investigate the impact of specific aromatic species on combustion noise vibration and instability.

5.2 Results

This section elaborates on the results obtained during the investigation. It should be noted that the fuels tested were A1-A9 and B2-B16 as well as Jet A1.

Figure 5.1 shows the single sided FFT for all 8 sensors for the fuel A2 at all three engine conditions. This set of results is indicative of all the FFT's derived from the other test points, which is in keeping with the literature as the FFT depicts the combustors characteristics and that has remained constant. The FFT's peaks vary in amplitude and frequency between conditions as can be seen from Fig. 5.1 due to the physical flow properties being varied. For a given condition it is expected that the peaks in terms of frequency location would stay constant and the amplitude would vary indicating either louder noise or more powerful vibrations as the fuel changed. Furthermore, it should be noted that the FFT only depicts the range from 0Hz to 6kHz this has been done to better illustrate the peaks within this range due to the fact that above this frequency no further details of note are visible. The sampling rate of this investigation was 25kHz which allows a Nyquist resolution of 12.5kHz. Furthermore, it should be noted that as this is a real valued data set (i.e. time is not less than 0) a single sided FFT suffices and the complex conjugate pairs are ignored (they are depicted in Fig 5.1 by the peaks at 0Hz) and the negative real amplitude content has been superimposed onto the positive axis by doubling the amplitude. Therefore, the FFT amplitude should not be considered absolute and should only be compared to similar FFT's which have undergone the same procedure as depicted in Appendix 1.

From Fig. 5.1 it is clearly visible that the accelerometers are dominated by the second condition depicted in green. This is in keeping with the operating condition's where the second condition has the greatest air and fuel flow rates and therefore the combustor is running extremely rich. Which in turn causes increased mass flow out of the exhaust and causes the large vibrations shown in the accelerometers. It should also be noted that accelerometers X2 and Y2 depict an almost identical FFT to X1 and Y1. This is also to be expected as they were placed in the experiment as a redundancy and to verify the results obtained by placing accelerometers in the same axis but slightly different locations.

Continuing on with the examinations of the accelerometers, it is clear that the second condition dominates the X axis vibrations with a natural mode at 4.6kHz and 4.8kHz. This

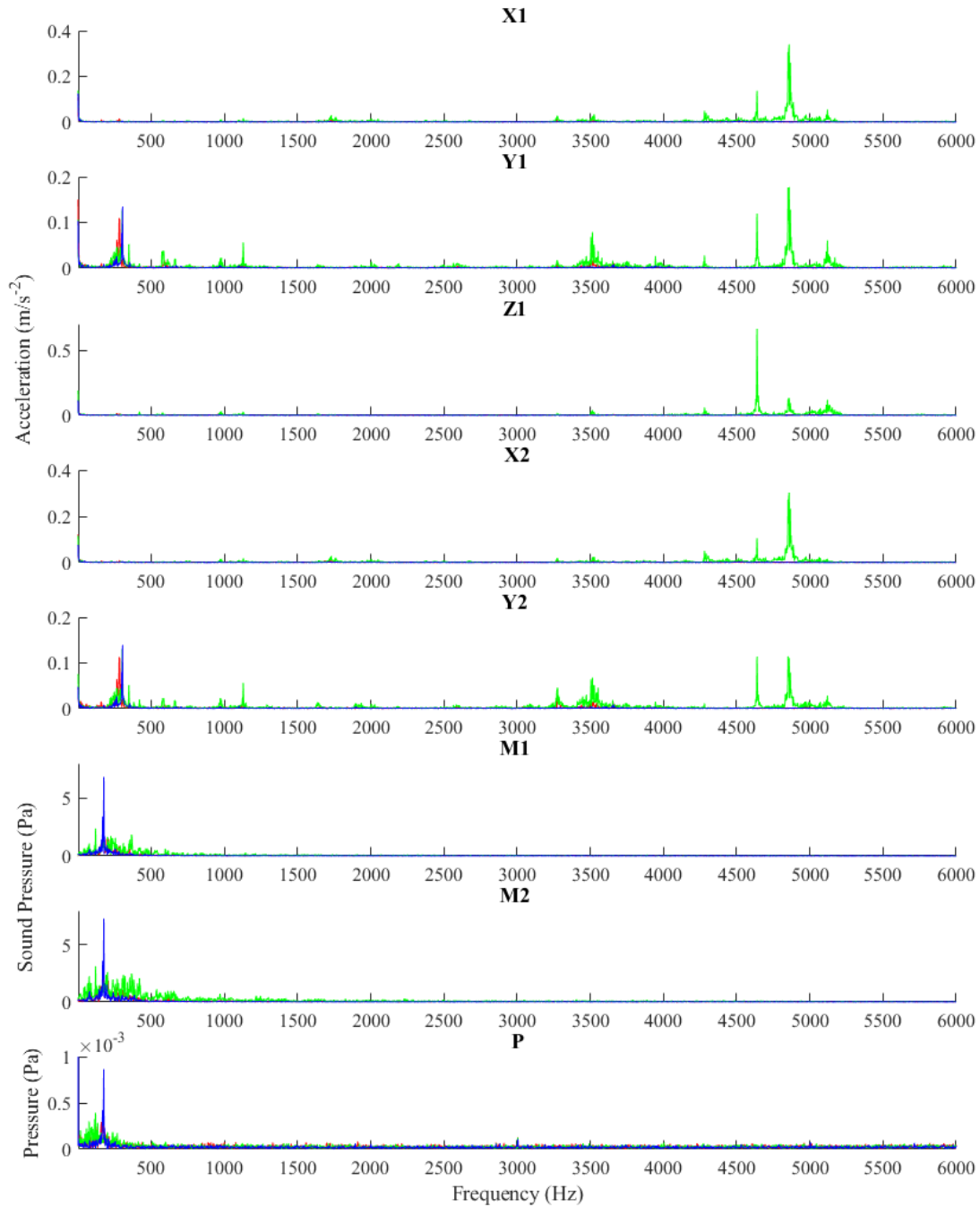


Figure 5.1: Single sided FFT of all 8 sensors (accelerometers (X1, Y1, Z1, X2 and Y2), microphones (M1 and M2) and pressure sensor (P)) for A2. Red, green and blue lines indicate conditions 1, 2 and 3 respectively.

mode was present in the FFT's for all the fuels at varying amplitudes suggesting that this is a combustor natural mode and hence is an intrinsic structural property of the combustor. Along the Y axis accelerometers, we see modes for the 1st and 3rd conditions at around

300Hz as well as the modes at 4.6 and 4.8kHz for the second condition. A small peak is visible here at 3.5kHz on the second mode as well.

Moving on to the microphone FFT's, we can clearly see that it is dominated by the blue of condition 3 at 176Hz. This was to be expected because during the testing of condition 3 for all fuels the noise generated by the combustor was audibly different in the sense that a piercing almost whistle like sound was heard. This indicated that at condition 3 operating parameters the combustor undergoes a Helmholtz resonance. Although condition 2 produced the overall loudest sound due to the increased fuel and air flow rates condition 3 produced the clearest resonance which at a given frequency which is possibly more harmful to component wear as well as from a health and safety perspective (i.e. auditory damage). These phenomena will be explored further in the Octave analysis.

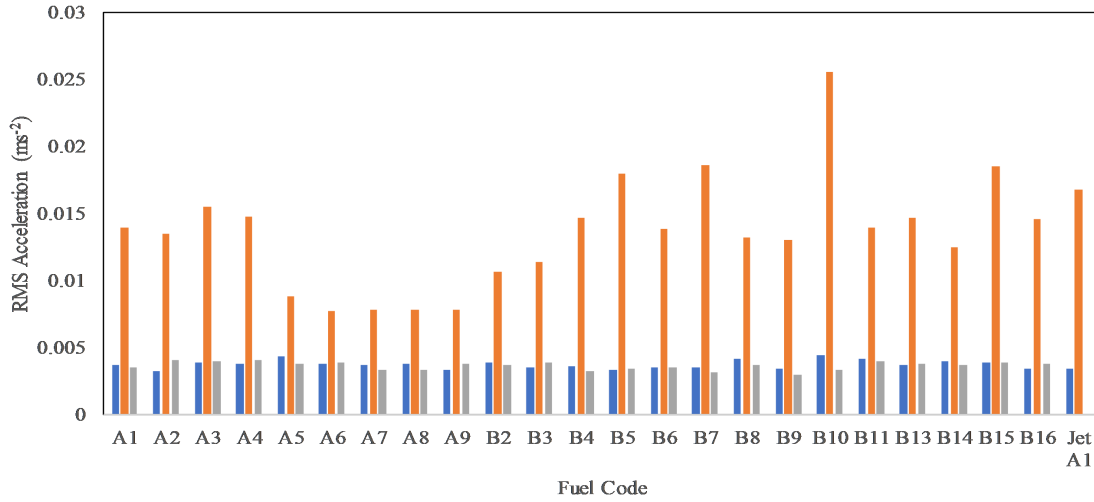
The final sensor depicted in Fig. 5.1 is the pressure oscillations from the optical pressure sensor inserted into the combustor. Here we see that condition 3 shows the sole peak at 176Hz. condition 2 also shows a broader peak less defined peak in this area suggesting increased pressure oscillations in a broad frequency spectrum. Furthermore, it is relatively obvious that the peaks from M1, M2 and P are closely linked. This is to be expected as it is well known that the pressure oscillations from the heat release of combustion is directly responsible for the acoustic noise emitted from combustion [72, 152]. In our case the pressure oscillations are varied amongst the fuels due to the impact fuel properties play upon the heat release rate, laminar flame speed and the bulk properties of the fuels which would impact the injection characteristics of the flame as has been evidenced in chapter 4. An investigation conducted by Dowling et al. describes in detail the formation mechanism for noise from combustion and derives that combustion noise is greatest between 125Hz to 1200Hz depending on operating condition this corroborates well with the results obtained in this investigation [153]. Whilst the noise and pressure are linked it should be noted that they are slightly out of phase due to the time taken for the acoustic waves to reach the microphones. However, this is negligible and does not impact the results as the data collection was started once the combustor was running and stable in terms of operating conditions. Furthermore, some frequency shift of the peaks was detected between the test points of around ± 10 Hz, which indicates that each fuel has an impact on the frequency

and rate of heat release, which is to be expected as the calorific values and reaction rates of the aromatic compounds are different. Whilst the peak frequency modes of the combustor are a function of the design geometry in the main it must be noted that the combustion zone gasses also act as a body (with mass and a stiffness constant) which has its own natural frequencies which are altered by the combustion of different fuels. The interaction between the combustion gasses and the combustor itself form a complex for which the mode shapes are prone to change with the variation in combustion variables.

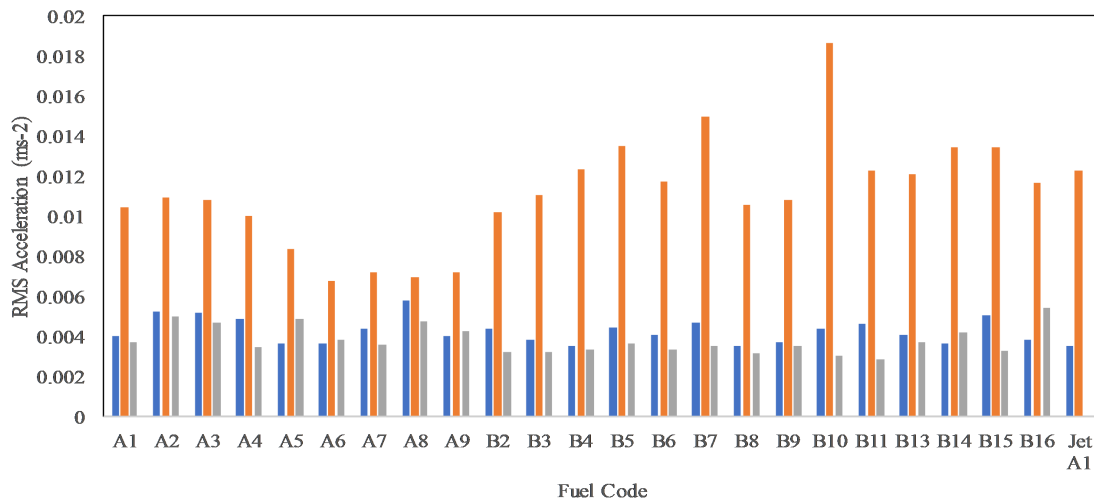
5.2.1 RMS Analysis

This section depicts the RMS (Root Mean Square) analysis of the vibration data for each fuel. RMS analysis has long been used as a tool to analyse random signals in that it can provide a single value for a dynamic signal which can then be compared. This is particularly useful in noise and vibration analysis as the RMS value in effect describes the power of a particular sound or vibration [109]. The mathematical formulation for the RMS value has been described in equation 2.8. A key feature of RMS analysis is that it is a mean power value that encompasses the entirety of the signal that has been acquired. This contrasts with an FFT or octave analysis where the focus is upon a particular section of the frequency domain which is of interest. A drawback of this approach is that the RMS value includes any noise in the signal, be it either physically induced noise (i.e. from a stray footstep near a sensor) or electronic noise from the DAQ and signal conditioners. This drawback is outweighed however by the fact that RMS provides a single comparative value from an entire signal which can be compared to another that has been processed in the same manner as is the case in this investigation. Moreover, as we can see from the FFT in Fig. 5.1 the noise present in these signals is quite minor compared to the peaks which indicates that the RMS is therefore influenced more by the peaks than the noise.

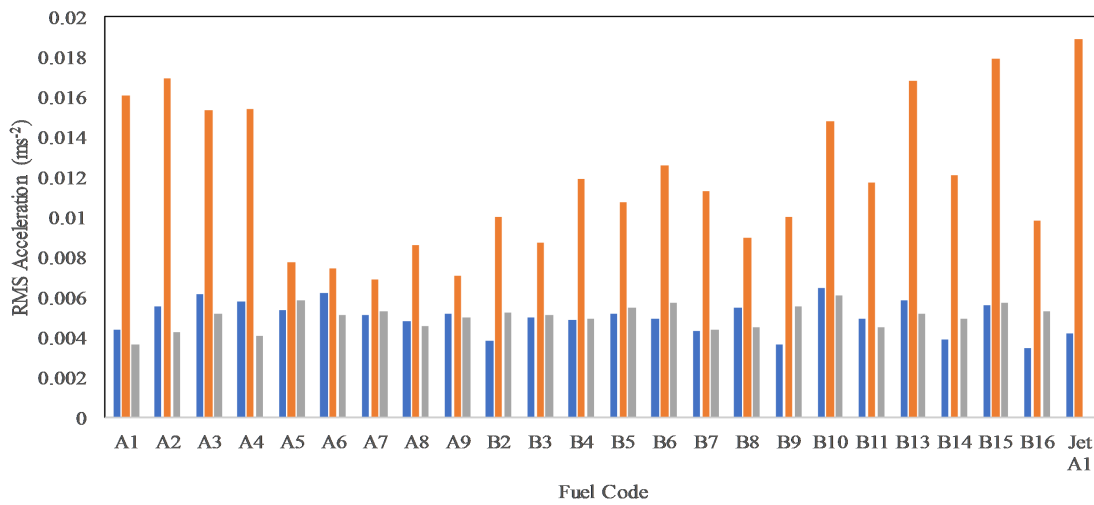
Figure 5.2 depicts the RMS acceleration values for all the tested fuels at the 3 combustor operating conditions (conditions 1, 2 and 3 in blue, orange and grey respectively). Sub figures 5.2a, 5.2b and 5.2c depict the RMS values in the 3 axis of X, Y and Z respectively. It is immediately visible that condition 2 dominates the RMS values on all 3 axes. This is to be expected due to the high air and fuel flow rates which lead to an overall larger reac-



(a) X1 RMS.

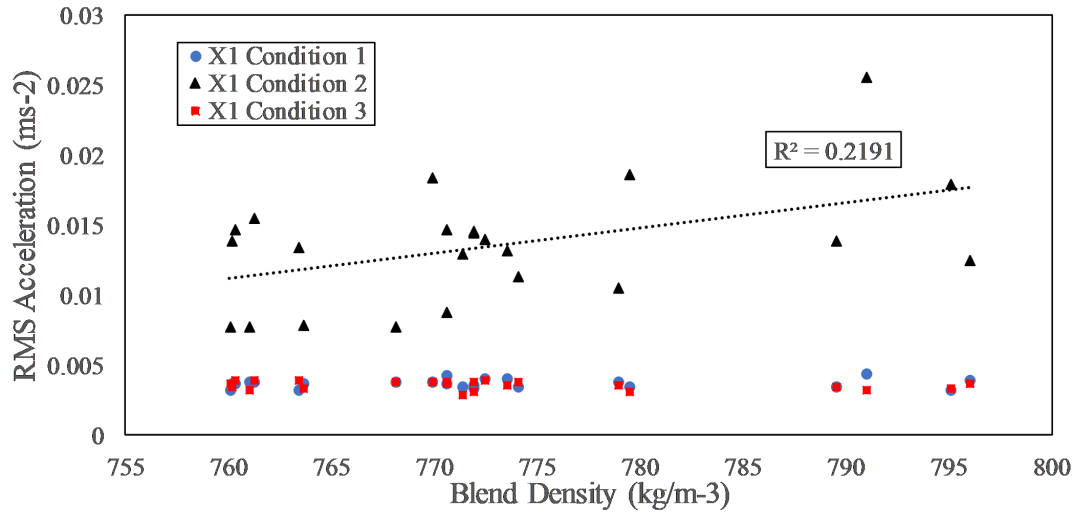


(b) Y1 RMS.

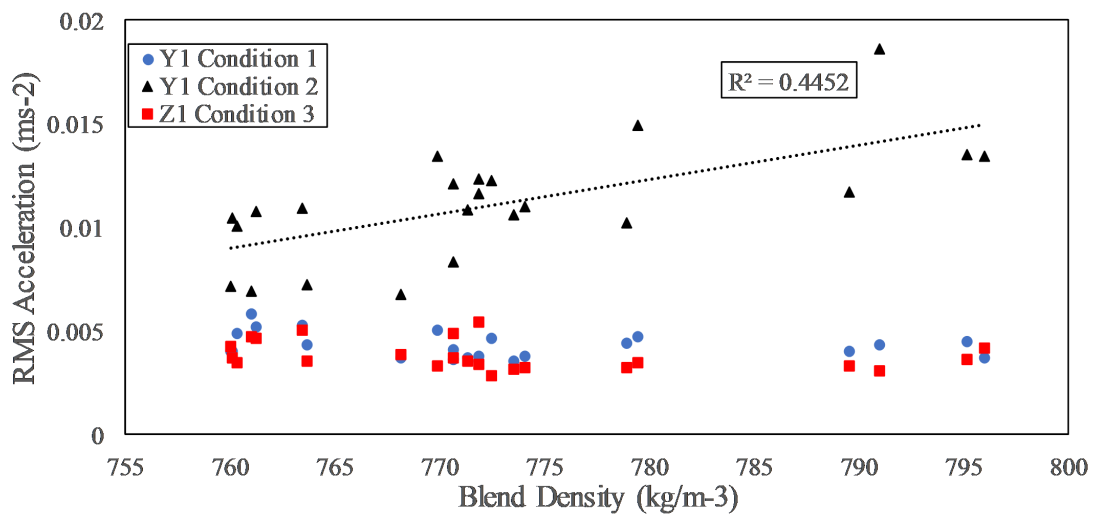


(c) Z1 RMS.

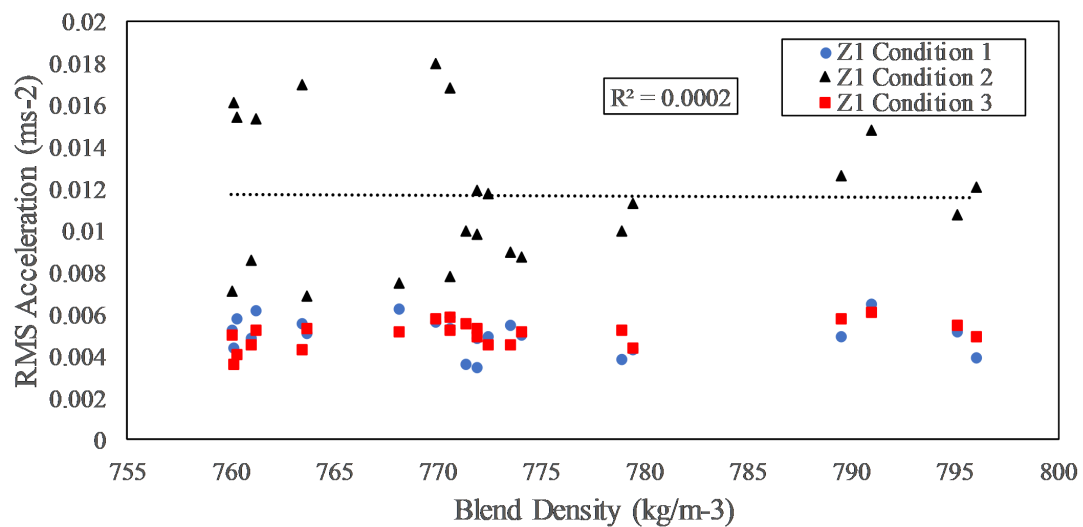
Figure 5.2: RMS data for A and B groups at Condition 1 (Blue) Condition 2(Orange) and Condition 3 (Grey).



(a) X1 RMS.



(b) Y1 RMS.



(c) Z1 RMS.

Figure 5.3: RMS accelerometer data compared to fuel blend density for all 3 conditions.

tion and heat release which then impact greatly upon the vibrations caused. Condition 1 and 2 overall produce the least amount of vibrations which again is to be expected as they share a common airflow rate. The highest vibrations are observed along the X axis which is axial to the airflow. The least amount of vibration is present in the Z axis which is the vertical axis and therefore encounters the greatest damping as the combustor is affixed to the floor in that direction, which means that the combustor cannot flex and vibrate as much in the Z direction.

Furthermore, it appears that there are significant differences in the vibrations amongst the various fuels indicating that the fuel plays a role in the combustion vibration caused. It is immediately visible that in the X and Y directions that B10 Tetralin has the highest vibrations. In addition, it is visible that the A group on average has lower vibrations than the B group which is in keeping with the knowledge that higher aromatic content causes poorer combustion.

Figure 5.3 depicts the RMS values plotted against blend density for the 3 combustor conditions in the 3 axis (X Y and Z). The second condition shows a positive correlation in the X and Y directions whereas the blend density increases the vibrations caused increase. This leads some credence to the fact that as the density of a fuel increase the combustion quality decreases. The Z direction shows no correlation. However, this can be attributed to the fact that the overall vibrations for the 3 conditions are very low in the Z direction due to the physical properties of the combustor as discussed previously. Condition 1 and 2 also show no correlation in any direction. This can be attributed to the fact that the overall mass flow in these conditions are too low to cause increased pressure oscillations via heat release to impact the vibrations of the combustor in a noticeable manner.

5.2.2 Octave band analysis

This section describes the octave band analysis conducted on the microphone data in this investigation. The octave band analysis in essence describes the frequency content in a given signal split into several bands whose upper bound is twice the lower bound and described by its centre frequency. This type of analysis combines the FFT and a sorting method to say along which portion of the frequency spectrum the bulk of a signal lies in

terms of decibels. This is particularly useful in acoustic analysis where a key goal is to determine the frequency range of a signal so that it may be mitigated using active or passive methods (noise cancelling or damping materials) in a particular frequency range. The octave bands centre frequencies have been defined in the ANSI/ASA S1.11-2014 and BS EN 61260 which are compatible to each other [111].

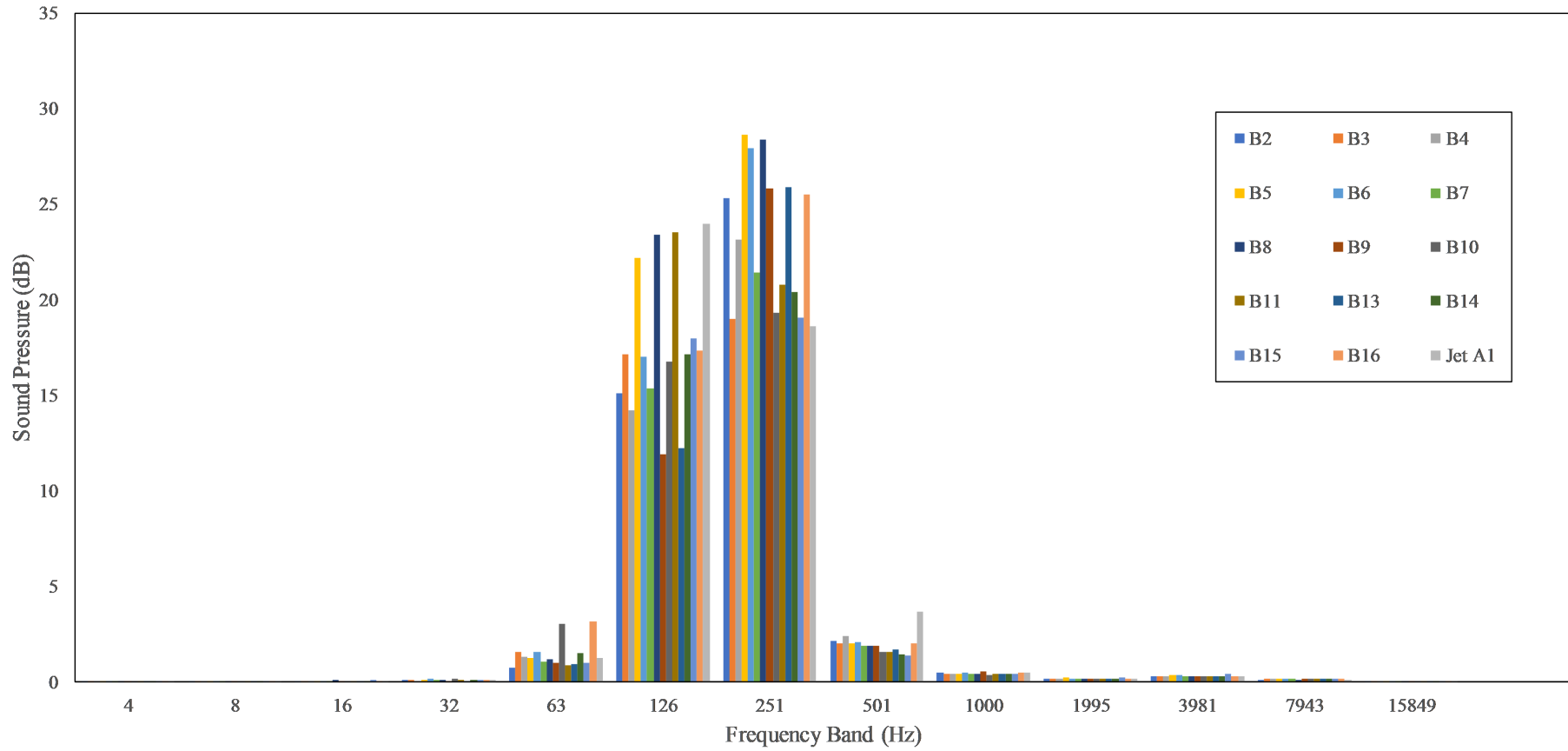


Figure 5.4: Octave band analysis for B group and Jet A1 for M2 at condition 1. Reference pressure $1Pa$.

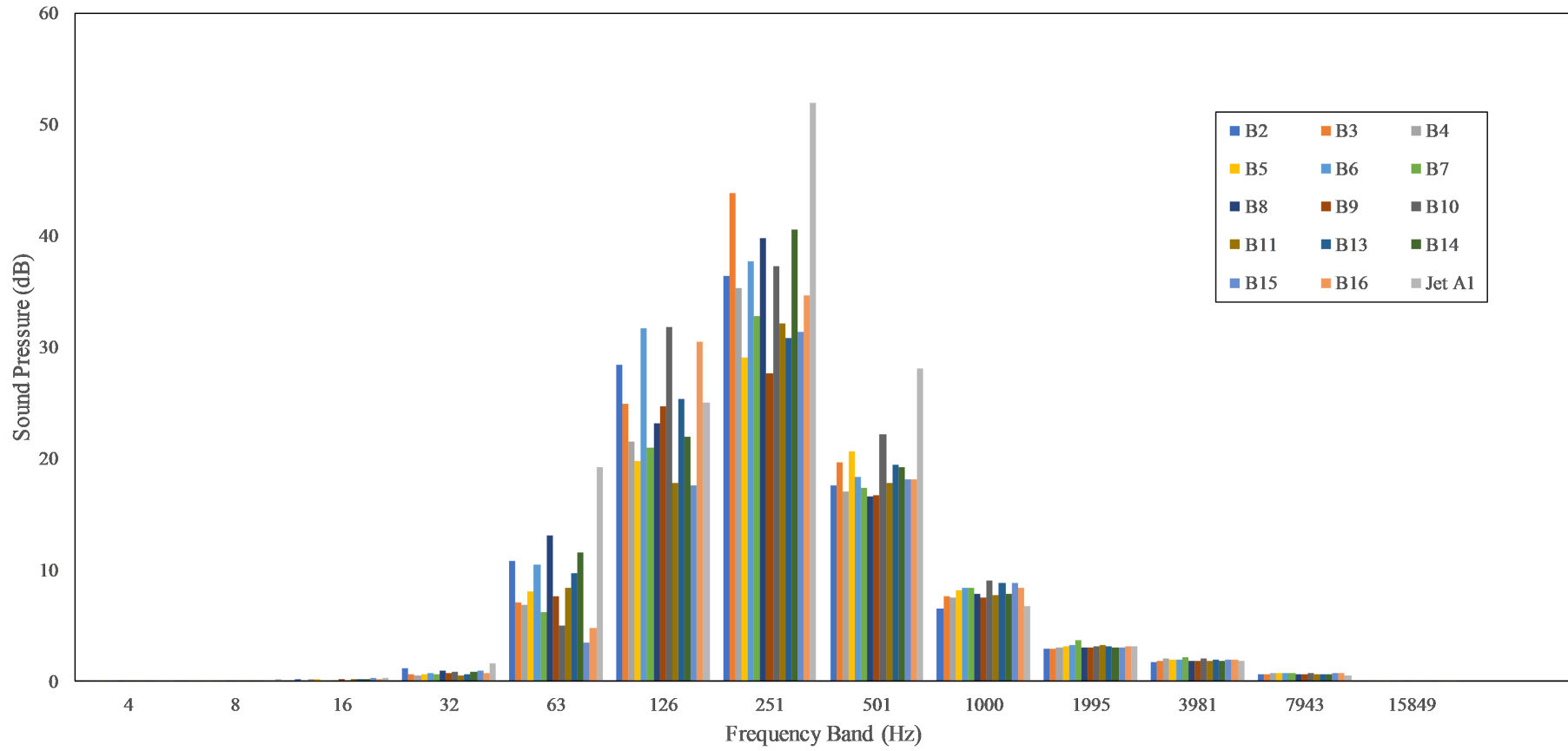


Figure 5.5: Octave band analysis for B group and Jet A1 for M2 at condition 2. Reference pressure 1 Pa.

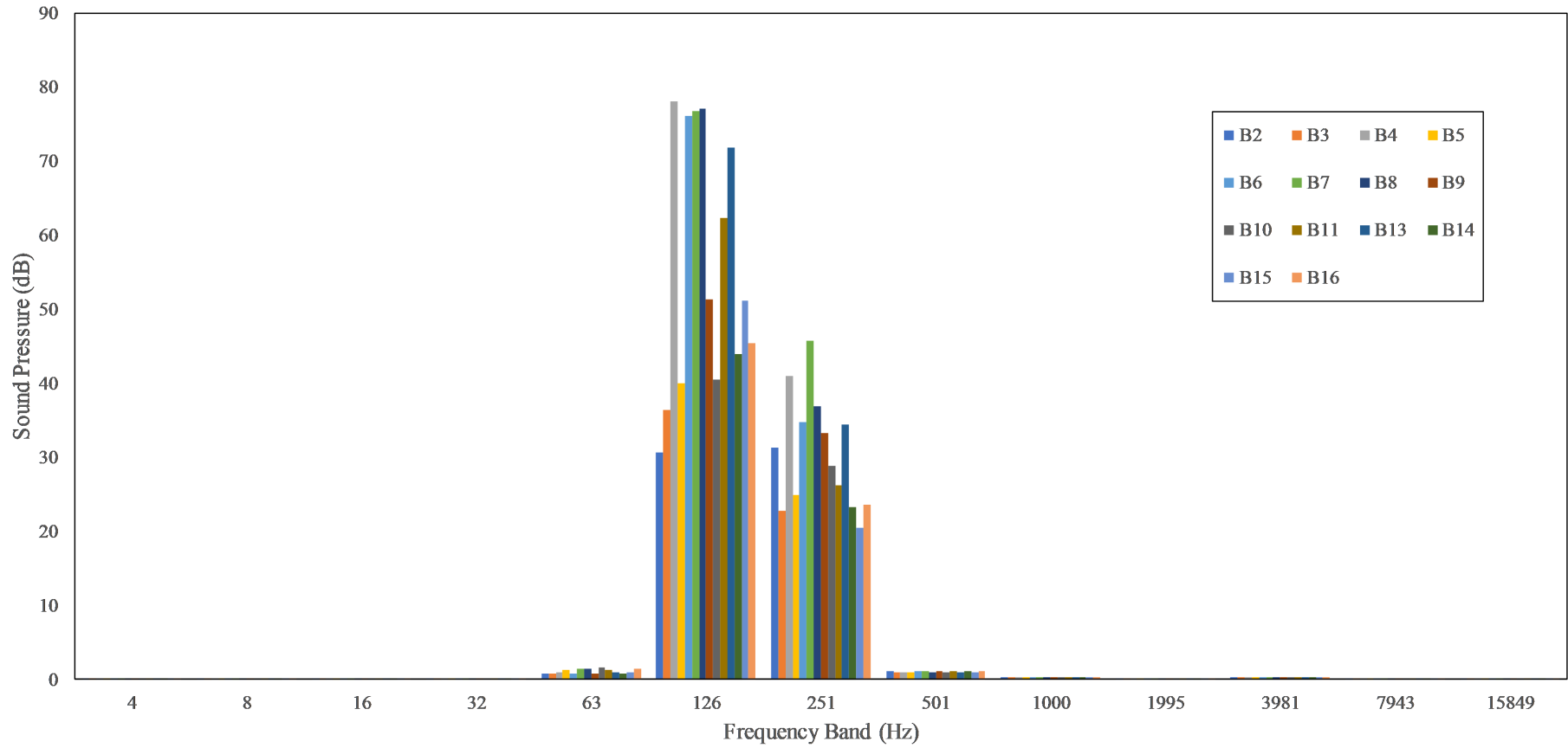


Figure 5.6: Octave band analysis for B group for M2 at condition 3. Reference pressure $1Pa$.

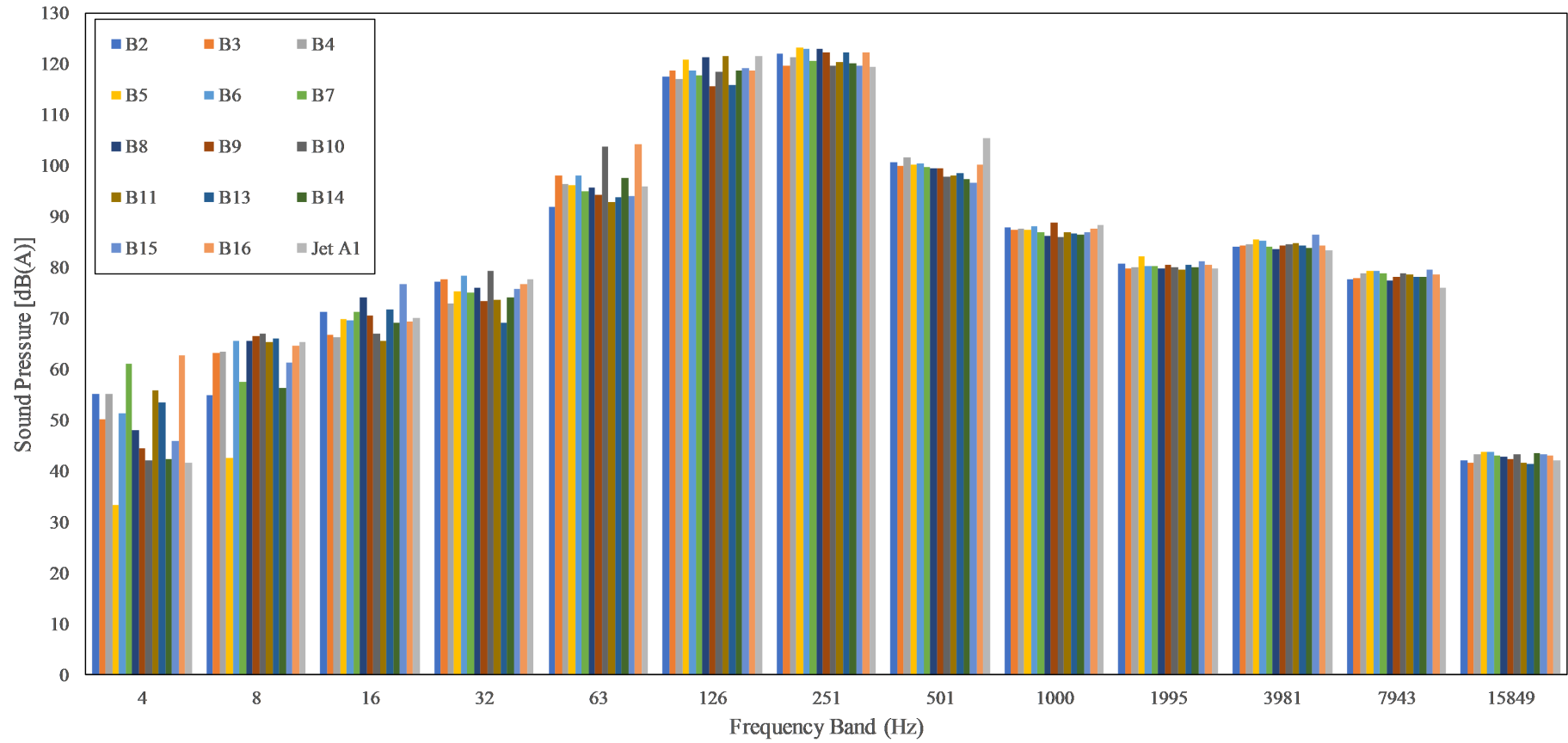


Figure 5.7: Octave band analysis for B group and Jet A1 for M2 at condition 1. Reference pressure $20\mu Pa$ which corresponds with human hearing range.

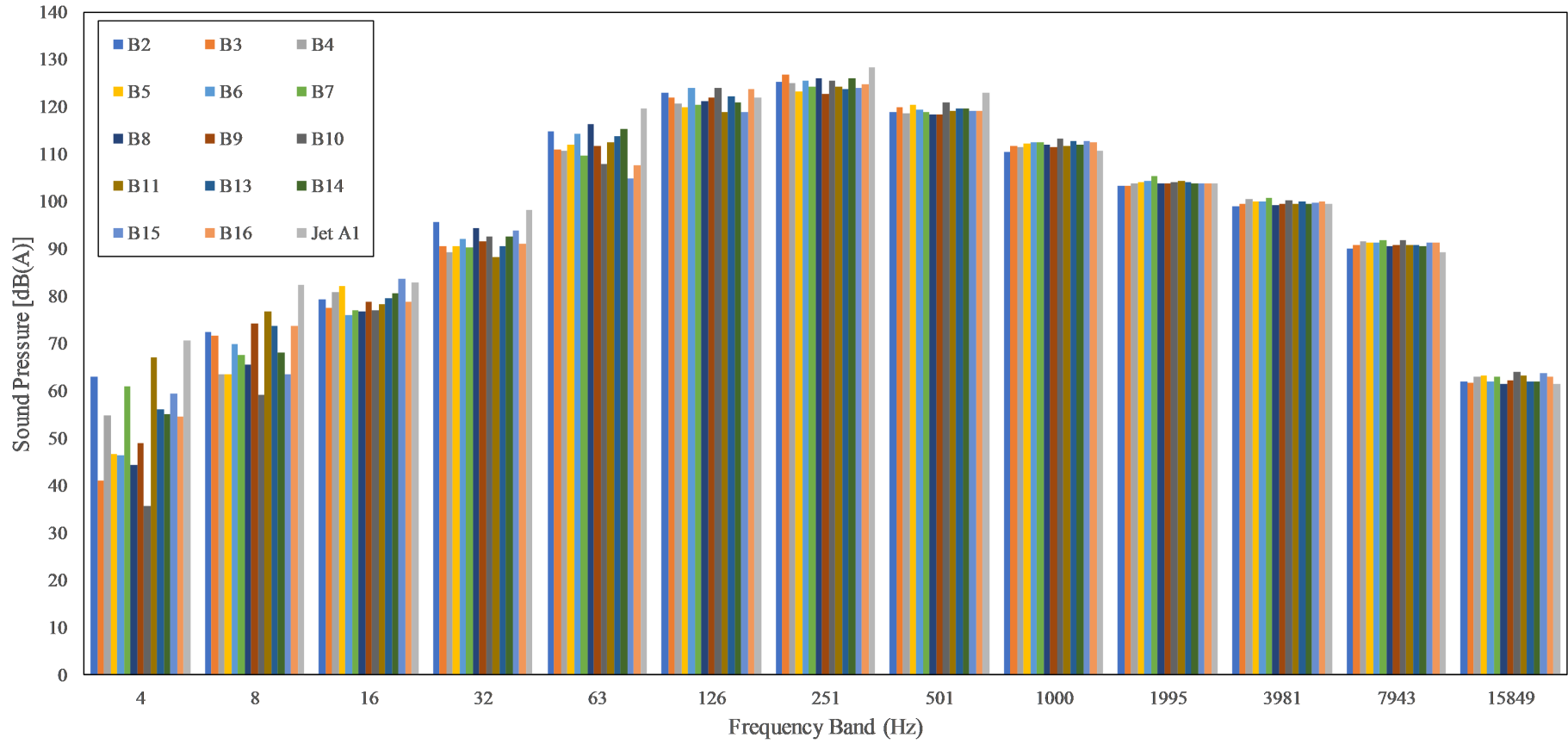


Figure 5.8: Octave band analysis for B group and Jet A1 for M2 at condition 2. Reference pressure $20\mu Pa$ which corresponds with human hearing range.

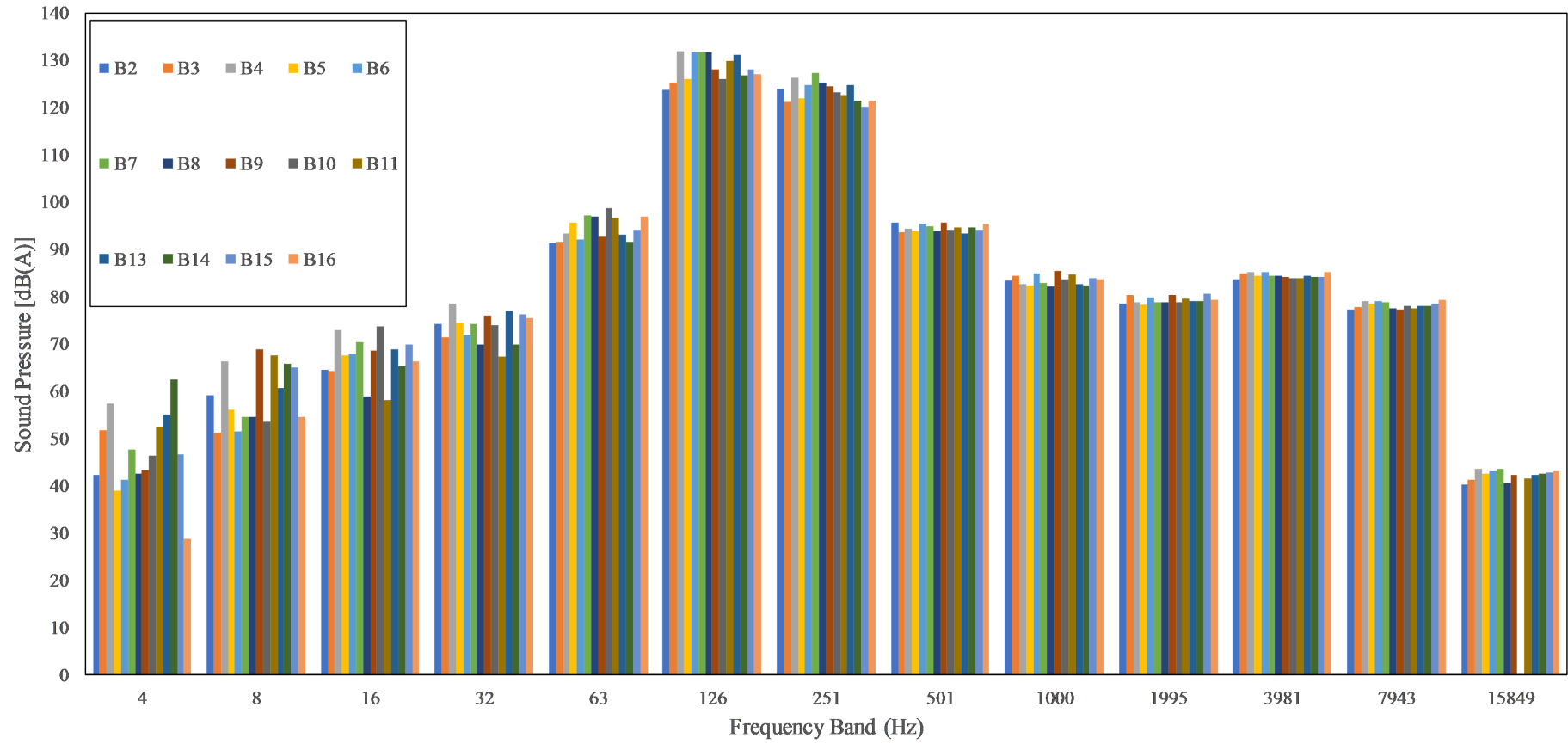


Figure 5.9: Octave band analysis for B group for M2 at condition 3. Reference pressure $20\mu Pa$ which corresponds with human hearing range.

The octave band analysis also translates the raw sound pressure acquired into decibels which is much more common in acoustic analysis via equation 2.9. The decibel range is a logarithmic non-linear range used to identify the variation in sound levels. Figures 5.4 through to Fig. 5.6 depict the octave analysis for the B group at condition 1,2 and 3 respectively for M2. It was decided to conduct the octave analysis using M2 since both microphones show near identical frequency content with the only difference being that M2 detected greater sound pressure levels with respect to M1 due to its closer proximity to the outlet of the combustor. This was to be expected as sound intensity decays according to the inverse square law. The decibel values for Fig. 5.4 through to Fig. 5.6 have been processed using reference pressure of $1Pa$ which in essence translates the raw sound pressures into the decibel range whilst preserving the magnitudes of the pressure levels making it easier to identify which particular test point contributed the most noise.

For all three conditions it can be seen from the Figs. 5.4, 5.5 and 5.6 That the bulk of the noise is emanated in the 126Hz and 251Hz bands. For condition 1 and 2 the greatest noise is emanated from the 251Hz octave band which has a lower limit of 177Hz and an upper limit of 355Hz. For condition 3 the bulk of the noise is propagated from the 126Hz band which has an upper limit of 177Hz and a lower limit of 89Hz. This is in keeping with what was visible from the FFT in Fig. 5.1, where it was clearly seen that for condition 3 there exists a clear peak in the 170Hz range. Moreover, we can see that for condition 2 the noise content is widely distributed amongst 5 octave bands from 63Hz band up-to the 1kHz band. This is in keeping with the assessment that the second condition releases greatest overall sound power along the spectrum. Condition 1 and 3 have a much narrower frequency distribution of noise, mainly constrained to the 126Hz and 251Hz bands, which indicates that the noise generated in these conditions is composed of a more singular note. Furthermore, it should be noted that condition 1 has the lowest decibel values indicating that it is the quietest condition by far with a peak sound pressure of 70dB. This is in keeping with what was heard audibly during the experiment. Condition 3 shows the highest decibel values of all conditions with a peak sound pressure of nearly 80dB. If the area of these bar charts were considered however the power of the sound emitted along the frequency spectrum can be arrived at in watts. From this definition it is clearly visible

that condition 2 emits the greatest sound power but in a wide frequency range. condition 3 on the other hand emits an overall lesser amount of power but it is concentrated in 2 frequency bands. The sound power emitted is a good indicator of the overall heat release by the combustor. This correlates well with the fact that at condition 2 one would expect the highest heat release due to the fact that the overall fuel and air mass flow rates are at these conditions. Condition 3's concentrated sound power can be explained by the fact that at this operating condition the combustor acts as Helmholtz resonator where the heat release due to combustion process is exciting a natural harmonic of the combustor and therefore amplifies the sound generated. This could be considered detrimental to the overall combustion performance as prolonged combustion at these conditions could cause increased wear on the combustor as well as any rotational parts such as turbines downstream of the combustor, as would be the case in practical situation.

From condition 2 (the overall loudest condition) Fig. 5.5, the worst performers in terms of noise in the 251Hz band were B3, B14 and Jet A1 which correspond to Styrene, Methyl-naphthalene respectively. The best performer in this band was Cumene emitting the least sound pressure in the 251Hz band.

Figures 5.7, 5.8 and 5.9 depict the octave bands of the 3 conditions with the decibel scale calibrated to the human hearing range with a reference pressure of $20\mu Pa$. This is known as the sound pressure level or SPL. it is useful to define sound pressures in this manner as humans do not perceive noises linearly and also from a comparison point of view with literature. Compared to the $1Pa$ reference pressure plots, the SPL plots overall show greater values up-to 130dB. In essence the SPL for all 3 conditions is between 30dB to 130dB for all the fuels along the octave bands. This conforms to what was audibly heard during the investigation in that it was quite noticeable when the combustor condition changed however no audible difference could be heard with respect to each fuel in a given condition.

A study conducted by Simons et al. investigated the noise and vibrations emitted from a miniature turbojet type gas turbine SR-30 [86]. They have also investigated 2 alternative fuels and Jet A and conducted an octave analysis on the noise data they obtained and is depicted in Fig.5.10. As is visible Simons SPL analysis closely matches that of

this investigation depicted in Fig. 5.8. The exception being the peak observed close to 10kHz which corresponds to their shaft speed, this is not visible in this investigation as this experiment involved no moving parts downstream of the fan used to induced airflow. An interesting phenomenon in both SPL plots is the increased variation between fuels in the sub 100Hz bands, indicating that fuel has an impact on the low frequency noise emitted during combustion. It is theorized that the variation in low frequency noise is due to the fact the direct noise caused by the combustion of the various fuels are depicted in this region therefore the fuel plays a role in the noise produced at these frequencies. The noise produced at the higher frequency ranges are the result of the noise generated by the high-speed flow exiting the nozzle of the combustor which tends to dominate the noise spectrum in the upper frequency bands. This high frequency noise would be largely unaffected as it is a function of the outlet flow speed of the combustor and the overall pressure increase caused by the combustion reaction, which is not expected to vary greatly with fuel composition.

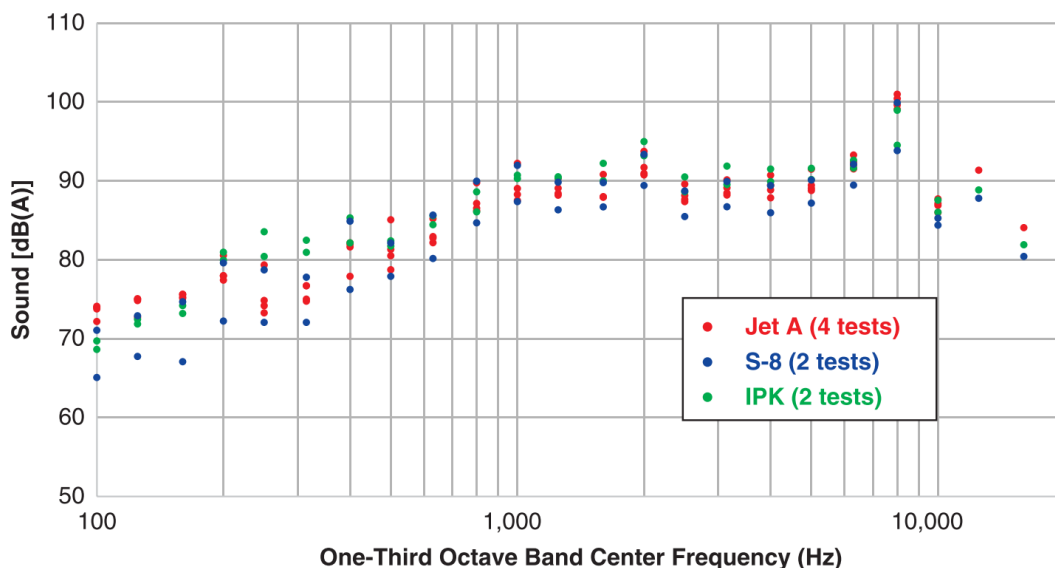


Figure 5.10: Octave band analysis conducted by Simons et al for Jet A and 2 alternative fuels [86].

5.2.3 Peak height analysis

The final analysis conducted in this investigation was a peak height analysis. Where individual peaks present in the FFT of each fuel was compared to each other and plotted against their blend density. The utility of this type of analysis with respect to RMS is that we manage to eradicate the impact of signal noise which interferes with the RMS value.

The first peak to be compared with the fuel blend density was The X acceleration peak found at 4.8kHz in condition 2 for all the fuels tested both A and B groups shown in Fig. 5.11. it is clearly visible here that there exists a positive correlation of increased vibratory acceleration axial to the combustion airflow as the fuel blend density increases. The correlation coefficient of 0.38 lends some credence to this.

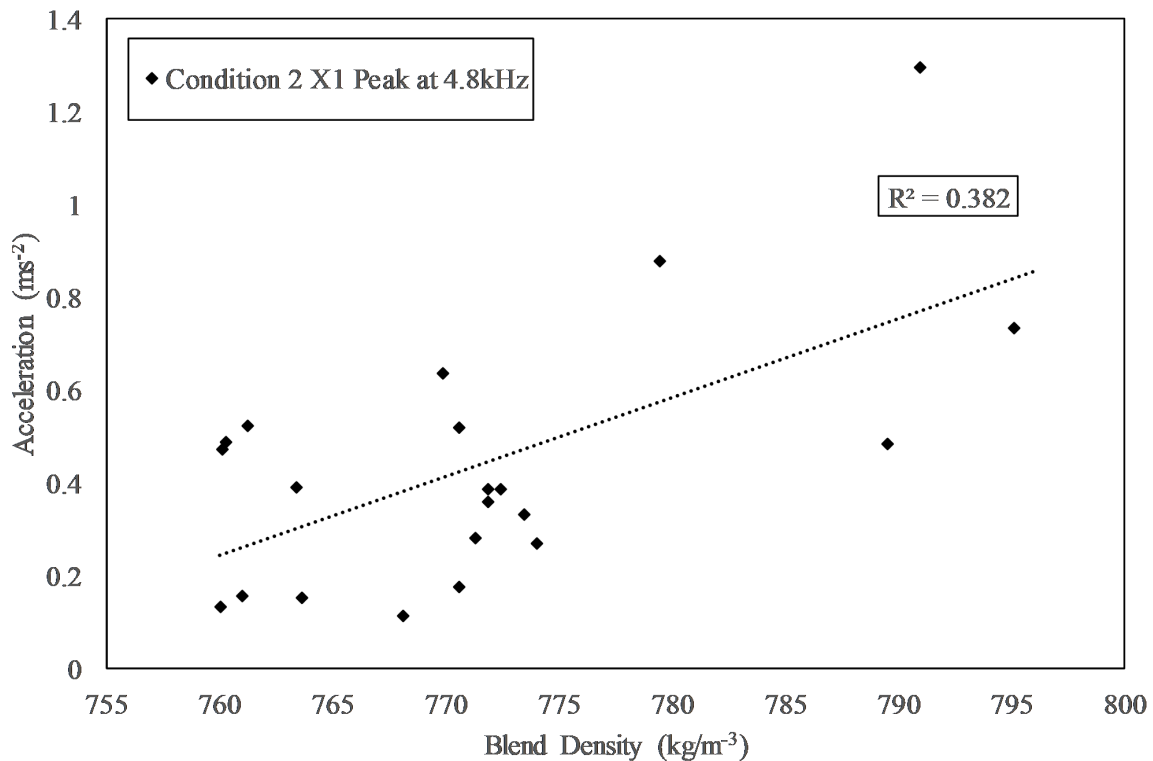


Figure 5.11: Peak height analysis for A and B groups for X1 at condition 2.

Figure 5.12 depicts the peak height against blend density for the Y direction acceleration for all fuels tested. Again, it is clear that a positive correlation exists with respect to increased vibration as fuel density increases. However, it should be noted that the overall vibrations are lower compared to the X direction which undergoes the harshest of the vibrations at $1.3ms^{-2}$ whereas the Y direction experiences only $0.75ms^{-2}$ at its peak.

Condition 2 was chosen for this comparison as it showed the highest overall vibrations of all 3 conditions. The effect of blend density on combustion vibration intensity is explained by the fact that post injection there exists a density gradient in the reaction mixture (all reactions contain a density gradient of reactants) This gradient is exacerbated in by the increased species density. This reaction gradient is responsible for the fluctuation in the heat release rate as well as the temperature gradient across the combustion chamber. This in turn induces vorticity and causes turbulence, which along with the pressure waves from the chemical reaction cause the increased vibration when interacting with the solid combustor walls.

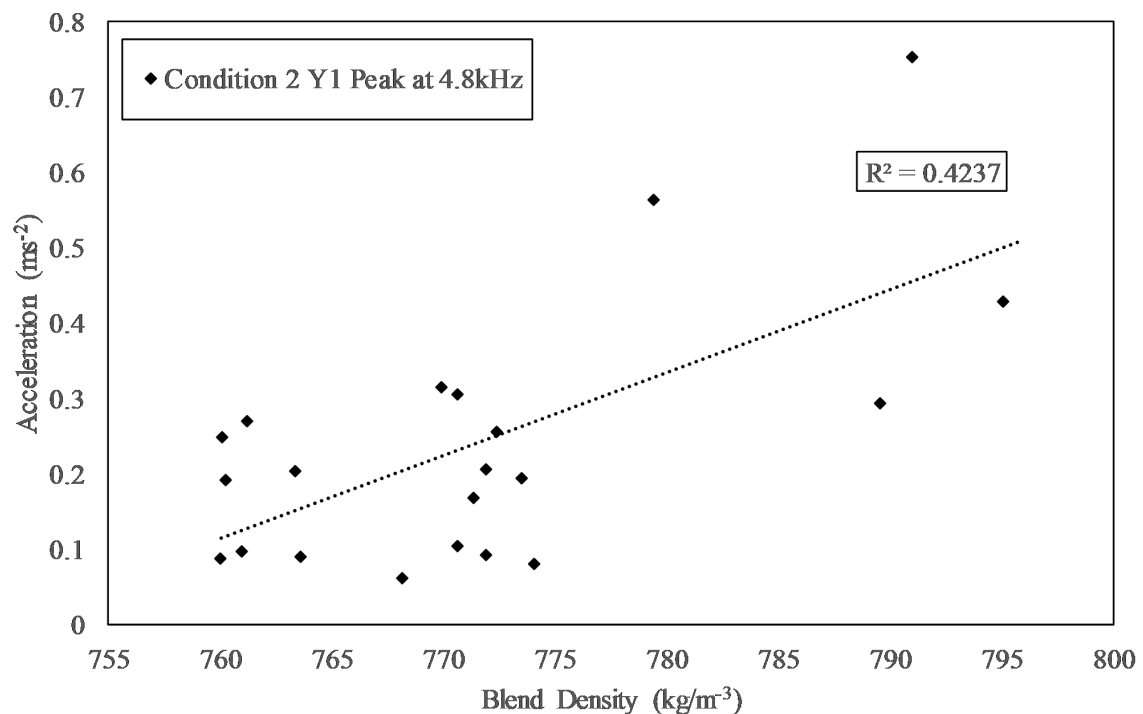


Figure 5.12: Peak height analysis for A and B groups for Y1 at condition 2.

Figure 5.13 depicts the pressure oscillations peak at 176Hz for condition 3 for all the fuels tested. As is visible there is no immediate correlation between the pressure oscillations and blend density. This can be explained by the fact that the pressure oscillations detected are extremely low in the order of $10^{-3} Pa$. This indicates that pressure waves reaching the sensor between the combustor casing and the combustion liner are being heavily attenuated. This is justifiable in that as this particular combustor was running on atmospheric inlet air pressure, it was not expected to see large spikes in pressure due to

combustion.

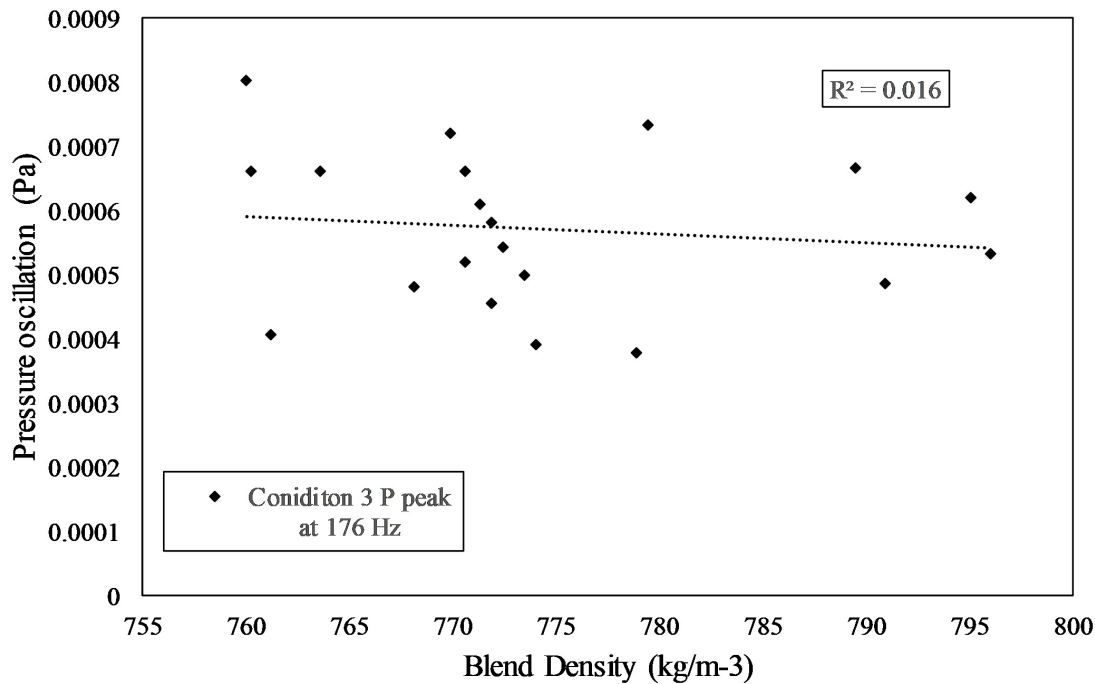


Figure 5.13: Peak height analysis for A and B groups for P at condition 3.

Figure 5.14 depicts the X1 direction peak height against the H/C ratio of the fuel blends tested. As can be seen there exists no correlation between the H/C ratio of the fuels tested and their acceleration peaks. This can be attributed to the fact that the range of the H/C ratio of the species tests is low ranging from 0.9-1.6. Furthermore, it should be noted that as the aromatics were blended with a solvent which would act to damp the overall H/C ratio of the blends towards the H/C ratio of the solvent which would be constant among fuels tested. Overall, the impact of the H/C ratio on vibrations would be clearer if the aromatics were tested on their own. However, this is neither practical nor realistic as jet fuel is composed in the main of straight chain aliphatic hydrocarbons similar to the solvent used in this investigation.

It can be said that this investigation has uncovered a link between fuel properties and combustion instability, as is evidenced by the fact that the 16 aromatic surrogates tested showed varied vibrations and noise with respect to Jet A1. This is explained by the fact that the combustor in question has been designed to run on Jet A1 as with fuel properties in the ranges defined in ASTM D1655 [25]. It is possible to design and modify a combus-

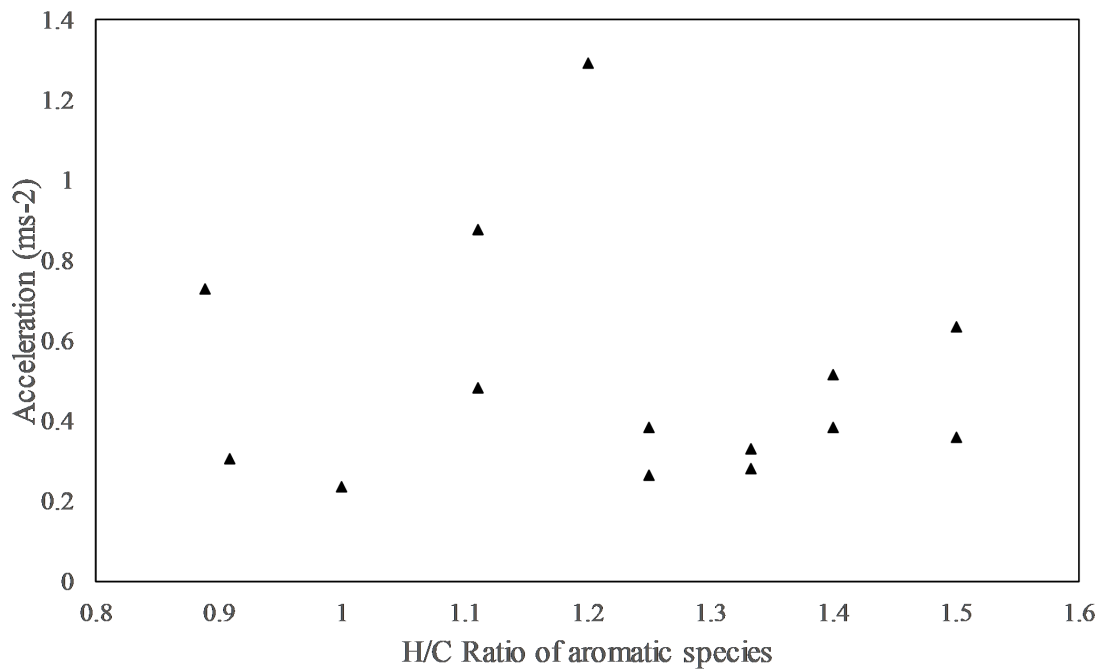


Figure 5.14: Peak height analysis for A and B groups for X1 at condition 2 with respect to H/C ratio.

tor to run on various types of fuels. This is achieved by means of injector modification (i.e. increasing nozzle size, varying injection pressures and air assist pressures) or swirler modification in premixed combustors. Moreover, to combat instabilities and excessive vibrations the combustor geometry itself can be modified to produce the necessary damping at a given frequency. This is achieved by means of adding baffle plates, vanes and redistributing the mass of the combustor to achieve better combustion performance. However, As no alternative fuel has gained wide acceptance as a replacement for Jet kerosene, and there are a myriad of contender as described in chapter 2.1 it would be futile to design the engine to suit the fuel. The better approach is to design the alternative fuel to suit the engine by varying it fuel properties. The novelty of this investigation is that it aids in the design of an alternative fuel by shedding light on the noise and vibrations characteristics of 16 aromatic compounds in an existing combustor design to be used as a drop-in fuel. The necessity for the incorporation of aromatics has been well described in the literature due to their lubricity and seal swell capability. Therefore, this investigation serves to show the least harmful aromatics to incorporate in an alternative fuel in terms of their combustion

instability characteristics.

5.3 Conclusions

Overall, in this investigation it has been observed that noise, and vibrations and combustion instabilities generated by a gas turbine combustor are impacted by the fuel composition and operating conditions of the combustor. Figure 5.1 serves to establish the noise, vibrations and instability characteristics of the Tay combustor used in this investigation. The reason for this is that it shows the pattern of peaks observed under the 3 tested conditions which remained constant for all the test points. The variation observed from thereon focussed upon the amplitudes of the peaks which denoted the power of the noise, vibrations and pressure oscillations observed with respect to each fuel.

A key finding of this instigation was that as aromatic content of the fuel increases by mass the noise and vibrations produced increase with the 18% B group performing worse compared to the 8% A group. Overall the worst aromatic was shown to be Tetralin and Methylnaphthalene performing poorly in the RMS octave and peak height analyses. This was to be expected as these are both poly aromatic hydrocarbons containing 2 rings of carbon- hydrogen atoms. The best performer from both C and A groups were Cumene in terms of vibrations and Styrene and O-Xylene with respect to Sound pressure emitted. This corroborates with the chemical composition in that they are all simple aromatics with only one ring with small methyl or ethyl groups attached. This is in keeping with the trends observed in chapter 5 where the SMD was also impacted by these factors.

Finally, it should be noted that while pressure oscillations were observed with the optical sensor used in this investigation, the results proved inconclusive. It is theorized that this is due to the fact that the combustion rig was run at atmospheric pressure with no significant compression of the inlet air. Furthermore, it is speculated that the combustion liner plays a role in attenuating the pressure waves generated by the heat release of combustion and serves to contain the combustion generated turbulent flow to within the combustion liner, in effect shielding the pressure sensor from the oscillations. Moreover, as has been observed by Chen et al. The inlet air temperature plays a key role in the observable pres-

sure oscillations [87]. As this combustor was run on ambient inlet air conditions the lack of a cohesive pressure oscillation conclusion is to be expected.

Overall contribution to knowledge from this chapter involves the testing of 16 aromatic compounds in 2 blend ratios for their noise, noise vibrations and instability characteristics which showed that the noise and vibrations observed were linked to their fuel properties mainly the fuel density and the chemical composition of the aromatic (i.e. its aromaticity in terms of carbon rings).

Chapter 6

APU testing

6.1 Introduction

This chapter describes the results of the noise and vibrations data obtained from the APU whilst running on the drop-in alternative fuels from table 3.3. The pure aromatic species were not tested on the APU due to the adverse effect they pose to the fuel system of the APU and the associated costs of replacing the high pressure fuel pump due to the wear caused by the blends listed in table 3.1.

The format of this chapter will be largely similar to chapter 5 in terms of the analysis conducted, the key difference here being the change in the equipment from a combustor to a complete gas turbine engine. The reasoning behind testing the noise and vibrations of a complete gas turbine is to observe the difference between the noise and vibrations produced by a combustor (which for all intents and purposes is purely generated by the combustion process) and that of an in-service gas turbine, which along with the combustor has a multitude of turbo-machinery attached to extract useful work from the combustion process. It is obvious that these rotational components will greatly impact the noise and vibrations characteristics of the engine, hence it is critical to observe the effect that noise and vibrations caused by fuel variation has on the operability of the gas turbine as a whole.

6.2 Results

Figure 6.1 depicts the single sided FFT for the 5 sensors used in this investigation for the fuel RF14 (reference Jet A1). The tooltips show peak amplitudes and their frequency locations for the 3 accelerometers and 2 microphones. Compared to the combustor FFT in Fig. 5.1 The vibrations of the APU are orders of magnitude higher in terms of amplitude and frequency. Whilst the combustors' frequency range was limited to within 6kHz the APU vibrates well into the 20kHz range. This is explained by the fact that the combustor is limited in its vibration to combustion and exhaust noise and vibrations whereas the APU vibrations and noise are dominated by its rotational component (e.g. turbine, compressor) noise and vibrations. An observation of note is the lower overall noise measurements, which as has been explained in chapter 3.6 is due to the microphones being placed outside the APU room. The reason for this is that the microphones used in this investigation have a dynamic range of 135dB and the noise inside the APU room exceeded this by an order of magnitude thereby saturating the microphones. Therefore, it should be noted that the noise results presented in this chapter are lower than they would be in practice due to the attenuation caused by the sound dampened walls of the APU room.

Furthermore, it should be noted that the FFT's for all the fuels tested follow the same pattern as Fig. 6.1 as the Frequency content largely determined by the engine operational conditions and the overall design of the rotational machinery of the APU which influence the natural modes of the engine. The key difference amongst the fuels stem from the intensity of the vibrations caused which vary with fuel type as will be shown further-on. With this in mind it is clearly visible from Fig.6.1 that the vibrations from X1, Y1 and Z1 form 3 distinct peak groupings. Firstly at 0.7kHz, secondly at 10kHz where the peak amplitudes are found and finally at 21kHz. The first peaks at 700Hz correspond to the shaft speed of the APU which varies between 40000 and 42000RPM depending on condition. The second set of peaks is most probably caused by the bleed valve. This reasoning for this is that the second condition shows larger peak than the 3rd condition here, even though it produces less power. Therefore it can be theorized that the partially opened bleed valve of the 2nd causes increased vibrations compared to the fully closed flush bleed valve from the first condition and the fully opened bleed valve position from the 3rd condition. The final

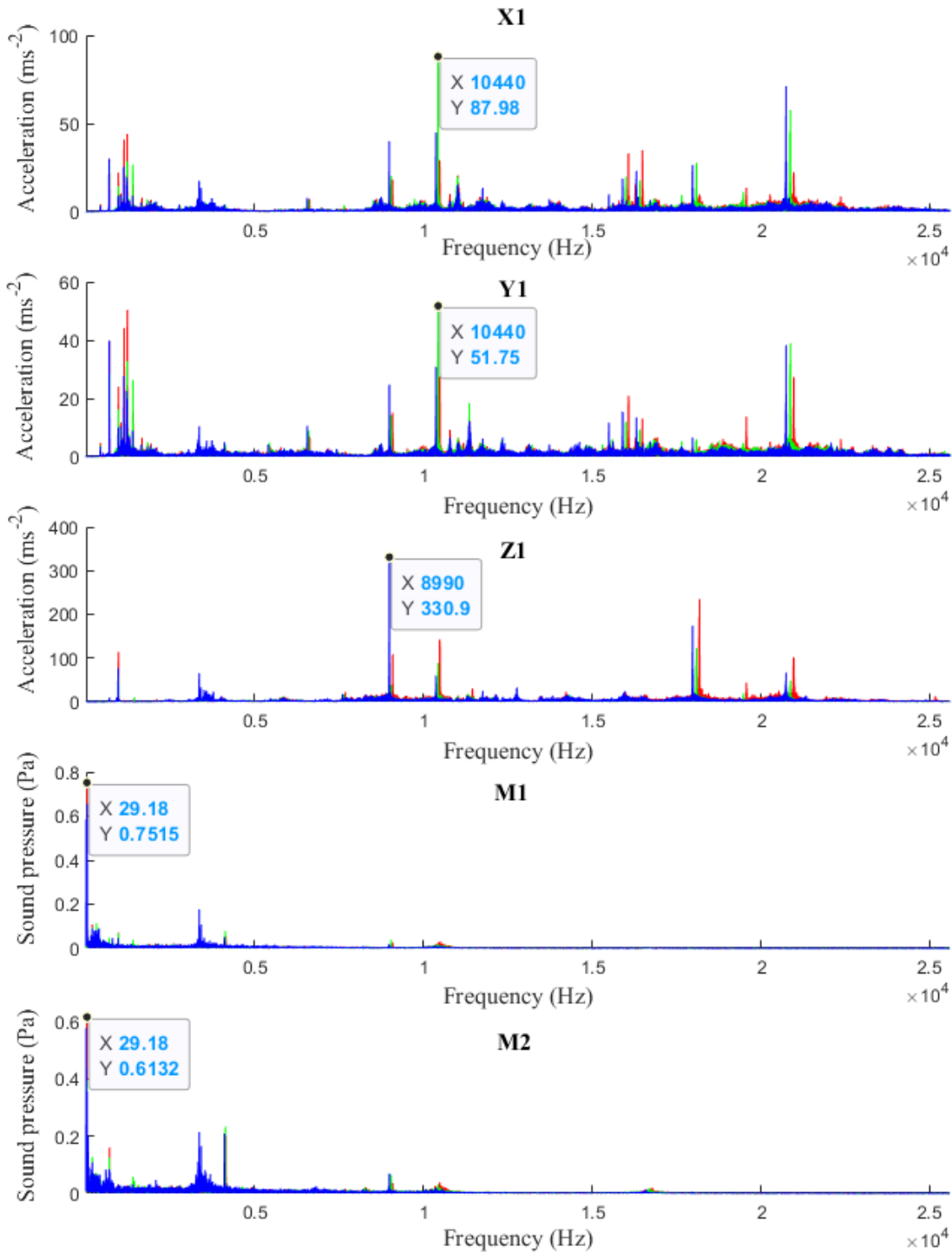


Figure 6.1: Single sided FFT of all 5 sensors (accelerometers (X1, Y1, Z1), microphones (M1 and M2) for RF14. Red, green and blue lines indicate conditions 1, 2 and 3 respectively. Tooltips indicate peak amplitudes and their corresponding frequency.

set of peaks is an exact multiple of the second set of peaks (2nd peak group at 10400Hz and 3rd peak group 20800Hz), hence it can be said that it is a resonance mode generated by

the shell and frame of the APU. Another interesting phenomenon we see is that in general the peaks tend to shift lower as engine condition increases. In the sense that for each set of peaks the red 3rd condition has a higher frequency compared to the green 2nd condition and the blue 1st condition.

When considering the sound pressure peaks from Fig. 6.1 it is clearly visible that the noise has been heavily damped and the peak sound pressure measured is in the order of 0.6-0.7Pa which corresponds to 90dB[A]. the two microphones largely show similar results with the 3rd condition showing slightly higher sound intensity.

Figure 6.2 depicts the FFT of X1 for RF14 for the 3 engine conditions. As can be seen the variation in peaks is not as straightforward as it was for the combustor, in that it is not immediately visible what the trend between the conditions are. At the 'A' location the peaks tend to increase as the engine condition increases, indicating increased vibrational intensity. This indicates that the peak at 20kHz is linked to the load placed on the engine and the associated decrease in AFR. Which in turn would indicate that this peak is directly caused by a component that is impacted by the richer combustion conditions (i.e. a hot section component). On the contrary the peaks at 17kHz and the low level back ground noise surrounding location 'A' show the opposite trend, showing a decrease in vibrational intensity as engine condition increases. This is indicative of the rotational components of the gas turbine as it is known that as the engine is loaded and made to produce increased amounts of bleed air the RPM decreases slightly. This is corroborated with the peak at location 'B' which is known to be the peak caused by the main shaft and associated components spinning at that speed. The final interesting peak from Fig.6.2 is the peak at 10.4kHz where the intensity is lowest at condition 1 with $29m.s^{-2}$, highest at condition 2 with $87m.s^{-2}$ and in-between at condition 3 with $45m.s^{-2}$. As this peak is present at all the condition 2 test points for all the fuels showing that it is not an anomaly, moreover as it is present but not as pronounced at the other 2 conditions it stands to reason that the cause of this peak is unique to condition 2 which would mean it can be concluded that it is due to turbulence and resonance caused by the bleed valve being partially opened at condition 2 as mentioned above. Where the fully closed valve causes the least resonance, the fully open valve causing increased resonance and finally the partially opened valve

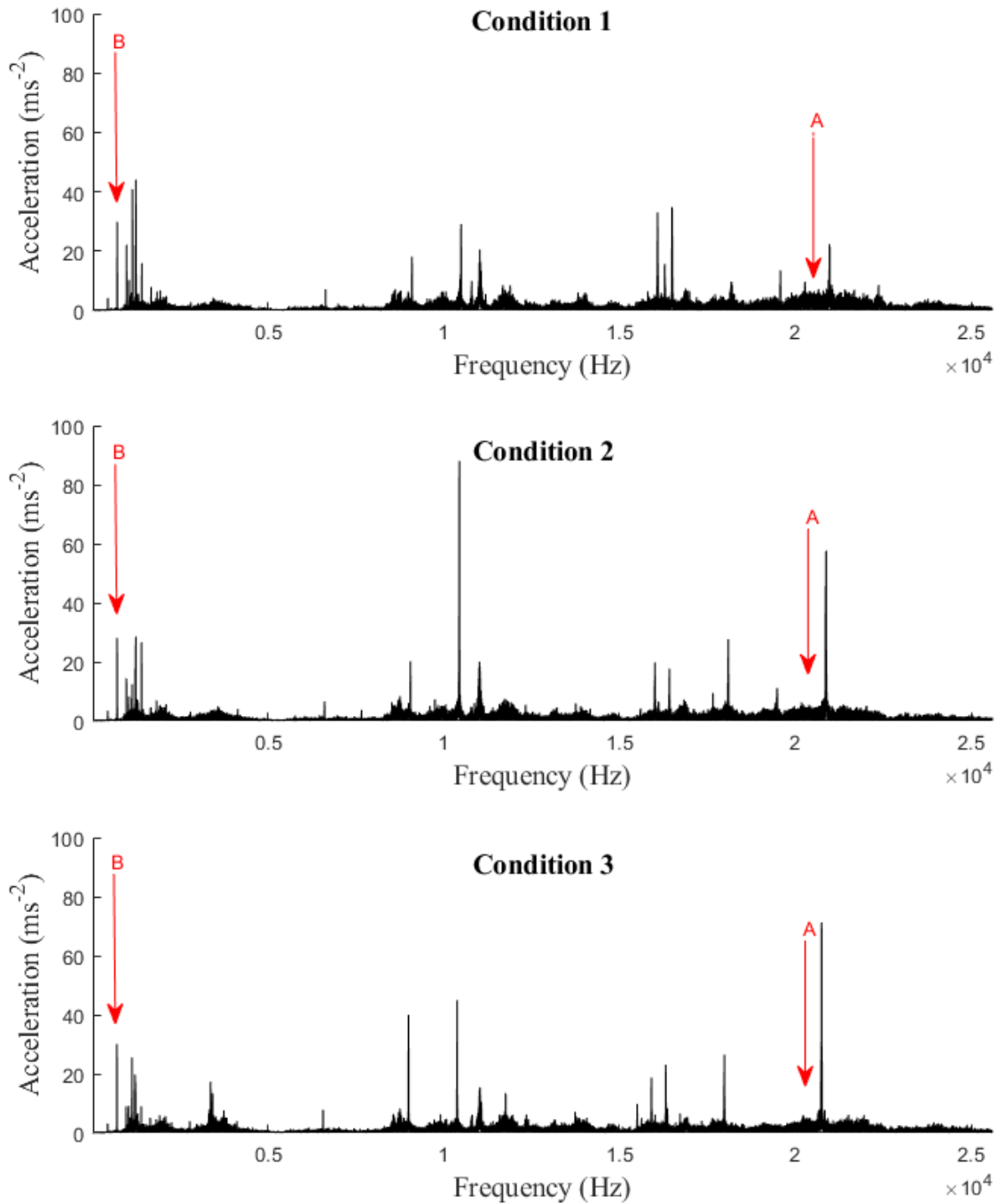


Figure 6.2: Single sided FFT of X1 for the three engine conditions with RF14 (reference Jet A1).

causing very high resonance and associated vibrations.

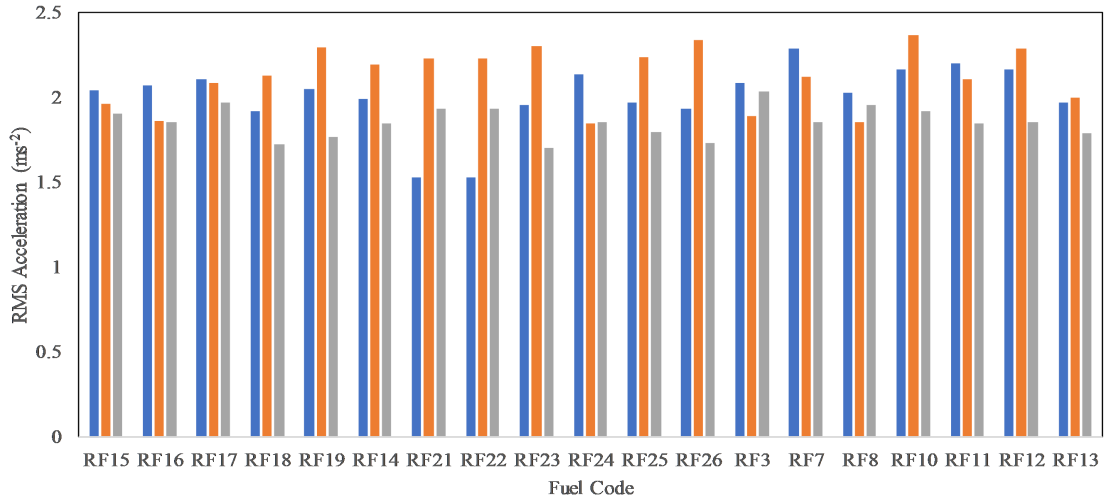
6.2.1 RMS Analysis

This section describes the RMS analysis conducted on the vibration data from the APU for all the test fuels as per table 3.3. Figure 6.3 also shows the extent of the fuels tested as not all the fuels mentioned in table 3.3 were available in sufficient quantities to be utilised in the APU. The procedure for conducting an RMS analysis has been described in chapter 2 as well a more detailed explanation in chapter 5. Figure 6.3 depicts the RMS values of all three accelerometers (X1 Fig. 6.3a, Y1 Fig.6.3b and Z1 Fig.6.3c). In the X axis from Fig.6.3a condition 1 and 2 dominate in terms of RMS for all the test points although the variation between test points is around $1ms^{-2}$. The most consistent of the conditions is condition 3. The mean RMS for condition 1 is $2.008ms^{-2}$, for condition 2 is $2.17ms^{-2}$ and $1.854ms^{-2}$ for condition 3.

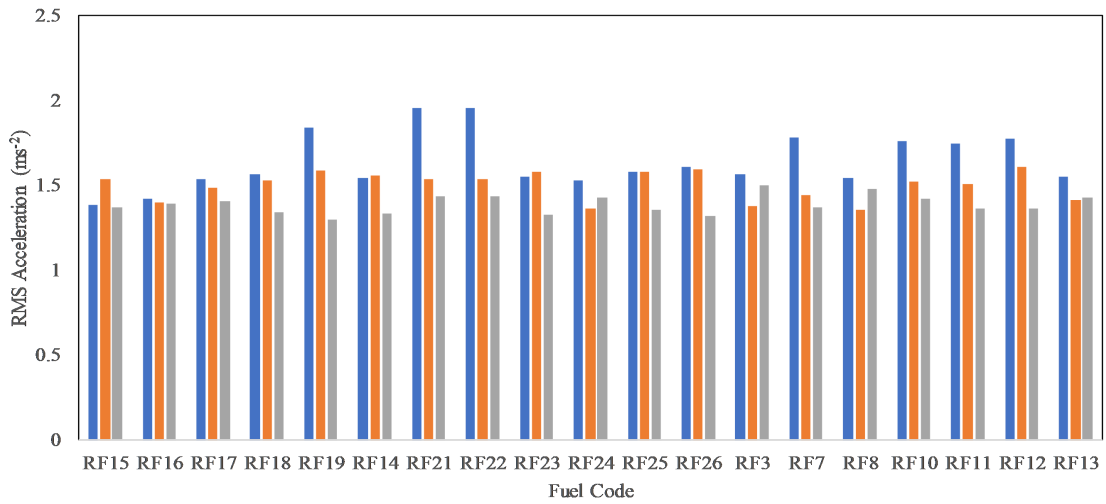
Figure 6.3b shows the RMS for the Y axis. The overall mean vibrations are lower in the axis with $1.639ms^{-2}$ for condition 1, $1.503ms^{-2}$ for condition 2 and lastly $1.386ms^{-2}$ for condition 3. This indicates that the overall vibrations for the Y axis are lower than those for the X axis.

Figure 6.3c shows the RMS values for the Z axis. This accelerometer has the highest RMS values of all the accelerometers captured. This is attributed to the fact that it was located on the frame support closest to the main shaft of the APU as is visible from Fig.3.23. The reason for not placing all 3 accelerometers on the same support was for redundancy purposes (i.e if one accelerometer were to fall off due to the vibrations caused or the adhesive melting the remainder would be operational.) as the wider experiment would not be stopped and test points repeated for the benefit of only one instrument. Figure 6.3c also shows the greatest variation amongst the fuels and engine conditions with a minimum RMS acceleration of $3ms^{-2}$ and maximum of $9ms^{-2}$. Condition 1 also appears to be the harshest vibratory condition due to the increased shaft speed recorded with an average RMS amongst the fuels of $6.29ms^{-2}$.

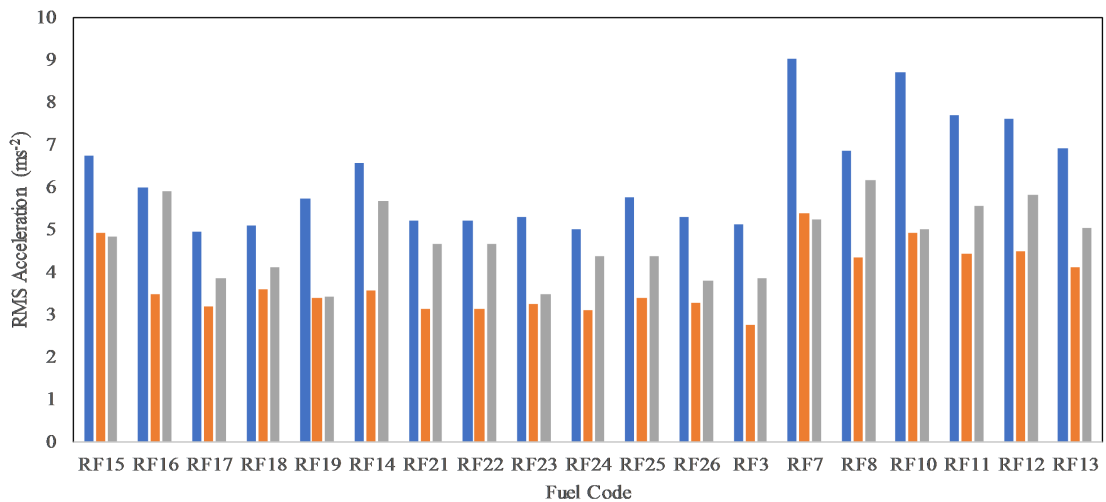
Considering the above information, it was decided to use condition 3 as the base condition with which to compare the fuel properties using the data from the X1 accelerometer. The reasoning behind this was as condition 3 has the lowest AFR and therefore the richest combustion condition, the impact of the fuel would be best shown by condition 3. The



(a) X1 RMS.



(b) Y1 RMS.



(c) Z1 RMS.

Figure 6.3: RMS data for each fuel at Condition 1 (Blue) Condition 2(Orange) and Condition 3 (Grey).

reason for using accelerometer X1 was because it had the median vibratory harshness of all 3 accelerometers. Clearly Z1 is severely impacted by the turbine blade oscillations which would serve to dilute the impact fuel properties impact on vibrations. This was proven to be the case upon further analysis where whilst all the accelerometers showed similar correlations, X1 condition 3 had the best clarity.

Furthermore Jet A1 (Fuel RF14) was repeated at the start of each day to determine the effects of ambient conditions on the results presented in this investigation and to preclude any random bias from the results. The results are shown in Fig. 6.4. As can be seen the 3 test points show near identical with a standard deviation of less than 0.05. This indicates that the variation of vibration seen can be attributed to the fuels' impact to a great extent.

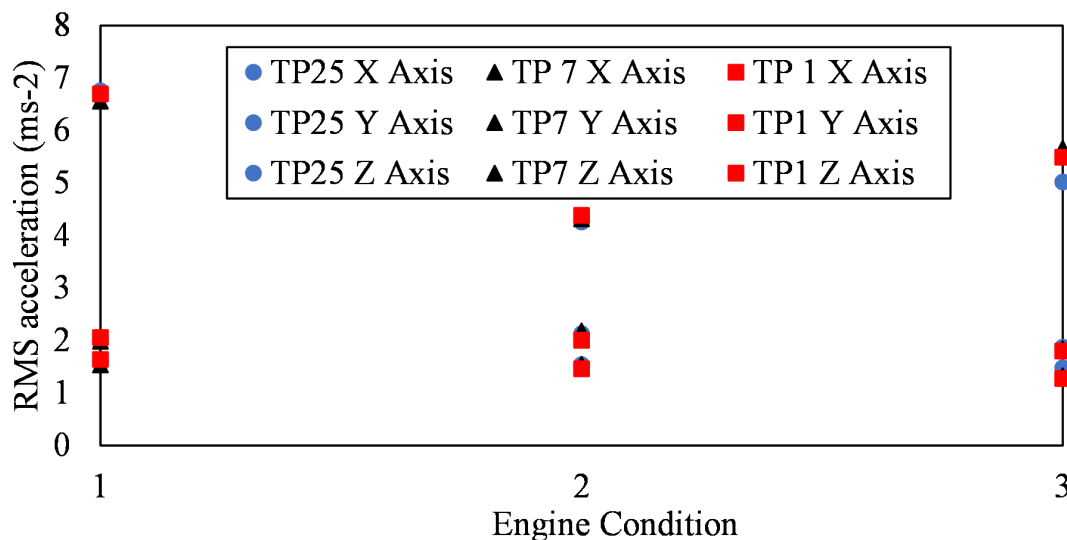


Figure 6.4: RMS Analysis of 3 Jet A1 repeats conducted with respect to engine condition

Figure 6.5 depicts the viscosity in centistokes (mm^2s^{-1}) for the fuels tested for which viscosity data was available as per table 3.3. It is clearly visible that there exists a positive correlation whereas the viscosity of the fuel increases the RMS acceleration produced also increases. A correlation coefficient of 0.33 supports this observation, as does the science which as determined in chapter 4 a viscous fuel tends to lead to poorer atomisation (increased fuel viscosity resists atomisation and requires higher injection pressures to atomise satisfactorily) which in turn causes poorer mixing of the fuel and air. This causes a increase in the variation of heat release from combustion due to richer and leaner ar-

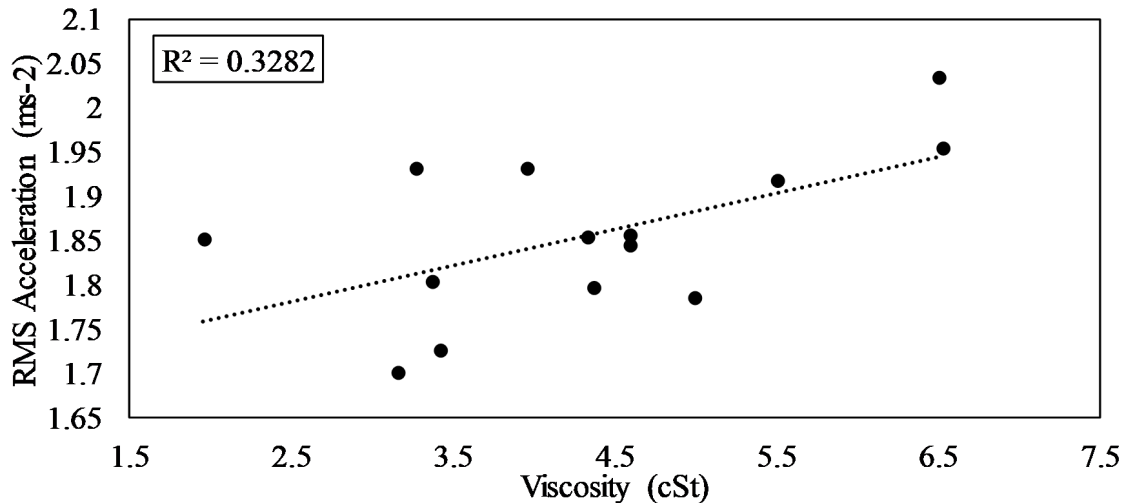


Figure 6.5: RMS acceleration of fuels tested in APU against the viscosity. Note not all fuels' viscosity data were available.

eas of the combustion mix, which goes on to cause increased vibrations which have been detected in Fig.6.5.

Figure 6.6 depicts the fuel density against the observed RMS accelerations for all fuels tested. Again a positive correlation is clearly visible with a correlation coefficient of 0.34. This was to be expected as the fuel testing on the combustor also showed similar results as in Fig.5.11. This is explained by the fact that denser fuel molecules are more difficult to oxidise as they contain more chemical bonds per volume of fuel which require more energy to break down again impacting the heat release rate which in turn can be observed from the RMS acceleration. Moreover, the increased density fuels have poorer injection characteristics as has been seen in chapter 4. This larger droplet size (caused by the increased pressure required to properly atomise denser fuels) leads to poorer mixing of the combustion mixture which leads to hot spots and oscillations of the heat release rate and acoustic couples' waves which would impact the vibrations observed.

Figure 6.7 shows the RMS acceleration against the fuels H/C ratio. As can be clearly seen there exists a negative correlation with a correlation coefficient of 0.34 indicating that as H/C ratio increases the RMS acceleration decreases. This is in keeping with the literature in that as the hydrogen content of a fuel increases the combustion becomes cleaner and more stable as it easily oxides as a molecule as well as in complex compounds. This finding has been supported by experiments conducted with gaseous fuels by Wang et al.

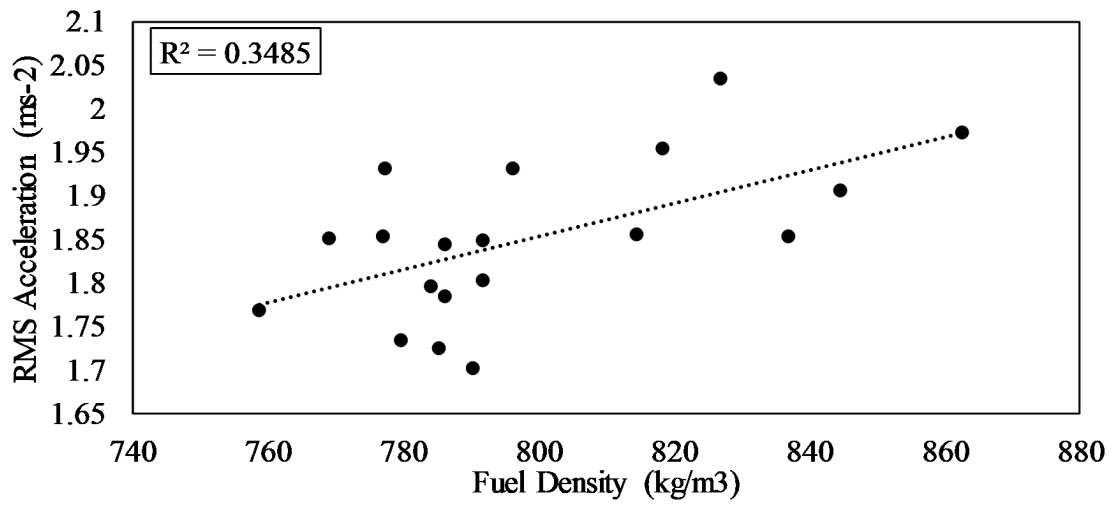


Figure 6.6: RMS acceleration of fuels tested in APU against the fuel density.

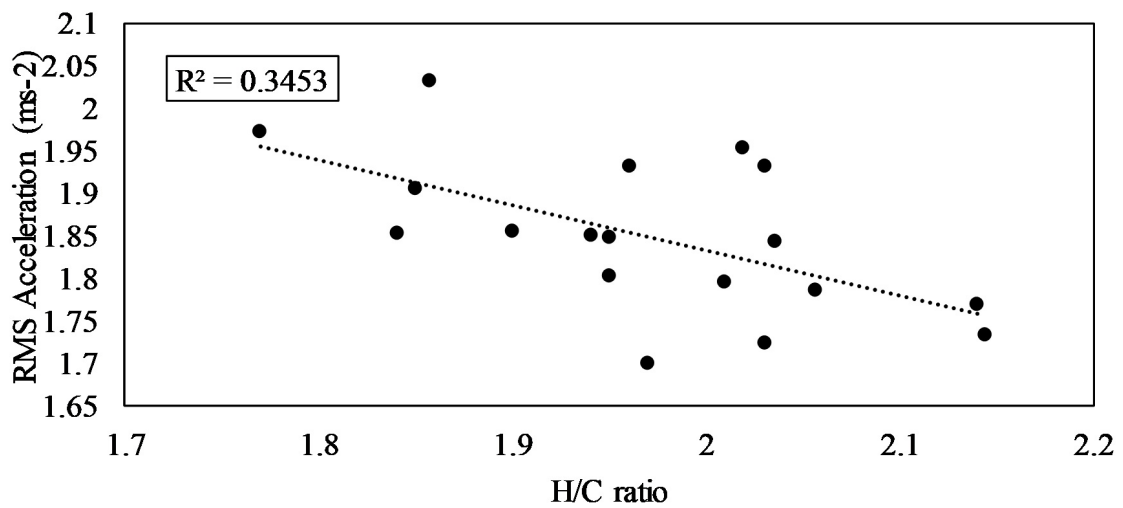


Figure 6.7: RMS acceleration of fuels tested in APU against the hydrogen to carbon ratio.

Note not all fuels' H/C ratio data were available.

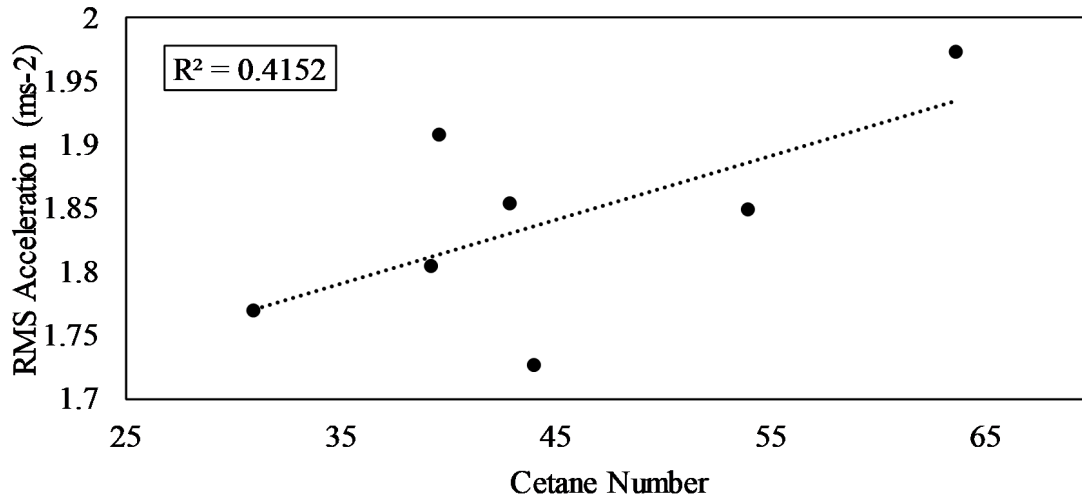


Figure 6.8: RMS acceleration of fuels tested in APU against the cetane number. Only fuels with cetane number available are depicted (RF3, RF7, RF8, RF10, RF11, RF12, RF13).

where the addition of extra hydrogen to methane fuel leads to lower acoustic oscillation in certain frequency ranges [154]. As RMS encompasses the entire frequency spectrum it can be said that this investigation finds that the increase in H/C ratio of a fuel tends to have a positive impact in terms of vibrations caused. This finding is supported by research conducted by Othman et al. who observed that as carbon to Hydrogen ratio increases vibrations also increase as shown in Fig. 2.28. This is in keeping with what has been observed in this particular investigation where we see a decrease in vibration intensity as H/C ratio increases (H/C ratio is the inverse of the C/H ratio).

The final fuel property with which a correlation has been achieved is cetane number as shown in Fig.6.8. It is seen that as the cetane number increases, the RMS vibrations increase. However, as only 7 data points were available due to the lack of testing of the cetane number of jet fuels as a standard this correlation should be viewed with sufficient scrutiny. That being said the correlation coefficient of 0.41 in keeping with the previous fuel properties. This finding is keeping with the definition of cetane number which is a parameter mainly used in the qualitative analysis of compression ignition (CI) engine fuels (i.e. Diesel). Cetane number is a parameter denoting the ignition delay (The time taken for diesel fuel to ignite after injection into a CI engine combustion chamber) of a fuel. A higher cetane number corresponds to a lower ignition delay and vice versa. A lower ignition delay could possibly indicate that such fuels are prone to unstable heat release

due to their chemical composition as cetane additives such as 2-ethylhexyl nitrate.

6.2.2 Octave analysis

This section depicts the octave analysis conducted on the noise data obtained from all the fuels tested in the APU. A description on the octave analysis process can be found in section 2.3.3. Overall, the data obtained from the microphones are of limited utility as they were placed outside the APU room and are therefore heavily damped by the sound insulation of the APU room walls. Figures 6.9, 6.10 and 6.11 depict the Sound pressure levels in decibels for Microphone 1 at condition 1, 2 and 3 respectively. The Frequency content has been divided into octaves as per ANSI standard S1.11-2014 [111]. In general, it is clearly visible that the APU noise is well distributed amongst the octave compared to the octave analysis of the combustor. With peaks visible in the 32Hz band for all 3 conditions. The lowest octave band for all 3 conditions is the 15kHz band. The highest overall sound pressure is located at condition 3 32Hz band at 102dB. However, the difference in sound pressure between the engine conditions are quite minimal due to the damping.

The largest variation in sound pressure is observed in the 4Hz band for all 3 conditions. This was also observed in the octave analysis of the combustor in chapter 5. It may be that the accuracy of the microphones drops towards the lower end of its sensitivity scale at 4dB which causes greater fluctuation in the sound pressure levels recorded in that octave band. However, it is more likely that this variation is caused by the equivalence ratio fluctuations at this low frequency variation of noise between the fuels was visible in the combustor testing as well. Furthermore, in the research conducted by Simons et al, this pattern is shown. This has been shown in Fig. 5.10. Moreover it is known in the literature that combustion instability is a relatively low frequency affair with variations occurring at sub 100hz [68, 155].

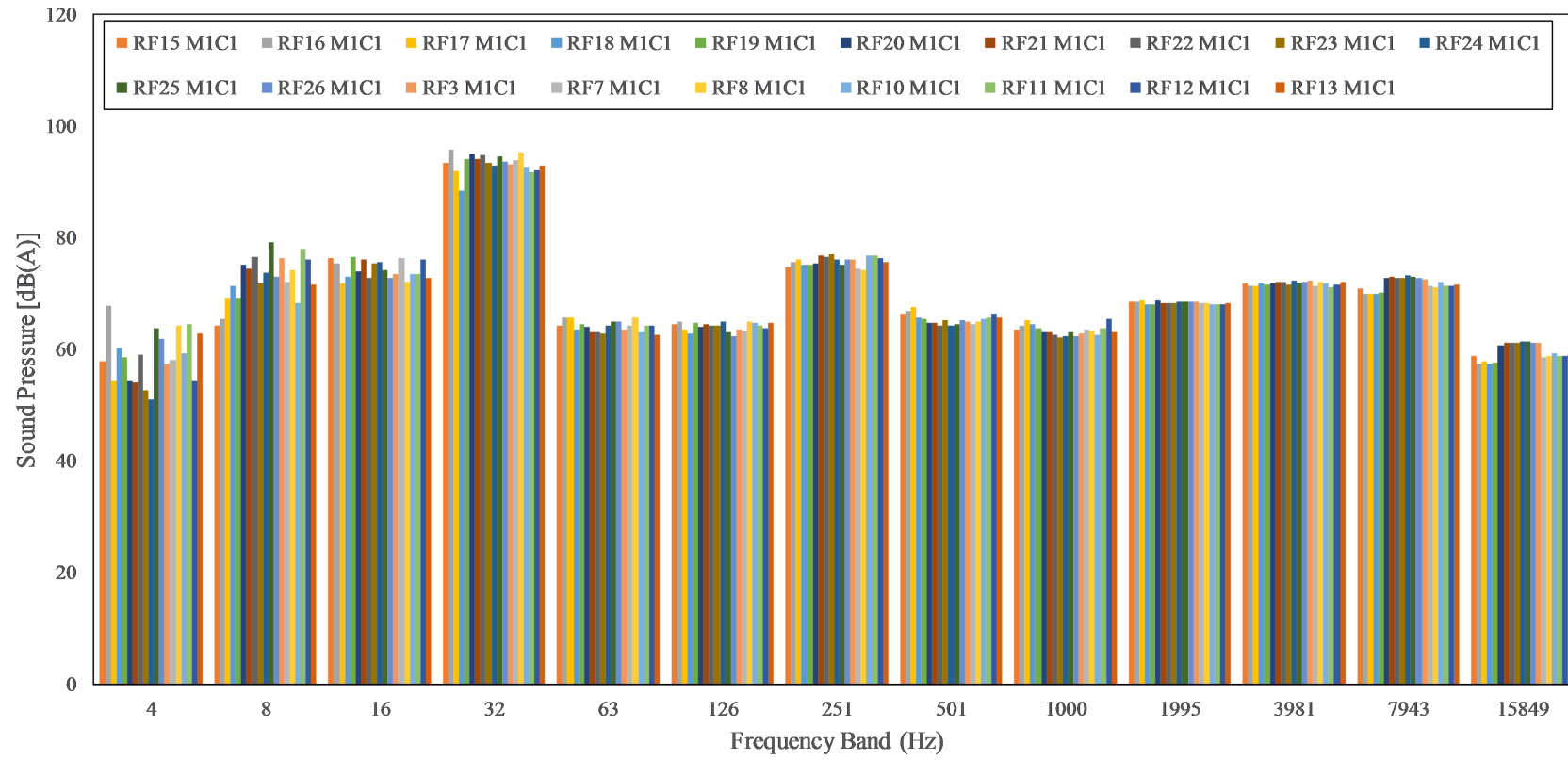


Figure 6.9: Octave band analysis M1 at condition 1. Reference pressure $20\mu Pa$ which corresponds with human hearing range.

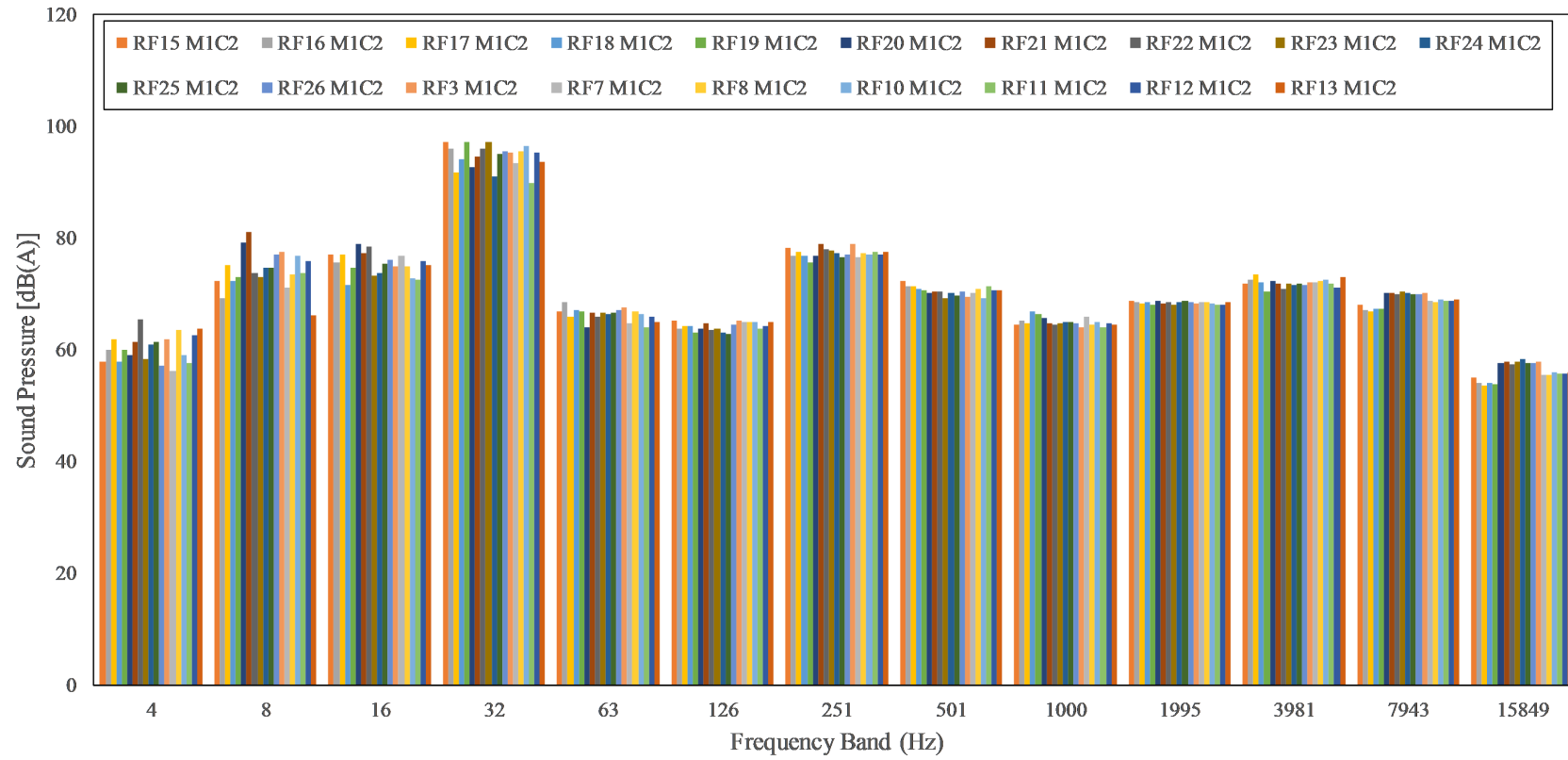


Figure 6.10: Octave band analysis M1 at condition 2. Reference pressure $20\mu Pa$ which corresponds with human hearing range.

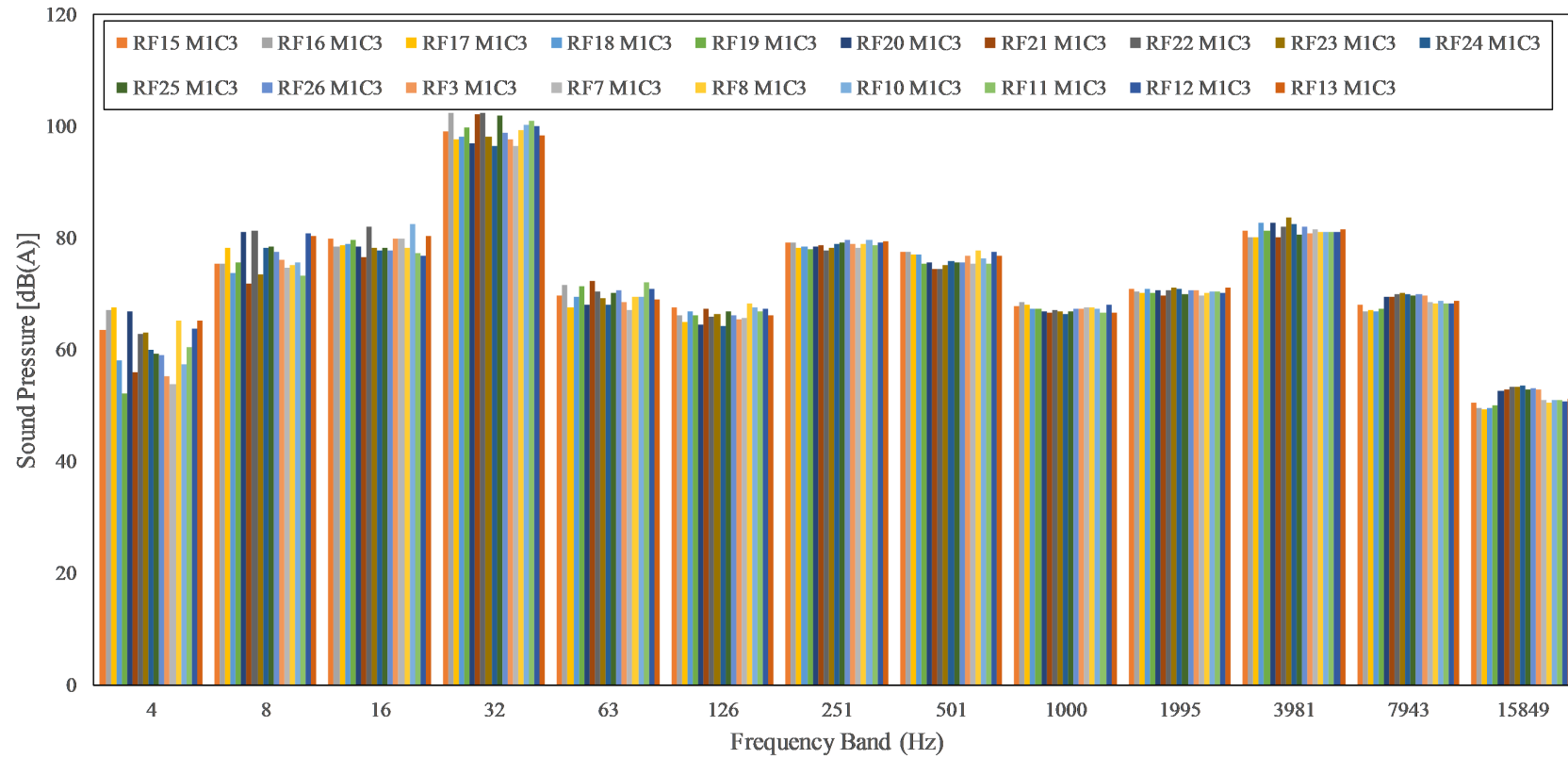


Figure 6.11: Octave band analysis M1 at condition 3. Reference pressure $20\mu Pa$ which corresponds with human hearing range.

6.3 Conclusions

Overall, in the experiments conducted with APU it can be conclusively said that fuel properties impact the vibrations and therefore the stability characteristics of the combustion produced by a full gas turbine adding to the knowledge. The noise and vibrations characteristics of the APU have been established by Fig.6.1.

Further findings of this investigation were the correlations derived with respect to RMS acceleration and fuel properties including density, viscosity, H/C ratio and cetane number, it is difficult to theorize as to which particular fluid property of these is contributing the most towards the vibrations generated as these variable are intrinsically linked to each other (i.e. fuels with a lower H/C ratio are generally denser as carbon is denser than hydrogen and the molecule is entirely formed of hydrogen and carbon molecules). Moreover, a foundation has been laid to derive an optimum fuel blend with respect to fuel properties by means of testing 20 drop-in alternative fuels and surrogates and measuring their instability characteristics and linking the instability to the fuel properties. All of the above are novel findings which add to the knowledge regarding the performance of alternative fuels instability characteristics on conventional gas turbines.

In addition, it should also be noted that vibrations observed in this chapter are caused by combustion, flow characteristics and the rotational mechanical components. It is clear that vibrations caused by combustion heat release fluctuation has a tendency to amplify the vibrations of rotational components. This explains the reason that RMS acceleration shows great variation with respect to fuel properties, where the RMS acceleration is in the main impacted by the turbo-machinery. This is clearly observed by the fact that condition 3 of the APU produces correlations with respect to fuel properties, while condition 1 and 2 do not or only show slight correlations. This is indicative of the fact that condition 1 and 2 of the APU is dominated by the non-combustion related turbulence vibrations and other machinery noise of the engine. However, with that being said, it is obvious that the combustion process and the noise and vibration caused by it go on to affect the turbo machinery of the APU. This is shown from the fact that the natural mode shapes of the APU are amplified by the combustion noise and vibration.

Moreover, it should be noted that this investigation has resulted in a proven method-

ology to detect combustion influenced noise and vibrations. This method can in future be used to determine the impact of any fuel on a gas turbine.

Chapter 7

Overall conclusions of alternative fuels and combustion instability and future work

This chapter describes the overall conclusions that have been gleaned from the combination of knowledge gained in the 3 results chapters. It also describes the potential future work that can be conducted to complement and enrich the understanding of combustion instability and how fuel variation impacts in the wider sense.

7.1 Overall conclusions

To validate the results from chapters 5 and 6 the SMD obtained from the droplet size analysis has been compared to the acceleration data obtained from the APU and the combustor. Figure 7.1 depicts the SMD vs RMS acceleration for the common fuels tested in the droplet size analysis and the APU for noise and vibrations. Fuels RF7-RF14 were tested for both droplet size and vibrations. The SMD was tested at 60psi injection pressure and the accelerometer was X1 and the APU condition was condition 3 (main engine start condition on table 3.6). A good positive correlation was observed showing that as droplet size increases the the combustion vibrations also increase in the APU. This is explained by the fact that as droplet size increases in the combustion chamber, this leads to poorer mixing

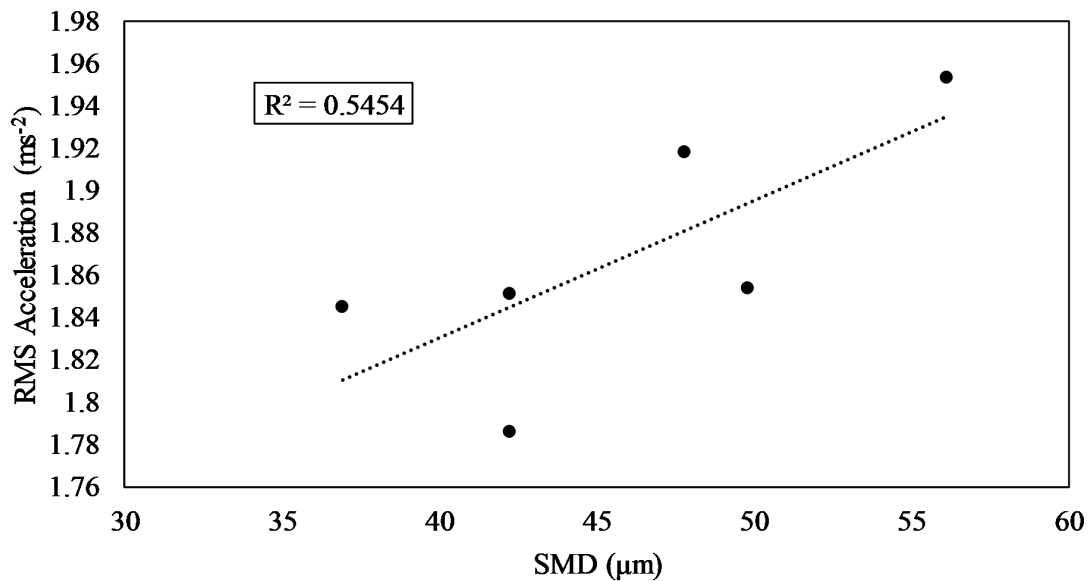


Figure 7.1: RMS acceleration for X1 condition 3 against the SMD at 60psi for fuels RF7, RF8, RF10, RF11, RF12 and RF13 for the APU.

which in turn causes variations in the density gradient of the fuel air mixture. Which itself leads to greater fluctuations in heat release and pressure waves in the combustor which when impinging upon the solid combustion chamber walls leads to increased vibrations.

Figure 7.2 shows the peak height for condition 2 (refer to table 3.5) X1 of the combustor against the SMD at 60psi for the A and B group fuels. The peak height has been chosen for this comparison instead of the RMS values as in the combustor investigation the RMS values are of less utility due to the overall peak height to noise ratio being lower. This is due to the fact that the combustor produces less overall vibrations with respect to the APU which is natural considering the lack of rotational components in the combustor. The correlation again here is that as SMD increase the magnitude of vibrations produced increases. leading to less stable combustion.

From this analysis it is possible to conclude that droplet size and atomisation plays a key role in combustion instability, which in turn means that fuel properties play a key role in combustion instability from an injection point of view. This view is supported in the literature as equivalence ratio fluctuations are a known cause of combustion instability [74, 77, 108, 153].

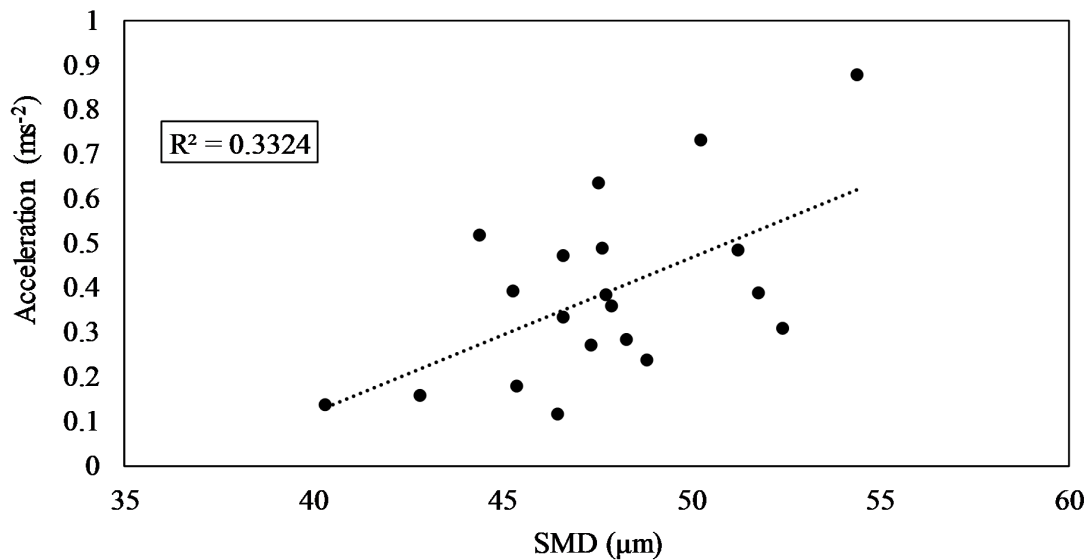


Figure 7.2: Peak height of T2 X1 against the SMD at 60psi for fuels both A and B group fuels tested on atmospheric combustor.

Further conclusions derived from this investigation is that mono-aromatic compounds with large aliphatic components attached to them performed well in the droplet size analysis and the combustor testing with respect to poly-aromatic compounds.

Another conclusion of this overall investigation is the establishment of a link between the viscosity, flashpoint fuel density, H/C ratio and cetane number of the fuels and combustion instability which has been observed by means of acoustics and vibrations. This makes sense as the fuel properties heavily influence the injection characteristics of the fuel which in turn cause oscillations in the heat release and acoustic coupled pressure waves which lead to increased noise and vibration. Furthermore, it should be noted that this increased noise and vibrations compared with conventional Jet A1 while minor, will lead to increased wear of the turbo machinery and combustion liners with prolonged use increasing the high-cycle fatigue of these components and therefore decrease in maintenance intervals which is detrimental to commercial operation.

A future impact of this work would be that designer fuels could be optimised for current combustions systems and future combustion technologies.

Therefore, in summary the contributions to knowledge of this work can be summarised

as follows;

- Impact of varying aromatic species and drop-in alternative fuels and their properties on droplet size distribution.
- The impact of fuel properties on droplet size has been investigated especially with respect to aromatic species which has not been done previously. Which in turn has allowed the determination of an optimum aromatic to be blended with future alternative jet fuels (Ethylbenzene and Cumene).
- Impact of aromatic species and their properties on noise, vibrations and combustion instability in a gas turbine combustor.
- Determining the impact of fuel properties on noise and vibrations of a full gas turbine using 20 drop-in alternative fuels and reference fuels. Deriving correlations between noise and vibrations and Fuel; density, viscosity, flash point, surface tension, cetane number and H/C ratio.
- Finally, Linking of fuel droplet size to vibrations produced.

7.2 Future work

This section describes the possible work that could be completed in the future to expand and enrich the findings of this investigation.

Firstly, it would be prudent to observe the variation of combustion vibrations and noise produced for various fuels at varying pressure ratios. This is important as the the overall pressure ratio (OPR) of commercial gas turbines vary from around 15 to 60 in the latest generation aviation turbines. Therefore, any variation in noise and vibration that can be attributed to combustion pressures can be observed independently of the vibration and noise caused by fuel variation.

Secondly, it would be useful to conduct a study on the seal swell capabilities of the aromatics tested in this investigation, particularly Cumene styrene and O-Xylene which performed the best in the noise and vibrations testing as well as the droplet size analysis. With this knowledge it is possible to say that adding these compounds to future alternative

fuels would satisfy the operational requirements with respect to fuel system lubricity and combustion instability.

Another work that could be considered in future would be an active control system to damp the noise and vibrations observed in this investigation which are caused by equivalence ratio fluctuation. This could take the form of variable geometry fuel injection system which can compensate for the alternative fuel used in the engine. Overall it could be used to vary the nozzle diameter, air assist pressures, injection pressures etc.

Bibliography

- [1] B. Khandelwal, C. J. Wijesinghe, and S. Sriraman, “Effect of Alternative Fuels on Emissions and Engine Compatibility,” in *Energy for Propulsion : A Sustainable Technologies Approach*, A. K. Runchal, A. K. Gupta, A. Kushari, A. De, and S. K. Aggarwal, Eds., Singapore: Springer Singapore, 2018, pp. 27–50, ISBN: 978-981-10-7473-8. DOI: 10.1007/978-981-10-7473-8_2.
- [2] C. J. Wijesinghe and B. Khandelwal, “Impact of alternative fuel on gas turbine noise, vibration and instability,” in *AIAA Scitech 2019 Forum*, ser. AIAA SciTech Forum, Reston, Virginia: American Institute of Aeronautics and Astronautics, Jan. 2019, ISBN: 978-1-62410-578-4. DOI: 10.2514/6.2019-0240.
- [3] C. Wijesinghe, Y. Ling, and B. Khandelwal, “Experimental Investigation and Assessment of Combustion Instability and Engine Vibrations; as an Impact of Using Novel Alternative Fuels with Low Aromatics in a Gas Turbine Engine,” GPPS, Sep. 2019. DOI: 10.33737/gpps19-bj-195.
- [4] P. King, A. Al-Sheboul, A. F. C. Dos Santos, C. Wijesinghe, and B. Khandelwal, “The feasibility of hydrogen assisted combustors and fuel reformation technologies,” in *AIAA Propulsion and Energy Forum and Exposition, 2019*, American Institute of Aeronautics and Astronautics Inc, AIAA, 2019, ISBN: 9781624105906. DOI: 10.2514/6.2019-4411.
- [5] B. Khandelwal, J. Cronly, I. Ahmed, C. Wijesinghe, and C. Lewis, “The effect of alternative fuels on gaseous and particulate matter (PM) emission performance in an auxiliary power unit (APU),” *The Aeronautical Journal*, vol. 123, no. 1263, pp. 617–634, May 2019, ISSN: 0001-9240. DOI: 10.1017/aer.2019.16.

- [6] A. Schäfer, “The Prospects for Biofuels in Aviation,” in *Biofuels for Aviation*, C. J. Chuck, Ed., Elsevier, 2016, pp. 3–16, ISBN: 978-0-12-804568-8. DOI: 10.1016/B978-0-12-804568-8.00001-9.
- [7] D. Ibarra, R. Ramírez-Mendoza, and E. López, “Noise emission from alternative fuel vehicles: Study case,” *Applied Acoustics*, vol. 118, pp. 58–65, Mar. 2017, ISSN: 1872910X. DOI: 10.1016/j.apacoust.2016.11.010.
- [8] A. L. Hansell, M. Blangiardo, L. Fortunato, S. Floud, K. de Hoogh, D. Fecht, R. E. Ghosh, H. E. Laszlo, C. Pearson, L. Beale, S. Beevers, J. Gulliver, N. Best, S. Richardson, and P. Elliott, “Aircraft noise and cardiovascular disease near Heathrow airport in London: small area study,” *BMJ*, vol. 347, no. oct08 3, f5432–f5432, Oct. 2013, ISSN: 1756-1833. DOI: 10.1136/bmj.f5432.
- [9] M. P. Norton and D. G. Karczub, “Fundamentals of Noise and Vibration Analysis for Engineers, 2nd Edition,” *Noise Control Engineering Journal*, vol. 55, no. 2, p. 275, 2007, ISSN: 07362501. DOI: 10.3397/1.2721371.
- [10] M. Leyko, F. Nicoud, S. Moreau, and T. Poinso, “Numerical and analytical investigation of the indirect combustion noise in a nozzle,” *Comptes Rendus Mécanique*, vol. 337, no. 6-7, pp. 415–425, Jun. 2009, ISSN: 16310721. DOI: 10.1016/j.crme.2009.06.025.
- [11] International Energy Agency, *Data tables – Data & Statistics - IEA*, 2017. [Online]. Available: <https://www.iea.org/data-and-statistics/data-tables?country=WORLD%7B%5C&%7Denergy=Oil%7B%5C&%7Dyear=2017> (visited on 01/16/2020).
- [12] BP, “BP Statistical Review of World Energy 2019,” Tech. Rep., 2019.
- [13] M. U. Kirschbaum, “Assessing the merits of bioenergy by estimating marginal climate-change impacts,” *The International Journal of Life Cycle Assessment*, vol. 22, no. 6, pp. 841–852, Jun. 2017, ISSN: 0948-3349. DOI: 10.1007/s11367-016-1196-4.

- [14] M. Brandão, A. Levasseur, M. U. Kirschbaum, B. P. Weidema, A. L. Cowie, S. V. Jørgensen, M. Z. Hauschild, D. W. Pennington, and K. Chomkham Sri, “Key issues and options in accounting for carbon sequestration and temporary storage in life cycle assessment and carbon footprinting,” *International Journal of Life Cycle Assessment*, vol. 18, no. 1, pp. 230–240, Jan. 2013, ISSN: 09483349. DOI: 10.1007/s11367-012-0451-6.
- [15] S. T. Omaye, “Metabolic modulation of carbon monoxide toxicity,” *Toxicology*, vol. 180, no. 2, pp. 139–150, Nov. 2002, ISSN: 0300483X. DOI: 10.1016/S0300-483X(02)00387-6.
- [16] H. Brunt and S. J. Jones, “A pragmatic public health-driven approach to enhance local air quality management risk assessment in Wales, UK,” *Environmental Science & Policy*, vol. 96, pp. 18–26, Jun. 2019, ISSN: 14629011. DOI: 10.1016/j.envsci.2019.02.008.
- [17] R. Wu, X. Song, Y. Bai, J. Chen, Q. Zhao, S. Liu, H. Xu, T. Wang, B. Feng, Y. Zhang, L. Zhong, X. Wang, F. Wu, and W. Huang, “Are current Chinese national ambient air quality standards on 24-hour averages for particulate matter sufficient to protect public health?” *Journal of Environmental Sciences*, vol. 71, pp. 67–75, Sep. 2018, ISSN: 10010742. DOI: 10.1016/j.jes.2018.01.017.
- [18] L. Zheng, C. Ling, E. A. Ubogu, J. Cronly, I. Ahmed, Y. Zhang, and B. Khandelwal, “Effects of Alternative Fuel Properties on Particulate Matter Produced in a Gas Turbine Combustor,” *Energy & Fuels*, vol. 32, no. 9, pp. 9883–9897, Sep. 2018, ISSN: 0887-0624. DOI: 10.1021/acs.energyfuels.8b01442.
- [19] K. Gupta, A. Rehman, and R. Sarviya, “Bio-fuels for the gas turbine: A review,” *Renewable and Sustainable Energy Reviews*, vol. 14, no. 9, pp. 2946–2955, Dec. 2010, ISSN: 13640321. DOI: 10.1016/j.rser.2010.07.025.
- [20] S. Yang, Y. Yang, R. K. Kankala, and B. Li, “Sustainability assessment of syn-fuels from biomass or coal: An insight on the economic and ecological burdens,” *Renewable Energy*, vol. 118, pp. 870–878, Apr. 2018, ISSN: 09601481. DOI: 10.1016/j.renene.2017.11.073.

- [21] U.S. Energy information Administration, *World oil transit chokepoints*, 2013. [Online]. Available: https://www.eia.gov/international/analysis/special-topics/World%7B%5C_%7D0il%7B%5C_%7DTransit%7B%5C_%7DChokepoints.
- [22] R. J. Heffron, D. McCauley, and B. K. Sovacool, “Resolving society’s energy trilemma through the Energy Justice Metric,” *Energy Policy*, vol. 87, pp. 168–176, Dec. 2015, ISSN: 03014215. DOI: 10.1016/j.enpol.2015.08.033.
- [23] J. Hileman and R. Stratton, “Alternative jet fuel feasibility,” *Transport Policy*, vol. 34, pp. 52–62, Jul. 2014, ISSN: 0967070X. DOI: 10.1016/j.tranpol.2014.02.018.
- [24] Ministry of Defence UK Aviation fuels committee, *Defence Standard 91-091*, 2016. [Online]. Available: https://global.ihs.com/doc%7B%5C_%7Ddetail.cfm?document%7B%5C_%7Dname=DEF%20STAN%2091-091%7B%5C_%7Ditem%7B%5C_%7Ds%7B%5C_%7Dkey=00450750.
- [25] ASTM, *ASTM D1655 18a Standard Specification for Aviation Turbine Fuels*, 2018. DOI: 10.1520/D1655-19A. [Online]. Available: <http://www.astm.org/cgi-bin/resolver.cgi?D1655>.
- [26] ASTM International, *D7566 - 18 Standard Specification for Aviation Turbine Fuel Containing Synthesized Hydrocarbons*, 2018. DOI: 10.1520/D7566-18. [Online]. Available: www.astm.org..
- [27] M. Bernabei, R. Reda, R. Galiero, and G. Bocchinfuso, “Determination of total and polycyclic aromatic hydrocarbons in aviation jet fuel,” *Journal of Chromatography A*, vol. 985, no. 1-2, pp. 197–203, Jan. 2003, ISSN: 00219673. DOI: 10.1016/S0021-9673(02)01826-5.
- [28] N. S. Mat Aron, K. S. Khoo, K. W. Chew, P. L. Show, W.-H. Chen, and T. H. P. Nguyen, “Sustainability of the four generations of biofuels – A review,” *International Journal of Energy Research*, vol. 44, no. 12, pp. 9266–9282, Oct. 2020, ISSN: 0363-907X. DOI: 10.1002/er.5557. [Online]. Available: <https://onlinelibrary.wiley.com/doi/10.1002/er.5557>.

- [29] R. C. de Cerqueira Leite, M. R. L. Verde Leal, L. A. Barbosa Cortez, W. M. Griffin, and M. I. Gaya Scandiffio, “Can Brazil replace 5% of the 2025 gasoline world demand with ethanol?” *Energy*, vol. 34, no. 5, pp. 655–661, May 2009, ISSN: 03605442. DOI: 10.1016/j.energy.2008.11.001.
- [30] M. Moreira, A. C. Gurgel, and J. E. A. Seabra, “Life Cycle Greenhouse Gas Emissions of Sugar Cane Renewable Jet Fuel,” *Environmental Science & Technology*, vol. 48, no. 24, pp. 14 756–14 763, Dec. 2014, ISSN: 0013-936X. DOI: 10.1021/es503217g.
- [31] F. Pierobon, I. L. Eastin, and I. Ganguly, “Life cycle assessment of residual lignocellulosic biomass-based jet fuel with activated carbon and liginosulfonate as co-products,” *Biotechnology for Biofuels*, vol. 11, no. 1, May 2018, ISSN: 17546834. DOI: 10.1186/s13068-018-1141-9.
- [32] I. Ganguly, F. Pierobon, T. C. Bowers, M. Huisenga, G. Johnston, and I. L. Eastin, “‘Woods-to-Wake’ Life Cycle Assessment of residual woody biomass based jet-fuel using mild bisulfite pretreatment,” *Biomass and Bioenergy*, vol. 108, pp. 207–216, Jan. 2018, ISSN: 18732909. DOI: 10.1016/j.biombioe.2017.10.041.
- [33] A. Gasparatos, P. Stromberg, and K. Takeuchi, “Sustainability impacts of first-generation biofuels,” *Animal Frontiers*, vol. 3, no. 2, pp. 12–26, Apr. 2013, ISSN: 2160-6056. DOI: 10.2527/af.2013-0011.
- [34] D. Wardle, “Global sale of green air travel supported using biodiesel,” *Renewable and Sustainable Energy Reviews*, vol. 7, no. 1, pp. 1–64, Feb. 2003, ISSN: 13640321. DOI: 10.1016/S1364-0321(03)00002-9.
- [35] W. Chu, J. Xu, J. Hong, T. Lin, and A. Khodakov, “Design of efficient Fischer Tropsch cobalt catalysts via plasma enhancement: Reducibility and performance (Review),” *Catalysis Today*, vol. 256, no. P1, pp. 41–48, Nov. 2015, ISSN: 09205861. DOI: 10.1016/j.cattod.2015.05.024.
- [36] T. Kandaramath Hari, Z. Yaakob, and N. N. Binitha, “Aviation biofuel from renewable resources: Routes, opportunities and challenges,” *Renewable and Sustainable Energy Reviews*, vol. 42, pp. 1234–1244, Feb. 2015, ISSN: 13640321. DOI:

- 10.1016/j.rser.2014.10.095. [Online]. Available: <https://linkinghub.elsevier.com/retrieve/pii/S1364032114009204>.
- [37] M. Fatih Demirbas, “Biorefineries for biofuel upgrading: A critical review,” *Applied Energy*, vol. 86, no. SUPPL. 1, S151–S161, Nov. 2009, ISSN: 03062619. DOI: 10.1016/j.apenergy.2009.04.043.
- [38] W. L. Roberts, “Bio Jet Fuels,” in *The 5th International Biofuels Conference*, 2008.
- [39] J. I. Hileman, H. M. Wong, I. A. Waitz, D. S. Ortiz, J. T. Bartis, M. A. Weiss, and P. E. Donohoo, “Near-Term Feasibility of Alternative Jet Fuels,” MIT, Tech. Rep. 6, 2009, pp. 1–150. [Online]. Available: https://www.rand.org/pubs/technical%7B%5C_%7Dreports/TR554.html.
- [40] S. Richter, M. Braun-Unkhoff, C. Naumann, and U. Riedel, “Paths to alternative fuels for aviation,” *CEAS Aeronautical Journal*, vol. 9, no. 3, pp. 389–403, Sep. 2018, ISSN: 1869-5582. DOI: 10.1007/s13272-018-0296-1.
- [41] E. Corporan, T. Edwards, L. Shafer, M. J. DeWitt, C. Klingshirn, S. Zabarnick, Z. West, R. Striebich, J. Graham, and J. Klein, “Chemical, Thermal Stability, Seal Swell, and Emissions Studies of Alternative Jet Fuels,” *Energy & Fuels*, vol. 25, no. 3, pp. 955–966, Mar. 2011, ISSN: 0887-0624. DOI: 10.1021/ef101520v.
- [42] Y. Liu and C. W. Wilson, “Investigation into the Impact of n-Decane, Decalin, and Isoparaffinic Solvent on Elastomeric Sealing Materials,” *Advances in Mechanical Engineering*, vol. 4, p. 127430, Jan. 2012, ISSN: 1687-8140. DOI: 10.1155/2012/127430.
- [43] W.-C. Wang and L. Tao, “Bio-jet fuel conversion technologies,” *Renewable and Sustainable Energy Reviews*, vol. 53, pp. 801–822, Jan. 2016, ISSN: 13640321. DOI: 10.1016/j.rser.2015.09.016.
- [44] L. Rye, S. Blakey, and C. W. Wilson, “Sustainability of supply or the planet: a review of potential drop-in alternative aviation fuels,” *Energy Environ. Sci.*, vol. 3, no. 1, pp. 17–27, 2010, ISSN: 1754-5692. DOI: 10.1039/B918197K.

- [45] BYOGY Renewables, “Alcohol To Jet (ATJ) emerging through ASTM,” 2011. [Online]. Available: https://www.icao.int/Meetings/EnvironmentalWorkshops/Documents/2011-SUSTAF/19%7B%5C_%7DWeiss.pdf.
- [46] S. Geleynse, K. Brandt, M. Garcia-Perez, M. Wolcott, and X. Zhang, “The Alcohol-to-Jet Conversion Pathway for Drop-In Biofuels: Techno-Economic Evaluation,” *ChemSusChem*, vol. 11, no. 21, pp. 3728–3741, Nov. 2018, ISSN: 18645631. DOI: 10.1002/cssc.201801690.
- [47] D. R. Tree and K. I. Svensson, “Soot processes in compression ignition engines,” *Progress in Energy and Combustion Science*, vol. 33, no. 3, pp. 272–309, Jun. 2007, ISSN: 03601285. DOI: 10.1016/j.pecs.2006.03.002.
- [48] A. Kugele, F. Jelinek, and R. Gaffal, “Aircraft Particulate Matter Emission Estimation through all Phases of Flight EEC/SEE/2005/0014,” Brussels, Tech. Rep., 2005. [Online]. Available: https://www.eurocontrol.int/sites/default/files/library/034%7B%5C_%7DAircraft%7B%5C_%7DParticulate%7B%5C_%7DMatter%7B%5C_%7DEmission%7B%5C_%7DEstimation.pdf.
- [49] A. Petzold and C. W. Wilson, “Physical and Chemical Properties of Aircraft Engine Exhaust Particles,” Oberpfaffenhofen. [Online]. Available: https://www.dlr.de/pa/Portaldata/33/Resources/dokumente/poster/D2%7B%5C_%7DPetzold%7B%5C_%7DPartEmis.pdf.
- [50] J. Kuenen, B. Gschwind, K. M. Drebszok, D. Stetter, R. Kranenburg, C. Hendriks, M. Lefèvre, I. Blanc, A. Wyrwa, and M. Schaap, “Estimating particulate matter health impact related to the combustion of different fossil fuels,” in *27th International Conference on Informatics for Environmental Protection*, B. Page, A. G. Fleischer, J. Göbel, and V. Wohlgemuth, Eds., Hambourg, Germany, Sep. 2013, p. 171. [Online]. Available: <https://hal-mines-paristech.archives-ouvertes.fr/hal-00858231>.
- [51] D. W. Dockery, C. A. Pope, X. Xu, J. D. Spengler, J. H. Ware, M. E. Fay, B. G. Ferris, and F. E. Speizer, “An Association between Air Pollution and Mortality in

- Six U.S. Cities,” *New England Journal of Medicine*, vol. 329, no. 24, pp. 1753–1759, Dec. 1993, ISSN: 15334406. DOI: 10.1056/NEJM199312093292401.
- [52] J. D. Sacks, L. W. Stanek, T. J. Luben, D. O. Johns, B. J. Buckley, J. S. Brown, and M. Ross, “Particulate Matter–Induced Health Effects: Who Is Susceptible?” *Environmental Health Perspectives*, vol. 119, no. 4, pp. 446–454, Apr. 2011, ISSN: 0091-6765. DOI: 10.1289/ehp.1002255.
- [53] T. REICHHARDT, “EPA particulate matter health effects document criticized,” *Environmental Science & Technology*, vol. 29, no. 10, 449A–449A, Oct. 1995, ISSN: 0013-936X. DOI: 10.1021/es00010a735.
- [54] P. Lobo, D. E. Hagen, and P. D. Whitefield, “Comparison of PM Emissions from a Commercial Jet Engine Burning Conventional, Biomass, and Fischer–Tropsch Fuels,” *Environmental Science & Technology*, vol. 45, no. 24, pp. 10 744–10 749, Dec. 2011, ISSN: 0013-936X. DOI: 10.1021/es201902e.
- [55] B. T. Brem, L. Durdina, F. Siegerist, P. Beyerle, K. Bruderer, T. Rindlisbacher, S. Rocci-Denis, □. M. Gurhan Andac, J. Zelina, O. Penanhoat, J. Wang, M. G. Andac, J. Zelina, O. Penanhoat, and J. Wang, “Effects of Fuel Aromatic Content on Nonvolatile Particulate Emissions of an In-Production Aircraft Gas Turbine,” *Environmental Science & Technology*, vol. 49, no. 22, pp. 13 149–13 157, Nov. 2015, ISSN: 0013-936X. DOI: 10.1021/acs.est.5b04167.
- [56] M. J. DeWitt, E. Corporan, J. Graham, and D. Minus, “Effects of Aromatic Type and Concentration in Fischer–Tropsch Fuel on Emissions Production and Material Compatibility,” *Energy & Fuels*, vol. 22, no. 4, pp. 2411–2418, Jul. 2008, ISSN: 0887-0624. DOI: 10.1021/ef8001179.
- [57] P. I. Williams, J. D. Allan, P. Lobo, H. Coe, S. Christie, C. Wilson, D. Hagen, P. Whitefield, D. Raper, and L. Rye, “Impact of Alternative Fuels on Emissions Characteristics of a Gas Turbine Engine – Part 2: Volatile and Semivolatile Particulate Matter Emissions,” *Environmental Science & Technology*, vol. 46, no. 19, pp. 10 812–10 819, Oct. 2012, ISSN: 0013-936X. DOI: 10.1021/es301899s.

- [58] A. Liati, B. T. Brem, L. Durdina, M. Vö Gtli, Y. Arroyo, R. Dasilva, □. Panayotis, D. Eggenschwiler, and J. Wang, “Electron Microscopic Study of Soot Particulate Matter Emissions from Aircraft Turbine Engines,” *Environmental Science and Technology*, vol. 48, pp. 10 975–10 983, 2014. DOI: 10 . 1021 / es501809b. [Online]. Available: <http://pubs.acs.org/doi/pdf/10.1021/es501809b>.
- [59] Rolls-Royce and FAA, “Rolls-Royce Alternative Fuels Program-Final Report (CLEEN),” U.S. Department of Transportation, Federal Aviation Administration, Rolls-Royce, Tech. Rep., 2015.
- [60] S. Christie, D. Raper, D. S. Lee, P. I. Williams, L. Rye, S. Blakey, C. W. Wilson, P. Lobo, D. Hagen, and P. D. Whitefield, “Polycyclic Aromatic Hydrocarbon Emissions from the Combustion of Alternative Fuels in a Gas Turbine Engine,” *Environmental Science & Technology*, vol. 46, no. 11, pp. 6393–6400, Jun. 2012, ISSN: 0013-936X. DOI: 10 . 1021 / es300301k.
- [61] E. W. Thomas, R. E. Fuller, and K. Terauchi, “Fluoroelastomer compatibility with biodiesel fuels,” in *SAE Technical Papers*, SAE International, 2007. DOI: 10 . 4271 / 2007 - 01 - 4061.
- [62] S. Z. Qamar, M. Akhtar, T. Pervez, and M. S. Al-Kharusi, “Mechanical and structural behavior of a swelling elastomer under compressive loading,” *Materials & Design*, vol. 45, pp. 487–496, Mar. 2013, ISSN: 02613069. DOI: 10 . 1016 / j . matdes . 2012 . 09 . 020. [Online]. Available: <https://linkinghub.elsevier.com/retrieve/pii/S0261306912006504>.
- [63] The Boeing Company and University of Dayton Research Institute, “CLEEN Report: Impact of Alternative Jet Fuel and Fuel Blends on Non-Metallic Materials Used in Commercial Aircraft Fuel Systems,” Tech. Rep., 2011. [Online]. Available: https://www.faa.gov/about/office%7B%5C_%7Dorg/headquarters%7B%5C_%7Doffices/apl/research/aircraft%7B%5C_%7Dtechnology/cleen/reports/.
- [64] J. L. Graham, R. C. Striebich, K. J. Myers, D. K. Minus, and W. E. Harrison, “Swelling of Nitrile Rubber by Selected Aromatics Blended in a Synthetic Jet

- Fuel,” *Energy & Fuels*, vol. 20, no. 2, pp. 759–765, Mar. 2006, ISSN: 0887-0624. DOI: 10.1021/ef050191x.
- [65] J. P. Baltrus, D. D. Link, P. H. Zandhuis, R. J. Gormley, and R. R. Anderson, “Screening of potential o-ring swelling additives for ultraclean transportation fuels,” in *ACS Symposium Series*, vol. 959, 2007, pp. 197–208, ISBN: 0841274096. DOI: 10.1021/bk-2007-0959.ch015.
- [66] A. Anuar, “Effect of Fuels, Aromatics and Preparation Methods On Seal-Swell,” Ph.D. dissertation, University of Sheffield, 2014.
- [67] Y. Çengel and M. Boles, *Thermodynamics an engineering approach*, 8 Edition. McGraw-Hill Education, 2018, ISBN: 978-0-07-339817-4.
- [68] A. H. Lefebvre and D. R. Ballal, *Gas Turbine Combustion; Alternative Fuels and Emissions*, 2. CRC Press, Apr. 2010, vol. 141, pp. 247–248, ISBN: 9780429141041. DOI: 10.1201/9781420086058. [Online]. Available: <https://www.taylorfrancis.com/books/9781420086058>.
- [69] Rolls-Royce, *The Jet Engine*, 5 Edition. Wiley, 1996, ISBN: 978-1-119-06599-9.
- [70] K. Ajay, “Gas turbine power plant (introduction),” [Online]. Available: <https://www.theengineerspost.com/gas-turbine-power-plant/>.
- [71] T. C. Lieuwen, *Unsteady Combustor Physics*. Cambridge University Press, 2012, ISBN: 9781107015999.
- [72] T. C. Lieuwen and V. Yang, *Gas turbine emissions*. Cambridge University Press, 2013, ISBN: 9781139015462.
- [73] J. Yoon, M.-K. Kim, J. Hwang, J. Lee, and Y. Yoon, “Effect of fuel–air mixture velocity on combustion instability of a model gas turbine combustor,” *Applied Thermal Engineering*, vol. 54, no. 1, pp. 92–101, May 2013, ISSN: 13594311. DOI: 10.1016/j.applthermaleng.2013.01.032.
- [74] K. R. McManus, T. Poinsot, and S. M. Candel, *A review of active control of combustion instabilities*, 1993. DOI: 10.1016/0360-1285(93)90020-F.

- [75] T. C. Lieuwen and V. Yang, *Combustion Instabilities In Gas Turbine Engines*. Reston ,VA: American Institute of Aeronautics and Astronautics, Jan. 2006, ISBN: 978-1-56347-669-3. DOI: 10 . 2514 / 4 . 866807. [Online]. Available: <http://arc.aiaa.org/doi/book/10.2514/4.866807>.
- [76] H. Kobayashi, H. Gotoda, S. Tachibana, and S. Yoshida, “Detection of frequency-mode-shift during thermoacoustic combustion oscillations in a staged aircraft engine model combustor,” *Journal of Applied Physics*, vol. 122, no. 22, p. 224 904, Dec. 2017, ISSN: 0021-8979. DOI: 10 . 1063/1 . 5003912.
- [77] S. Candel, “Combustion dynamics and control: Progress and challenges,” *Proceedings of the Combustion Institute*, vol. 29, no. 1, pp. 1–28, Jan. 2002, ISSN: 15407489. DOI: 10 . 1016/S1540-7489(02)80007-4.
- [78] J. W. S. Rayleigh, *The theory of sound*, 2 edition, R. B. Lindsay and J. W. Strutt, Eds. New York: New York : Dover, 1945, 1945, ISBN: 0486602931.
- [79] M. Rabs, F.-K. Benra, and O. Schneider, “Emergence of Kelvin-Helmholtz Instabilities in Gas Turbine Rim Cavities: A Parameter Study,” in *ASME Turbo Expo 2012*, American Society of Mechanical Engineers, Jun. 2012, pp. 2097–2106, ISBN: 978-0-7918-4470-0. DOI: 10 . 1115/GT2012-68834.
- [80] F. E. Marble and S. M. Candel, “Acoustic disturbance from gas non-uniformities convected through a nozzle,” *Journal of Sound and Vibration*, vol. 55, no. 2, pp. 225–243, Nov. 1977, ISSN: 10958568. DOI: 10 . 1016/0022-460X(77)90596-X.
- [81] K. H. Yu, A. Trouvé, and J. W. Daily, “Low-frequency pressure oscillations in a model ramjet combustor,” *Journal of Fluid Mechanics*, vol. 232, no. -1, p. 47, Nov. 1991, ISSN: 0022-1120. DOI: 10 . 1017/S0022112091003622.
- [82] M. C. Janus, G. A. Richards, M. J. Yip, and E. H. Robey, “Effects of Ambient Conditions and Fuel Composition on Combustion Stability,” in *American Society of Mechanical Engineers (ASME)/International Gas Turbine Institute (IGTI) Turbo Expo Meeting*, Orlando, Florida: American Society of Mechanical Engineers, Jun. 1997, V002T06A035, ISBN: 978-0-7918-7869-9. DOI: 10 . 1115/97-GT-266.

- [83] U. Vandsburger, K. McManus, and C. Bowman, “Effect of fuel spray vaporization on the stability characteristics of a dump combustor,” in *AIAA/ASM E/SAE/ASEE 25th Joint Propulsion Conference*, ser. Joint Propulsion Conferences, Monterey, CA: American Institute of Aeronautics and Astronautics, Jul. 1989. DOI: 10.2514/6.1989-2436.
- [84] J. Mehta, P. Mungur, W. Dodds, D. Bahr, and S. Clouser, “Fuel effects on gas turbine combustor dynamics,” in *26th Joint Propulsion Conference*, ser. Joint Propulsion Conferences, Reston, Virginia: American Institute of Aeronautics and Astronautics, Jul. 1990. DOI: 10.2514/6.1990-1957.
- [85] B. Khandelwal, S. Roy, C. Lord, and S. Blakey, “Comparison of Vibrations and Emissions of Conventional Jet Fuel with Stressed 100% SPK and Fully Formulated Synthetic Jet Fuel,” *Aerospace*, vol. 1, no. 2, pp. 52–66, Aug. 2014, ISSN: 2226-4310. DOI: 10.3390/aerospace1020052.
- [86] E. Simons and V. Soloiu, “Reduction of Aircraft Gas Turbine Noise with New Synthetic Fuels and Sound Insulation Materials,” *Transportation Research Record: Journal of the Transportation Research Board*, vol. 2603, no. 1, pp. 50–64, Jan. 2017, ISSN: 0361-1981. DOI: 10.3141/2603-06.
- [87] F. Chen, C. Ruan, T. Yu, W. Cai, Y. Mao, and X. Lu, “Effects of fuel variation and inlet air temperature on combustion stability in a gas turbine model combustor,” *Aerospace Science and Technology*, vol. 92, pp. 126–138, Sep. 2019, ISSN: 12709638. DOI: 10.1016/j.ast.2019.05.052.
- [88] M. Othman, Y. Najjar, and T. Abou-Arab, “Fuel effect on induced vibration in gas turbine engines,” *Fuel*, vol. 67, no. 3, pp. 321–326, Mar. 1988, ISSN: 00162361. DOI: 10.1016/0016-2361(88)90313-4.
- [89] A. Mansour and N. Chigier, “Dynamic behavior of liquid sheets,” *Physics of Fluids A: Fluid Dynamics*, vol. 3, no. 12, pp. 2971–2980, Dec. 1991, ISSN: 0899-8213. DOI: 10.1063/1.857839.

- [90] L. Rayleigh, "On The Instability Of Jets," *Proceedings of the London Mathematical Society*, vol. s1-10, no. 1, pp. 4–13, Nov. 1878, ISSN: 00246115. DOI: 10.1112/plms/s1-10.1.4.
- [91] R. P. Fraser, P. Eisenklam, N. Dombrowski, and D. Hasson, "Drop formation from rapidly moving liquid sheets," *AIChE Journal*, vol. 8, no. 5, pp. 672–680, Nov. 1962, ISSN: 0001-1541. DOI: 10.1002/aic.690080522.
- [92] M. M. Elkotb, "Fuel atomization for spray modelling," *Progress in Energy and Combustion Science*, vol. 8, no. 1, pp. 61–91, Jan. 1982, ISSN: 03601285. DOI: 10.1016/0360-1285(82)90009-0.
- [93] H. Hiroyasu and T. Kadota, "Fuel Droplet Size Distribution in Diesel Combustion Chamber," in *SAE Technical Papers*, vol. 83, SAE International, Feb. 1974, pp. 2615–2624. DOI: 10.4271/740715.
- [94] S. NUKIYAMA and Y. TANASAWA, "An Experiment on the Atomization of Liquid by Means of an Air Stream (the 2nd Report).," *Transactions of the Japan Society of Mechanical Engineers*, vol. 4, no. 15, pp. 138–143, 1938, ISSN: 0029-0270. DOI: 10.1299/kikai1938.4.15_138.
- [95] A. H. Lefebvre, "Energy considerations in twin-fluid atomization," *Journal of Engineering for Gas Turbines and Power*, vol. 114, no. 1, pp. 89–96, Jan. 1992, ISSN: 15288919. DOI: 10.1115/1.2906311.
- [96] C. Shao, K. Luo, M. Chai, and J. Fan, "Sheet, ligament and droplet formation in swirling primary atomization," *AIP Advances*, vol. 8, no. 4, p. 045211, Apr. 2018, ISSN: 2158-3226. DOI: 10.1063/1.5017162. [Online]. Available: <https://doi.org/10.1063/1.5017162>.
- [97] M. DELACRUZGARCIA, E. MASTORAKOS, and A. DOWLING, "Investigations on the self-excited oscillations in a kerosene spray flame," *Combustion and Flame*, vol. 156, no. 2, pp. 374–384, Feb. 2009, ISSN: 00102180. DOI: 10.1016/j.combustflame.2008.11.018.

- [98] C. Liu, F. Liu, J. Yang, Y. Mu, and G. Xu, “Investigations of the effects of spray characteristics on the flame pattern and combustion stability of a swirl-cup combustor,” *Fuel*, vol. 139, pp. 529–536, Jan. 2015, ISSN: 00162361. DOI: 10.1016/j.fuel.2014.08.072.
- [99] J. Lovett, T. Brogan, D. Philippona, B. Kiel, and T. Thompson, “Development Needs for Advanced Afterburner Designs,” in *40th AIAA/ASME/SAE/ASEE Joint Propulsion Conference and Exhibit*, Reston, Virginia: American Institute of Aeronautics and Astronautics, Jul. 2004, ISBN: 978-1-62410-037-6. DOI: 10.2514/6.2004-4192.
- [100] H. Ebrahimi, “Overview of Gas Turbine Augmentor Design, Operation, and Combustion Oscillation,” in *42nd AIAA/ASME/SAE/ASEE Joint Propulsion Conference & Exhibit*, vol. 7, Reston, Virginia: American Institute of Aeronautics and Astronautics, Jul. 2006, pp. 5658–5673, ISBN: 978-1-62410-038-3. DOI: 10.2514/6.2006-4916.
- [101] B. Lewis and G. Von Elbe, *Physics of flames and explosions of gases*, 3rd. Academic Press, 1987, ISBN: 9780323138024.
- [102] A. Vouros, A. Vouros, and T. Panidis, “Spray Characteristics of Alternative Aviation Fuel Blends,” *Aerospace*, vol. 4, no. 2, p. 18, Mar. 2017, ISSN: 2226-4310. DOI: 10.3390/aerospace4020018.
- [103] D. Sivakumar, S. K. Vankeswaram, R. Sakthikumar, and B. N. Raghunandan, “Analysis on the atomization characteristics of aviation biofuel discharging from simplex swirl atomizer,” *International Journal of Multiphase Flow*, vol. 72, pp. 88–96, Jun. 2015, ISSN: 03019322. DOI: 10.1016/j.ijmultiphaseflow.2015.02.009.
- [104] R. C. Tolman, “The effect of droplet size on surface tension,” *The Journal of Chemical Physics*, vol. 17, no. 3, pp. 333–337, Mar. 1949, ISSN: 00219606. DOI: 10.1063/1.1747247.
- [105] T. Buschhagen, R. Z. Zhang, A. J. Bokhart, R. M. Gejji, S. V. Naik, R. P. Lucht, J. P. Gore, P. E. Sojka, C. D. Slabaugh, and S. Meyer, “Effect of Aviation Fuel

- Type and Fuel Injection Conditions on Non-reacting Spray Characteristics of a Hybrid Airblast Fuel Injector,” in *54th AIAA Aerospace Sciences Meeting*, Reston, Virginia: American Institute of Aeronautics and Astronautics, Jan. 2016, pp. 1–18, ISBN: 978-1-62410-393-3. DOI: 10.2514/6.2016-1154.
- [106] K. Kannaiyan and R. Sadr, “Experimental investigation of spray characteristics of alternative aviation fuels,” *Energy Conversion and Management*, vol. 88, pp. 1060–1069, Dec. 2014, ISSN: 01968904. DOI: 10.1016/j.enconman.2014.09.037.
- [107] J. Zhao, B. Zhao, X. Wang, and X. Yang, “Atomization performance and TG analysis of Fischer–Tropsch fuel compared with RP-3 aviation fuel,” *International Journal of Hydrogen Energy*, vol. 42, no. 29, pp. 18 626–18 632, Jul. 2017, ISSN: 03603199. DOI: 10.1016/j.ijhydene.2017.04.137.
- [108] W. Lang, T. Poinsot, and S. Candel, “Active control of combustion instability,” *Combustion and Flame*, vol. 70, no. 3, pp. 281–289, Dec. 1987, ISSN: 00102180. DOI: 10.1016/0010-2180(87)90109-X.
- [109] A. Brandt, *Noise and Vibration Analysis*. Chichester, UK: John Wiley & Sons, Ltd, Feb. 2011, ISBN: 9780470978160. DOI: 10.1002/9780470978160.
- [110] H. Nyquist, “Thermal Agitation of Electric Charge in Conductors,” *Physical Review*, vol. 32, no. 1, pp. 110–113, Jul. 1928, ISSN: 0031-899X. DOI: 10.1103/PhysRev.32.110.
- [111] Acoustic Society of America, *ANSI/ASA S1.11-2014/Part 1/IEC 61260-1:2014 (R2019) - Electroacoustics - Octave-band and Fractional-octave-band Filters - Part 1: Specifications (a nationally adopted international standard)*, 2014. [Online]. Available: <https://webstore.ansi.org/Standards/ASA/ANSIASAS1112014PartIEC61260-1-2391664> (visited on 07/07/2020).
- [112] Y. Voronenko and M. Puschel, “Algebraic Signal Processing Theory: Cooley–Tukey Type Algorithms for Real DFTs,” *IEEE Transactions on Signal Processing*, vol. 57, no. 1, pp. 205–222, Jan. 2009, ISSN: 1053-587X. DOI: 10.1109/TSP.2008.2006152.

- [113] D. C. K. Rao, S. Karmakar, and S. Basu, “Atomization characteristics and instabilities in the combustion of multi-component fuel droplets with high volatility differential,” *Scientific Reports*, vol. 7, no. 1, p. 8925, Dec. 2017, ISSN: 2045-2322. DOI: 10.1038/s41598-017-09663-7.
- [114] A. L. Pillai, J. Nagao, R. Awane, and R. Kurose, “Influences of liquid fuel atomization and flow rate fluctuations on spray combustion instabilities in a backward-facing step combustor,” *Combustion and Flame*, vol. 220, pp. 337–356, Oct. 2020, ISSN: 00102180. DOI: 10.1016/j.combustflame.2020.06.031.
- [115] J. Grohmann, B. Rauch, T. Kathrotia, W. Meier, and M. Aigner, “Influence of single-component fuels on gas-turbine model combustor lean blowout,” in *Journal of Propulsion and Power*, vol. 34, American Institute of Aeronautics and Astronautics Inc., Jan. 2018, pp. 97–107. DOI: 10.2514/1.B36456.
- [116] A. García, J. Monsalve-Serrano, B. Heuser, M. Jakob, F. Kremer, and S. Pischinger, “Influence of fuel properties on fundamental spray characteristics and soot emissions using different tailor-made fuels from biomass,” *Energy Conversion and Management*, vol. 108, pp. 243–254, Jan. 2016, ISSN: 01968904. DOI: 10.1016/j.enconman.2015.11.010.
- [117] B. Ahn, J. Lee, S. Jung, and K. T. Kim, “Low-frequency combustion instabilities of an airblast swirl injector in a liquid-fuel combustor,” *Combustion and Flame*, vol. 196, pp. 424–438, Oct. 2018, ISSN: 00102180. DOI: 10.1016/j.combustflame.2018.06.031.
- [118] G. Vignat, D. Durox, K. Prieur, and S. Candel, *An experimental study into the effect of injector pressure loss on self-sustained combustion instabilities in a swirled spray burner*, 2018. DOI: 10.1016/j.proci.2018.06.125.
- [119] C. A. Moses and P. N. Roets, “Properties, characteristics, and combustion performance of sasol fully synthetic jet fuel,” *Journal of Engineering for Gas Turbines and Power*, vol. 131, no. 4, 2009, ISSN: 07424795. DOI: 10.1115/1.3028234. [Online]. Available: <https://asmedigitalcollection.asme.org/>

- gasturbinespower/article-pdf/131/4/041502/5706818/041502%7B%5C_%7D1.pdf.
- [120] M. Colket, T. Edwards, F. Dryer, S. Williams, N. Cernansky, D. Miller, F. Egolfopoulos, F. Dryer, and J. Bellan, “Identification of Target Validation Data for Development of Surrogate Jet Fuels,” in *46th AIAA Aerospace Sciences Meeting and Exhibit*, Reston, Virginia: American Institute of Aeronautics and Astronautics, Jan. 2008, ISBN: 978-1-62410-128-1. DOI: 10.2514/6.2008-972.
- [121] K. Chen, H. Liu, and Z. Xia, “The Impacts of Aromatic Contents in Aviation Jet Fuel on the Volume Swell of the Aircraft Fuel Tank Sealants,” *SAE International Journal of Aerospace*, vol. 6, no. 1, pp. 2013-01-9001, Sep. 2013, ISSN: 1946-3901. DOI: 10.4271/2013-01-9001.
- [122] R. Friedman, “RECENT TRENDS IN AVIATION TURBINE FUEL PROPERTIES,” Cleveland, OH, 1982. [Online]. Available: <https://ntrs.nasa.gov/search.jsp?R=19830003070>.
- [123] T. Schripp, B. Anderson, E. C. Crosbie, R. H. Moore, F. Herrmann, P. Oßwald, C. Wahl, M. Kapernaum, M. Köhler, P. Le Clercq, B. Rauch, P. Eichler, T. Mikoviny, and A. Wisthaler, “Impact of Alternative Jet Fuels on Engine Exhaust Composition During the 2015 ECLIF Ground-Based Measurements Campaign,” *Environmental Science & Technology*, vol. 52, no. 8, pp. 4969–4978, Apr. 2018, ISSN: 0013-936X. DOI: 10.1021/acs.est.7b06244.
- [124] Shell Oil Company, *Civil Aviation Fuel | Jet Fuel Specifications | Shell Global*. [Online]. Available: <https://www.shell.com/business-customers/aviation/aviation-fuel/civil-jet-fuel-grades.html>.
- [125] Energy Institute, *IP 160: Crude petroleum and liquid petroleum products - Laboratory determination of density - Hydrometer method | EI - Publishing*. [Online]. Available: <https://publishing.energyinst.org/topics/fuel-quality-and-control/ip-test-methods/ip-160-crude-petroleum-and-liquid-petroleum-products-laboratory-determination-of-density-hydrometer-method> (visited on 06/18/2020).

- [126] ———, “Crude petroleum and petroleum products — Determination of density — Oscillating U-tube method,” vol. 2001, p. 12 185, 2001. [Online]. Available: <https://publishing.energyinst.org/ip-test-methods/full-list-of-ip-test-methods-publications/ip-365-crude-petroleum-and-petroleum-products-determination-of-density-oscillating-u-tube-method2>.
- [127] ASTM, *D4052*, 2019. DOI: 10.1520/D4052-18A. [Online]. Available: www.astm.org (visited on 06/18/2020).
- [128] A. N. Standard, *ASTM D445: Standard Test Method for Kinematic Viscosity of Transparent and Opaque Liquids (And Calculation of Dynamic Viscosity)*, 1988. [Online]. Available: <https://www.astm.org/Standards/D445.htm> (visited on 07/27/2020).
- [129] Malvern Instruments, *Malvern Instruments 2600 User Manual*. 1991.
- [130] F. Barreras, A. Lozano, J. Barroso, and E. Lincheta, “EXPERIMENTAL CHARACTERIZATION OF INDUSTRIAL TWIN-FLUID ATOMIZERS,” *Atomization and Sprays*, vol. 16, no. 2, pp. 127–146, 2006, ISSN: 1045-5110. DOI: 10.1615/AtomizSpr.v16.i2.10.
- [131] J. S. Chin, W. M. Li, and Y. Zhang, “Experimental study of the effect of dense spray on drop size measurement by light scattering technology,” *Journal of Engineering for Gas Turbines and Power*, vol. 114, no. 1, pp. 82–88, Jan. 1992, ISSN: 15288919. DOI: 10.1115/1.2906310.
- [132] P. B. Kowalczyk and J. Drzymala, “Physical meaning of the Sauter mean diameter of spherical particulate matter,” *Particulate Science and Technology*, vol. 34, no. 6, pp. 645–647, Nov. 2016, ISSN: 0272-6351. DOI: 10.1080/02726351.2015.1099582.
- [133] A. Pacek, C. Man, and A. Nienow, “On the Sauter mean diameter and size distributions in turbulent liquid/liquid dispersions in a stirred vessel,” *Chemical Engineering Science*, vol. 53, no. 11, pp. 2005–2011, Jun. 1998, ISSN: 00092509. DOI: 10.1016/S0009-2509(98)00068-2.

- [134] Malvern Instruments, “A basic guide to particle characterization,” 2015. [Online]. Available: https://www.cif.iastate.edu/sites/default/files/uploads/0ther%7B%5C_%7DInst/Particle%20Size/Particle%20Characterization%20Guide.pdf.
- [135] I. Macafee, “The Development and Introduction of High Temperature Optical Pressure Sensors in Gas Turbine Combustion Monitoring Applications,” Tech. Rep. [Online]. Available: <https://oxsensis.com/wp-content/uploads/2019/08/The-development-and-introduction-of-high-temperature-optical-pressure-sensors-in-gas-turbine-combustion-monitoring-applications-0xsensis-paper-2019.pdf>.
- [136] Oxsensis Ltd, “Oxsensis Dynamic Pressure Measurement System Reference Guide,” Tech. Rep., 2011.
- [137] Dytran Instruments, *Series 3225F|Miniature Sensor|Dytran*. [Online]. Available: <https://www.dytran.com/Model-3225F-Miniature-Accelerometer-P1346/> (visited on 06/01/2020).
- [138] PCB Piezotronics, *PCB Model HT378B02*. [Online]. Available: <http://www.pcb.com/Products.aspx?m=HT378B02> (visited on 06/01/2020).
- [139] Baumgart, *Technologie-Entwicklung Baumgart*. [Online]. Available: <http://www.te-baumgart.de/Gasturbines/GTCP85/gtcp85.html> (visited on 03/17/2020).
- [140] A. E. S. E. T. Alajmi, N. M. Adam, A. A. Hairuddin, and L. C. Abdullah, “Fuel atomization in gas turbines: A review of novel technology,” *International Journal of Energy Research*, vol. 43, no. 8, pp. 3166–3181, Jun. 2018, ISSN: 0363-907X. DOI: 10.1002/er.4415.
- [141] K. P. Shanmugasdas, S. R. Chakravarthy, R. N. Chiranthan, J. Sekar, and S. Krishnaswami, “Characterization of wall filming and atomization inside a gas-turbine swirl injector,” *Experiments in Fluids*, vol. 59, no. 10, p. 151, 2018, ISSN: 07234864. DOI: 10.1007/s00348-018-2606-0.

- [142] J. Sallevelt, J. Gudde, A. Pozarlik, and G. Brem, “The impact of spray quality on the combustion of a viscous biofuel in a micro gas turbine,” *Applied Energy*, vol. 132, pp. 575–585, Nov. 2014, ISSN: 03062619. DOI: 10.1016/j.apenergy.2014.07.030.
- [143] A. P. Crayford, F. Lacan, J. Runyon, P. J. Bowen, S. Balwadkar, J. Harper, and D. G. Pugh, “Manufacture, characterization and stability limits of an AM prefilming air-blast atomizer,” in *Proceedings of the ASME Turbo Expo*, vol. 4B-2019, 2019, ISBN: 9780791858622. DOI: 10.1115/GT2019-91624.
- [144] S. Penner and F. Williams, “Recent studies on flame stabilization of premixed turbulent gases,” *Applied Mechanics Reviews*, vol. 10, no. 6, pp. 229–237, 1957, ISSN: 0003-6900.
- [145] G. Charalampous and Y. Hardalupas, “How do liquid fuel physical properties affect liquid jet development in atomisers?” *Physics of Fluids*, vol. 28, no. 10, p. 102 106, Oct. 2016, ISSN: 10897666. DOI: 10.1063/1.4965447.
- [146] I. S. Carvalho and M. V. Heitor, “Liquid film break-up in a model of a prefilming airblast nozzle,” *Experiments in Fluids*, vol. 24, no. 5-6, pp. 408–415, 1998, ISSN: 07234864. DOI: 10.1007/s003480050190.
- [147] P. Gogate, “The use of ultrasonic atomization for encapsulation and other processes in food and pharmaceutical manufacturing,” in *Power Ultrasonics*, Elsevier, Jan. 2015, pp. 911–935, ISBN: 9781782420361. DOI: 10.1016/B978-1-78242-028-6.00030-2.
- [148] B. Li, B. Shi, X. Zhao, K. Ma, D. Xie, D. Zhao, and J. Li, “Oxy-fuel combustion of methane in a swirl tubular flame burner under various oxygen contents: Operation limits and combustion instability,” *Experimental Thermal and Fluid Science*, vol. 90, pp. 115–124, Jan. 2018, ISSN: 08941777. DOI: 10.1016/j.expthermflusci.2017.09.001.
- [149] R. M. Flores, M. M. Miyasato, V. G. McDonell, and G. S. Samuelsen, “Response of a Model Gas Turbine Combustor to Variation in Gaseous Fuel Composition,”

- Journal of Engineering for Gas Turbines and Power*, vol. 123, no. 4, pp. 824–831, Oct. 2000, ISSN: 0742-4795. DOI: 10.1115/1.1377011.
- [150] T. M. Muruganandam, S. Nair, D. Scarborough, Y. Neumeier, J. Jagoda, T. Lieuwen, J. Seitzman, and B. Zinn, “Active Control of Lean Blowout for Turbine Engine Combustors,” *Journal of Propulsion and Power*, vol. 21, no. 5, pp. 807–814, Sep. 2005, ISSN: 0748-4658. DOI: 10.2514/1.7254.
- [151] D. Allgood, S. Murugappan, S. Acharya, and E. Gutmark, “Infrared measurements of thermoacoustic instabilities in a swirl-stabilized combustor,” *Combustion Science and Technology*, vol. 175, no. 2, pp. 333–355, Feb. 2003, ISSN: 0010-2202. DOI: 10.1080/00102200302398.
- [152] S. Nair and T. Lieuwen, “Acoustic detection of blowout in premixed flames,” *Journal of Propulsion and Power*, vol. 21, no. 1, pp. 32–39, Jan. 2005, ISSN: 07484658. DOI: 10.2514/1.5658.
- [153] A. P. Dowling and Y. Mahmoudi, “Combustion noise,” *Proceedings of the Combustion Institute*, vol. 35, no. 1, pp. 65–100, 2015, ISSN: 15407489. DOI: 10.1016/j.proci.2014.08.016. [Online]. Available: <https://linkinghub.elsevier.com/retrieve/pii/S1540748914004003>.
- [154] M. Wang, Y. Zhong, and K. Deng, “Experiment investigation of the effects of hydrogen content on the combustion instability of methane/hydrogen lean premixed swirl flames under different acoustic frequency ranges,” *AIP Advances*, vol. 9, no. 4, p. 045 206, Apr. 2019, ISSN: 2158-3226. DOI: 10.1063/1.5091617.
- [155] M. MACQUISTEN and A. DOWLING, “Low-frequency combustion oscillations in a model afterburner□,” *Combustion and Flame*, vol. 94, no. 3, pp. 253–264, Aug. 1993, ISSN: 00102180. DOI: 10.1016/0010-2180(93)90072-B.

Appendices

Appendix 1 VI Data Acquisition block diagram

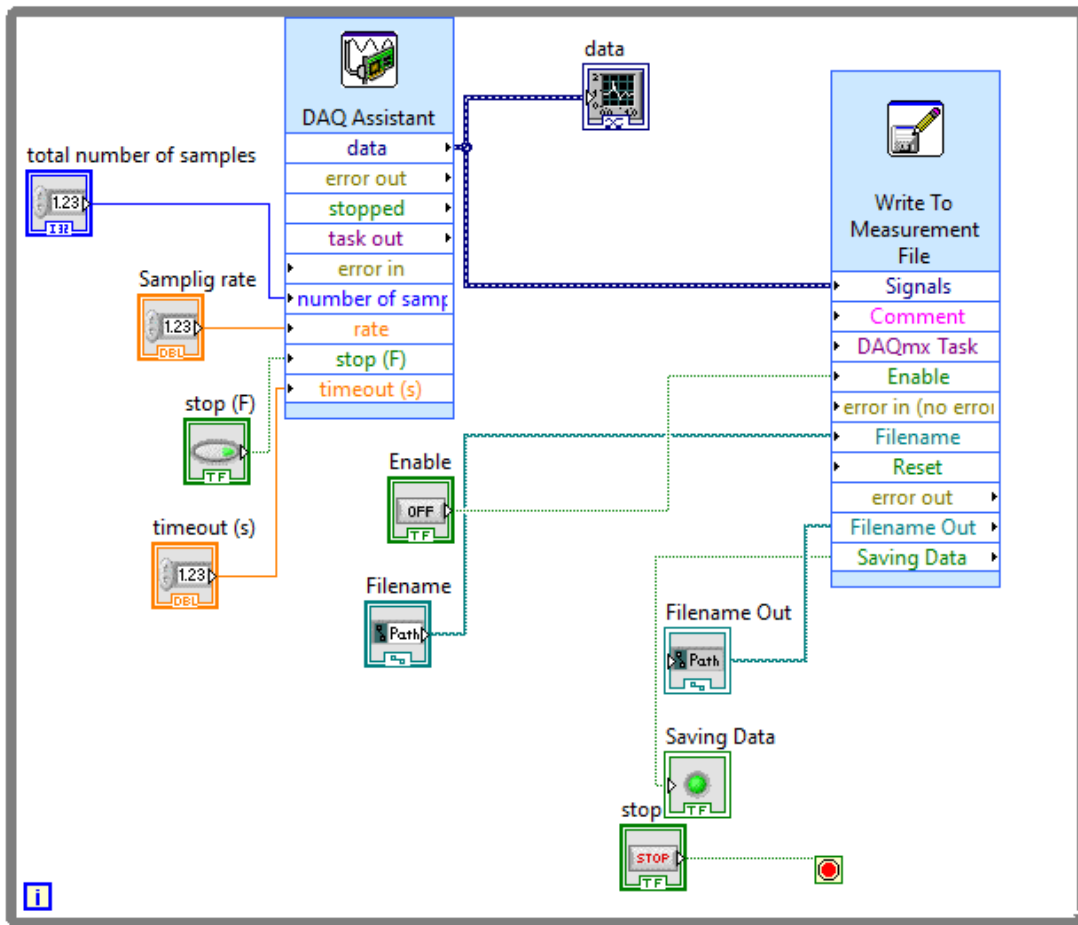


Figure 7.3: Data acquisition VI for acceleration, noise and pressure.

Appendix 2 Matlab Code

```

1 %sampling Frequency
2 fs =25000;
3
4 % Process to convert imported data into array format. t1-t3
   are cobmuster conditions.
5 JetA1t1=table2array(JetA1t1);
6 JetA1t2=table2array(JetA1t2);
7 JetA1t3=table2array(JetA1t3);

```

```

8
9 % Process to check the timestamps of the data for any
    corruptions in the files like NaN's where the aquisition
    computer could not keep up with the aquisition rate.
10 idt1 = find(isnan(JetA1t1(:,1)));
11 idt2 = find(isnan(JetA1t2(:,1)));
12 idt3 = find(isnan(JetA1t3(:,1)));
13
14 %process to delete the corrupted rows.
15 JetA1t1(idt1,:) = [];
16 JetA1t2(idt2,:) = [];
17 JetA1t3(idt3,:) = [];
18
19 % selecting the analysis window
20 t_sel = 500000:510000;
21
22
23 %naming Variables
24 t1=JetA1t1(t_sel,1);
25 t2=JetA1t2(t_sel,1);
26 t3=JetA1t3(t_sel,1);
27
28 x1t1=JetA1t1(t_sel,2);
29 x1t2=JetA1t2(t_sel,2);
30 x1t3=JetA1t3(t_sel,2);
31
32 y1t1=JetA1t1(t_sel,3);
33 y1t2=JetA1t2(t_sel,3);
34 y1t3=JetA1t3(t_sel,3);
35

```

36

37 z1t1=JetA1t1(t_sel,4);

38 z1t2=JetA1t2(t_sel,4);

39 z1t3=JetA1t3(t_sel,4);

40

41

42 x2t1=JetA1t1(t_sel,5);

43 x2t2=JetA1t2(t_sel,5);

44 x2t3=JetA1t3(t_sel,5);

45

46

47 y2t1=JetA1t1(t_sel,6);

48 y2t2=JetA1t2(t_sel,6);

49 y2t3=JetA1t3(t_sel,6);

50

51

52 m1t1=JetA1t1(t_sel,7);

53 m1t2=JetA1t2(t_sel,7);

54 m1t3=JetA1t3(t_sel,7);

55

56

57 m2t1=JetA1t1(t_sel,8);

58 m2t2=JetA1t2(t_sel,8);

59 m2t3=JetA1t3(t_sel,8);

60

61

62 p1t1=JetA1t1(t_sel,9);

63 p1t2=JetA1t2(t_sel,9);

64 p1t3=JetA1t3(t_sel,9);

65

```

66 %% plotting the timespacing to determine the actually
    sampling rate
67 figure (1)
68 plot(diff(t1))
69 figure (2)
70 plot(diff(t2))
71 figure (3)
72 plot(diff(t3))
73 %% Resampling the data to required sampling frequency as
    nessacary
74
75 [x1rt1 , t1r] = resample(x1t1 , t1 , fs);
76 [x1rt2 , t2r] = resample(x1t2 , t2 , fs);
77 [x1rt3 , t3r] = resample(x1t3 , t3 , fs);
78
79 [y1rt1 , t1r] = resample(y1t1 , t1 , fs);
80 [y1rt2 , t2r] = resample(y1t2 , t2 , fs);
81 [y1rt3 , t3r] = resample(y1t3 , t3 , fs);
82
83 [z1rt1 , t1r] = resample(z1t1 , t1 , fs);
84 [z1rt2 , t2r] = resample(z1t2 , t2 , fs);
85 [z1rt3 , t3r] = resample(z1t3 , t3 , fs);
86
87 [x2rt1 , t1r] = resample(x2t1 , t1 , fs);
88 [x2rt2 , t2r] = resample(x2t2 , t2 , fs);
89 [x2rt3 , t3r] = resample(x2t3 , t3 , fs);
90
91 [y2rt1 , t1r] = resample(y2t1 , t1 , fs);
92 [y2rt2 , t2r] = resample(y2t2 , t2 , fs);
93 [y2rt3 , t3r] = resample(y2t3 , t3 , fs);

```

94

95 [m1rt1 , t1r] = resample (m1t1 , t1 , fs);

96 [m1rt2 , t2r] = resample (m1t2 , t2 , fs);

97 [m1rt3 , t3r] = resample (m1t3 , t3 , fs);

98

99 [m2rt1 , t1r] = resample (m2t1 , t1 , fs);

100 [m2rt2 , t2r] = resample (m2t2 , t2 , fs);

101 [m2rt3 , t3r] = resample (m2t3 , t3 , fs);

102

103 [p1rt1 , t1r] = resample (p1t1 , t1 , fs);

104 [p1rt2 , t2r] = resample (p1t2 , t2 , fs);

105 [p1rt3 , t3r] = resample (p1t3 , t3 , fs);

106

107 %% FFT generation where S_FFT is the code used. see next
section.

108 [whzt1 , X1t1]=S_FFT (t1 , x1t1);

109 [whzt2 , X1t2]=S_FFT (t2 , x1t2);

110 [whzt3 , X1t3]=S_FFT (t3 , x1t3);

111

112 [whzt1 , Y1t1]=S_FFT (t1 , y1t1);

113 [whzt2 , Y1t2]=S_FFT (t2 , y1t2);

114 [whzt3 , Y1t3]=S_FFT (t3 , y1t3);

115

116 [whzt1 , Z1t1]=S_FFT (t1 , z1t1);

117 [whzt2 , Z1t2]=S_FFT (t2 , z1t2);

118 [whzt3 , Z1t3]=S_FFT (t3 , z1t3);

119

120 [whzt1 , X2t1]=S_FFT (t1 , x2t1);

121 [whzt2 , X2t2]=S_FFT (t2 , x2t2);

122 [whzt3 , X2t3]=S_FFT (t3 , x2t3);

```

123
124 [ whzt1 , Y2t1 ]=S_FFT( t1 , y2t1 );
125 [ whzt2 , Y2t2 ]=S_FFT( t2 , y2t2 );
126 [ whzt3 , Y2t3 ]=S_FFT( t3 , y2t3 );
127
128 [ whzt1 , M1t1 ]=S_FFT( t1 , m1t1 );
129 [ whzt2 , M1t2 ]=S_FFT( t2 , m1t2 );
130 [ whzt3 , M1t3 ]=S_FFT( t3 , m1t3 );
131
132 [ whzt1 , M2t1 ]=S_FFT( t1 , m2t1 );
133 [ whzt2 , M2t2 ]=S_FFT( t2 , m2t2 );
134 [ whzt3 , M2t3 ]=S_FFT( t3 , m2t3 );
135
136 [ whzt1 , Pt1 ]=S_FFT( t1 , p1t1 );
137 [ whzt2 , Pt2 ]=S_FFT( t2 , p1t2 );
138 [ whzt3 , Pt3 ]=S_FFT( t3 , p1t3 );
139
140 %% Plotting of the data
141 subplot(8,1,1)
142 hold on
143 plot( whzt1 , abs( X1t1 ) , 'r' )
144 plot( whzt2 , abs( X1t2 ) , 'g' )
145 plot( whzt3 , abs( X1t3 ) , 'b' )
146 xlim([5 6000])
147
148 title( 'X1 ' )
149
150 subplot(8,1,2)
151 hold on
152 plot( whzt1 , abs( Y1t1 ) , 'r' )

```

```
153 plot (whzt2 , abs (Y1t2) , 'g')
154 plot (whzt3 , abs (Y1t3) , 'b')
155 xlim ([2 6000])
156 title ('Y1 ')
157
158 subplot (8 ,1 ,3)
159 hold on
160 plot (whzt1 , abs (Z1t1) , 'r')
161 plot (whzt2 , abs (Z1t2) , 'g')
162 plot (whzt3 , abs (Z1t3) , 'b')
163 xlim ([2 6000])
164
165 title ('Z1 ')
166
167 subplot (8 ,1 ,4)
168 hold on
169 plot (whzt1 , abs (X2t1) , 'r')
170 plot (whzt2 , abs (X2t2) , 'g')
171 plot (whzt3 , abs (X2t3) , 'b')
172 xlim ([2 6000])
173
174 title ('X2')
175
176 subplot (8 ,1 ,5)
177 hold on
178 plot (whzt1 , abs (Y2t1) , 'r')
179 plot (whzt2 , abs (Y2t2) , 'g')
180 plot (whzt3 , abs (Y2t3) , 'b')
181 xlim ([2 6000])
182 title ('Y2 ')
```

```
183
184 subplot(8,1,6)
185 hold on
186 plot(whzt1,abs(M1t1),'r')
187 plot(whzt2,abs(M1t2),'g')
188 plot(whzt3,abs(M1t3),'b')
189 xlim([2 6000])
190
191 title('M1')
192
193 subplot(8,1,7)
194 hold on
195 plot(whzt1,abs(M2t1),'r')
196 plot(whzt2,abs(M2t2),'g')
197 plot(whzt3,abs(M2t3),'b')
198 xlim([2 6000])
199
200 title('M2')
201
202 subplot(8,1,8)
203 hold on
204 plot(whzt1,abs(Pt1),'r')
205 plot(whzt2,abs(Pt2),'g')
206 plot(whzt3,abs(Pt3),'b')
207 xlim([2.56 6000])
208
209
210 title('P')
211
212 hold off
```

```

213
214 %% RMS acceleration generation
215 C16RMS=[rms(abs(X1t1)) rms(abs(X1t2)) rms(abs(X1t3)); rms(
        abs(Y1t1)) rms(abs(Y1t2)) rms(abs(Y1t3));rms(abs(Z1t1))
        rms(abs(Z1t2)) rms(abs(Z1t3))];
216 C16RMStble=array2table(C16RMS,'VariableNames',{ 'T1', 'T2', '
        T3'});
217 %% process to show spectrogram to determine if singals are
        stationary
218
219 subplot(3,2,1)
220 spectrogram(x1t2,2000,1000, linspace(0,12.5e3,12.5e3),25e3)
221 title('X1')
222 subplot(3,2,2)
223 spectrogram(y1t2,2000,1000, linspace(0,12.5e3,12.5e3),25e3)
224 title('Y1')
225 subplot(3,2,3)
226 spectrogram(z1t2,2000,1000, linspace(0,12.5e3,12.5e3),25e3)
227 title('Z1')
228 subplot(3,2,4)
229 spectrogram(m1t2,2000,1000, linspace(0,12.5e3,12.5e3),25e3)
230 title('M1')
231 subplot(3,2,5)
232 spectrogram(m1t2,2000,1000, linspace(0,12.5e3,12.5e3),25e3)
233 title('M2')
234 subplot(3,2,6)
235 spectrogram(p1t2,2000,1000, linspace(0,12.5e3,12.5e3),25e3)
236 title('P')

1 function varargout = S_FFT(t,x)
2

```

```

3 % Code to Create single sided FFT
4 %
5 % [freq ,X] = S_FFT(t ,x)
6
7 % t = time signal (s)
8 % x = position signal
9 % whz = frequency (Hz)
10 % X = Fourier Transform of x
11
12
13
14
15 % transpose data
16 t = s (:);
17 x = x (:);
18
19 % the FFT algorithm works best with an even number of data
    points
20 n = length(t);
21 if n/2 ~= round(n/2) ,
22     t = t(1:end-1);
23     x = x(1:end-1);
24     n = n-1;
25 end
26
27 % derive the fft magnitudes
28 Y = fft(x);
29 X = [Y(1); 2*Y(2:(n/2+1))] / n;
30
31 % derive the frequency points

```

```
32 dt = mean(diff(t));
33 whz = [0:n/2]'/n/dt;
34
35
36
37 if nargin == 0,
38
39 end
40
41 % error meesages
42
43 if nargin > 0,
44     varargout{1} = whz;
45 end
46
47 if nargin > 1,
48     varargout{2} = X;
49 end
```